Relating Mechanical Properties of Paper to Papermaking Variables

A Dissertation Submitted By

Dana L. Ingalsbe

B.S. 1995, Roberts Wesleyan College

M.S. 1997, The Institute of Paper Science and Technology

This Thesis is in Partial Fulfillment of the Requirements from

The Institute of Paper Science and Technology

for the Degree of Doctor of Philosophy

Atlanta, Georgia

June 2001

"Thinking cannot be carried on without the materials of thought; and the materials of thought are facts, or else assertions that are presented as facts. A mass of details stored up in the mind does not in itself make a thinker; but on the other hand thinking is absolutely impossible without that mass of details. And it is just this latter impossible operation of thinking without the materials of thought which is being advocated by modern pedagogy and is being put into practice only too well by modern students. In the presence of this tendency, we believe that facts and hard work ought to be allowed to come to their rights. It is impossible to think with an empty mind."

-J. Gresham Machen (1881-1935)

TABLE OF CONTENTS

LIST OF FIGURES

LIST OF TABLES

LIST OF SYMBOLS

a.d.	Air dry
C_{ij}	Elastic stiffness coefficient
$\overline{C}_{ij}$	Specific elastic stiffness coefficient
$\overline{C}_{11}$	MD specific stiffness
$\overline{C}_{22}$	CD specific stiffness
$\overline{C}_{33}$	ZD specific stiffness
CDS	CD Shrinkage
e_{ij}	Strain tensor
E_p	Sheet modulus
E_f	Fiber modulus
E_x	Young's modulus (MD)
E_y	Young's modulus (CD)
FO	Fiber orientation ratio (max/min)
FR	Freeness (mLs)
G_f	Fiber shear modulus
G_{xy}	Shear modulus in the plane of the sheet
g	Grammage (kg/m^2)
JW	Jet-to-wire speed ratio
K	Constant: product of fiber modulus and fiber density
L	Average fiber length
OCA	Optical contact area
o.d.	Oven dry

Q_{ij}	Planar stiffness coefficient
$\overline{Q}_{ij}$	Specific planar stiffness coefficient
RBA	Relative bonded area
R.H.	Relative humidity
R_{xy}	Elastic stiffness ratio
ΔS	Change in scattering coefficient
S_{ij}	Compliance tensor
V	Velocity
V_{45}	Velocity at 45 degrees
WP	Wet-pressing level
WS	Wet-straining level
x, y, z	Principal directions in a rectangular Cartesian coordinate system
$\overline{Z}$	Specific Z-toughness
w	Mean fiber width
ρ	Apparent density
ν_{ij}	Poisson's ratio
σ_{ij}	Stress tensor
θ	Angle of measurement
ϕ	Angle of fiber orientation misalignment from MD
K	von Mises fitting parameter

ABSTRACT

The importance of on-line process control has been recognized by the pulp and paper industry as a major cost saving initiative. Traditional quality monitoring involves sampling and testing from the finished reel, possibly hours after production has occurred. This destructive testing is limited and may not relate directly to the end-use performance of a grade. Conversely, elastic stiffness properties are fundamental mechanical properties that serve to characterize a material in all three dimensions. Elastic stiffnesses may be detected in moving webs using acoustic techniques. The detection of elastic stiffnesses on-line is therefore aptly suited for application in papermaking process control.

Real-time process control (1) requires the use of sensors, algorithms and actuators to detect changes in elastic stiffness and fiber orientation properties, interpret those changes, and respond immediately with adjustments to papermaking parameters, such as jet-to-wire ratio or wet-pressing pressure. The benefits of time savings, materials savings, and energy savings are countless.

Significant research investigating the effects of manufacturing variables upon the nondestructive properties of paper has been previously conducted. However, the inverse problem of predicting changes in manufacturing variables from nondestructive paper properties has not been addressed.

This doctoral dissertation work focused upon the development of an empirical model relating the nondestructive mechanical and physical properties of a reprographic

sheet to papermaking variables such as refining, wet-pressing, and restrained drying, among others. Such a model may serve to further advance on-line process control.

An experimental handsheet program was executed. Handsheets were formed on the Formette Dynamique under different controlled process conditions. The sheets were then characterized using in-plane and out-of-plane ultrasonic stiffness measurements and image analysis of dyed fibers in the sheets.

A series of five equations describing each of the measured nondestructive properties as a function of machine variables was obtained by performing several multiple nonlinear regression analyses of the data.

The inverse relationship was produced, describing the machine variables as functions of nondestructive sheet properties. Two simulations testing the precision of the inverse equations were instrumental in determining that the inverse equations effectively predicted freeness, jet-to-wire, and CD shrinkage values.

INTRODUCTION

Traditional methods of paper testing involve a limited battery of destructive tests that are performed on samples taken from the end of a particular reel. There are inherent limitations with this practice as it relates to the economy and quality control of a paper machine. Primarily, there is a significant time lag between reel turn up and the completion of dry lab testing. This makes such testing an impossible means of real-time quality control. Secondly, the tests are destructive and do not necessarily relate to the final, end-use parameters of the paper itself.

Elastic stiffness measurements characterize a material in its three dimensions. Such measurements can be performed nondestructively using acoustic methods and have the capability of being performed both on the moving web and in the laboratory. Elastic stiffness measurements may be correlated to traditional measurements of strength (2). However, stiffness itself is an important measurement in and of itself and will be emphasized in this dissertation.

The detection of elastic stiffnesses in real time entails an important step towards improved papermaking process control. In addition to elastic stiffness measurements, fiber orientation distributions may also be detected nondestructively using on-line instrumentation. Optical properties such as brightness, opacity, and smoothness are routinely measured on-line using optical scanning devices.

The ultimate goal of real-time stiffness and fiber orientation detection is to

provide monitoring that allows papermakers to "close the loop" in the quest to better control the papermaking process and improve sheet uniformity. The cost-savings and waste-minimization possibilities offered by the development of real-time, on-machine testing are countless.

Understanding the relationships between elastic stiffness measurements, fiber orientation measurements, apparent densities, and different papermaking processes is important for determining the effects of manufacturing variables. It is also necessary to measure properties that provide independent information about different papermaking parameters. Several studies have investigated the effects of individual papermaking processes upon the mechanical stiffnesses of paper. It has been found, for instance, that MD longitudinal stiffness is sensitive to several machine variables such as fiber orientation, wet-pressing, and wet-straining. Methods of separating the influences of fiber orientation from other papermaking variables were proposed by Baum (3). He proposed the simultaneous detection of in-plane and out-of-plane stiffness properties, partially on the basis that in-plane properties are sensitive to fiber orientation but out-of-plane longitudinal stiffness is not.

The final product of this work is a model that relates changes in nondestructive mechanical properties of the sheet to manufacturing variables. In a series of controlled experiments, sheets were made with different levels of five independent manufacturing variables: stock freeness, jet-to-wire speed ratio, wet-pressing level, MD wet-straining, and CD shrinkage/restraint. After TAPPI standard conditioning, in-plane stiffness

properties, out-of-plane ZD stiffness, fiber orientation distribution, and apparent density were measured. The resulting data were analyzed using regression analysis to describe each dependent variable as a polynomial function of the independent variables. The final step was to construct the inverse relationships, that is, to describe the independent variables as an expression of the dependent variables.

The outcome of the data analysis is a series of equations that relate changes in the measured nondestructive properties of the sheet to changes that occurred in the manufacturing process. While such a model on a laboratory scale is rudimentary, it is a necessary first step in approaching the large-scale issue of reaching true process control on a paper machine.

The conditions for sheet making modeled reprographic bond paper (copy paper). This grade accounts for about 30% of total North American uncoated free-sheet shipments, the largest segment of the printing/writing paper sector in terms of tonnage (4). Copy paper is a commodity grade and information about this grade was readily available. On the other hand, if a grade such as tissue had been used, it would have been difficult, if not impossible, to get information about the grade from any of the manufacturers. Linerboard would have been a good choice, but in the proposal stage of this project it was thought that linerboard would be studied concurrently as part of a DOE project; that did not happen.

While several researchers have investigated the individual contributions of different machine variables to the stiffness properties of the sheet, no one has attempted

to decouple the effects of a number of variables and develop a corresponding descriptive model.

BACKGROUND

Elastic Properties of Paper

The elastic properties of materials are typically reported with dimensions of force per unit area, corresponding to the initial slope of a stress-strain curve. Because of paper's rough surface, variable thickness, and unique compressibility, the mass specific stiffness (or specific stiffness or tensile stiffness index), $\overline{C}_{ij}$, is conventionally used: the elastic stiffness divided by the mass density of paper, ρ, written as:

$$\overline{C}_{ij} = C_{ij}/\rho \qquad [1]$$

where the dimensions of mass specific stiffness are reported as a squared velocity, $(km/sec)^2$, or force length per unit mass, MNm/kg (5). Coefficients i and j may each equal 1, 2, 3, 4, 5, or 6.

The elastic stiffness ratios provide descriptors for the degree of orthotropy of a sheet (2).

$$R_{MD\text{-}CD} = R_{xy} = C_{11}/C_{22} \qquad [2]$$

$$R_{MD\text{-}ZD} = R_{xz} = C_{11}/C_{33} \qquad [3]$$

$$R_{CD\text{-}ZD} = R_{yz} = C_{22}/C_{33} \qquad [4]$$

Another parameter of significance is the geometric mean:

$$\text{Geometric Mean} = (C_{11} \cdot C_{22})^{1/2} \qquad [5]$$

The geometric mean stiffness value is approximately constant at different degrees of anisotropy and is thus considered a predictor of an invariant property (6).

The Orthotropic Model of Paper

Paper is a three-dimensional anisotropic structure. Paper is also described as orthotropic: having three mutually perpendicular planes of symmetry (7). The three planes are: machine direction (x or MD), cross machine direction (y or CD) and thickness direction (z or ZD). At small strains, it can be assumed that paper behaves in accordance with Hooke's Law: in an elastic solid the strain is proportional to the stress imposed on the material.

To understand the orthotropic model, it is helpful to envision a cube of material aligned with a Cartesian coordinate system (1, 2, 3). There are three possible stresses acting on each face of this cube. There are three normal stresses: σ_{11}, σ_{22}, and σ_{33}. A normal stress is one acting perpendicular to the cut surface. There are six shear stresses: σ_{12}, σ_{13}, σ_{23}, σ_{21}, σ_{31}, and σ_{32}. A shear stress is one which acts in a direction parallel to the cut surface. The 1, 2, and 3 subscripts refer to the x, y, and z coordinate directions of the sheet, respectively. The first subscript references the direction normal to the plane of action while the second subscript references the direction of the stress. When a body is in equilibrium and the net moment on the cube is zero, $\sigma_{ij} = \sigma_{ji}$.

The deformation of a solid can be described using a displacement vector field, $\vec{u}$ (x, y, z). The vector $\vec{u}$ is the difference between the location of a particle after

deformation occurs and its original location with respect to a system of fixed coordinates. The strain of a solid at a point can be defined in terms of the displacement vector field:

$$\begin{aligned} e_{11} &= (\partial u_x)/\partial_x, \quad e_{12} = e_{21} = (\partial u_x)/\partial_y + (\partial u_y)/\partial_x \\ e_{22} &= (\partial u_y)/\partial_y, \quad e_{13} = e_{31} = (\partial u_x)/\partial_z + (\partial u_z)/\partial_x \\ e_{33} &= (\partial u_z)/\partial_z, \quad e_{23} = e_{32} = (\partial u_y)/\partial_z + (\partial u_z)/\partial_y \end{aligned} \qquad [6]$$

The strain tensor is symmetric with $e_{ij} = e_{ji}$.

The nine stresses that act upon a material can be reduced to six independent stresses and redefined using the following notation:

$$\begin{aligned} \sigma_{11} &= \sigma_1 \qquad \sigma_{23} = \sigma_4 \\ \sigma_{22} &= \sigma_2 \qquad \sigma_{13} = \sigma_5 \\ \sigma_{33} &= \sigma_3 \qquad \sigma_{12} = \sigma_6 \end{aligned} \qquad [7]$$

Hooke's Law assumes each of the stresses can be expressed as a linear combination of the strains. The six independent stresses and six independent strains can be expressed as a generalized Hooke's Law with 21 stiffness terms since $C_{12} = C_{21}$ and $C_{ij} = C_{ji}$. However, in an orthotropic material such as paper, the 21 stiffnesses can be reduced to nine and the constitutive relationship can be expressed as:

$$\begin{bmatrix} \sigma_{11} \\ \sigma_{22} \\ \sigma_{33} \\ \sigma_{23} \\ \sigma_{13} \\ \sigma_{12} \end{bmatrix} = \begin{bmatrix} C_{11} & C_{12} & C_{13} & 0 & 0 & 0 \\ C_{12} & C_{22} & C_{23} & 0 & 0 & 0 \\ C_{13} & C_{23} & C_{33} & 0 & 0 & 0 \\ 0 & 0 & 0 & 2 \cdot C_{44} & 0 & 0 \\ 0 & 0 & 0 & 0 & 2 \cdot C_{55} & 0 \\ 0 & 0 & 0 & 0 & 0 & 2 \cdot C_{66} \end{bmatrix} \begin{bmatrix} \varepsilon_{11} \\ \varepsilon_{22} \\ \varepsilon_{33} \\ \varepsilon_{23} \\ \varepsilon_{13} \\ \varepsilon_{12} \end{bmatrix} \qquad [8]$$

By inverting Equation [8], Hooke's Law can be written using the compliance tensor [S]:

$$\begin{bmatrix} \varepsilon_{11} \\ \varepsilon_{22} \\ \varepsilon_{33} \\ \varepsilon_{23} \\ \varepsilon_{13} \\ \varepsilon_{12} \end{bmatrix} = \begin{bmatrix} S_{11} & S_{12} & S_{13} & 0 & 0 & 0 \\ S_{12} & S_{22} & S_{23} & 0 & 0 & 0 \\ S_{13} & S_{23} & S_{33} & 0 & 0 & 0 \\ 0 & 0 & 0 & \frac{S_{44}}{2} & 0 & 0 \\ 0 & 0 & 0 & 0 & \frac{S_{55}}{2} & 0 \\ 0 & 0 & 0 & 0 & 0 & \frac{S_{66}}{2} \end{bmatrix} \begin{bmatrix} \sigma_{11} \\ \sigma_{22} \\ \sigma_{33} \\ \sigma_{23} \\ \sigma_{13} \\ \sigma_{12} \end{bmatrix} \qquad [9]$$

In practice, the stiffnesses can be measured using ultrasonic wave propagation through the paper. The compliances directly relate to the engineering constants. The compliances may be expressed as moduli; the distinction between a stiffness (C_{ii}) and a modulus ($1/S_{ii}$) is that a stiffness coefficient is the ratio of stress to strain without lateral strain, while a modulus is the ratio of stress to strain without lateral stresses (8).

If paper was much thicker than the wavelength emitted by a normal ultrasonic transducer, C_{11} and C_{22} constants could be determined by propagating bulk longitudinal waves along the MD and CD. Since paper is a relatively thin material, the construction of paper stacks is required to propagate bulk waves in the plane of the paper (9). For a single sheet, the top sheet surface is unrestrained, and σ_{33}, σ_{13}, and σ_{23} are zero throughout the sheet. The sheet is thin compared to the wavelength of ultrasound in the out-of-plane direction and thus the "plane stress" condition is adopted. Under the plane stress condition, the bulk (C) stiffness coefficients are replaced by the planar (Q) stiffness coefficients (the matrices in Equation [8] is reduced to a 3-column matrices with Q

coefficients replacing the C coefficients and all terms with an out-of-plane component replaced with 0 values). The planar stiffness is between the corresponding Young's modulus and bulk stiffness in magnitude (8).

The relationships between the stiffnesses, compliances, and engineering constants are as follows (9):

$$E_{11} = \frac{1}{S_{11}} = Q_{11} - \frac{Q_{12}^2}{Q_{22}} \quad [10]$$

$$E_{22} = \frac{1}{S_{22}} = Q_{22} - \frac{Q_{12}^2}{Q_{11}} \quad [11]$$

$$E_{33} = \frac{1}{S_{33}} = \frac{C_{11} \cdot C_{22} \cdot C_{33} + 2 \cdot C_{12} \cdot C_{13} \cdot C_{23} - C_{11} \cdot C_{23}^2 - C_{22} \cdot C_{13}^2 - C_{33} \cdot C_{12}^2}{C_{11} \cdot C_{22} - C_{12}^2} \quad [12]$$

$$G_{44} = \frac{1}{S_{44}} = C_{44} \quad [13]$$

$$G_{55} = \frac{1}{S_{55}} = C_{55} \quad [14]$$

$$G_{66} = \frac{1}{S_{66}} = Q_{66} \quad [15]$$

$$\upsilon_{12} = \frac{-S_{12}}{S_{22}} = \frac{C_{12} \cdot C_{33} - C_{13} \cdot C_{23}}{C_{11} C_{33} - C_{13}^2} = \frac{Q_{12}}{Q_{11}} \quad [16]$$

$$\upsilon_{23} = \frac{-S_{23}}{S_{33}} = \frac{C_{23} \cdot C_{11} - C_{12} \cdot C_{23}}{C_{11} \cdot C_{22} - C_{12}^2} = \frac{Q_{13}}{Q_{12}} \quad [17]$$

$$\upsilon_{21} = \frac{-S_{12}}{S_{11}} = \frac{C_{12} \cdot C_{33} - C_{13} \cdot C_{23}}{C_{22} \cdot C_{33} - C_{23}^2} = \frac{Q_{12}}{Q_{22}} \quad [18]$$

where E_{11}, E_{22}, and E_{33} are Young's moduli; C_{44}, C_{55}, and C_{66} are shear moduli; and υ_{12}, υ_{13}, υ_{23}, υ_{21}, υ_{31}, and υ_{32} are Poisson's ratios. In practice, C_{13} and C_{23} are very small

(9).

A nondestructive method to quantify elastic stiffness is to measure the velocity of ultrasonic waves as they propagate through paper. The wave velocity is proportional to the elastic stiffness. Both longitudinal and shear waves can be propagated through paper: a longitudinal wave has particle motion parallel to the axis of propagation while a shear wave has particle motion perpendicular to the axis of propagation.

The velocity of waves traveling through the sheet are measured using two systems, one specifically for out-of-plane and one for in-plane measurements. These systems are described later. In-plane measurements are performed at 80 kHz (10) while out-of-plane measurements are made at 1 MHz (11).

In-Plane Elastic Stiffness Measurements

The nondestructive and rapid nature of ultrasonic elastic stiffness determinations make this method attractive for characterizing the elastic properties of paper. Craver and Taylor first conducted experiments using ultrasonic velocity measurements on paper in the 1960s (12). Since then, further work has led to significant development and techniques for ultrasonic testing of paper.

Ultrasonic testing requires a transducer that emits a wave through the sheet and a receiver that intercepts the wave signal. The delay times between the transducer and receiver are measured and repeated at several locations on the sheet and the delay times are then averaged for a given position. The velocities taken at different positions on the sample are then averaged to determine an average stiffness measurement for the paper.

The in-plane stiffness coefficients are obtained by measuring the velocity of a longitudinal waves propagated in the MD or CD orientations:

$$Q_{11} = \rho V^2_{L\text{-}MD} \qquad [19]$$

$$Q_{22} = \rho V^2_{L\text{-}CD} \qquad [20]$$

The coefficient Q_{66} is obtained by measuring the velocity of a shear wave, V_s, propagated in either the x or y direction and then polarized in the y or x direction, respectively (2).

$$Q_{66} = \rho V_s^{\,2} \qquad [21]$$

The Q_{12} value must be determined from a fourth measurement, typically a shear wave, polarized in the MD-CD plane, at a direction of 45° to both the MD and CD axes.

$$Q_{12} = \{[2\rho V_{45}^2 - \tfrac{1}{2}(Q_{11} + Q_{22}) - Q_{66}]^2 - [(Q_{11} - Q_{22})^2/2]\}^{1/2} - Q_{66} \qquad [22]$$

Q_{12} can also be obtained from a polar plot of longitudinal stiffnesses and Q_{66}.

Out-of-Plane Elastic Stiffness Measurements

As discussed previously, paper can be considered a three-dimensional bulk material. Three of the nine stiffness constants are out-of-plane measurements; that is, they are measured by waves propagated in the z direction of the sheet. As such:

$$C_{33} = \rho V^2_{L\text{-}ZD} \qquad [23]$$

$$C_{44} = \rho V^2_{S\text{-}CD\text{-}ZD} \qquad [24]$$

$$C_{55} = \rho V^2_{S\text{-}MD\text{-}ZD} \qquad [25]$$

where $V_{L\text{-}ZD}$ is the velocity of the ZD bulk longitudinal wave, $V_{S\text{-}CD\text{-}ZD}$ is the velocity of the ZD bulk shear wave oriented in the CD direction, and $V_{S\text{-}MD\text{-}ZD}$ is the velocity of the ZD bulk shear wave oriented in the MD direction.

Fiber Orientation Distribution

On a paper machine, there is a preferential orientation of fibers in the MD. This is caused by flow patterns established in the headbox and is largely influenced by the jet-to-wire speed differential and transverse flows. There is a positive correlation between increased fiber orientation distribution in the MD and MD stiffness measurements. As more fibers become aligned in the MD, the MD stiffness measurement increases and the CD stiffness measurement decreases.

The fiber orientation distribution describes the distribution of fibers with respect to angle as determined by the weighted fiber length or another similar factor. Fiber orientation distribution may be mathematically described using a distribution function. At least three functions (13) have proven to be of interest: the cosine distribution function, the von Mises distribution function , and the wrapped Cauchy distribution function.

- Cosine Distribution Function:

$$f(\phi - \theta) \equiv (1 - \pi) \cdot \left[(1) + a_1 \cdot \cos(2\,(\phi - \theta)) + a_2 \cdot \cos(4\,(\phi - \theta)) + \ldots a_n \cdot \cos(2 \cdot n(\phi - \theta)) \right] \quad [26]$$

- von Mises Distribution Function:

$$f(\phi - \theta) \equiv \frac{\left[a_0 \exp(\kappa \cdot \cos(2\,(\phi - \theta))) \right]}{\pi \cdot I_0 \cdot \kappa} \quad [27]$$

- Wrapped Cauchy Distribution Function:

$$\pi \cdot f_c(\phi - \theta) = \frac{\left(1 - \rho^2\right)}{1 + \rho^2 - 2 \cdot \rho \cos(2\,(\phi - \theta))} \qquad [28]$$

In the above equations, θ denotes the angle of fiber orientation misalignment from the machine direction and ϕ denotes the angle of measurement. All of these distributions assume symmetry about $\phi = \theta$.

The difference between stiffness orientation and fiber orientation distributions merits explanation. Fiber orientation describes the preferential orientation of fibers in the machine direction. In addition to fiber orientation, the stiffness orientation distribution is affected by dried-in stresses, such as those caused by wet-straining, restrained drying, or shrinkage of the sheet. Stiffness orientation distribution can be described by a polar plot of stiffness values. For an orthotropic elastic material, longitudinal stiffness at an angle (ϕ-θ) from the MD axis is:

$$Q_{rr} = Q_{11}\cos^4(\phi-\theta) + 2(Q_{12} + 2Q_{66})\cos^2(\phi-\theta)\sin^2(\phi-\theta) + Q_{22}\sin^4(\phi-\theta) \qquad [29]$$

where Q_{rr} is a longitudinal stiffness in the radial direction at a specified angle.

Fiber orientation is measured by image analysis of dyed fibers incorporated into the sheet while stiffness orientation is determined from a polar plot of ultrasonic measurements.

Process Control Algorithms for Paper Machine Control

Papermakers have traditionally controlled paper machines based on the results of dry lab testing, manipulating variables that the particular machine tender considers key to control the quality parameters. These adjustments are arbitrary based on the machine tender's experience and estimations.

With the competitive nature of the paper industry in recent years, the importance of process monitoring has become more apparent. Automatic control of the paper machine is a desirable economic asset to any paper mill. Automatic control of the paper machine requires three primary components (1). These include sensors for the measurement of process and paper parameters during manufacture, algorithms for relating input variables to output variables, and actuators for adjustment of the appropriate machine variables.

This research thesis focuses on the development of a predictive empirical model based on fiber orientation and elastic stiffness measurements using statistical methods. Manufacturing variables covered as large a range as possible in the laboratory setting. On a paper machine, the range of variables can be expected to be even less.

One application for predicting paper machine quality data is the neural network approach (14). A neural network "learns" the nonlinear response surface of machine behavior based on a quantity of process data. A backpropagation algorithm is trained using prior knowledge of actual outputs and results to predict the response surface. The

neural network approach is desirable because it is flexible for different systems, is insensitive to noise in the data, and does not require an understanding of the particular system. The drawback of this method is the quantity of data required for training the neural network. Schweiger and Rudd (14) collected one month's worth of data at a sample rate frequency of two minutes from a linerboard machine in order to predict Concora medium test (CMT) and porosity (a total of approximately 21, 900 sample points in a one month period). In the laboratory setting, achieving such a data collection would be an impossible task in a reasonable amount of time.

Genetic algorithms are another developing method for optimization of manufacturing systems (15). Genetic algorithms are based on Darwin's theory of evolution (16) and its postulate that living organisms evolve by one of two processes, natural selection or reproduction. The fitness of an organism determines whether it will survive or reproduce. Reproduction ensures recombination of genes among offspring, making offspring more adaptable to environmental changes. This recombination of genetic material allows more rapid evolution of an organism than if the genetic material of the organism was simply copied from one generation to the next. On this principle, the genes are analogous to possible solutions for a control problem Evolution is analogous to the search for an ideal solution to the control problem. Using a population of data, genetic algorithms determine the fitness values of each possible solution and extract pairs of solutions with high fitness values. These solutions "mate"; their genetic material is exchanged to produce offspring with a combination of parental genetic material. This process repeats until a new population is created. After several repetitions of this pattern,

the genetic algorithm reaches an optimal solution to the problem. Such a method also requires a large pool of initial data.

The need for control algorithms is such that current popular methods do not consider nor address the empirical relationship between machine variables and paper properties. The purpose of this research effort is to look at those fundamental relationships between changes in the nondestructive mechanical properties of the sheet and the changes that occurred in the manufacturing process. A better understanding of how papermaking variables are described in terms of paper properties (1) is of interest to the paper physicist and in the long run will better serve the papermaker and the papermaking process by explaining the relationship between properties and controlled manufacturing conditions.

Effects of Papermaking Variables on Elastic Properties

Refining

During the refining process, fibers are cut, curled, internally and externally fibrillated, and fines are produced.

Berger and Baum (17) found that the changes in the cell wall brought about by increased refining or decreased pulping yield (lignin and hemicellulose removed) had a direct influence upon the in-plane and the ZD properties of paper. They postulated that z directional fiber properties related directly to the z directional sheet properties. Z directional sheet properties were more sensitive to changes in yield and refining than were the in-plane properties. Higher yield samples had a slightly lower Q_{11} stiffness at constant density than lower yield samples. C_{33} increased by a factor of about 45% over a range of apparent densities (17). At constant density C_{33} increased by a factor of 2 due to refining. Also at a constant density, increasing the yield caused a decrease in C_{33} by about 40%. C_{44} and C_{55} values varied with density and refining just like C_{33}. Increased refining had a greater effect on these two out-of-plane shear stiffnesses than did wet-pressing.

Stratton (18) examined both the z-toughness and the out-of-plane elastic stiffness C_{33} as measures of fiber-fiber bond strength. The specific Z-toughness ($\overline{Z}$) is the bond breaking energy per unit of bond broken optical contact area. The difference in scattering coefficient (ΔS) of a paper sheet between 2 transparent tapes before and after

delamination was first determined. The change in optical contact area per unit of geometric area, ΔOCA, was then:

$$\Delta OCA = (\Delta S)(g) \qquad [30]$$

where g was the grammage. The specific Z-toughness, $\overline{Z}$, was then calculated as:

$$\overline{Z} = (Z)/\Delta OCA \qquad [31]$$

The tensile strength of a sample was dependent upon whether the density was achieved by wet-pressing or refining. Stratton wanted to determine if the C_{33} stiffness and z-toughness measurements responded in a similar manner. It was discovered that at a given density, different degrees of refining had a small effect upon C_{33}. Wet-pressing at a constant refining level increased the C_{33} stiffness by as much as a factor of four, in agreement with Berger and Baum (17). There was a nonlinear relationship between variations of C_{33} with density. Page (19) explained the phenomenon by hypothesizing that with increased beating, fibers swelled more and more shrinkage of the fibers occurred during the drying process. During restrained drying, the forces of shrinkage removed kinks and microcompressions and produced a tighter network structure. This "tightening" resulted in increased modulus and therefore higher tensile measurements.

Jet-to-Wire Speed Differential

Fibers are preferentially oriented in the machine direction of the sheet. The degree of fiber orientation is primarily dependent upon conditions at the slice such as jet-to-wire ratios and transverse slice flows (20).

Cox performed an analysis of the effect of orientation of the fibers on the stiffness and strength of paper and other fibrous materials (21). He reasoned that any fiber orientation could be described as the cosine distribution function, Equation [29]. This function, along with the fiber modulus and fiber density, were then used to predict the in-plane stiffnesses of the sheet:

$$Q_{11} = (K/16) \cdot (6 + 4a_1 + a_2) \qquad [32]$$

$$Q_{22} = (K/16) \cdot (6 - 4a_1 + a_2) \qquad [33]$$

$$Q_{12} = Q_{66} = (K/16) \cdot (2 - a_2) \qquad [34]$$

where K was a constant, the product of fiber modulus and fiber density (21).

In a study of the physical mechanisms of fiber orientation in the Fourdrinier process, Niskanen (22) suggested that in an oriented shear field, the fiber orientation distribution could be approximated by an elliptical distribution function while the flow of the suspension was assumed to be laminar. The anisotropy of the sheet could only be increased to a certain plateau; according to Niskanen the corresponding velocity difference was approximately 20 m/min, regardless of the machine. This finding suggested a universal mechanism giving rise to a plateau in paper anisotropy. If the speed of the suspension grew too large, a turbulent boundary layer developed to dissipate shear stresses imposed by the growing fluid speed.

Ishisaki (23) used three methods of measurement (laser diffusion, image analysis, and ultrasonic tests) to analyze three jet-to-wire ratios and three degrees of misalignment

(0°, 7.5°, and 15°). Image analysis and laser diffusion fiber orientation measurements were insensitive to built-in stresses caused by MD wet-straining and drying restraints. The fiber orientation angle of misalignment (a simulation of on-machine transverse slice flows) as measured by image analysis and laser diffusion did not change due to wet straining or drying restraint. On the other hand, ultrasonic stiffness measurements indicated that the stiffness orientation angle was affected by built-in stresses, as was the max-min stiffness anisotropy ratio.

Wet-Pressing

Wet-pressing densifies the network of fibers. Wet fibers are flexible and conform to one another. The well-bonded network therefore has higher stiffness values in all three planes.

In a series of experiments, Baum (2) found that increased pressing produced increases in MD, CD, and ZD elastic moduli. Combining different levels of wet-straining and jet-to-wire ratios did not alter the impact of pressing upon the apparent density. While the MD and CD moduli experienced significant increases due to wet-pressing, the increases in ZD moduli were much more dramatic: a tenfold increase over the range of densities studied (in combination with wet-straining).

Fleischman et al. (24) found that C_{33} was not sensitive to changes in jet-to-wire ratios but was extremely sensitive to wet-pressing pressure, wet-straining, and drying restraints. Increasing the wet-pressing pressure caused significant increases in ZD stiffness and in the out-of-plane shear stiffnesses, in agreement with Baum (2).

As mentioned earlier, Berger and Baum (17) varied the levels of wet-pressing in a collection of experiments to determine the effects of yield and refining on ZD properties. Mirroring the results of Fleischman (24), C_{33} increased by a factor of about 45% over the range of densities studied. This result was four or five times greater than the results obtained by Fleischman over the same range of densities.

MD Wet-Straining

Open draws on the paper machine stretch the sheet in the machine direction. Such stretching of the wet web causes the mechanical properties in the direction of strain to increase. Wet-straining pulls kinks and microcompressions out of the fibers, resulting in a stiffer fiber network. This theory may explain the increase in in-plane anisotropy that takes place during wet-straining.

Using ultrasonic measurements, Fleischman et al. (24) found that z direction properties were highly dependent on the degree of wet-straining in the sheet. The C_{33} value depended very strongly on the apparent density of the sheet. When wet-straining was increased in the x direction of the sheet by 2.4%, C_{33} was reduced by half its average value. (Sheets were unrestrained in the CD during straining, then clamped during drying). Fleischman concluded that the fibers oriented in the direction of wet-straining were "straightened" (essentially, kinks and microcompressions were minimized) by the process of wet-straining and when later subjected to a load, the fibers responded equally, resulting in a stiffer sheet (24). The mechanism by which wet-straining enhanced the elastic anisotropy of the sheet did not involve a large fiber reorientation.

Hess (25) verified a significant insensitivity of fiber orientation to MD wet-straining. In comparing fiber orientation and stiffness orientation polar plots under conditions of wet-straining, it was found that wet-straining induced a large difference between the fiber orientation distribution and stiffness orientation distribution, regardless of the drying conditions. Hess found that the greater the degree of MD wet-straining, the

greater the disparity between the stiffness orientation measurements and fiber orientation measurements. This was due to the fact that stiffness properties were sensitive to such treatment while fiber orientation properties were not.

Setterholm and Kuenzi (26) studied the effects of MD wet-straining and fiber orientation upon tensile strength and modulus of elasticity. Handsheets with different degrees of jet-to-wire ratios were clamped in the MD and either stretched or allowed to shrink during the drying process. Fiber orientation had a greater influence on tensile strength than did restraint during drying (change in MD dimension between wet and dry). Increasing the fiber orientation ratio from 0.5 to 2.5 resulted in a threefold increase in tensile strength while going from –7.6% to 4.0% drying restraint resulted in a tensile strength increase of between 30%-40%. The moduli of elasticity were as dependent upon restraint during drying as they were upon fiber orientation differences over the examined range. At lower levels of fiber orientation, drying under restraint increased the modulus of elasticity by 250,000 psi, while at higher levels of orientation, the restraint during drying increased elasticity by 600,000 psi: a comparable pair of increases of approximately 300%.

Transverse flows cause the maximum angle of the fiber distribution to be misaligned from the MD axis. Baum and Brennan (20) found that drying conditions did not affect the angle of deviation from the MD of specific elastic stiffness polar diagrams. When a sample was rewet and dried freely there was a decrease in the enclosed area of the specific stiffness polar diagram. Such results confirmed that the specific stiffness

polar plot's angle of deviation from the machine direction was not influenced by dried-in stresses but by fiber orientation where the maximum of the distribution was not along the MD, in agreement with Hess (25). The relief from dried-in stresses when the samples were rewet and dried freely accounted for the decrease in the area of the plot.

CD Shrinkage and Drying Restraint

A sheet dried without any type of CD restraint may shrink up to 15%. The degree of fiber shrinkage and thus sheet shrinkage is related to the wood species, the type of pulping, the pulping yield, and the amount of refining.

The amount of CD restraint varies across the width of the paper machine. In the center of the web the sheet is more fully restrained than along the edges of the web.

Wahlstrom (27) investigated the effects of different drying strategies using a biaxial drying device. In a study where paper was dried under different conditions of MD and CD strain (from –10% CD shrinkage to 2% CD stretch; from –3% MD shrinkage to 2% MD stretch), there was a 200% increase in CD tensile stiffness index and a 100% increase in MD tensile stiffness index. Another study (27) investigating the interaction between MD and CD found that CD shrinkage did not affect MD properties of the sheet (sheets were allowed to shrink to differing degrees in the CD while restrain-dried in the MD). The MD and CD properties were thus uncoupled.

Finally, Wahlstrom (27) investigated how MD and CD stiffness properties developed during the drying process for three different drying strategies. During restrained drying, the development of tensile stiffness index in the MD and CD increased exponentially with decreasing moisture ratio, with most of the stiffness increase taking place during the final stages of the drying process. Imposing 2% MD stretch, full drying restraint, and free shrinkage upon three different sheets, it was found that all three dried

with the same exponential increase trend in tensile stiffness index, but that the final tensile stiffness index was highest for the sheet subjected to 2% MD stretch. The stiffness did not increase immediately upon stretching the sample, but instead increased as the moisture ratio decreased.

Htun (28) investigated the relationship between internal stress, final drying stress and yield stress in strained and restrain-dried sheets. Regardless of refining level, the amount of wet pressing, or the incorporation of different fiber fractions in the sheet, the internal stress and the final drying stress were found to be equivalent. Both parameters gave essentially the same information about the mechanical properties of the sheet. Examining sheets made from a variety of pulps, the final drying stresses were compared to the yield stresses (yield stress being defined as the stress at the proportional limit). It was found that the yield stress was equal to the limit reached by the final drying stress. There was strong evidence that in paper, the final drying stress, the internal stress, and the yield stress, were equivalent. Examining mechanical properties, Htun compared a wide variety of pulps' elastic moduli to drying stresses. They found that a sheet dried under restraint had a universal yield strain value of 0.16%, but had no explanation for the apparently universal value.

Htun and Fellers (6) studied the merits of using the geometric mean value as an invariant measure of the mechanical properties of paper. Directional handsheets made at different anisotropies and dried under conditions of no restraint, full MD-CD restraint, and CD free-drying and 2% MD stretch were compared. The geometric mean was

constant under identical drying conditions in the MD and CD, and was independent of the fiber orientation of the sheet.

Ishisaki (23) found that under conditions of full MD-CD drying restraint and 0% wet-straining, there was no change in the stiffness angle (sheets were cut at various "nominal" angles). However, when uniaxial restrained drying was implemented with 2% MD wet-straining, the stiffness angle was less than the nominal angle by as much as 10^{o}, showing that the stiffness polar angle was affected by straining. CD shrinkage had no influence upon the fiber orientation. CD shrinkage did, however, affect the stiffness orientation; there was CD shrinkage of the polar plot when MD uniaxial drying restraint was used, and when MD restraint was coupled with wet-straining, CD shrinkage and MD elongation of the polar plot resulted. Ishisaki also found that uniaxial drying restraint (MD) increased the ZD specific stiffness value compared with full MD-CD drying restraint as a result of CD shrinkage.

PREDICTIVE MODELS FOR PAPER MECHANICAL BEHAVIOR

There are several models that are useful in analyzing the mechanical behavior of paper. Four models will be discussed here, but there are others that may be equally effective. It must be kept in mind that these are all limited models and may only be valid under particular conditions.

The Cox Model

As briefly described in the previous section, the Cox model (21) was based upon an assumption of uniform strain. The Cox model considered only the in-plane fiber orientation distribution, without consideration of the network structure or the nature of bonds within the structure.

For the case of an isotropic sheet (random fiber distribution), the coefficients of the cosine distribution function for fiber orientation distribution were all zero. Cox predicted that in such a case, the following equations would hold:

$$E_x \text{ (Young's Modulus)} = 1/S_{11} = K/3 \quad [35]$$

$$G_{xy} \text{ (Shear Modulus)} = 1/S_{66} = K/8 \quad [36]$$

$$\nu_{ij} \text{ (Poisson's Ratio)} = -S_{12}/S_{11} = 1/3 \quad [37]$$

While this model was instrumental in predicting the elastic moduli from the fiber modulus and the fiber density, it was a simple network model and did not fully account for the interaction of the fibers and the network of orthotropic sheets. However, the Cox

model was effective in the case of a random handsheet. In an oriented handsheet, the Cox model underestimated the shear modulus and overpredicted the Poisson's ratio (5).

The Page and Seth Model

Building upon the work of Cox, Page and Seth (19) set about to develop an equation that applied to less well-bonded sheets, as Cox's model was developed for highly bonded sheets.

The final equation that related the modulus of the handsheet to the modulus of the fibers, fiber dimensions, and relative bonded area was:

$$E_p = \frac{1}{3} E_f \left[(1) - \frac{w}{L \cdot RBA} \cdot \left(\sqrt{\frac{E_f}{2 \cdot G_f}} \right) \tanh \left(\frac{L \cdot RBA}{w} \cdot \sqrt{\frac{2\,G_f}{E_f}} \right) \right] \qquad [38]$$

where E_p was the modulus of the sheet, E_f was the average modulus of the fibers, G_f was the shear modulus of the fiber, L was the average fiber length, w was the mean fiber width, and RBA was the relative bonded area. The coefficient of 1/3 represented a random fiber distribution.

Through a series of experiments to verify this equation, Page and Seth discovered that, for a variety of pulps, moduli, and RBA values, the equation was able to accurately predict the elastic modulus of a sheet. In summary, with a decrease in fiber modulus, fiber length, or RBA, there was a subsequent and predictable decrease in the modulus of a sheet.

Empirical Equations

The Baum Relationship

Baum et al. (7) discovered that the geometric mean of the in-plane Poisson's ratio remained fairly constant at different apparent densities of a variety of handsheets and machine-made papers:

$$\sqrt{\upsilon_{12}\cdot\upsilon_{21}}=0.293 \qquad [39]$$

Good agreement was also found between the measured shear compliance and the following predictive equation:

$$S_{66}=2\sqrt{S_{11}\cdot S_{22}}\cdot\left(\sqrt{\upsilon_{12}\cdot\upsilon_{21}}+1\right)=2.586\cdot\sqrt{S_{11}\cdot S_{22}} \qquad [40]$$

In this instance the fixed value of the geometric mean of the Poisson's ratio meant that there were only two independent elastic properties remaining.

Similarly, the shear modulus may also be predicted using the geometric mean of the in-plane stiffnesses, a variation on Baum's relationship, in [41]. This equation will be investigated in a subsequent section:

$$Q_{66}=b\cdot\sqrt{Q_{11}\times Q_{22}}=0.353\cdot\sqrt{Q_{11}\times Q_{22}} \qquad [41]$$

The Campbell Relationship

Campbell (29) studied paper's elastic properties under the condition of stress

parallel to the plane of the sheet.

The in-plane Young's modulus at angle θ to the cross direction was given by:

$$\frac{1}{E_\theta} = \frac{\cos^4\theta}{E_x} + \left(\frac{1}{G_{xy}} - \frac{\nu_{xy}}{E_x} - \frac{\nu_{yx}}{E_y}\right)\cdot\left(\sin^2\theta\cdot\cos^2\theta\right) + \frac{\sin^4\theta}{E_y} \qquad [42]$$

where

$$\nu_{xy}/E_x = \nu_{yx}/E_y \qquad [43]$$

and the elastic constants of interest were:

- E_x , Young's modulus (CD)
- E_y, Young's modulus (MD)
- ν_{xy} , Poisson's Ratio (CD tension, MD contraction)
- ν_{yx} , Poisson's Ratio (MD tension, CD contraction)
- G_{xy} , shear modulus in the plane of the sheet

Campbell went on to explain that experimental curves of Young's modulus as a function of angle were expressed by:

$$\frac{1}{E_\theta} = \frac{\cos^2\theta}{E_x} + \frac{\sin^2\theta}{E_y} \qquad [44]$$

Equation [44] held for a wide variety of paper and paperboards. Equation [43] is true for elastic orthotropic sheets. Therefore, Equation [42] reduced to Equation [44] if and only if:

$$\frac{1}{G_{xy}} = \frac{1+\nu_{xy}}{E_x} + \frac{1+\nu_{yx}}{E_y} \qquad [45]$$

suggesting that if Equation [45] held for all paper, the in-plane shear modulus could be calculated from the in-plane values of Young's modulus and Poisson's ratio. Equation [45] can also be written in terms of compliance:

$$S_{66} = S_{11} + S_{22} - 2S_{12} \qquad [46]$$

OBJECTIVES

The primary purpose of this thesis was to develop an empirical model that could relate the changes in mechanical properties to changes in the papermaking variables. The objective was to investigate the relationships between the mechanical properties of reprographic paper and the manufacturing variables using parameters available or potentially available during papermaking.

Specifically, the objectives of the project were as follows:

1. Develop and conduct an experimental program to build a database providing the necessary information to relate paper mechanical properties to machine variables, and vice versa, for the case of reprographic paper.

2. Manufacture a series of sheets according to the experimental design, varying the following parameters: stock freeness, jet-to-wire speed ratio, wet-pressing, MD wet-straining, and CD shrinkage.

3. Test the sheets nondestructively, using the following methods: in-plane ultrasonic testing, ZD ultrasonic testing, and image analysis fiber orientation measurements.

4. From the data, investigate the inverse problem of predicting machine variables from mechanical properties for the case of reprographic paper by way of an empirical model.

5. Verify the model using existing data and lab-generated data.

EXPERIMENTAL PROGRAM

General

Bleached kraft hardwood and softwood pulps were obtained in wet lap form from International Paper's Riverdale Mill in Selma, Alabama. The pulp arrived at approximately 13% consistency and was stored at 37°C.

The pulp was diluted and refined using a Valley beater according to TAPPI Method T-200 (30). Hardwood and softwood furnishes were refined separately. All of the pulp was refined in this manner to reach specific target freenesses. The refined pulp was stored at 37°C until use.

Method Used to Dye Black Fibers

It was necessary to incorporate dyed fibers into the sheets to determine the fiber orientation distriibutions. A sample of the bleached fibers were taken from the pulp supply and dyed using Chlorazol Black E.

Forty grams of oven-dried fibers were taken from the thick stock and diluted to 800 mL. 1200 mL of deionized water were heated on a hot plate until boiling. The pulp was added to the water. 0.8 g of Chlorazol Black E powder was dissolved in a smaller beaker of hot water and then added to the pulp suspension. The suspension was stirred with a stirring rod for about 10 minutes. 8 g of NaCl was added to the pulp mixture and it was then allowed to cool for 12 hours.

The following day the slurry was divided into three even portions. Each portion was washed in the Bauer-McNett fiber classifier. The 100-mesh screen was placed in the first position and each sample was washed for a total of 40 minutes. The washing step removed fines from the pulp suspension and removed the unattached dye from the fibers in the slurry. The dyed fibers were removed, dewatered, and then placed in a sealed plastic bag in cold storage at approximately 18% consistency until they were needed for sheet making.

The dyed fibers were taken from the pad, weighed out, and then dispersed in a bottle of slurry by shaking. The slurry and dyed fibers were then added to the large mixing container of pulp.

Sheet Formation Procedure

Stock was prepared in a 30-gallon container for each sheet-making session. Hardwood and softwood pulps were combined in a 60/40 ratio (o.d. basis). The pulps were then diluted to approximately 0.40% consistency. An amount of dyed fibers equal to 0.25% of the total o.d. fiber content was added. The stock was thoroughly mixed using an upright stand mixer.

Sheets were made using the Formette Dynamique directional handsheet former manufactured by Techpap. The unit has a rotating centrifugal jar where stock is sprayed onto a forming wire. A fine plastic mesh wire was used as a backing wire and a bronze metal mesh wire was used as the forming wire.

With the forming wire and backing wire in place, the jar was started and set to a predetermined angular velocity. As the jar rotated, deionized water from a hand-held water hose was sprayed onto the wire until a water wall developed. The stock was sprayed directly onto this water wall as opposed to being sprayed onto the wire itself.

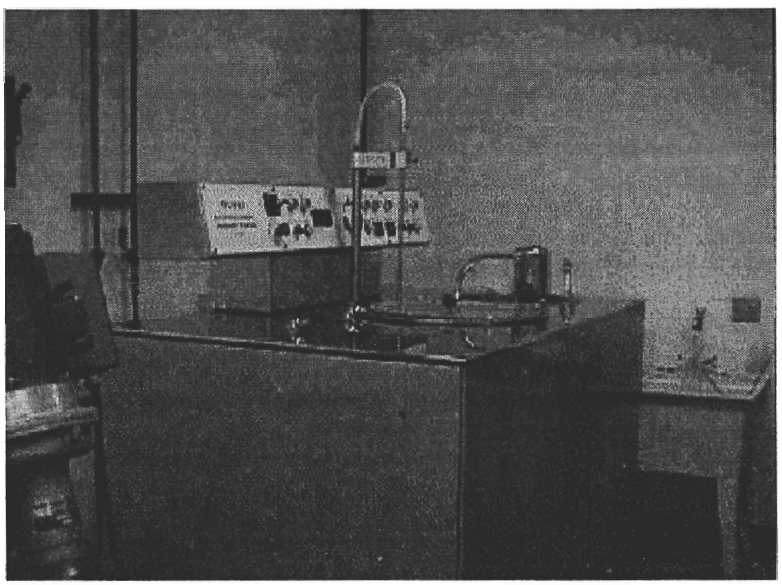

Figure 1. The Formette Dynamique Handsheet Former

The nozzle used for spraying the stock was a Techpap #2504 nozzle. The nozzle was maintained in a neutral position on the spray arm. The wires, nozzle, and mechanical configuration for the Formette Dynamique were maintained constant for all of the sheets.

The two main variables that were adjustable on the Formette Dynamique were the jar speed and the pump pressure. The Formette was capable of jar speeds up to 1500 meters per minute. The pump pressure was variable from 0 to approximately 2 bars. Jet-to-wire speed ratios were adjusted by changing either the pump pressure, the jar speed, or

both. The settings necessary for achieving a variety of MD/CD stiffness ratios were determined during preliminary experimentation.

The speed of the jar was reported on the front panel of the Formette Dynamique. The jet velocity required a calculation to be determined. An empty 2 L graduated cylinder was held under the nozzle and water was sprayed at a specified pressure into the cylinder for a one minute period. After the one minute, the volume of the water was recorded and the jet velocity was calculated using the following equation (31) :

$$\text{Jet Velocity}_{m/min} = (\text{Volume}_{liters/min}/1.37) \times 1000 \qquad [47]$$

Each handsheet was made in the same manner. Approximately 7500 mL of slurry at 0.4% consistency were necessary to make an 80 g/m^2 sheet. Before making a sheet, a calculated amount of pulp was taken from the mixing container and transferred to a smaller 5-gallon bucket. About 1 liter of deionized water was sprayed into the pulp holding tank of the Formette. After the water wall was formed, the "cycle" button was depressed and the water from the stock tank was sprayed into the jar. The pressure of the flow was set immediately according to the specific experiment being run. When the water was almost completely drained from the tank, the premeasured slurry was poured from the 5-gallon bucket into the stock holding tank. After the stock had been sprayed to form the sheet, approximately one to two additional liters of deionized water were added to the pulp holding tank. The additional water served to clean out the pump and the nozzle before the next sheet was to be made.

The Formette Dynamique automatically drained the sheet (called "scooping") and applied the brake to the jar. The number of "sweeps" made by the jet over the wire was programmed by the user. Also programmed by the user was the point at which drainage began. Upon recommendation by the manufacturer, the drainage process began 2 sweeps before the final sweep count (for example, if the jet was programmed to sweep 80 times, drainage would begin after 78 sweeps). The drainage process was initiated when a small flap behind the rotating jar moved forward and broke the water wall, causing it to collapse. After drainage was completed, the Formette Dynamique automatically brought the jar to a stop.

After the jar stopped, the wet sheet was removed with the bronze wire intact. The nozzle and nozzle arm were removed from the jar and placed to the side. The sheet and wire combination were carefully removed from the jar.

The sheet and wire combination were laid wire-side down on a flat table atop a Plexiglas plate of the same dimensions as the wire. A blotter was placed smooth-side down on top of the sheet and wire. Another Plexiglas plate was placed on top of the blotter. Because the sheets showed a tendency to stick to the blotters, the blotters were first treated with a spray lubricant. This lubricant prevented the sheets from sticking to the blotters. The sandwich of sheet, wire, blotter, and plates was then flipped over and the wire carefully removed. Three to four (depending on the number of subsheets desired) 10-inch blotters were placed on top of the sheet, perpendicular to the sheet edges. Approximately 2 inches was left between the blotter and the top and bottom edges of the

master sheet. A new blotter was placed on top of these and the plate was replaced. The sandwich was flipped again and square blotters were aligned on the felt side of the sheet. Using a sharp precision cutting wheel, each of the 10-inch subsheets was cut from the master by cutting the sheet around the perimeter of each blotter. The sheet was immediately pressed between the two blotters in the nip press, felt-side up.

While the sheets made in the lab were pressed over the full range of capabilities for the nip press (2 bars to 6 bars pressure), the full range of the press did not produce a good range of apparent densities. The range of densities from 2 bars pressing to 6 bars pressing was 398 kg/m^3 to 570 kg/m^3, a range of 172 kg/m^3. After the sheets had been made and data analysis was being performed, a series of sheets were made in the lab with coded conditions of zero for freeness and jet-to-wire ratio. The sheets were pressed using a Noble & Wood handsheet press located in PTB lab 379 over a range of 2 bars to 8 bars pressure. Because the sheets from the original experiment had been pressed using a nip press, the dwell time for each of the sheets in the Noble & Wood press was only a couple of seconds in an effort to simulate nip-press conditions. Finally, the sheets were dried under full restraint using the biaxial testing device. No MD wet-straining was subjected upon the sheets. Figure 2 shows the linear relationship between pressing and apparent density for the sheets.

As stated, the range of apparent densities for nip pressing was 172 kg/m^3: from 398 kg/m^3 to 570 kg/m^3. The range of densities for static pressing was 139 kg/m^3. Static pressing pressures did not produce the same apparent densities at equivalent pressures as

the nip press, likely because of the difference in pressing mechanism. The highest apparent density achieved with the Noble & Wood press was 665.1 kg/m^3. Even if the nip press had possessed higher pressing capabilities, the increase in apparent densities would have been nominal.

The mechanical reliability of the nip press itself was also a problem. Between the time that the sheets were made for the screening experiment and the time the sheets were made for the central composite design experiment, the press was repaired. Water had contaminated the compressed-air supply and personnel from Cybermetrics repaired the press. Looking at the data from the sheets made for the screening experiment, the range of densities was 143.63 kg/m^3 over a pressing range of 3 bars to 5 bars (before the press was broken and repaired). The same range from 2 bars to 6 bars in the central composite experiment (after repair) was 164.36 kg/m^3, but the maximum was 570 kg/m^3 over the entire range of pressings (-2 to +2 coded). The maximum apparent density at +1 coding for the screening experiment was 563 kg/m^3. A greater range of pressing could have been achieved had the press been functioning in the central composite experiment as it was during the screening experiment -- its range of pressures had been decreased.

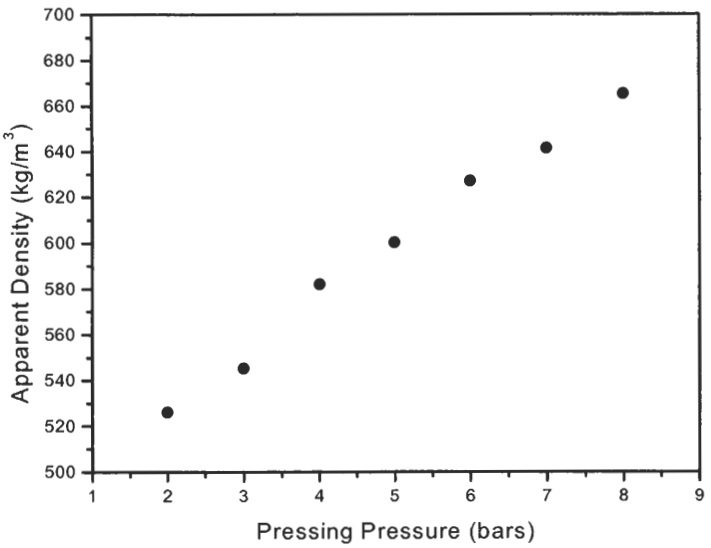

Figure 2. Pressing vs. Apparent Density for Sheets Pressed Using the Noble & Wood Press

At the beginning of experimentation, the apparent densities for a variety of commercial reprographic papers were measured. The range of apparent densities was from 762 kg/m^3 for CopyPlus brand to 924 kg/m^3 for LaserPlus brand. The laboratory-made sheets did not come close to these apparent densities; however, there may be reasons besides laboratory pressing limitations. The commercial reprographic sheets may have as much as 18% ash (filler) content (32). The presence of filler particles in the otherwise unoccupied voids between fibers makes the sheet more dense. Another difference between the lab-made sheets and commercial sheets is the absence of calendering in the laboratory sheets. Calendering increased the density of the sheet appreciably; in previous experiments on a variety of paper grades the density increased as

much as 65% (33).

Wet-Straining and Drying

After pressing, each sheet/blotter sandwich was placed in a moisture saturated environment to prevent ambient drying. The saturated environment was created by placing wet paper towels in a large lock-top plastic bag. The sample was then placed in a plastic pouch inside the large bag to prevent direct contact with the wet paper towels. According to experimentation performed by Hess (25), the solids level remained unchanged while the sample was stored in the saturated environment.

The biaxial straining device was modeled after several similar instruments in existence. It was engineered and built by Katsuhiko Terada of Japan. The computer interface was written in LabView by Joe Gerhardstein. The instrument has a maximum load output of 50 kgf and can accommodate samples as small as 13 cm x 13 cm and as large as 22.5 cm x 22.5 cm. The displacement of the jaws in each direction reaches a maximum of 40 mm on either axis. Both x- and y-axis movement is facilitated by 10V stepper motors. Each axis is also equipped with load cells to determine the load in each direction as the sheet is being strained and restrained during the drying process. The LabView interface supports real-time plots of both x- and y-position displacement (cm) and x- and y-axis forces (N). These plots were saved and reviewed to study the drying patterns of sheets as they are strained and dried under restraint during different sheet-making conditions.

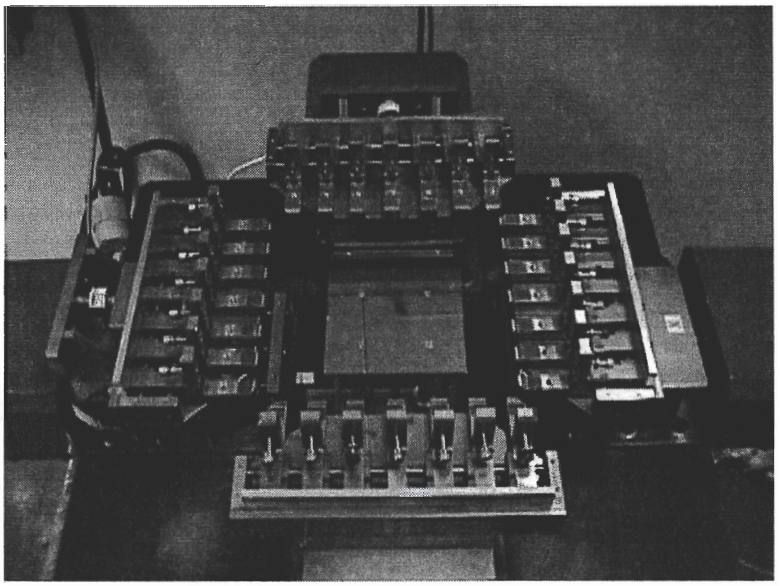

Figure 3. The IPST Biaxial Device

The sheet to be strained was placed in the drying frame with the center support platform in the highest position to support the wet sample. Aluminum combs were placed between the clamps to ensure uniform spacing, as the clamps are able to move freely on bearings. The sample was aligned squarely on the clamps, and the clamps were then closed. The screws that secure the clamps were then tightened using the electric drill. After all of the clamps were tightened, the support platform was lowered out of the way and the combs carefully removed to allow free movement of the sheet during stretching or shrinking.

The LabView program was prepared to be activated as soon as the sheet was secured in place. The biaxial device can be programmed to do many things to the sheet: the sheet can be held without any clamp movement to allow fully restrained drying in both the MD and CD; the sheet may be strained in the MD while it is fully restrained in

the CD; the sheet may be strained in the MD and allowed to shrink in the CD under a specified load. There are many variations and they can be specified by the operator of the program.

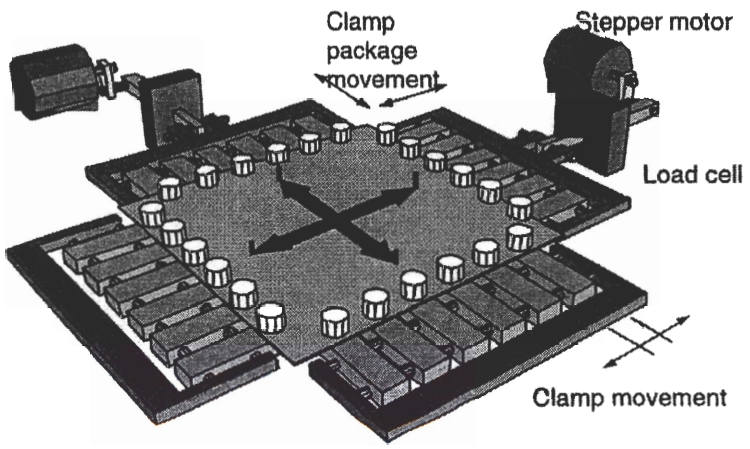

Figure 4. Schematic Diagram of Paper Sample in Biaxial Device (27)

Once the LabView program was activated to run, a radiant-heating plate was lowered into place approximately 2 inches from the surface of the sheet. This heater can be set to a range of temperatures and is monitored by a thermocouple on the rear of the heating surface. Fans placed on either side of the biaxial device provided air circulation around the sheet to assist the drying process.

After the sheet dried completely as determined by the force profile generated during drying, the heating plate was lifted out of place and the screws were loosened. The sheet was taken out of the drying frame and the edges trimmed where the clamps were gripping the edges. The sheet was then labeled along the edge with the straining and drying conditions and the name of the data file to which the force and displacement

files were stored.

DESIGN OF EXPERIMENTS

The experimental design used for this project was structured to investigate the effect of five process variables on measured nondestructive properties.

The first step in experimentation determined the significance of the variables. The first set of experiments was a half-replicate of a 2^5 factorial design consisting of 16 sheets. This half-replicate was designed to exhibit the degree of interaction among variables and show if one or more of the variables is insignificant. Table 1 shows the screening experiment used to begin the study. This screening design is a subset of the full central composite design.

After examination of the screening experiment data, the 62 experiments of the central composite design were carried out to complete the work, as shown in Table 2. Because the press was repaired between the screening experiment and the final experiment, all 62 sheets were made, instead of just the 46 sheets required to complete the central composite design experiment.

Table 1. Statistical Design for Screening Experiment

Sheet ID	Refining	J/W	Pressing	Straining	Drying
1	-1	-1	-1	-1	+1
2	+1	-1	-1	-1	-1
3	-1	+1	-1	-1	-1
4	+1	+1	-1	-1	+1
5	-1	-1	+1	-1	-1
6	+1	-1	+1	-1	+1
7	-1	+1	+1	-1	+1
8	+1	+1	+1	-1	-1
9	-1	-1	-1	+1	-1
10	+1	-1	-1	+1	+1
11	-1	+1	-1	+1	+1
12	+1	+1	-1	+1	-1
13	-1	-1	+1	+1	+1
14	+1	-1	+1	+1	-1
15	-1	+1	+1	+1	-1
16	+1	+1	+1	+1	+1

Table 2. Double Central Composite Design Experiment

Sheet ID	Refining	J/W	Pressing	Straining	Drying
1	-1	-1	-1	-1	-1
2	1	-1	-1	-1	-1
3	-1	1	-1	-1	-1
4	1	1	-1	-1	-1
5	-1	-1	1	-1	-1
6	1	-1	1	-1	-1
7	-1	1	1	-1	-1
8	1	1	1	-1	-1
9	-1	-1	-1	1	-1
10	1	-1	-1	1	-1
11	-1	1	-1	1	-1
12	1	1	-1	1	-1
13	-1	-1	1	1	-1
14	1	-1	1	1	-1
15	-1	1	1	1	-1
16	1	1	1	1	-1
17	0	0	0	0	-1
18	0	0	0	0	-1
19	0	0	0	0	-1
20	0	0	0	0	-1
21	0	0	0	0	-1
22	0	0	0	0	-1
23	0	0	0	0	-1
24	-2	0	0	0	-1
25	2	0	0	0	-1
26	0	-2	0	0	-1
27	0	2	0	0	-1
28	0	0	-2	0	-1
29	0	0	2	0	-1
30	0	0	0	-2	-1
31	0	0	0	2	-1
32	-1	-1	-1	-1	1
33	1	-1	-1	-1	1
34	-1	1	-1	-1	1
35	1	1	-1	-1	1
36	-1	-1	1	-1	1
37	1	-1	1	-1	1
38	-1	1	1	-1	1
39	1	1	1	-1	1
40	-1	-1	-1	1	1
41	1	-1	-1	1	1
42	-1	1	-1	1	1
43	1	1	-1	1	1
44	-1	-1	1	1	1
45	1	-1	1	1	1
46	-1	1	1	1	1
47	1	1	1	1	1
48	0	0	0	0	1
49	0	0	0	0	1
50	0	0	0	0	1
51	0	0	0	0	1
52	0	0	0	0	1
53	0	0	0	0	1
54	0	0	0	0	1
55	-2	0	0	0	1
56	2	0	0	0	1
57	0	-2	0	0	1
58	0	2	0	0	1
59	0	0	-2	0	1
60	0	0	2	0	1
61	0	0	0	-2	1
62	0	0	0	2	1

RESULTS AND DISCUSSION

Validity of Shear Modulus Predictions

In the following section, it should be noted that shear modulus is not included as an independent variable in the analysis of the data. This is because of its expected dependence on longitudinal moduli predicted with Campbell's (29) and the relationship set forth by Baum (7) to determine if the Q_{66} quantity is an independent in-plane variable.

Determining Q_{66} using Campbell's Equation [47] and comparing it to Q_{66} obtained using in-plane elastic stiffness measurements produced the following data shown in Figure 5, the ratio of predicted Q_{66} values versus MD/CD stiffness ratios:

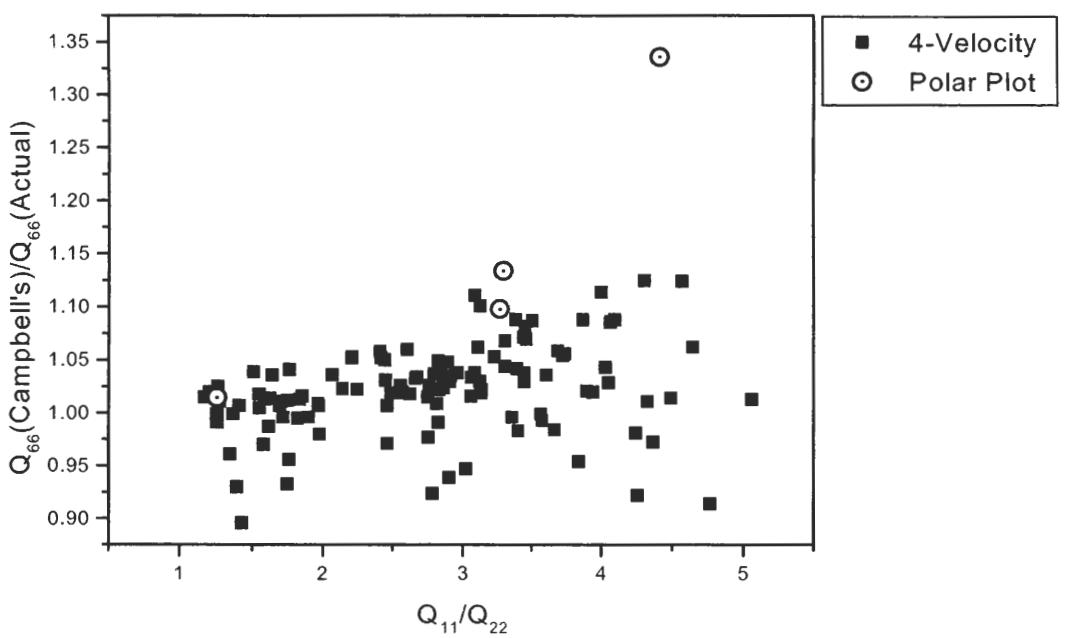

Figure 5. Comparing Q_{66} as Obtained by Campbell's with Measured Q_{66} Values

The data show a general trend that as the MD/CD stiffness ratio increased, Campbell's gave a poor estimate of the Q_{66} value. Taking four sheets from the full range of stiffness ratios to compare the results obtained for polar plot measurements revealed a greater disparity between the Q_{66} value obtained by Campbell's relationship and the actual measured Q_{66} value.

Q_{66} was calculated using Baum's Equation [40]. The data plotted out as shown in Figure 6:

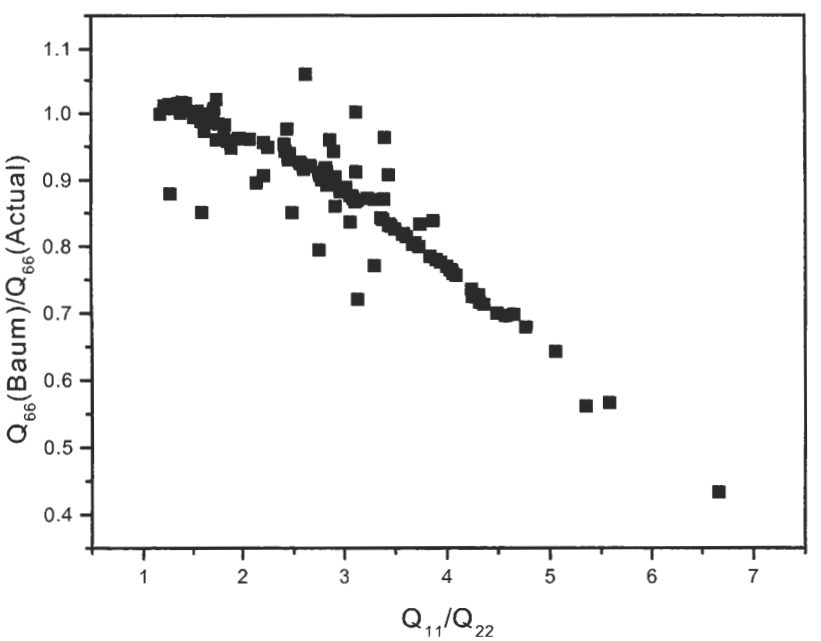

Figure 6. Q_{66} as Determined by Baum vs. Q_{11}/Q_{22}

The ability of Q_{66} to be predicted by using the S_{11} and S_{22} compliances decreased

with increasing stiffness ratio. A linear trend was evident.

Q_{66} was calculated using the geometric mean of the in-plane stiffnesses Q_{11} and Q_{22} (Equation [41]). Plotting ultrasonic in-plane Q_{11}/Q_{22} data versus calculated Q_{66} produced the following fit of the data, as shown in Figure 7:

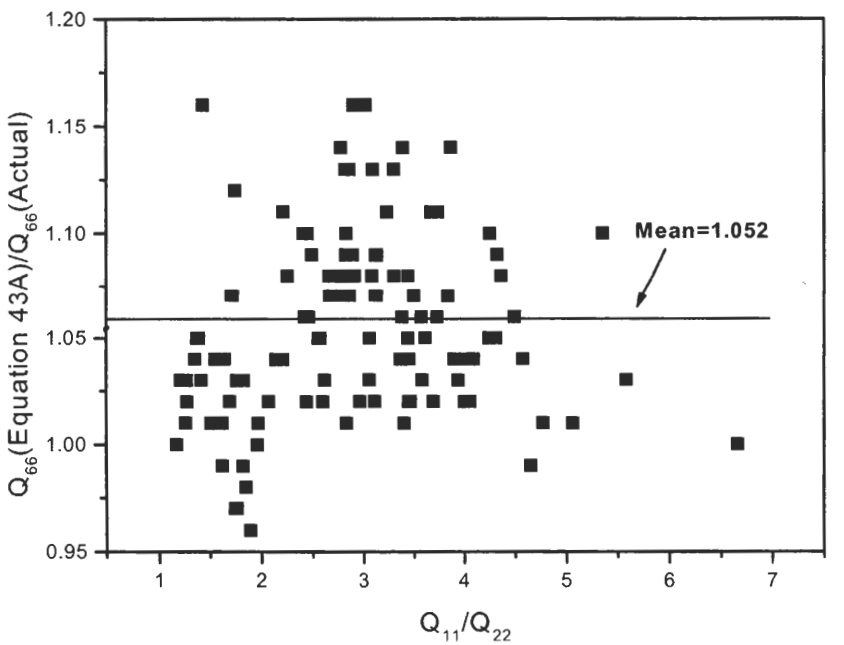

Figure 7. Q_{66} as Determined by Equation [43A] vs. Measured Q_{66} From Ultrasonic Measurements

The data fit Equation [41], approximately as well as they fit the Campbell equation but there was no observed trend as the orthotropy of the sheets increased.

The results of determining Q_{66} with the Equation [41] led to the conclusion that Q_{66} was not an independent in-plane variable. Campbell's equation gave relatively good predictions for the first series of data, but was not precise when the sheets were

re-measured using full polar plot measurements to verify the results. Determining Q_{66} using the geometric mean of the in-plane stiffnesses gave similar results to Campbell's equation.

Analysis of Screening Experiment

The 16 sheets were tested for grammage, soft-platen caliper, fiber orientation distribution, in-plane stiffness values, and out-of-plane stiffness values.

The data were analyzed to determine if the manufacturing conditions at coded values of −1 and +1 were sufficiently extreme to bring about significant changes in the measured properties. The five controlled manufacturing variables were: refining, jet-to-wire speed ratio, wet-pressing, MD wet-straining, and CD shrinkage. The actual conditions for these sheets (uncoded) were:

Table 3. Variable Levels for Screening Experiment

Independent Variable	-1 Level	+1 Level
Freeness (HW/SW)	400 mLs/432 mLs	491 mLs/586 mLs
Jet-to-Wire Ratio (Jet Vel./Wire Vel.)	1.18	0.63
Wet-Pressing	3 bars x 3 passes	5 bars x 3 passes
MD Wet-Straining	1.35%	0.45%
CD Shrinkage	3%	0%

After testing the sheets, the data were analyzed using a Yates algorithm. Sheets were manufactured in duplicate. The sum of the measurements was divided by two to

obtain an average value. The Yates model hypothesized that the effect of the variable in question was 0, and the summary of the effect was given using an F-ratio test of significance at the 99% confidence level. The worksheets for each of the five variables are presented in Appendix I.

Duplicate production of the sheets allowed for an accurate measurement of error in each of the five analyses. The S_{yy} value is the sum of squares due to differences between duplicates. To determine the S_{yy} value, each individual measurement was first squared and the sum of the squared values was calculated. The individual measurements were also summed, then squared and divided by 32, the total number of samples. The summed, squared and divided value was subtracted from the sum of the squared values to produce the S_{yy} value. The S_{yy} value was subtracted from the sum of squares due to the effects and interactions to give a sum of squares due to error (SSE). The sum of squares due to error was used as a direct determinant of the F-ratio for each of the individual and interactive terms.

The following table indicates whether each of the manufacturing variables was significant at the 99% confidence level, as determined by the indicated measured variables:

Table 4. Significance of Machine Variables as Determined by Measured Variables

		Measured Variables				
	Source	**MD Stiffness (Q_{11})**	**CD Stiffness (Q_{22})**	**ZD Stiffness (C_{33})**	**Apparent Density (AD)**	**Fiber Orientation Ratio (FO)**
Machine Variables	**Freeness (FR)**	No	No	Yes	Yes	Yes
	Jet-to-Wire Ratio (JW)	Yes	Yes	No	No	Yes
	Wet-Pressing (WP)	No	No	Yes	Yes	No
	Wet-Straining (WS)	Yes	No	Yes	No	No
	CD Shrinkage (CDS)	No	Yes	Yes	Yes	No

It was determined that the independent variables were indeed sufficiently extreme to warrant changes in the measured dependent variables. Thus, it was appropriate to proceed with the full experiment at the same levels, in addition to more extreme levels (-2 and +2 coded) and center points (0 coded).

Analysis of the Central Composite Design

62 sheets were made according to the central composite design in Table 2. After testing the sheets as previously described, the raw data was organized in spreadsheet format (please refer to Appendix II). The coded variable conditions are summarized in Table 5.

Table 5. Variable Levels for Central Composite Design Experiment

Independent Variable	-2 Level	-1 Level	0 Level	+1 Level	+2 Level
Freeness (HW/SW)	200 mLs	307 mLs	414 mLs	521 mLs	628 mLs
Jet-to-Wire	1.23	1.18	0.92	0.63	0.44
Wet Pressing	2 bars x 3 passes	3 bars x 3 passes	4 bars x 3 passes	5 bars x 3 passes	6 bars x 3 passes
MD Wet-Straining	0%	0.45%	0.9%	1.35%	1.8%
CD Shrinkage	--	3%	--	0%	--

The first step in the data analysis strategy was a linear regression analysis of the coded data in order to determine the effects of the input variables upon the measured nondestructive properties of the sheets. This analysis was performed using the NCSS (Number Crunching Statistical Software) package.

After the initial fit of the data, it was concluded that the data were not linear

(based on the poor fits of the linear equations). The linear regression also did not allow for any interactions between the variables.

The poor linear fits suggested that the next step in the analysis was determining a polynomial fit for the data, implementing squared terms of the coded inputs along with interaction terms (2 term interactions) of the input variables.

Proceeding to a polynomial fit from the linear fit improved all of the equations in question. In order to further optimize the fit of the data, it was necessary to look closely at the data to determine the presence of outliers and analyze their presence in the data set.

An outlier is a data point that deviates from the usual assumption $E(E_i) = 0$ for a specific value of *i*. If there is reason to assert that a particular data point is an outlier exerting a large influence upon the fitted regression model, one may look at the residuals of the data set to identify that point. The term residual means the difference between the actual data point and the data point predicted by the regression equation. A specific type of residual is the R-Student value (t_i):

$$t_i = \frac{e_i}{s_{-i}\sqrt{1 - h_{ii}}}, i = 1, 2, \ldots . n \qquad [48]$$

where s_{-i} is an estimate of error standard deviation, calculated with the *i*th data point deleted. The R-Student statistic provides an exact t-test for the detection of an outlier at a specific data location. Plots of R-Student residuals show data points where the error of fit is larger than that expected by chance.

Plotting residuals is useful in data analysis of regressions. While plotting the residual values against expected values may be useful, studentized residuals are a superior statistic to plot; contrary to a plot of residuals, studentized residuals provide a set of statistics that behave in a standard way under ideal conditions.

Figure 8 shows a sample plot of studentized residuals versus expected values for ZD specific stiffness. Some points fell outside the randomly scattered pattern of heterogeneity that was expected of the data. In the first nonlinear fitting of the data, those points that fell beyond the range of -2 to +2 for R-Student values were examined and investigated.

Some of the points were outliers because the machine conditions were incorrectly described (for example, pressing was at -1 instead of +1); in such cases, the data spreadsheet was corrected. Two coefficients for jet-to-wire ratio were changed from -1 to +1 after recognizing that they had been misreported by looking at the sheets' high MD values, values that were identical to other sheets made under that same condition. A total of six CD shrinkage coefficients were changed from -1 to +1 or vice versa after examining the output graphs from the biaxial tester and discovering that those coefficients had been recorded incorrectly. After correcting these points, it was not necessary to remove any of the data points from the set. Many computer packages flag points that have a studentized residual with an absolute value larger than 2, but one must keep in mind that even in an idealized situation, about 5% of the data points are expected to have a studentized residual with an absolute value larger than 2, and about 1% of the

data points are expected to have a standardized residual with an absolute value greater than 2.5 (34).

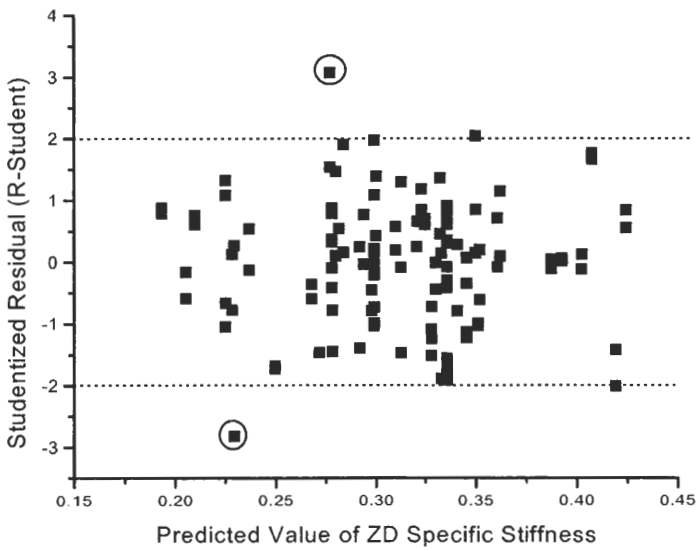

Figure 8. R-Student Values Plotted Against Predicted Values for ZD Specific Stiffness

Fitting of the jet-to-wire ratio data was a challenge. After thoroughly investigating the data for incorrect values, it was suspected that the lowest coded levels of jet-to-wire ratio (-2) were incorrect. The lowest jet-to-wire coded value of -2 should actually have been -1.23, after remeasuring the jet velocities in the lab to confirm the speculation that the lowest coded jet-to-wire ratios were incorrect. Correcting these coded values affected only 2 data points but drastically improved the fit of the data overall.

After examining the points that were greater than an absolute value of 2 and correcting points as necessary, a second nonlinear fit was implemented with the best

results:

$$Q_{11} = -0.526 FR + 0.226 FR^2 + 2.235 JW - 1.017 JW^2 \ldots + 0.345 WP - 0.146 WP^2 + 0.857 WS + 0.448 CDS \ldots + 0.304 FR \cdot JW + 0.184 FR \cdot WP + 0.244 FR \cdot CDS \ldots + -0.169 JW \cdot CDS + 16.116 \qquad R^2 = 0.915 \qquad [49]$$

$$Q_{22} = -0.397 FR - 1.605 JW + 0.701 JW^2 + 0.104 WP \ldots + 0.951 CDS + -0.169 JW \cdot CDS + 0.124 WP \cdot WS + 5.541 \qquad R^2 = 0.952 \qquad [50]$$

$$C_{33} = -0.0429 FR - 0.00456 FR^2 + 0.0178 WP - 0.00567 WP^2 \ldots + -0.0189 WS - 0.0179 CDS + 0.0102 FR \cdot JW \ldots + 0.00860 FR \cdot CDS + 0.00693 JW \cdot CDS + 0.315 \qquad R^2 = 0.860 \qquad [51]$$

$$FO = -0.225 FR^2 + 4.766 JW - 1.250 JW^2 \ldots + -0.570 CDS - 0.533 JW \cdot CDS + 8.927 \qquad R^2 = 0.935 \qquad [52]$$

$$AD = -19.897 FR + 5.354 JW - 3.946 JW^2 + 16.842 WP \ldots + -6.026 WP^2 - 6.348 WS - 3.181 WS^2 - 7.366 CDS \ldots + 5.056 FR \cdot WP + 5.026 FR \cdot CDS - 4.879 JW \cdot WS \ldots + 5.936 WP \cdot WS + 512.811 \qquad R^2 = 0.818 \qquad [53]$$

Taking Equation [49] as an example, the following graphs depict how changes in MD stiffness were predicted by the jet-to-wire speed ratio and MD wet-straining. The effects of freeness, wet-pressing, and CD shrinkage were removed using the coefficients given in Equation [49]. In order to make a surface plot of the predicted values versus the actual values, the two most significant manufacturing variables were selected.

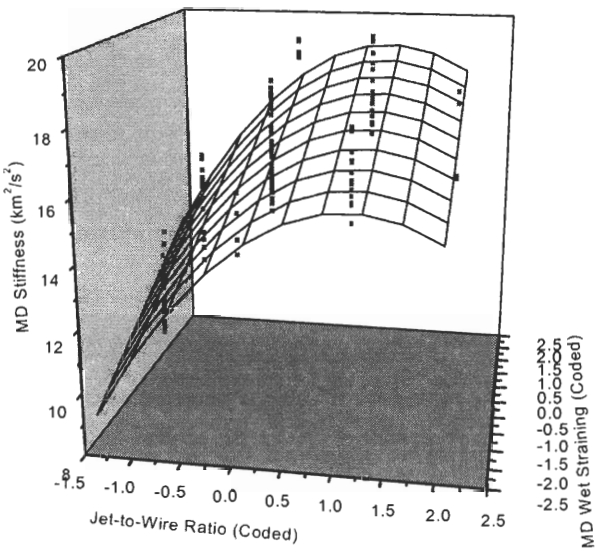

Figure 9. Q_{11} Predicted vs. Q_{11} Actual (View 1)

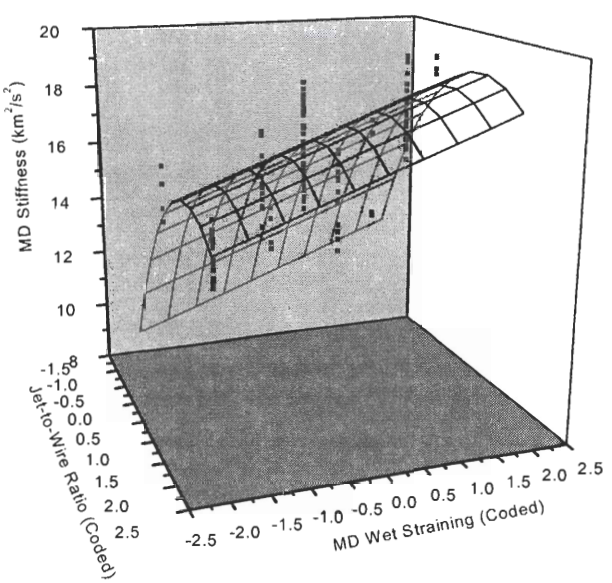

Figure 10. Q_{11} Predicted vs. Q_{11} Actual (View 2)

The Precision of the Regression

To verify that the regression equation was a good fit to the data, the actual MD data values were plotted against the predicted MD stiffness values as calculated using Equation [49]. Figure 11 gives a better visual representation of the fit with $R^2 = 0.915$. The coefficient of determination (R^2) is an important parameter in the fitting process. The coefficient of determination is the ratio of the sum of squares due to regression and the total sum of squares. R^2 is reported as a value between 0 and 1, with R^2 values closer to 1 showing that there is a smaller sum of squares for error, SSE, with respect to the sum of squares for the regression line, SSR. Therefore, the R^2 value is the fraction of the variability in MD that can be accounted for by the fit of this model.

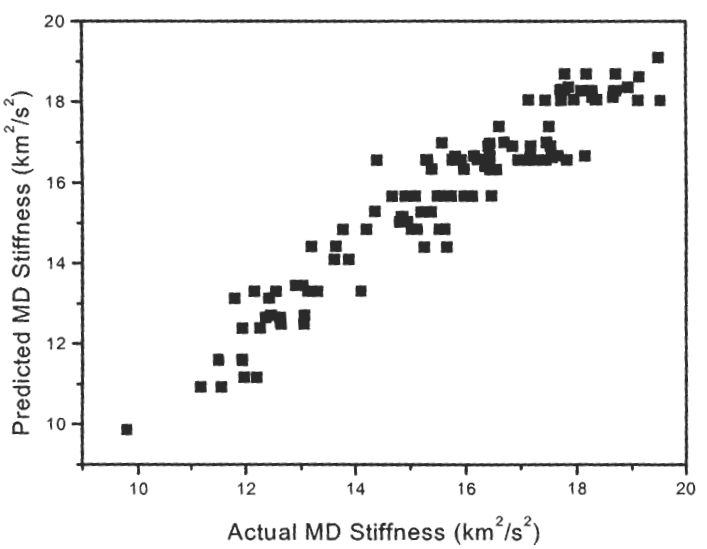

Figure 11. Actual MD Stiffness vs. Predicted MD Stiffness (R^2=0.9153)

There is a general 1:1 relationship between the predicted values for MD stiffness

and the actual measured values for MD stiffness. However, while the data fit the model quite well, one must also examine the variability of the data from the values predicted by the regression. In such a case, it is helpful to partition the sum of squares and construct an analysis of variance table for the regression. The SSR is calculated from the regression coefficients and has n-1 degrees of freedom. The SSE provides an estimate of the variance about the regression. The analysis of variance (AOV) table for MD stiffness is:

Table 6. AOV Table for MD Stiffness (Q_{11})

Source	DF	SS	MS	F-Ratio
Due to Regression	19	554.3459	29.1761	59.1748
Residual	104	51.27712	0.4930	
Total	123	605.623	4.9237	

The F-ratio provides an unbiased estimation of whether the model adequately estimates the data system. The F-ratio is calculated by dividing the mean squared value due to regression by the residual mean squared value. Comparing the F-ratios of the MD response and other responses gives one a description of the amount of variance in the system: higher F-ratios indicate that more variance is due to the regression than due to experimental error. A summary table of AOV responses is as follows for the forward equations:

Table 7. Summary of Analyses of Variance Results for Regression Equations 49-53

	SSR	SSE	MSR	MSE	F-Ratio	R^2
Q_{11} (Eq. 49)	554.345	51.277	29.176	0.493	59.174	0.915
Q_{22} (Eq. 50)	354.971	17.789	18.682	0.171	109.220	0.952
C_{33} (Eq. 51)	0.329	$5.339E^{-02}$	$1.733E^{-02}$	$5.134E^{-04}$	33.761	0.860
FO (Eq. 52)	1880.509	130.100	98.974	1.250	79.118	0.935
AD (Eq. 53)	97413.09	21648.8	5127.005	208.161	24.629	0.818

In alignment with their R^2 values, it is apparent that the greater the F-ratio, the less variance in the data is due to experimental error. For example, for Equation [50], the F-ratio of 109.220 suggests that most of the variance in Q_{22} can be accounted for by the regression itself. Only a small percentage of the variance is due to experimental error.

In a manner similar to F-ratios, T-values show the variance of a coeffient in a regression equation. The T-value is obtained by dividing the regression coefficient by its standard error value. Higher T-values indicate that the coefficient has little variance due to experimental error. The following table summarizes the T-values for the five manufacturing variables in each of the forward equations.

Table 8. Summary of T-Values for Coefficients in Regression Equations 49-53

	FR	JW	WP	WS	CDS
Q_{11} (Eq. 49)	-7.037	26.2705	4.5241	10.4629	6.5882
Q_{22} (Eq. 50)	-9.0258	-32.0236	2.3201	0.0923	23.7480
C_{33} (Eq. 51)	-17.8134	1.1606	7.2558	-7.1853	-8.1933
FO (Eq. 52)	0.2091	35.1638	0.3707	1.3739	-5.2654
AD (Eq. 53)	-12.9530	3.0619	10.7476	-3.7720	-5.2696

In an effort to determine the "goodness" of the data, one may observe that there is significant variability in the jet-to-wire data in the equations where jet-to-wire effects are significant at the 95% significance level. Despite a good fit of the data to the model for fiber orientation ratio (R^2=0.935), the variability in the jet-to-wire ratio data is a concern when performing a regression for the purpose of predicting machine variables from changes in paper properties. There is also some variability in the data for freeness, although it is not as noticeable as the variability in jet-to-wire data.

Regression Equations to Form Predictive Model

The next step in the analysis was solving the series of five equations in the inverse manner. Specifically, the multiple regression routine was performed on the data once again, but the independent variables were now the measured properties, not the machine variables. The independent variables in the inverse case were: apparent density (AD), MD stiffness (Q_{11}), CD stiffness (Q_{22}), ZD stiffness (C_{33}), and fiber orientation ratio (FO). The dependent variables were: freeness (FR), jet-to-wire ratio (JW), wet-pressing (WP), MD wet-straining (WS), and CD shrinkage (CDS). The following set of equations summarize the fit of the data in the inverse situation:

$$FR = 0.191 \cdot AD - 0.000188 \cdot AD^2 - 49.243 \cdot C_{33} + 57.898 \cdot C_{33}^2 - 38.690 \qquad R^2 = 0.539 \qquad [54]$$

$$JW = -0.0485 \cdot FO + 0.0200 \cdot FO^2 - 1.102 \qquad R^2 = 0.992 \qquad [55]$$

$$WP = -33.132 \qquad R^2 = 0.304 \qquad [56]$$

$$WS = 1.457 \cdot Q_{11} - 0.0302 \cdot Q_{11}^2 - 0.796 \cdot FO + 0.0333 \cdot FO^2 - 11.210 \qquad R^2 = 0.563 \qquad [57]$$

$$CDS = 1.603 \cdot Q_{22} - 0.0595 Q_{22}^2 - 19.645 C_{33} + 21.077 C_{33}^2 \ldots + 0.500 FO - 0.0161 FO^2 - 5.892 \qquad R^2 = 0.854 \qquad [58]$$

The two equations with the best R^2 values were Equations [55] and [58]. Looking at Figure 8, it is apparent that there was some spread in the fiber orientation data at the different jet-to-wire levels. The variation in fiber orientation ratio was influenced by refining, MD straining, and shrinkage (Equation [52]). However, the influences of these

variables were not statistically significant in contrast with the effects of jet-to-wire ratio.

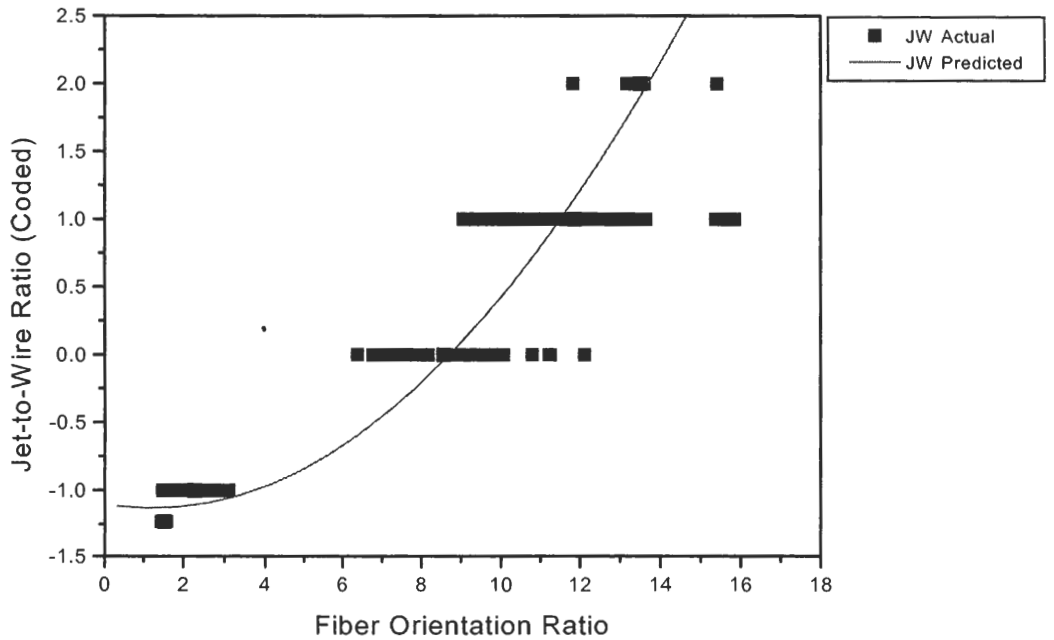

Figure 12. Fiber Orientation vs. JW Actual and JW Predicted

Looking more closely at the fiber orientation measurements showed that indeed there was a broad range in the fiber orientation data. These results verify the hight T-values for jet-to-wire data discussed previously. Specifically, sheets that were made under the same conditions often did not have a similar fiber orientation. For instance, samples 49-2 and 54-2 were made under identical conditions but have fiber orientation ratios of 10.79 and 7.40, respectively. Images of these samples are shown below in Figures 13 and 14:

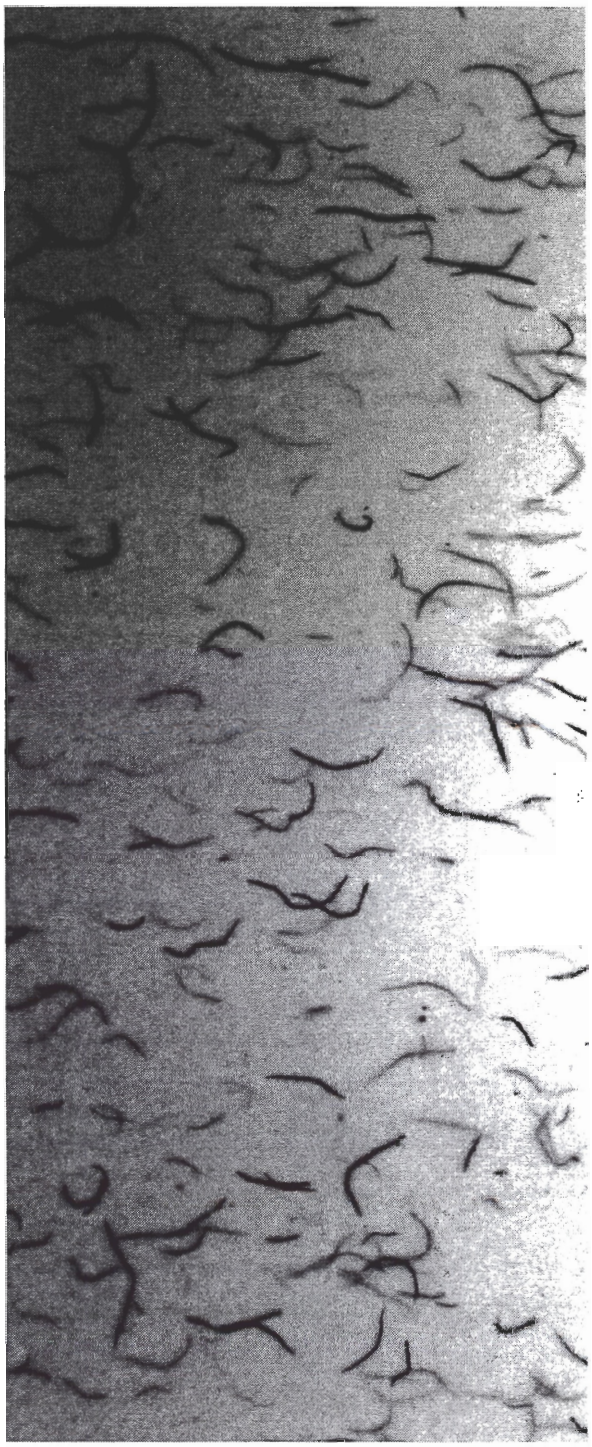

Figure 13. Fiber Analysis Image (MD Horizontal) of Sample 49-2, FO Ratio = 10.79

Figure 14. Fiber Analysis Image (MD Horizontal) of Sample 54-2, FO Ratio = 7.40

At first glance, these samples may not have visibly different appearances, but looking closer showed that Sample 49-2 had a definite strong trend of fiber alignment in the MD orientation. That trend was not as obvious with Sample 54-2, the fiber segments did not seem to have the same MD alignment as in 49-2. There was poor agreement in fiber orientation between the two samples. On the other hand, looking at fiber orientation ratios between duplicates showed very good agreement and repeatability. The duplicates were cut from the same master sheet and therefore the problem could not be traced to the fiber orientation image analysis system. The problem with poor repeatability seemed to be at an earlier point in the manufacturing process, likely changes in jet pressure or jar speed on the Formette Dynamique.

The second equation with a strong fit was Equation [58], the relationship between CD shrinkage and CD stiffness, ZD stiffness, and fiber orientation ratio. Correcting the CD shrinkage values for the relatively small effects of fiber orientation, there was an excellent fit of the CD shrinkage data to the predicted CD shrinkage/CD stiffness/ZD stiffness surface, as shown in Figures 15 and 16.

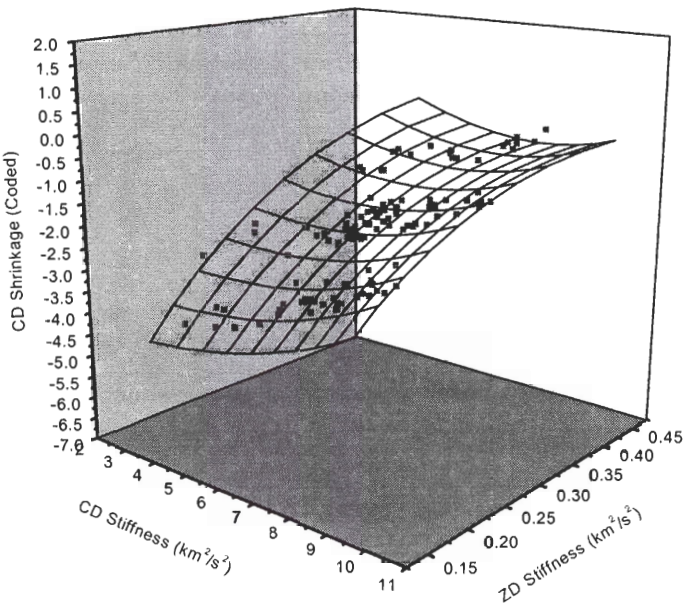

Figure 15. CD Shrinkage as a Function of CD Stiffness and ZD Stiffness (View 1)

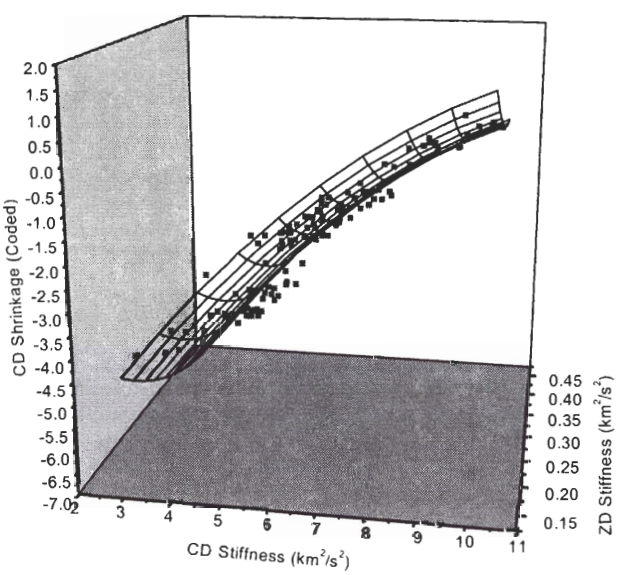

Figure 16. CD Shrinkage as a Function of CD Stiffness and ZD Stiffness (View 2)

The other three equations had fits with lower R^2 values than the CD shrinkage and jet-to-wire equations. Equation [54] related stock freeness to apparent density and ZD stiffness. Figures 17 and 18 show three-dimensional representations of the equation.

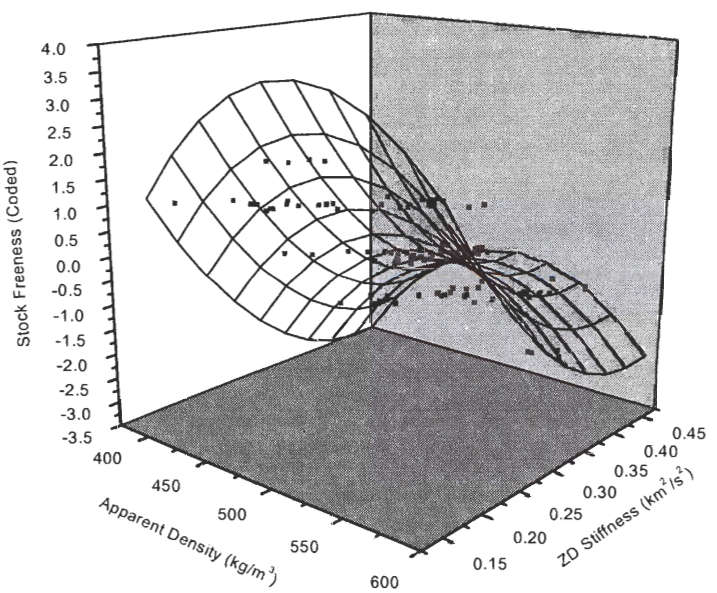

Figure 17. Stock Freeness as a Function of Apparent Density and ZD Stiffness (View 1)

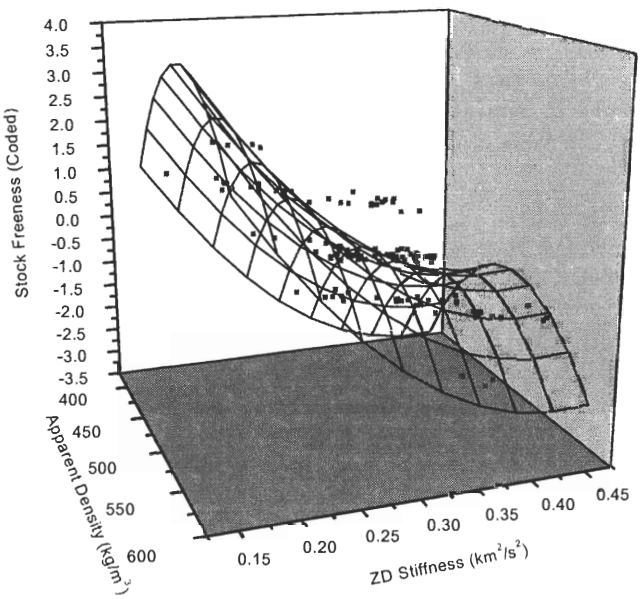

Figure 18. Stock Freeness as a Function of Apparent Density and ZD Stiffness (View 2)

The poor fit in the stock freeness case may have been caused by the relatively small range of apparent densities and secondly by the challenge of measuring ZD stiffness values on a thin sheet.

One obstacle to accurate ZD measurements was the limitation of ZD testing on thin sheets. The sheets made in the lab had an average caliper of 150 μm. The wavelengths used for out-of-plane stiffness testing were in the range of 1.0 to 2.0 MHz. When the ultrasound wavelength λ is of a similar magnitude to the sample caliper, it is difficult to obtain accurate measurements due to scattering of the waves in the sheet. Wavelength decreases with frequency; therefore, using the highest frequency possible makes the sample effectively "thicker". A limitation in this practice arises when the

wavelength decreases to a similar magnitude as fiber thickness. In such a case, the ultrasonic wave may not propagate through the sheet properly, due to difficulties with scattering (35). Conversely, the CD shrinkage prediction implemented ZD stiffness as a coefficient. The range of CD shrinkage may have been more suitable for predictions than was the range of freeness values.

The second equation that exhibited a poor fit to the data was wet-pressing [56]. None of the measured variables could be used to predict the pressing quantity. Looking back to the equations relating machine variables to measured nondestructive variables, pressing influenced MD stiffness, ZD stiffness, and apparent density measurements at statistically significant levels. While wet-pressing represented only a small factor in the MD and ZD stiffness measurements, it was a large factor in the apparent density measurements. In the inverse regression analysis, the small range of apparent densities did not produce a significantly robust data set to show the effects of apparent density upon pressing in the inverted regression. The small range magnified the effects of errors and the least-squares regression routine was unable to deem any of the coefficients as significant when tested using F-ratios.

Equation [57] related wet-straining to MD stiffness and fiber orientation ratio. The R^2 value for the equation was 0.563. The poor fit may be attributable to different factors. The most likely of these was the measurement and/or replication of fiber orientation ratio conditions. Five fiber orientation ratio measurements were taken for each sample: images of each sample were taken in 90° increments; the sample was then

turned over and one additional image was recorded. The average fiber orientation ratio measurements for the five images was recorded. The five ratios were very close to one another, but the ratios for different samples made under identical conditions had noticeable differences. Based upon these observations, it may be that the imaging system was overly or insufficiently sensitive to the effects of curled fiber fragments, short fibers, or other anomalies of dyed fibers in the samples. As mentioned previously, another possibility is that the jet-to-wire ratios were not held constant between identical conditions. Another possibility is that the range of straining was not sufficient, although it was enough to produce statistically significant changes in the screening experiment.

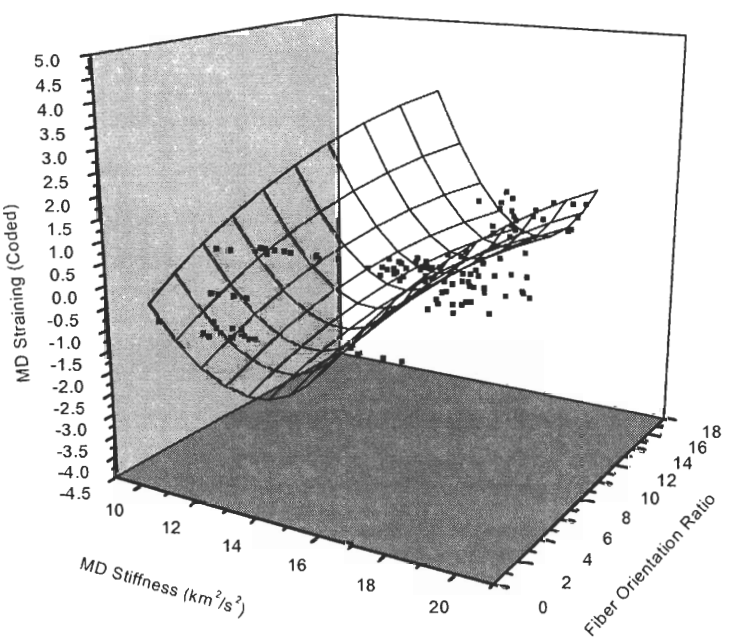

Figure 19. MD Wet-Straining as a Function of MD Stiffness and Fiber Orientation Ratio (View 1)

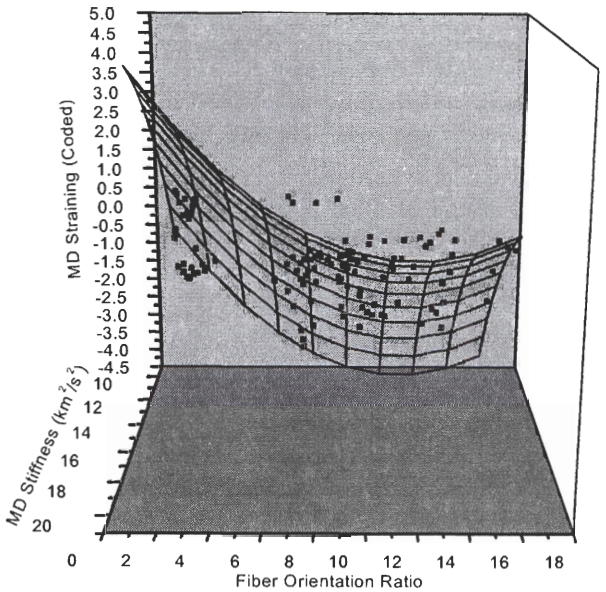

Figure 20. MD Wet-Straining as a Function of MD Stiffness and Fiber Orientation Ratio (View 2)

Equations [54] through [58] separated and decoupled many of the machine variable effects from the measured properties, as shown in Table 9. The advantage of using coded variables during the multiple regression process was that the relative magnitudes of the measured effects were evident in the equations.

Because of the effective decoupling of the different machine variables, one may reason that in an actual paper mill situation, on-line measurement of such stiffness and fiber orientation measurements could indeed be used for real-time control. A summary table of the inverse relationships is shown below:

Table 9. Machine Variables as Functions of Nondestructive Properties

Variable	As a Function of:				
	Apparent Density	MD Stiffness	CD Stiffness	ZD Stiffness	F.O. Ratio
Stock Freeness	✔			✔	
Jet-to-Wire Ratio					✔
Wet-straining		✔			✔
CD Shrinkage			✔	✔	✔

Numerical Inversion of Forward Equations to Obtain a Predictive Model

Another method of analyzing the ability of the data to be analyzed to form a predictive model is by numerical inversion of the "forward" equations -- Equations [50] through [54]. Numerical inversion of the equations was performed using MathCad and stating "guess" values for the machine variables in the forward equations. Using an iterative process, the MathCad program found the least squares solutions to the series of equations to converge upon a set of five values that fit the equations under the stated conditions of MD stiffness, CD stiffness, etc.

The following graphs compare the actual values for the machine variables to the predicted values as given by numerical inversion of the equations. For comparison, the graphs showing the actual values for the machine variables versus actual values for the regression analysis are also shown.

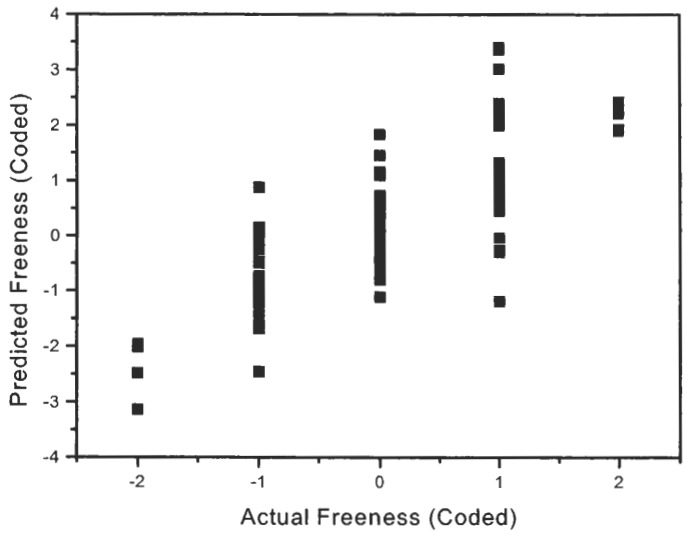

Figure 21. Actual vs. Predicted Freeness for Numerical Inversion

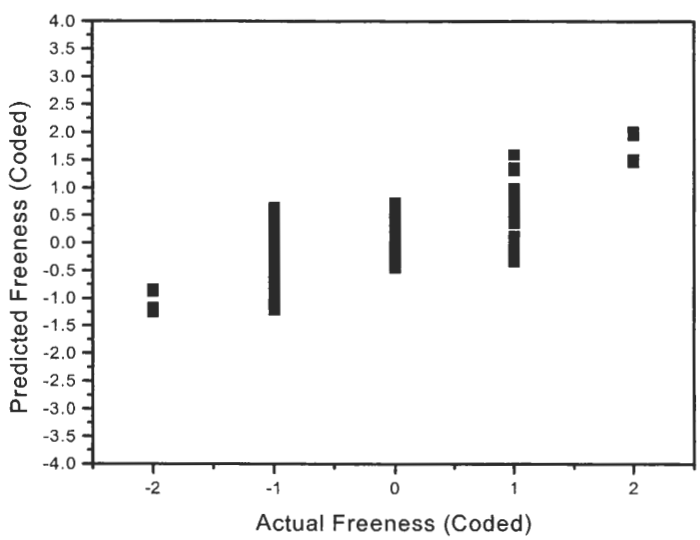

Figure 22. Actual vs. Predicted Freeness for Regression

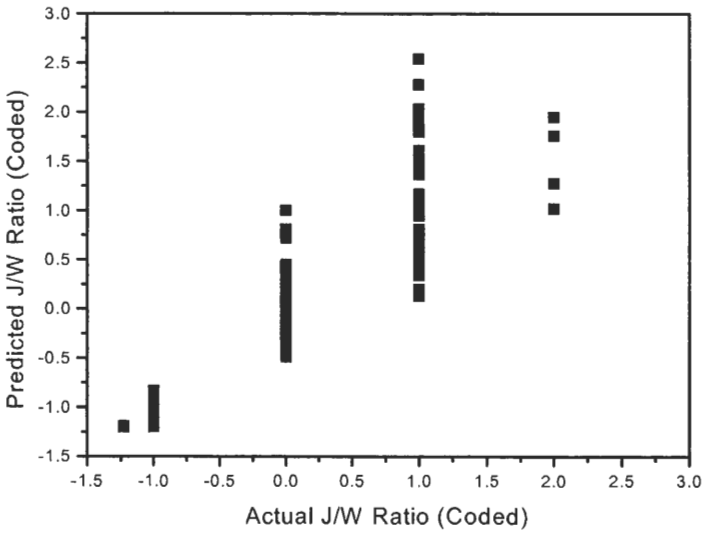

Figure 23. Actual vs. Predicted Jet-to-Wire for Numerical Inversion

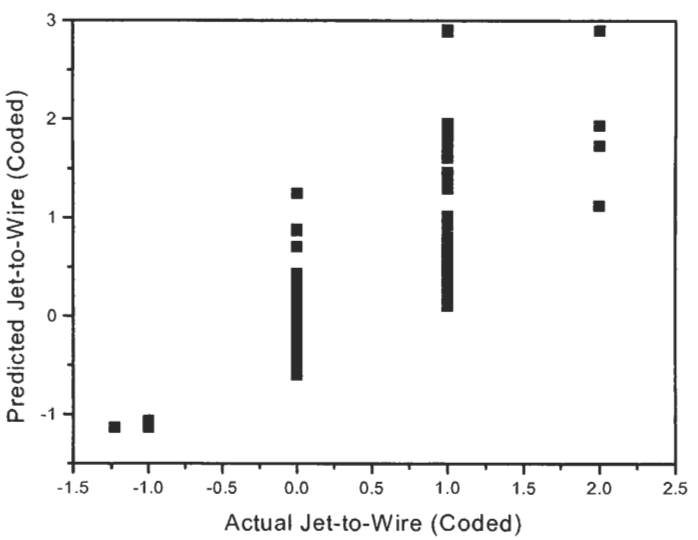

Figure 24. Actual vs. Predicted Jet-to-Wire for Regression

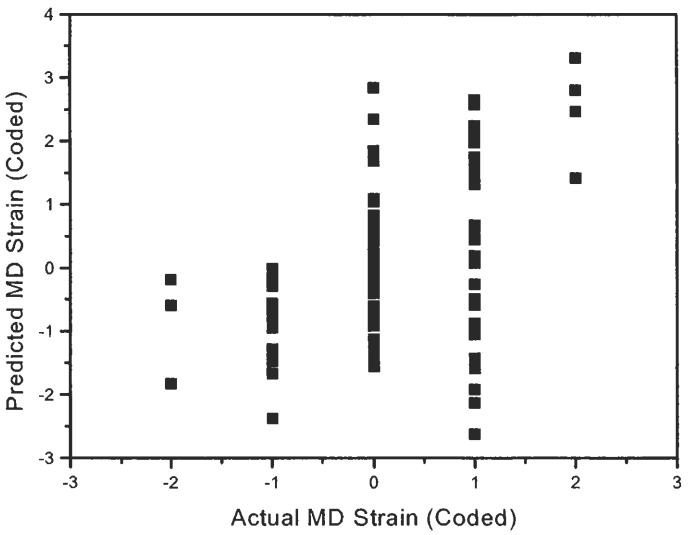

Figure 25. Actual vs. Predicted MD Strain for Numerical Inversion

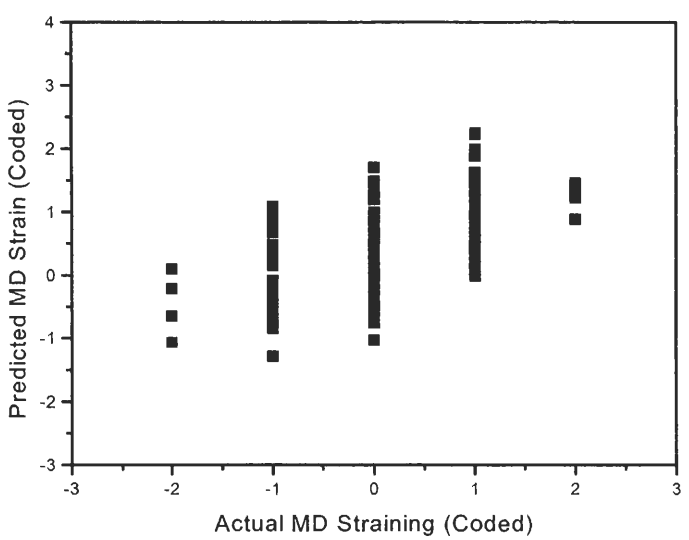

Figure 26. Actual vs. Predicted MD Strain for Regression

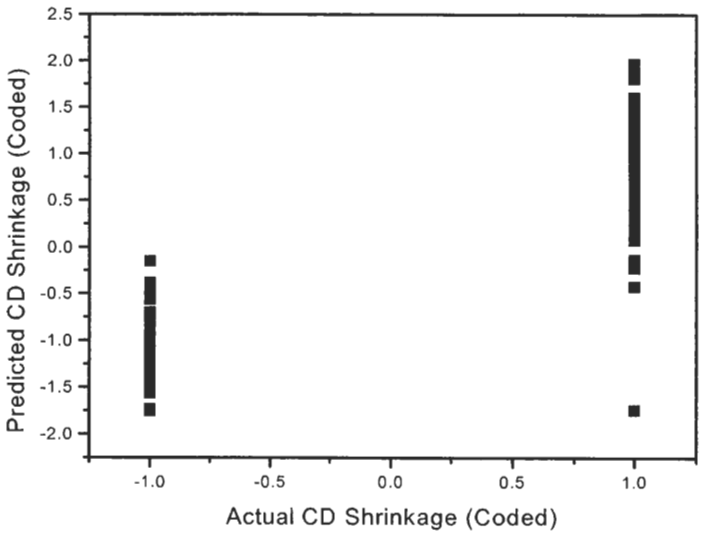

Figure 27. Actual vs. Predicted CD Shrinkage for Numerical Inversion

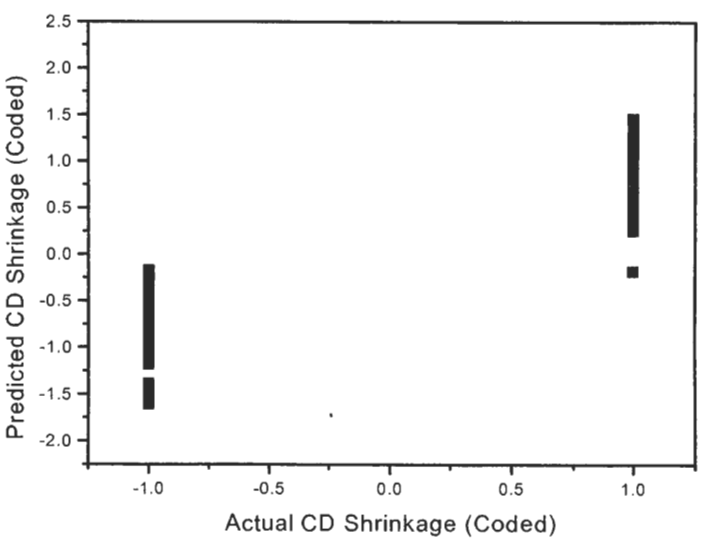

Figure 28. Actual vs. Predicted CD Shrinkage for Regression

While numerical inversion of the forward equations allows prediction of the

machine variables, the method is not as precise as the method of regression discussed in the previous section. Clearly, the spread of the data is large, making it difficult to use such a method for successful predictions.

Comparing to the Work of Fleischman

Similar work conducted by Fleischman (24) produced data that was investigated to compare to the results of this thesis (Ingalsbe). While Fleischman's work had a different purpose, sheets were made in a similar manner and some of the same manufacturing variables were investigated. Multiple regression analysis and inversion of equations of Fleischman's data could bring about complementary results to the work of Ingalsbe.

Fleischman sought to investigate the way in which fiber orientation and drying restraint affected the elastic and dielectric properties in all three principal directions of paper. Sheets were manufactured using a Formette Dynamique directional handsheet former at a basis weight of 400 a.d. kg/m^2. Sheets were made at low, medium, and high levels of fiber orientation, then pressed at different levels using a platen-style press. Each sheet was dried under restraint; some sheets were clamped biaxially and allowed to dry without any dimensional change while some sheets were clamped in the MD and wet-strained either 1.2% or 2.4% while the sheet freely contracted in the CD. After MD straining was completed, the sheet was clamped and restrained in the CD during the drying process.

Multiple non-linear regressions were performed on a series of data from 35 of Fleischman's sheets. The raw data are included in Appendix III. The "forward" equations related the three principal stiffness measurements and the apparent density measurements to the machine variables. The three machine variables were:

jet-to-wire ratio, wet pressing level, and wet straining level. Equations [59] through [62] show these relationships:

$$Q_{11} = 1.908 \cdot JW - 1.812 \cdot JW^2 + 0.870 \cdot PR + 0.241 \cdot JW \cdot PR \ldots + 1.018 \cdot WS - 0.608 \cdot WS^2 + 15.114 \qquad R^2 = 0.987 \qquad [59]$$

$$Q_{22} = -1.068 \cdot JW + 0.940 \cdot JW^2 + 0.273 \cdot PR - 0.0900 \cdot JW \cdot PR \ldots + -0.755 \cdot WS - 0.0926 \cdot WS^2 - 0.0661 \cdot JW \cdot PR \cdot WS + 3.493 \qquad R^2 = 0.997 \qquad [60]$$

$$C_{33} = 0.011 \cdot JW + 0.0136 \cdot PR - 0.0503 \cdot WS - 0.00969 \cdot JW \cdot WS + 0.126 \qquad R^2 = 0.955 \qquad [61]$$

$$AD = 14.735 \cdot JW - 17.068 \cdot JW^2 + 40.181 \cdot PR + 5.076 \cdot JW \cdot PR \ldots + -43.280 \cdot WS - 8.283 \cdot WS^2 - 6.135 \cdot JW \cdot WS + 745.500 \qquad R^2 = 0.987 \qquad [62]$$

All of the "forward" equations fit very well, with R^2 values of 0.95 or greater. Figures 29 and 30 show two perspectives of Equation [60], relating Q_{22} to machine variables:

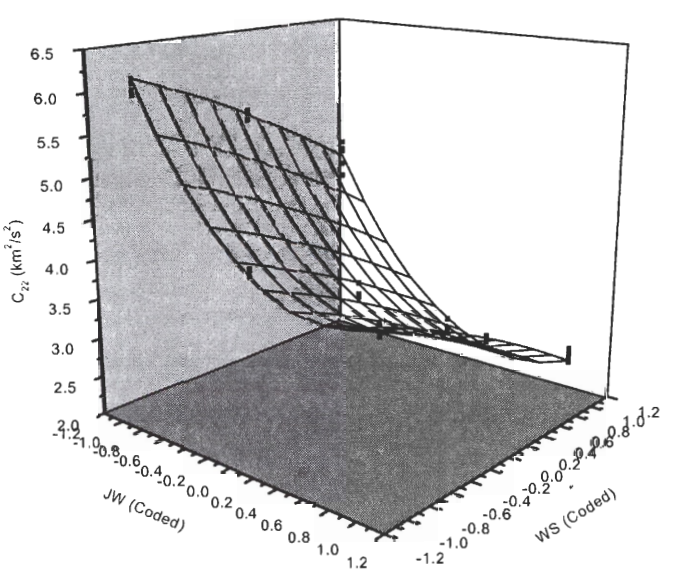

Figure 29. Q_{22} as a Function of Jet-to-Wire Ratio and Wet-Straining (Fleischman) (View 1)

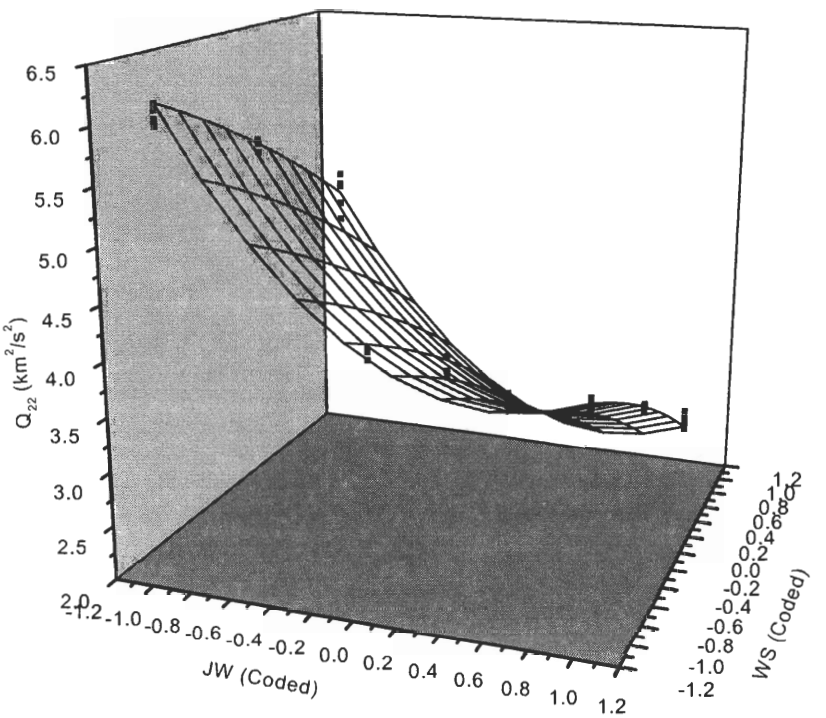

Figure 30. Q_{22} as a Function of Jet-to-Wire Ratio and Wet-Straining (Fleischman) (View 2)

The data fit very well in the forward equations. The data were next fit in the inverse manner, with the three primary stiffness measurements and the apparent density measurements set as the independent variables and the machine variables set as the dependent variables. The multiple regression routine was carried out in the same manner as for the reprographic sheets:

$$JW = -1.135 \cdot Q_{22} \qquad R^2 = 0.828 \qquad [63]$$

$$WP = 0.668 \cdot Q_{22} - 58.301 \cdot C_{33} + 177.730 C_{33}^2 \ldots + 0.0911 \cdot AD - 0.000053 \cdot AD^2 - 42.095 \qquad R^2 = 0.959 \qquad [64]$$

$$WS = 0.173 \cdot Q_{11} + 0.165 \cdot Q_{22} - 41.28 \cdot C_{33} + 98.05 \cdot C_{33}^2 \qquad R^2 = 0.981 \qquad [65]$$

Comparing the results of Fleischman's inverted multiple regressions to the results of the inverted regressions of Ingalsbe's data, there are some notable differences. Fleischman's "forward" equations possessed greater R^2 values than did Ingalsbe's "forward" equations. This in turn allowed the inverted equations to have better fits. In particular, the pressing equation had a very good fit with Fleischman's data, while with Ingalsbe's data, the pressing equation had the lowest R^2 value of the five equations produced. The thicker sheets produced by Fleischman allowed more precise measurements in the thickness direction of the sheet and thus better apparent density and C_{33} measurements due to the avoidance of problems as discussed previously.

Fleischman's Equation [63], relating the jet-to-wire ratio of the sheet to machine variables, was difficult to compare to Ingalsbe's jet-to-wire ratio Equation [55] because Ingalsbe measured the fiber orientation of the sheet while Fleischman did not emphasize such measurements. Fleischman did measure fiber orientation distributions, but the system of measurement was not advanced and not every sample was measured. Equation [63] therefore related the jet-to-wire ratio of the sheet to the Q_{22} stiffness and not to the fiber orientation ratio as in Equation [55]. While in the "forward" equations the jet-to-wire ratio was an independent variable in each of the four equations, only the Q_{22} stiffness was a factor in the inverse jet-to-wire relationship. The uncontrolled CD shrinkage in the series of sheets by Fleischman may have made it the most robust variable and its effects were more evident than the others in the inverse case.

The wet-straining inverse Equation [65] had the best fit of the three inverted equations. While Ingalsbe's inverse Equation [57] for wet-straining had coefficients for Q_{11} and fiber orientation ratio, Fleischman's Equation [65] had coefficients for Q_{11}, Q_{22}, and C_{33}. Fleischman's results were affected by the action of MD wet-straining the sheets and allowing the sheet to shrink freely in the CD during the straining action. This action was surely the reason for Q_{22}'s incorporation into the inverse equation. Fleischman also found that C_{33} was affected by wet straining. Such observations were not made in Ingalsbe's data, due likely to the Ingalsbe's small range of apparent densities. Fitting Fleischman's data to Equation [65] in Figures 31 and 32:

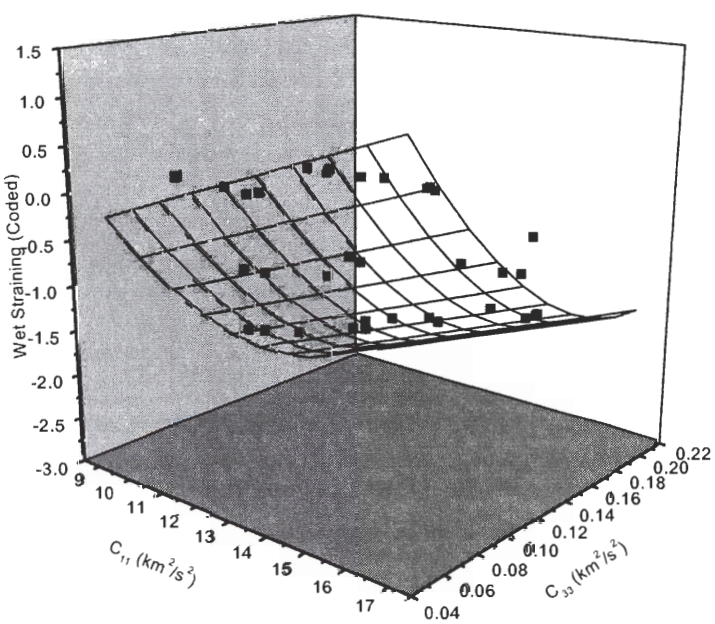

Figure 31. Wet Straining as a Function of Q_{11} and C_{33} (Fleischman) (View 1)

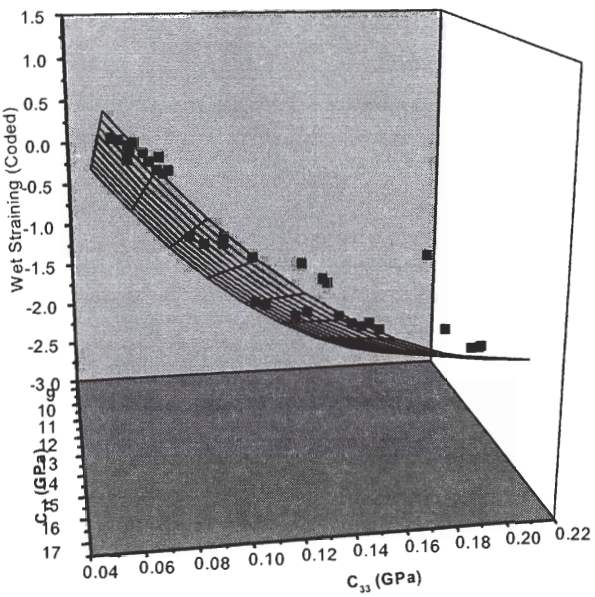

Figure 32. Wet Straining as a Function of Q_{11} and C_{33} (Fleischman) (View 2)

Simulated Application of the Model

The series of inverted Equations ([54] through [58]) were tested using a simulated model; no additional sheets were made. A series of sheet conditions were proposed and the resulting stiffness properties and fiber orientation properties were determined using Equations [49] through [53] (the "forward" equations).

Table 10. Proposed Manufacturing Conditions and the Resulting Properties

Independent Variables				Dependent Variables					
FR	JW	WS	CDS	Q_{11}	Q_{22}	C_{33}	FO	AD	Geo. Mean
0.00	0.00	0.00	0.00	16.00	5.39	0.32	8.99	513.09	9.29
0.00	2.00	0.75	0.00	18.12	4.73	0.31	14.25	510.28	9.26
0.00	1.00	1.20	0.00	18.51	4.66	0.30	12.21	499.24	9.29
0.00	0.00	-2.00	0.10	14.11	6.12	0.04	7.84	512.04	9.30
0.00	-1.23	-1.30	-0.55	11.08	7.81	0.35	1.61	506.57	9.30

In the initial simulation, the manufacturing conditions predicted properties that differed while the geometric mean of the in-plane stiffnesses remained constant. Freeness and pressing (pressing not shown) were kept at constant values because the inverted equations for freeness and pressing had low R^2 values. Jet-to-wire ratio, MD straining, and CD shrinkage were arbitrarily changed to keep the geometric mean constant at approximately 9.29 over a range of conditions. The MD, CD, and ZD stiffnesses, along with the fiber orientation ratio and apparent density value, were calculated using "forward" Equations [49] through [53].

After setting the coefficients to keep the geometric mean constant and solving for the sheet properties, the next step was solving the inverted equations. The solutions to

the inverted Equations [54] through [58] were obtained by taking the values of the measured variables (MD, CD, and ZD stiffness; fiber orientation ratio and apparent density) from Table 10 and substituting them into the equations:

Table 11. Solving the Inverted Equations with Data from Table 10

Independent Variables					Dependent Variables			
Q_{11}	Q_{22}	C_{33}	FO	AD	FR	JW	WS	CDS
16.00	5.39	0.32	8.99	513.09	0.01	0.52	-0.09	0.10
18.12	4.73	0.31	14.25	510.28	0.07	1.57	0.70	0.13
18.51	4.66	0.30	12.21	499.24	0.26	1.26	0.66	0.01
14.11	6.12	0.04	7.84	512.04	-0.39	0.22	-0.85	0.29
11.08	7.81	0.35	1.61	506.57	-0.35	-1.03	0.03	-0.55

The next step was comparing the predicted dependent variables from Table 11 to the independent variables from Table 10. Table 12 summarizes these results:

Table 12. Initial Coefficients vs. Calculated Values for the Series of Inverted Equations

Independent Variables				Dependent Variables			
FR	JW	WS	CDS	FR	JW	WS	CDS
0.00	0.00	0.00	0.00	0.01	0.52	-0.09	0.10
0.00	2.00	0.75	0.00	0.07	1.57	0.70	0.13
0.00	1.00	1.20	0.00	0.26	1.26	0.66	0.01
0.00	0.00	-2.00	0.10	-0.39	0.22	-0.85	0.29
0.00	-1.23	-1.30	-0.55	-0.35	-1.03	0.03	-0.55

Examining the independent variables compared to the resulting dependent variables, there were some interesting observations. Freeness values were all set at zero and the predicted freeness variables were all close to zero also, with only slight deviations. Jet-to-wire predictions had a positive correlation with their independent set values and the predictions were very close to the set values. Wet-straining predictions

were most accurate at independent set values between 0 and 1. At low levels of straining (-2 coded) the prediction was also negative. When a negative straining level was combined with a negative jet-to-wire prediction and CD shrinkage, the wet-straining predicted value was not satisfactory. Finally, CD shrinkage predictions were very good, regardless of the other set independent variables of jet-to-wire or wet-straining.

A second simulation to test the predictability of the inverse equations required a series of sheets with MD stiffness values held constant:

Table 13. Proposed Manufacturing Conditions and Predicted Properties

Independent Variables				Dependent Variables				
FR	JW	WS	CDS	Q_{11}	Q_{22}	C_{33}	FO	AD
0.00	0.00	0.00	0.00	16.00	5.39	0.32	8.99	513.09
0.00	-0.87	2.00	1.00	16.00	8.34	0.25	3.09	477.83
0.00	1.00	-1.50	0.25	16.01	5.06	0.35	11.69	526.26
0.00	2.00	-1.75	0.80	16.00	6.03	0.36	12.19	535.34
0.00	-0.50	1.60	-1.00	16.02	6.06	0.30	6.20	500.92

The predicted mechanical properties from the series of "forward" equations were then substituted into the series of inverted equations to yield the predictive values for the machine variables:

Table 14. Solving the Inverted Equations with Data from Table 13

Independent Variables				Dependent Variables				
Q_{11}	Q_{22}	C_{33}	FO	AD	FR	JW	WS	CDS
16.00	5.39	0.32	8.99	513.09	0.01	0.52	-0.09	0.10
16.00	8.34	0.25	3.09	477.83	1.04	-0.84	2.22	1.17
16.01	5.06	0.35	11.69	526.26	-0.41	1.16	-0.38	0.04
16.00	6.03	0.36	12.19	535.34	-0.57	1.26	-0.39	0.95
16.02	6.06	0.30	6.20	500.92	0.19	-0.19	0.72	0.10

Summarizing the results of the second simulation:

Table 15. Initial Coefficients vs. Calculated Values for the Series of Inverted Equations

Independent Variables				Dependent Variables			
FR	JW	WS	CDS	FR	JW	WS	CDS
0.00	0.00	0.00	0.00	0.01	0.52	-0.09	0.10
0.00	-0.87	2.00	1.00	1.04	-0.84	2.22	1.17
0.00	1.00	-1.50	0.25	-0.41	1.16	-0.38	0.04
0.00	2.00	-1.75	0.80	-0.57	1.26	-0.39	0.95
0.00	-0.50	1.60	-1.00	0.19	-0.19	0.72	0.10

The predicted freeness values in the second simulation were not nearly as precise as those in the first simulation. The independent freeness values were held constant at zero for all sheets while the predicted freeness values ranged from –0.57 to 1.04. The predicted jet-to-wire ratios were quite good for all of the sheets and over the entire range of independent values. At the highest (+2) level of set independent jet-to-wire, the predicted value fell short at 1.26; however, a similar shortfall was experienced during the first simulation. Figure 12 showed that predicted jet-to-wire ratios were expected to fall short of actual jet-to-wire ratios in spite of the fitting equation having an R^2 value of 0.992. Predicted wet-straining values were positively correlated to the independent set values for wet-straining. At negative set values of wet-straining, the predictions fell substantially short. The precision of the inverse equation for the case of wet-straining in the second simulation was similar to its precision in the first simulation. Finally, CD shrinkage predictions were very good until the case of –1 set independent shrinkage combined with +1.60 wet-straining. The series of predictions for CD shrinkage in the second simulation were comparable to the precision in the first simulation.

Obtaining a Robust Data Set

In an effort to use a set of laboratory data to predict machine variables from changes in non-destructive properties of the sheet, it is necessary that the data set be "robust". In other words, the data need to be of significant range and precision that one is able to go "back and forth" between the measured and predicted values with minimal error and good precision. Obtaining that robust data set was a challenge in this series of experiments and therefore it ought to be discussed as to what is necessary in order to obtain such a set of data.

Initially, it should be emphasized that obtaining a set of good data in the lab is an entirely different venture than collecting such data in a mill or manufacturing situation. Conditions in the lab are highly controlled and variables may be minimized. In addition, in the mill setting, there are far more variables than one may control at once, adding to the challenge of getting a desirable set of data. One of the major advantages of collecting data on-line, however, is the ability to collect mass quantities of data and reduce the error significantly as compared to the amount that could be physically collected in the lab.

In order to go "back and forth", data need to be precise; i.e., when performing the regressions on the data, the T-values for the coefficients should be large, showing a minimal standard error or variance. It is impossible to state necessary T-values as these change according to the quantity of data collected and thus standard errors vary. However, in looking at the results of Fleischman, who was quite able to go "back and forth" with predictive equations fitting quite well, R^2 values for the regression

equations need to be at least 0.90 and the T-values for the coefficients need to be at least 2, but higher values are preferable. For instance, Equation [57], predicting MD wet-straining, has an R^2 value of 0.957 and each of the significant coefficients (at the 95% level) possess absolute T-values of 6.125, 2.960, 9.299, and 5.752, respectively. This data set was obtained by using machine variables that varied the measured variables significantly, such as wet pressing that varied the apparent density over a much greater range than did the wet pressing in Ingalsbe's experiments.

As stated in a previous section, there was a significant amount of variance in the jet-to-wire speed ratios in Ingalsbe's sheets. In future, similar, lab work, it will be essential to determine the source of the variation (the pump or the jar speed) and make a special effort to keep that variable stable.

Obtaining a robust dataset in the mill environment should prove to be a challenge because of control issues. However, the mass quantity of data that can be collected over a short period of time may make it possible for analysis with neural networks or similar tools.

CONCLUSIONS

The problem of predicting changes in machine variables from non-destructive sheet properties is a challenging and complicated procedure. Many conditions need to be met in order for successful data collection to occur. These include: stable machine variables (i.e. little variation in set machine conditions), a broad range of possible manufacturing conditions available to the experimenter, and accurate measurement tools to detect the non-destructive mechanical sheet properties. If even one of these conditions is not present, then it is difficult, if not impossible, to complete the task of predicting changes in machine variables from non-destructive sheet properties.

This research work confirmed that G_{12} is not an independent physical variable in paper and thus should not be used in predictive algorithms for paper.

Due to variations in jet-to-wire ratio and a small range of wet-pressing available, it was not possible to achieve a truly predictive model as was set forth in this research proposal. However, it was possible to obtain a series of equations that could somewhat predict the directional trends in machine variable directions based on sheet measurements. The results would be useful in verifying the predictions made by an on-line tool such as neural networks, but could not be used on their own as a control method.

In light of the results achieved by Fleischman in the early 1980's, it is apparent that a higher basis weight sheet and a greater range of pressing conditions may contribute to a set of data, thus, a series of accurate predictive equations. While such a set of

predictive equations is useful in the laboratory setting, for true practicality it would be superior to use data actually produced on a full-scale paper machine. On the other hand, for the purpose of ascertaining the relationships between the manufacturing variables and non-destructive sheet properties, a study such as this is quite beneficial. Another benefit of comparing this work to that of Fleischman's is the confirmation that the relationships between non-destructive properties are highly dependent on the drying routine of the paper (i.e. whether shrinkage was allowed, etc.).

Paper machine data would not vary as much as laboratory data due to a more narrow range of conditions and therefore could not be analyzed in the same manner that our laboratory data were. It can be concluded that the spread in our laboratory data was too large in order to get a good model. For true applicability to the real-world problem of paper machine process control, a large set of data over a narrow range of manufacturing conditions would be necessary to produce a predictive model by means of neural networks and the like. A major obstacle in such testing is the detection of characteristics such as stiffness orientation, fiber orientation, CD shrinkage and MD straining on-line. Fiber orientation and stiffness orientation measurements have been developed or are under development, but shrinkage and straining measurements are not currently available. This work reveals that shrinkage measurements, fiber orientation measurements and stiffness measurements are all necessary to detect the nondestructive mechanical changes that occur in paper during the manufacturing process.

ACKNOWLEDGEMENTS

I would like to give special thanks to Dr. Douglas Coffin, my immediate advisor, for profitable discussions and encouragement. Thank you to Dr. Gary Baum and Dr. Charles Habeger for their guidance as they served on my thesis committee. I would also like to recognize my former advisor, Dr. Pierre Brodeur, for his help during the initial stages of my research.

I appreciate Dr. Hiroki Nanko and Dr. Timothy Patterson for serving on my final thesis defense committee. Dr. Nanko also assisted with the procurement of the biaxial testing device.

Mr. Joe Gerhardstein and Mr. Ted Jackson both provided valuable LabView programming services for several pieces of equipment. I am grateful for their help.

At one time or another, every member of the Institute faculty and staff has made a contribution to this project, either directly or indirectly. I am indebted to everyone at IPST for making this part of my life enjoyable and worthwhile.

I am grateful to the supporting member companies of The Institute of Paper Science and Technology for giving me the opportunity to study and learn at a wonderful institution such as this. My experience here has been positive and enriching.

Mr. Leo Leewenburg of Techpap in Grenoble, France, provided excellent training and customer support related to the Formette Dynamique sheet former. Mr. Katsuhiko Terada designed and built the biaxial testing device. International Paper's Riverdale Mill in Selma, Alabama, provided the wood pulp for this project.

Finally, my family members have given me generous support during my years at the Institute. I appreciate their encouragement as I worked toward this degree. I would like to especially recognize my husband, Thomas, for helping me as I achieved my goal.

LITERATURE CITED

1. Baum, G.A. Prospects in Paper Technology. Acta Polytechnica Scandinavia, Chemical Technology Series No. 272. Published by the Finnish Academy of Technology. Espoo, Finland. 30 pp. (1999).

2. Baum, G.A. Elastic Properties, Paper Quality, and Process Control. *Appita Journal.* **40**(4):288-294 (1987).

3. Baum, G.A. Polar Diagrams of Elastic Stiffnesses: Effect of Machine Variables. *TAPPI 1987 Paper Physics Conference Proceedings.* pp. 161-166 (1987).

4. *Pulp and Paper 1997 North American Factbook.* pp. 197-210 Miller Freeman Publications Limited (1997).

5. Coffin, D.W. Elastic Properties of Paper. *Handbook of Elastic Properties of Solids, Liquids and Gases (Levy, Bass and Stern, Editors). Vol. III: Elastic Properties of Solids: Biological and Organic Materials, Earth and Marine Sciences.* pp. 91-103. Academic Press (2001).

6. Htun, M. and Fellers, C. The Invariant Mechanical Properties of Oriented Handsheets. *TAPPI Journal.* **65**(4):113-117 (1982).

7. Baum, G.A.; Brennan, D.G.; and Habeger, C.C. Orthotropic Elastic Constants of Paper. *TAPPI Journal.* **64**(8):97-101 (1981).

8. Habeger, C.C. Ultrasonic Determinations of Stiffness Parameters. *Handbook of Physical Testing of Paper: Volume 1, Second Edition, Revised and Expanded.* pp.257-312. Marcel Dekker, Inc. (2001).

9. Mann, R.W. Elastic Wave Propagation in Paper. Doctoral Thesis, Institute of Paper Chemistry, Appleton, Wisconsin. 149 pages. (1978).

10. Habeger, C.C., et al. Using a Robot-Based Instrument to Measure the In-Plane Ultrasonic Velocities of Paper. *TAPPI Journal.* **72**(7):171-175 (1989).

11. Habeger, C.C. and Wink, W.A. Ultrasonic Velocity Measurements in the Thickness Direction of Paper. *Journal of Applied Polymer Science.* **32**:4503-4540 (1986).

12. Craver, J. and Taylor, D. Nondestructive sonic measurement of paper elasticity. *TAPPI Journal.* **48**(3):142-147 (1965).

13. Schulgasser, K. Fibre Orientation in Machine-Made Paper. *Journal of Materials Science.* **20**(1985):859-866 (1985).

14. Schweiger, C.A. and Rudd, J.B. Process and Control of Paper Machine Parameters Using Adaptive Technologies in Process Modeling. TAPPI Journal. **77**(11):201-208 (1994).

15. Kumar, A. and Hand, V.C. Using Genetic Algorithms and Neural Networks to Predict and Optimize Coated Board Brightness. Proceedings of the TAPPI 1999 Conference. pp. 161-170. (1999).

16. Darwin, C. On the Origin of Species. London: Murray, 1859. Reprinted, New York: Penguin, 1984.

17. Berger, B.F. and Baum, G.A. Z Direction Properties: The Effects of Yield and Refining. Papermaking Raw Materials (Punton, Ed.) Vol. 1:339-362. Mechanical Engineering Publications Limited. (1985).

18. Stratton, R.A. Characterization of Fibre-Fibre Bond Strength From Out-of-Plane Paper Mechanical Properties. *Journal of Pulp and Paper Science.* **19**(1):6-12 (1993).

19. Page, D.H. and Seth, R.S. The Elastic Modulus of Paper: II. The Importance of Fiber Modulus, Bonding, and Fiber Length. *TAPPI Journal.* **63**(6):113-116 (1980).

20. Baum, G.A. and Brennan, D.G. Transverse Jet Flows Affect Paper Properties. *TAPPI 1987 Process Control Conference Proceedings.* pp. 9-16 (1987).

21. Cox, H.L. The Elasticity and Strength of Paper and Other Fibrous Materials. *British Journal of Applied Physics.* (3):72-79 (1952).

22. Niskanen, K.J. Distribution of Fiber Orientations in Paper. *Transcript of the 9th Fundamental Research Symposium, Cambridge.* Baker, C.F. and Punton, V.W., Editors. Mechanical Engineering Publications Ltd., London, **1**:275-308 (1989).

23. Ishisaki, M. Comparative Study of Fiber and Stiffness Orientation Distributions. A190 Independent Research Project, IPST (1997).

24. Fleischman, E.H. An Investigation of the Elastic and Dielectric Anisotropy of Paper. Doctoral Thesis, Institute of Paper Chemistry, Appleton, Wisconsin, 155 pages (1981).

25. Hess, T.R. The Stiffness Polar Plot's Relationship With Stress-Strain Response and Fiber Orientation. A190 Independent Research Project, IPST (1994).

26. Setterholm, V. and Kuenzi, E.W. Fiber Orientation and Degree of Restraint During Drying: Effect on Tensile Anisotropy of Paper Handsheets. *TAPPI Journal.* **53**(10):1915-1920 (1970).

27. Wahlstrom, T. Influence of Shrinkage and Stretch During Drying on Paper Properties. Licentiate Thesis. Department of Pulp and Paper Chemistry and Technology, Royal Institute of Technology, Stockholm, Sweden. (1999).

28. Htun, M. Internal Stress in Paper. Paper: Structure and Properties (Bristow and Kolseth, ed.), Chap. 11: 227-239. Marcel Dekker. (1986).

29. Campbell, J.G. The In-Plane Elastic Constants of Paper. *Australian Journal of Applied Science.* **12**:356-357 (1961).

30. TAPPI Test Methods 1994-1995. TAPPI Press, Atlanta, Georgia. (1994).

31. Formette Dynamique User's Manual. Techpap Inc. pp. 35 (1999).

32. Schulz, C.E. (International Paper). Personal correspondence. March 12, 1999.

33. Charles, L.A. and Waterhouse, J.F. The Effect of Supercalendering on the Strength Properties of Paper. Proceedings of the 1987 International Paper Physics Conference. pp. 177-184. (1987).

34. Hayter, A.J. Probability and Statistics for Scientists and Engineers. PWS Publishing Company, Boston, Massachusetts (1996).

35. Habeger, C.C. and Wink, W.A. Ultrasonic Velocity Measurements in the Thickness Direction of Paper. Journal of Applied Polymer Science. 32:4503-4540. (1986).

APPENDIX I -- YATES ALGORITHM ANALYSES

Yates Algorithm For Analyzing Effects	
(Experiment Performed in Duplicate)	

Treatment Combination	MD Stiffness	(1)	(2)	(3)	(4)	Effect	Estimate of Effect	Sum of Squares	Mean Squares
1.00	25.90	48.50	111.34	229.51	489.15	Total			
2.00	22.61	62.83	118.17	259.64	-4.40	A	-0.27	1.21	0.60
3.00	32.93	53.88	129.23	-5.51	48.48	B	3.03	146.89	73.45
4.00	29.90	64.29	130.42	1.11	3.26	AB	0.20	0.67	0.33
5.00	27.14	58.18	-6.32	24.74	8.02	C	0.50	4.02	2.01
6.00	26.74	71.04	0.81	23.74	3.96	AC	0.25	0.98	0.49
7.00	31.54	59.77	2.14	1.86	-5.90	BC	-0.37	2.18	1.09
8.00	32.75	70.65	-1.03	1.40	-0.04	DE	0.00	0.00	0.00
9.00	28.90	-3.29	14.33	6.83	30.14	D	1.88	56.76	28.38
10.00	29.28	-3.03	10.41	1.19	6.62	AD	0.41	2.74	1.37
11.00	34.64	-0.39	12.86	7.13	-0.99	BD	-0.06	0.06	0.03
12.00	36.40	1.20	10.88	-3.17	-0.46	CE	-0.03	0.01	0.01
13.00	30.14	0.38	0.27	-3.92	-5.64	CD	-0.35	1.99	1.00
14.00	29.62	1.76	1.60	-1.98	-10.30	BE	-0.64	6.63	3.32
15.00	35.58	-0.52	1.39	1.33	1.95	AE	0.12	0.24	0.12
16.00	35.07	-0.51	0.01	-1.38	-2.71	E	-0.17	0.46	0.23
							Syy=	224.83	

AOV Table

Source	DF	Effects	SS	MS	F-Ratio	F (1, 16)	Significance (99%)
Freeness (A)	1.00	-0.27	0.60	0.60	1.92	<99%	no
Jet-to-Wire Ratio (B)	1.00	3.03	73.45	73.45	232.54	>99%	yes
AB	1.00	0.20	0.33	0.33	1.05	<99%	no
Wet Pressing (C)	1.00	0.50	2.01	2.01	6.36	<99%	no
AC	1.00	0.25	0.49	0.49	1.55	<99%	no
BC	1.00	-0.37	1.09	1.09	3.44	<99%	no
DE	1.00	0.00	0.00	0.00	0.00	<99%	no
Wet Straining (D)	1.00	1.88	28.38	28.38	89.86	>99%	yes
AD	1.00	0.41	1.37	1.37	4.33	<99%	no
BD	1.00	-0.06	0.03	0.03	0.10	<99%	no
CE	1.00	-0.03	0.01	0.01	0.02	<99%	no
CD	1.00	-0.35	1.00	1.00	3.15	<99%	no
BE	1.00	-0.64	3.32	3.32	10.50	>99%	yes
AE	1.00	0.12	0.12	0.12	0.38	<99%	no
Shrinkage (E)	1.00	-0.17	0.23	0.23	0.73	<99%	no
Error	16.00		5.05	0.32			
Total	31.00		117.47				

Check	Syy=	224.83	Syy(alg)=	224.83	OK!

Yates Algorithm For Analyzing Effects	
(Experiment Performed in Duplicate)	

Treatment Combination	CD Stiffness	(1)	(2)	(3)	(4)	Effect	Estimate of Effect	Sum of Squares	Mean Squares
1.00	13.10	31.86	50.68	103.30	205.20	Total			
2.00	18.76	18.82	52.62	101.90	-11.49	A	-0.72	8.24	4.12
3.00	11.68	30.95	49.26	-4.14	-38.87	B	-2.43	94.42	47.21
4.00	7.14	21.68	52.64	-7.35	-3.68	AB	-0.23	0.84	0.42
5.00	18.18	29.27	1.12	-22.31	5.33	C	0.33	1.78	0.89
6.00	12.77	19.99	-5.26	-16.56	-3.39	AC	-0.21	0.72	0.36
7.00	10.76	29.96	-5.17	-4.64	5.78	BC	0.36	2.08	1.04
8.00	10.92	22.68	-2.18	0.96	7.72	DE	0.48	3.72	1.86
9.00	17.06	5.67	-13.04	1.95	-1.40	D	-0.09	0.12	0.06
10.00	12.21	-4.54	-9.27	3.39	-3.21	AD	-0.20	0.64	0.32
11.00	10.16	-5.42	-9.28	-6.39	5.76	BD	0.36	2.07	1.04
12.00	9.83	0.15	-7.27	3.00	5.60	CE	0.35	1.96	0.98
13.00	14.64	-4.84	-10.21	3.77	1.44	CD	0.09	0.13	0.06
14.00	15.32	-0.33	5.57	2.01	9.38	BE	0.59	5.50	2.75
15.00	12.77	0.69	4.51	15.78	-1.76	AE	-0.11	0.19	0.10
16.00	9.91	-2.86	-3.55	-8.07	-23.85	E	-1.49	35.54	17.77
							Syy=	157.96	

AOV Table

Source	DF	Effects	SS	MS	F-Ratio	F (1, 16)	Significance (99%)
Freeness (A)	1.00	-0.72	4.12	4.12	8.03	<99%	no
Jet-to-Wire Ratio (B)	1.00	-2.43	47.21	47.21	91.96	>99%	yes
AB	1.00	-0.23	0.42	0.42	0.82	<99%	no
Wet Pressing (C)	1.00	0.33	0.89	0.89	1.73	<99%	no
AC	1.00	-0.21	0.36	0.36	0.70	<99%	no
BC	1.00	0.36	1.04	1.04	2.03	<99%	no
DE	1.00	0.48	1.86	1.86	3.62	<99%	no
Wet Straining (D)	1.00	-0.09	0.06	0.06	0.12	<99%	no
AD	1.00	-0.20	0.32	0.32	0.63	<99%	no
BD	1.00	0.36	1.04	1.04	2.02	<99%	no
CE	1.00	0.35	0.98	0.98	1.91	<99%	no
CD	1.00	0.09	0.06	0.06	0.13	<99%	no
BE	1.00	0.59	2.75	2.75	5.36	<99%	no
AE	1.00	-0.11	0.10	0.10	0.19	<99%	no
Shrinkage (E)	1.00	-1.49	17.77	17.77	34.61	>99%	yes
Error	16.00		8.21	0.51			
Total	31.00		87.19				

Check	Syy= 157.96	Syy(alg)= 157.96	OK!

Yates Algorithm For Analyzing Effects	
(Experiment Performed in Duplicate)	

Treatment Combination	ZD Stiffness	(1)	(2)	(3)	(4)	Effect	Estimate of Effect	Sum of Squares	Mean Squares
1.000	0.427	0.752	1.470	3.159	6.054	Total			
2.000	0.325	0.718	1.689	2.895	-0.478	A	-0.030	0.014	0.007
3.000	0.393	0.828	1.387	-0.267	0.031	B	0.002	0.000	0.000
4.000	0.325	0.861	1.508	-0.211	0.047	AB	0.003	0.000	0.000
5.000	0.415	0.694	-0.171	-0.001	0.339	C	0.021	0.007	0.004
6.000	0.413	0.693	-0.096	0.032	0.083	AC	0.005	0.000	0.000
7.000	0.477	0.738	-0.109	-0.058	0.099	BC	0.006	0.001	0.000
8.000	0.383	0.770	-0.102	0.105	0.056	DE	0.003	0.000	0.000
9.000	0.365	-0.103	-0.034	0.219	-0.264	D	-0.016	0.004	0.002
10.000	0.329	-0.069	0.032	0.120	0.056	AD	0.004	0.000	0.000
11.000	0.384	-0.002	-0.001	0.075	0.033	BD	0.002	0.000	0.000
12.000	0.310	-0.094	0.033	0.008	0.163	CE	0.010	0.002	0.001
13.000	0.430	-0.036	0.034	0.066	-0.098	CD	-0.006	0.001	0.000
14.000	0.308	-0.074	-0.092	0.033	-0.067	BE	-0.004	0.000	0.000
15.000	0.375	-0.123	-0.038	-0.126	-0.033	AE	-0.002	0.000	0.000
16.000	0.396	0.021	0.144	0.182	0.308	E	0.019	0.006	0.003
							Syy=	0.036	

AOV Table

Source	DF	Effects	SS	MS	F-Ratio	F (1, 16)	Significance (99%)
Freeness (A)	1.000	-0.030	0.007	0.007	65.278	>99%	yes
Jet-to-Wire (B)	1.000	0.002	0.000	0.000	0.272	<99%	no
AB	1.000	0.003	0.000	0.000	0.638	<99%	no
Wet Pressing (C)	1.000	0.021	0.004	0.004	32.811	>99%	yes
AC	1.000	0.005	0.000	0.000	1.952	<99%	no
BC	1.000	0.006	0.000	0.000	2.802	<99%	no
DE	1.000	0.003	0.000	0.000	0.892	<99%	no
Wet Straining (D)	1.000	-0.016	0.002	0.002	19.812	>99%	yes
AD	1.000	0.004	0.000	0.000	0.898	<99%	no
BD	1.000	0.002	0.000	0.000	0.309	<99%	no
CE	1.000	0.010	0.001	0.001	7.609	<99%	no
CD	1.000	-0.006	0.000	0.000	2.768	<99%	no
BE	1.000	-0.004	0.000	0.000	1.292	<99%	no
AE	1.000	-0.002	0.000	0.000	0.309	<99%	no
Shrinkage (E)	1.000	0.019	0.003	0.003	26.981	>99%	yes
Error	16.000		0.002	0.000			
Total	31.000		0.020				

Check	Syy= 0.036	Syy(alg)= 0.036	OK!

Yates Algorithm For Analyzing Effects	
(Experiment Performed in Duplicate)	

Treatment Combination	Apparent Density	(1)	(2)	(3)	(4)	Effect	Estimate of Effect	Sum of Squares	Mean Squares
1.00	1270.49	2431.49	4903.63	10346.07	20578.84	Total			
2.00	1161.00	2472.14	5442.44	10232.77	-866.84	A	-54.18	46963.22	23481.61
3.00	1327.70	2739.85	4903.68	-469.57	15.00	B	0.94	14.06	7.03
4.00	1144.44	2702.59	5329.09	-397.27	-8.24	AB	-0.52	4.24	2.12
5.00	1383.10	2468.50	-292.75	3.39	964.22	C	60.26	58107.51	29053.76
6.00	1356.75	2435.18	-176.82	11.61	163.26	AC	10.20	1665.86	832.93
7.00	1426.53	2642.08	-222.30	-197.89	0.34	BC	0.02	0.01	0.00
8.00	1276.06	2687.01	-174.97	189.65	169.18	DE	10.57	1788.87	894.43
9.00	1286.09	-109.49	40.65	538.81	-113.30	D	-7.08	802.31	401.15
10.00	1182.41	-183.26	-37.26	425.41	72.30	AD	4.52	326.71	163.35
11.00	1276.90	-26.35	-33.32	115.93	8.22	BD	0.51	4.22	2.11
12.00	1158.28	-150.47	44.93	47.33	387.54	CE	24.22	9386.70	4693.35
13.00	1415.93	-103.68	-73.77	-77.91	-113.40	CD	-7.09	803.72	401.86
14.00	1226.15	-118.62	-124.12	78.25	-68.60	BE	-4.29	294.12	147.06
15.00	1336.10	-189.78	-14.94	-50.35	156.16	AE	9.76	1524.12	762.06
16.00	1350.91	14.81	204.59	219.53	269.88	E	16.87	4552.20	2276.10
							Syy=	126237.89	63118.94

AOV Table

Source	DF	Effects	SS	MS	F-Ratio	F (1, 16)	Significance (99%)
Freeness (A)	1.00	-54.18	23481.61	23481.61	109.05	>99%	yes
Jet-to-Wire Ratio (B)	1.00	0.94	7.03	7.03	0.03	<99%	no
AB	1.00	-0.52	2.12	2.12	0.01	<99%	no
Wet Pressing (C)	1.00	60.26	29053.76	29053.76	134.93	>99%	yes
AC	1.00	10.20	832.93	832.93	3.87	<99%	no
BC	1.00	0.02	0.00	0.00	0.00	<99%	no
DE	1.00	10.57	894.43	894.43	4.15	<99%	no
Wet Straining (D)	1.00	-7.08	401.15	401.15	1.86	<99%	no
AD	1.00	4.52	163.35	163.35	0.76	<99%	no
BD	1.00	0.51	2.11	2.11	0.01	<99%	no
CE	1.00	24.22	4693.35	4693.35	21.80	>99%	yes
CD	1.00	-7.09	401.86	401.86	1.87	<99%	no
BE	1.00	-4.29	147.06	147.06	0.68	<99%	no
AE	1.00	9.76	762.06	762.06	3.54	<99%	no
Shrinkage (E)	1.00	16.87	2276.10	2276.10	10.57	>99%	yes
Error	16.00		3445.11	215.32			
Total	31.00		66564.06				

Yates Algorithm For Analyzing Effects	
(Experiment Performed in Duplicate)	

Treatment Combination	Fiber Orientation	(1)	(2)	(3)	(4)	Effect	Estimate of Effect	Sum of Squares	Mean Squares
1.00	5.76	16.11	73.19	134.18	264.73	Total			
2.00	10.35	57.08	60.99	130.55	35.21	A	2.20	77.50	38.75
3.00	27.82	10.98	66.94	18.02	157.89	B	9.87	1558.02	779.01
4.00	29.26	50.01	63.61	17.19	19.65	AB	1.23	24.13	12.06
5.00	4.27	14.96	6.03	80.00	-15.53	C	-0.97	15.08	7.54
6.00	6.71	51.98	11.99	77.89	-0.65	AC	-0.04	0.03	0.01
7.00	20.23	11.37	11.90	3.96	1.91	BC	0.12	0.23	0.11
8.00	29.78	52.24	5.29	15.69	3.51	DE	0.22	0.77	0.39
9.00	7.31	4.59	40.97	-12.20	-3.63	D	-0.23	0.82	0.41
10.00	7.65	1.44	39.03	-3.33	-0.83	AD	-0.05	0.04	0.02
11.00	20.21	2.44	37.02	5.96	-2.11	BD	-0.13	0.28	0.14
12.00	31.77	9.55	40.87	-6.61	11.73	CE	0.73	8.60	4.30
13.00	5.48	0.34	-3.15	-1.94	8.87	CD	0.55	4.91	2.46
14.00	5.89	11.56	7.11	3.85	-12.57	BE	-0.79	9.88	4.94
15.00	23.68	0.41	11.22	10.26	5.79	AE	0.36	2.10	1.05
16.00	28.56	4.88	4.47	-6.75	-17.01	E	-1.06	18.08	9.04
							Syy=	1720.46	

AOV Table

Source	DF	Effects	SS	MS	F-Ratio	F (1, 16)	Significance (99%)
Freeness (A)	1.00	2.20	38.75	38.75	16.05	>99%	yes
Jet-to-Wire Ratio (B)	1.00	9.87	779.01	779.01	322.58	>99%	yes
AB	1.00	1.23	12.06	12.06	4.99	<99%	no
Wet Pressing (C)	1.00	-0.97	7.54	7.54	3.12	<99%	no
AC	1.00	-0.04	0.01	0.01	0.01	<99%	no
BC	1.00	0.12	0.11	0.11	0.05	<99%	no
DE	1.00	0.22	0.39	0.39	0.16	<99%	no
Wet Straining (D)	1.00	-0.23	0.41	0.41	0.17	<99%	no
AD	1.00	-0.05	0.02	0.02	0.01	<99%	no
BD	1.00	-0.13	0.14	0.14	0.06	<99%	no
CE	1.00	0.73	4.30	4.30	1.78	<99%	no
CD	1.00	0.55	2.46	2.46	1.02	<99%	no
BE	1.00	-0.79	4.94	4.94	2.05	<99%	no
AE	1.00	0.36	1.05	1.05	0.43	<99%	no
Shinkage (E)	1.00	-1.06	9.04	9.04	3.74	<99%	no
Error	16.00		38.64	2.41			
Total	31.00		898.87				

Check	Syy=	1720.46	Syy(alg)=	1720.46	OK!

APPENDIX II -- CENTRAL COMPOSITE DATASET

Sample ID	HW/SW Free	J/W	Press	MD Strain	CD Shrinkage	Apparent Density	MD Stiffness	CD Stiffness	ZD Stiffness	Fiber Orientation Ratio
	(ml)		(bars)	(%)	(%)	(kg/m^3)	(km^2/s^2)	(km^2/s^2)	(km/s)^2	
1-1	-1	-1.00	-1	-1	-1	536.212	12.258	6.686	0.444	2.762
1-2	-1	-1.00	-1	-1	-1	537.359	11.940	6.301	0.442	2.796
2-1	1	-1.00	-1	-1	-1	442.657	9.796	5.796	0.241	1.988
2-2	1	-1.00	-1	-1	-1	442.657	9.796	5.796	0.241	1.988
3-1	-1	1.00	-1	-1	-1	537.796	16.275	4.368	0.388	13.072
3-2	-1	1.00	-1	-1	-1	545.673	16.210	4.545	0.385	10.180
4-1	1	1.00	-1	-1	-1	503.653	15.369	3.570	0.293	13.500
4-2	1	1.00	-1	-1	-1	509.591	15.189	3.186	0.310	15.420
5-1	-1	-1.00	1	-1	-1	560.296	13.063	6.620	0.442	2.184
5-2	-1	-1.00	1	-1	-1	563.028	12.460	7.099	0.436	2.483
6-1	1	-1.00	1	-1	-1	511.073	11.561	6.569	0.314	2.556
6-2	1	-1.00	1	-1	-1	499.009	11.181	6.037	0.322	3.104
7-1	-1	1.00	1	-1	-1	546.345	17.179	4.361	0.400	12.406
7-2	-1	1.00	1	-1	-1	551.605	17.534	4.500	0.405	13.160
8-1	1	1.00	1	-1	-1	509.620	15.964	3.436	0.330	12.920
8-2	1	1.00	1	-1	-1	507.717	15.382	3.846	0.321	11.518
9-1	-1	-1.00	-1	1	-1	519.063	13.881	7.049	0.386	2.646
9-2	-1	-1.00	-1	1	-1	510.355	13.614	6.931	0.364	2.548
10-1	1	-1.00	-1	1	1	448.668	13.300	8.595	0.211	2.556
10-2	1	-1.00	-1	1	1	450.565	14.110	8.224	0.203	2.594
11-1	-1	1.00	-1	1	-1	506.542	17.715	4.358	0.341	13.638
11-2	-1	1.00	-1	1	-1	516.607	17.776	4.190	0.348	15.380
12-1	1	1.00	-1	1	-1	432.178	17.465	2.624	0.212	12.232
12-2	1	1.00	-1	1	-1	448.567	16.699	3.120	0.231	13.175
13-1	-1	-1.00	1	1	-1	538.613	13.186	7.559	0.393	2.118
13-2	-1	-1.00	1	1	-1	539.720	13.648	7.510	0.394	1.948
14-1	1	1.00	1	1	-1	512.167	18.340	4.241	0.309	12.378
14-2	1	1.00	1	1	-1	532.935	17.952	3.547	0.339	12.600
15-1	-1	1.00	1	1	-1	528.224	19.138	4.385	0.339	13.343
15-2	-1	1.00	1	1	1	532.360	18.700	4.643	0.356	15.860

Sample ID	HW/SW Free	J/W	Press	MD Strain	CD Shrinkage	Apparent Density	MD Stiffness	CD Stiffness	ZD Stiffness	Fiber Orientation Ratio
	(ml)		(bars)	(%)	(%)	(kg/m^3)	(km^2/s^2)	(km^2/s^2)	(km/s)^2	
16-1	1	1.00	1	1	-1	494.844	17.143	3.749	0.262	13.008
16-2	1	1.00	1	1	-1	477.169	18.357	3.289	0.248	15.620
17-1	0	0.00	0	0	-1	509.077	16.469	4.866	0.300	9.634
17-2	0	0.00	0	0	-1	506.792	15.684	4.475	0.292	9.160
18-1	0	0.00	0	0	-1	505.649	16.119	4.668	0.296	9.288
18-2	0	0.00	0	0	-1	513.462	15.717	4.570	0.296	9.186
19-1	0	0.00	0	0	-1	515.495	15.492	4.984	0.350	9.763
19-2	0	0.00	0	0	-1	521.445	15.731	5.143	0.357	8.622
20-1	0	0.00	0	0	-1	513.177	15.049	5.177	0.350	6.998
20-2	0	0.00	0	0	1	502.577	15.760	7.125	0.343	6.778
21-1	0	0.00	0	0	-1	529.476	14.669	5.192	0.353	8.102
21-2	0	0.00	0	0	-1	522.478	14.909	5.034	0.326	7.926
22-1	0	0.00	0	0	-1	521.262	16.102	4.364	0.353	9.340
22-2	0	0.00	0	0	-1	519.154	16.104	4.196	0.344	11.256
23-1	0	0.00	0	0	-1	514.857	15.969	4.615	0.329	12.124
23-2	0	0.00	0	0	-1	517.988	15.681	4.553	0.334	11.220
24-1	-2	0.00	0	0	-1	564.374	18.657	5.218	0.389	9.794
24-2	-2	0.00	0	0	-1	570.636	18.285	5.449	0.377	6.962
25-1	2	0.00	0	0	-1	481.085	14.812	3.297	0.226	9.183
25-2	2	0.00	0	0	-1	471.256	14.942	3.649	0.223	9.023
26-1	0	-1.23	0	0	-1	515.502	11.967	7.369	0.330	1.457
26-2	0	-1.23	0	0	-1	510.726	12.200	7.554	0.329	1.447
27-1	0	2.00	0	0	-1	522.134	16.352	4.037	0.361	15.412
27-2	0	2.00	0	0	-1	524.925	16.438	3.865	0.342	13.600
28-1	0	0.00	-2	0	-1	477.939	15.659	4.342	0.286	7.358
28-2	0	0.00	-2	0	-1	468.656	15.249	4.159	0.276	9.518
29-1	0	0.00	2	0	1	529.201	16.150	6.201	0.341	7.926
29-2	0	0.00	2	0	1	521.314	16.441	6.151	0.311	7.682
30-1	0	0.00	0	-2	1	504.640	15.022	6.233	0.347	7.400
30-2	0	0.00	0	-2	1	504.501	15.617	6.109	0.338	7.464
31-1	0	0.00	0	2	1	494.591	18.087	6.795	0.297	6.978
31-2	0	0.00	0	2	1	485.892	18.663	6.682	0.295	7.190

Sample ID	HW/SW Free	J/W	Press	MD Strain	CD Shrinkage	Apparent Density	MD Stiffness	CD Stiffness	ZD Stiffness	Fiber Orientation Ratio
	(ml)		(bars)	(%)	(%)	(kg/m^3)	(km^2/s^2)	(km^2/s^2)	(km/s)^2	
32-1	-1	-1.00	-1	-1	1	482.734	11.805	10.054	0.305	1.483
32-2	-1	-1.00	-1	-1	1	486.766	12.425	9.879	0.296	1.826
33-1	1	-1.00	-1	-1	1	465.732	11.943	9.440	0.253	2.106
33-2	1	-1.00	-1	-1	1	462.735	11.512	9.517	0.248	1.694
34-1	-1	1.00	-1	-1	1	496.137	15.805	6.183	0.324	9.064
34-2	-1	1.00	-1	-1	1	506.633	15.801	6.418	0.347	9.968
35-1	1	1.00	-1	-1	1	490.316	16.559	5.483	0.282	10.894
35-2	1	1.00	-1	-1	1	479.371	16.441	5.330	0.311	10.372
36-1	-1	-1.00	1	-1	1	516.472	13.030	9.667	0.353	2.204
36-2	-1	-1.00	1	-1	1	507.681	12.905	9.280	0.393	2.082
37-1	1	-1.00	1	-1	1	464.826	12.620	8.366	0.255	2.323
37-2	1	-1.00	1	-1	1	466.520	12.365	8.770	0.260	1.840
38-1	-1	1.00	1	-1	1	513.419	16.436	6.395	0.376	10.770
38-2	-1	1.00	1	-1	1	502.538	15.570	6.326	0.359	10.486
39-1	1	1.00	1	-1	1	503.926	17.508	5.585	0.326	9.828
39-2	1	1.00	1	-1	1	503.156	16.599	5.739	0.335	9.160
40-1	-1	-1.00	-1	1	1	485.683	15.520	8.895	0.288	2.660
40-2	-1	-1.00	-1	1	1	485.771	15.122	8.855	0.281	2.348
41-1	1	-1.00	-1	1	1	419.398	13.126	8.003	0.210	2.593
41-2	1	-1.00	-1	1	1	434.244	13.187	8.514	0.212	2.570
42-1	-1	1.00	-1	1	1	474.108	17.855	5.701	0.297	10.766
42-2	-1	1.00	-1	1	1	470.466	18.927	5.580	0.262	9.498
43-1	1	1.00	-1	1	1	398.660	17.440	4.506	0.171	10.224
43-2	1	1.00	-1	1	1	455.278	17.729	5.365	0.235	11.580
44-1	-1	-1.00	1	1	1	495.320	14.842	9.336	0.293	2.658
44-2	-1	-1.00	1	1	1	506.056	14.865	9.426	0.336	2.504
45-1	1	-1.00	-1	1	1	436.014	12.161	8.896	0.214	1.520
45-2	1	-1.00	-1	1	1	449.591	12.546	8.790	0.213	1.650
46-1	-1	1.00	1	1	1	501.982	17.794	6.784	0.340	9.214
46-2	-1	1.00	1	1	1	502.331	18.176	6.463	0.338	10.144
47-1	1	1.00	1	1	1	501.428	19.505	5.663	0.287	11.360
47-2	1	1.00	1	1	1	530.266	19.487	5.212	0.324	11.068

Sample ID	HW/SW Free	J/W	Press	MD Strain	CD Shrinkage	Apparent Density	MD Stiffness	CD Stiffness	ZD Stiffness	Fiber Orientation Ratio
	(ml)		(bars)	(%)	(%)	(kg/m^3)	(km^2/s^2)	(km^2/s^2)	(km/s)^2	
48-1	0	0.00	0	0	1	524.194	16.954	6.165	0.332	8.934
48-2	0	0.00	0	0	1	522.313	17.161	6.063	0.310	9.062
49-1	0	0.00	0	0	1	508.464	17.351	6.284	0.302	6.372
49-2	0	0.00	0	0	1	515.069	16.985	6.003	0.302	10.796
50-1	0	0.00	0	0	1	502.486	14.393	6.524	0.282	9.376
50-2	0	0.00	0	0	1	512.624	15.304	6.260	0.299	7.486
51-1	0	0.00	0	0	1	506.549	15.917	6.497	0.275	9.134
51-2	0	0.00	0	0	1	504.026	15.279	6.802	0.276	7.744
52-1	0	0.00	0	0	-1	511.113	15.029	4.421	0.324	8.178
52-2	0	0.00	0	0	-1	514.167	15.084	4.926	0.344	10.066
53-1	0	0.00	0	0	1	497.821	17.819	5.519	0.304	9.310
53-2	0	0.00	0	0	1	490.931	17.429	5.999	0.294	8.982
54-1	0	0.00	0	0	1	505.420	17.445	6.091	0.298	8.028
54-2	0	0.00	0	0	1	521.357	17.174	6.175	0.324	7.400
55-1	-2	0.00	0	0	1	552.731	19.113	6.770	0.368	7.884
55-2	-2	0.00	0	0	1	554.875	19.528	7.095	0.368	7.238
56-1	2	0.00	0	0	1	469.021	16.407	5.251	0.202	7.208
56-2	2	0.00	0	0	1	457.920	16.850	5.460	0.193	7.604
57-1	0	-1.23	0	0	1	506.344	13.053	10.259	0.293	1.580
57-2	0	-1.23	0	0	1	507.108	12.635	10.048	0.293	1.588
58-1	0	2.00	0	0	1	510.862	17.173	5.500	0.313	11.833
58-2	0	2.00	0	0	1	503.213	17.558	5.316	0.302	13.180
59-1	0	0.00	-2	0	1	457.421	15.319	6.156	0.248	8.478
59-2	0	0.00	-2	0	1	444.204	14.359	5.932	0.234	7.690
60-1	0	0.00	2	0	1	512.422	18.149	6.255	0.281	9.848
60-2	0	0.00	2	0	1	511.817	17.661	6.066	0.281	7.536
61-1	0	0.00	0	-2	1	497.958	14.211	6.642	0.321	7.294
61-2	0	0.00	0	-2	1	506.452	13.766	6.664	0.319	7.812
62-1	0	0.00	0	2	1	500.112	18.714	6.546	0.285	8.074
62-2	0	0.00	0	2	1	492.382	18.268	6.457	0.269	8.894

APPENDIX III -- FLEISCHMAN DATA

	JW Ratio	Pressing	Wet-Straining	C11	C22	C33	AD
Sample ID				(km^2/s^2)	(km^2/s^2)	(km/s)^2	(kg/m^3)
240	0	1	1	16.60	2.78	0.07	728
241	0	-1	-1	12.45	3.89	0.15	733
242	0	-1	1	14.68	2.37	0.06	658
243	1	-1	0	13.52	3.21	0.10	690
244	1	0	0	15.34	3.31	0.18	744
245	1	-1	-1	12.25	3.70	0.14	726
246	-1	-1	0	10.98	5.18	0.09	682
247	-1	1	0	12.20	5.78	0.12	753
248	-1	0	-1	10.06	6.16	0.14	741
250	0	1	0	16.16	3.71	0.13	783
251	0	-1	0	13.85	3.35	0.10	691
252	1	1	0	16.60	3.56	0.13	798
253	1	1	-1	14.55	4.17	0.21	832
254	1	-1	1	14.35	2.38	0.06	644
255	-1	0	0	11.27	5.50	0.10	708
256	-1	1	1	12.55	4.80	0.06	691
257	-1	1	-1	10.68	6.32	0.17	787
258	-1	-1	1	10.83	4.32	0.06	631
259	-1	-1	-1	9.67	5.67	0.13	708
260	-1	0	1	11.86	4.72	0.06	670
261	0	1	-1	14.33	4.53	0.20	827
263	0	0	-1	13.17	4.23	0.17	777
264	0	0	0	15.35	3.48	0.13	760
265	0	0	1	15.64	2.65	0.07	699
267	1	1	1	16.71	2.67	0.07	717
268	1	0	-1	13.62	3.97	0.20	781
269	1	0	1	15.32	2.61	0.07	680
279	1	-1	-1	13.08	3.83	0.16	745
280	1	-1	1	14.72	2.49	0.06	657
281	1	1	-1	14.53	4.30	0.21	835
283	1	1	1	16.81	2.80	0.07	723
284	-1	-1	1	10.83	4.42	0.06	635
285	-1	1	1	12.45	4.97	0.07	705
286	-1	-1	-1	9.32	5.71	0.13	703
287	-1	1	-1	10.90	6.40	0.17	793

APPENDIX IV -- FIBER ORIENTATION POLAR PLOTS

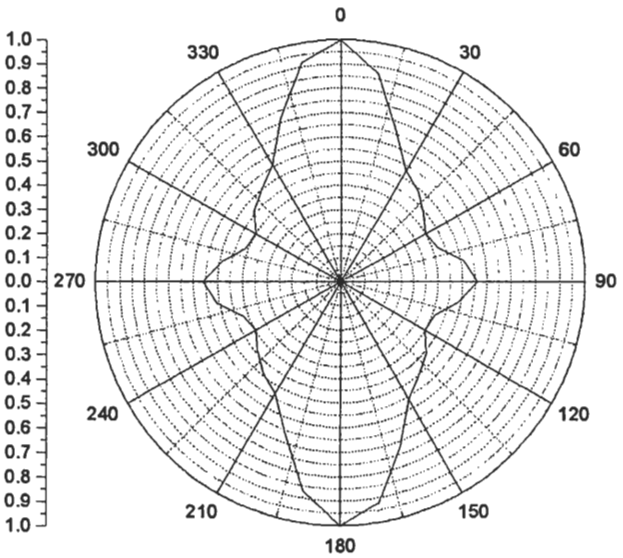

Sample 1-1

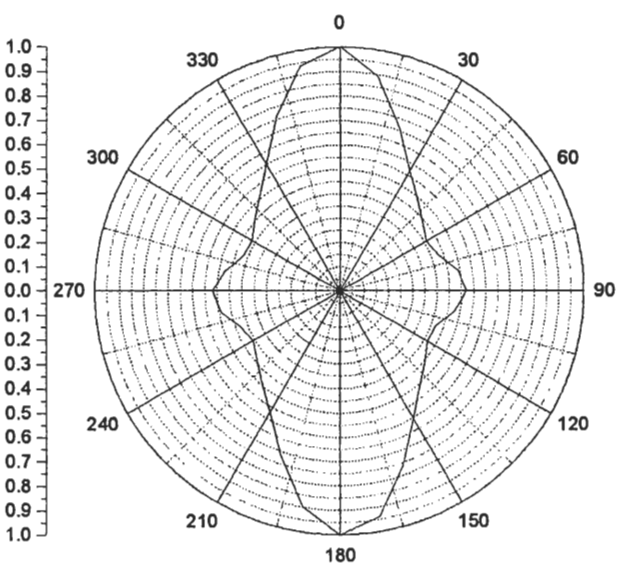

Sample 2-1

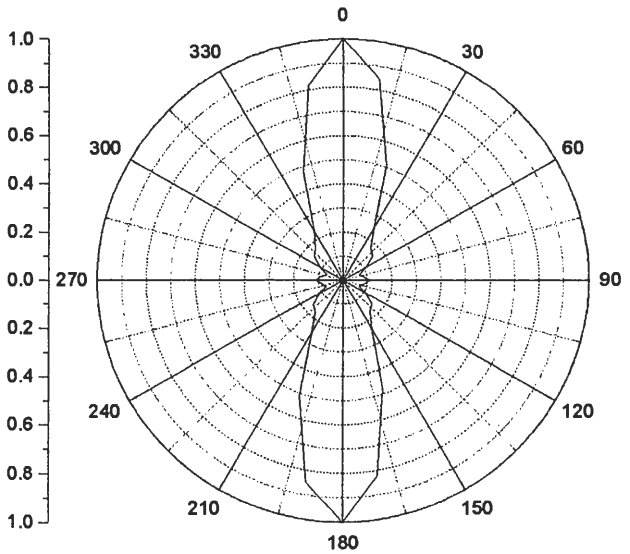

Sample 3-1

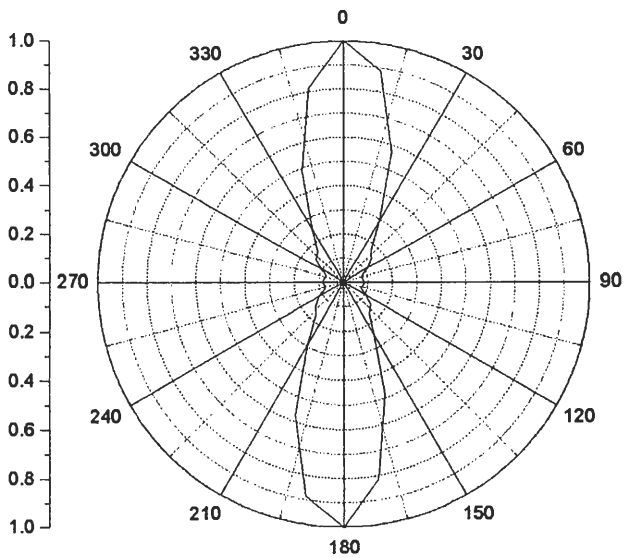

Sample 4-1

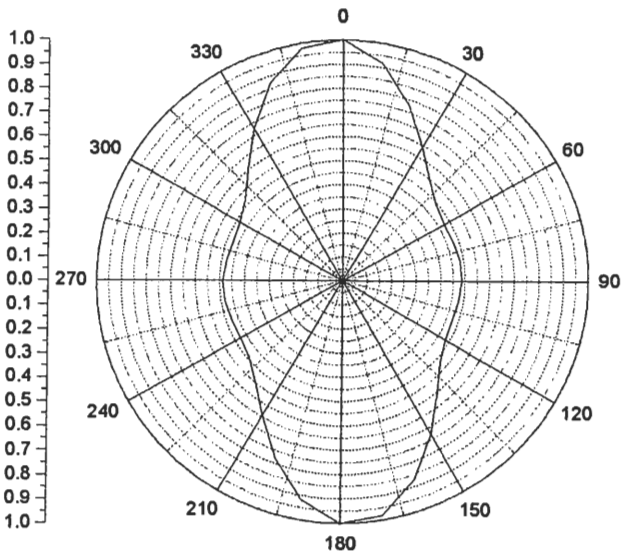

Sample 5-1

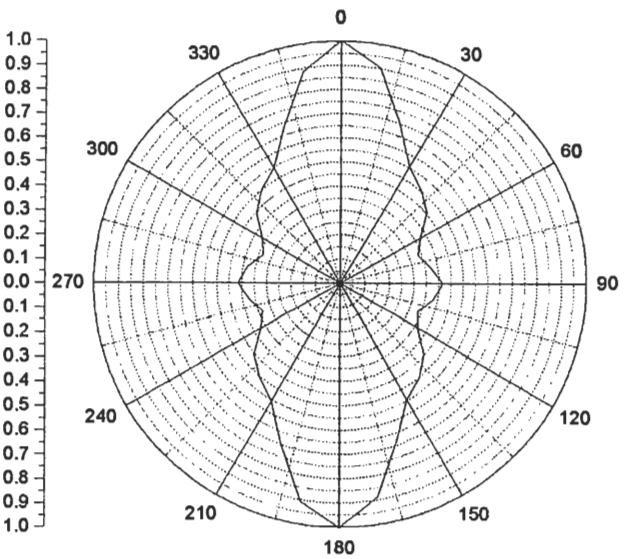

Sample 6-1

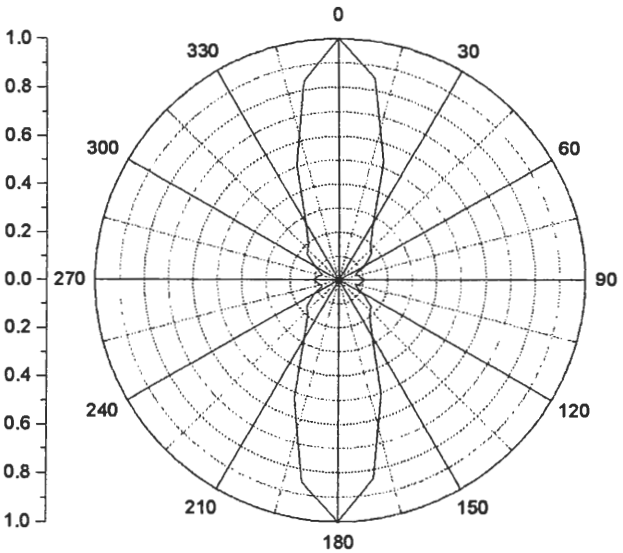

Sample 7-1

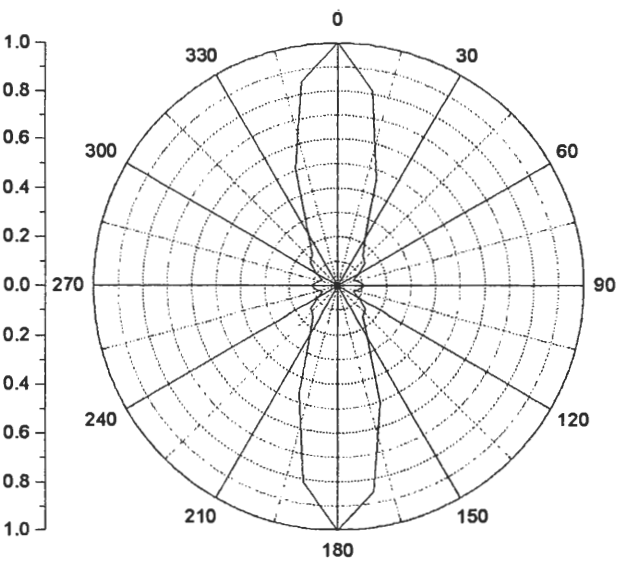

Sample 8-1

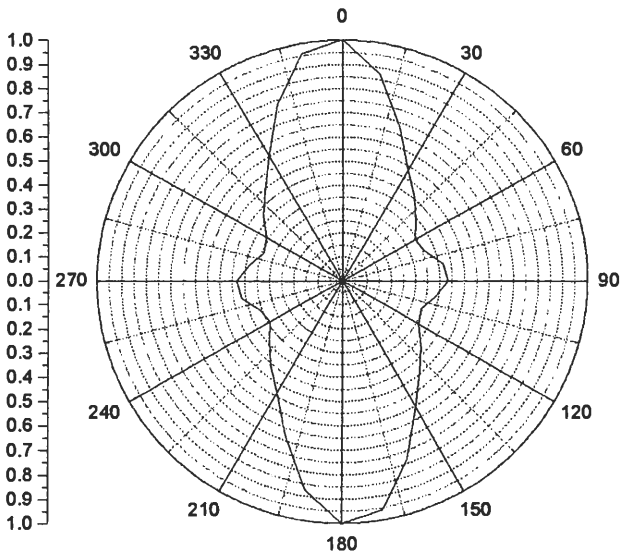

Sample 9-1

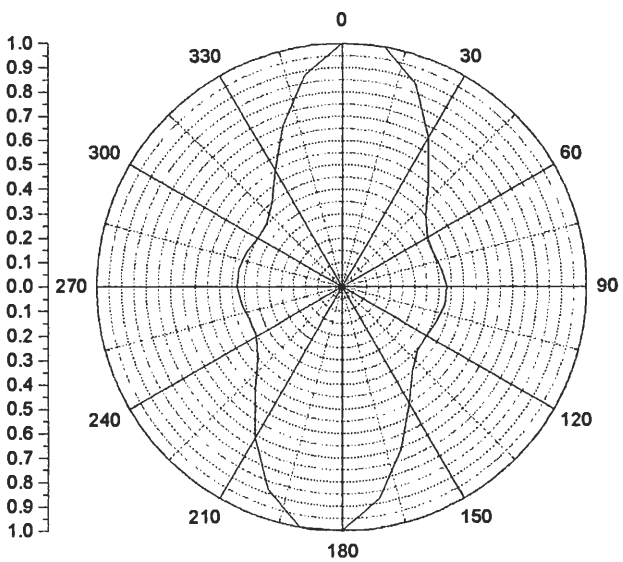

Sample 10-1

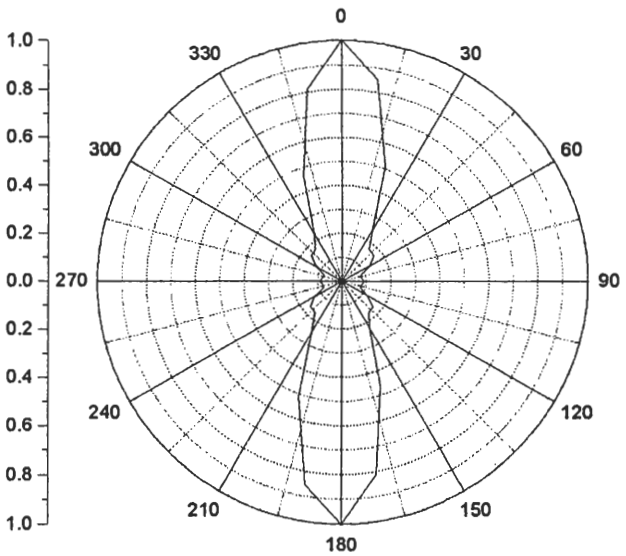

Sample 11-1

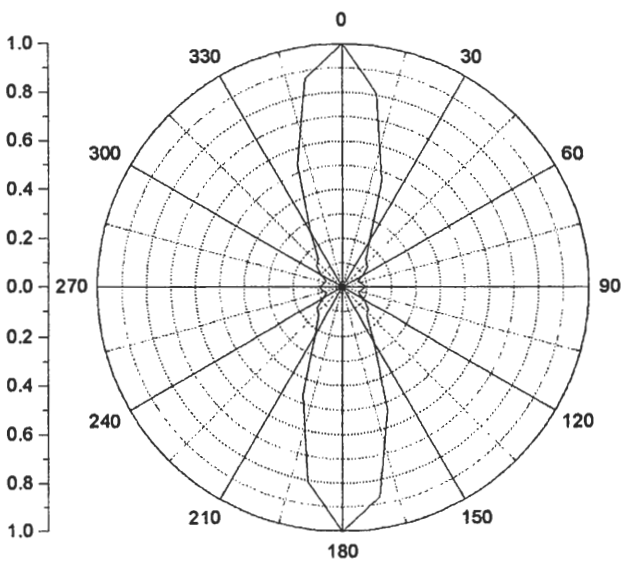

Sample 12-1

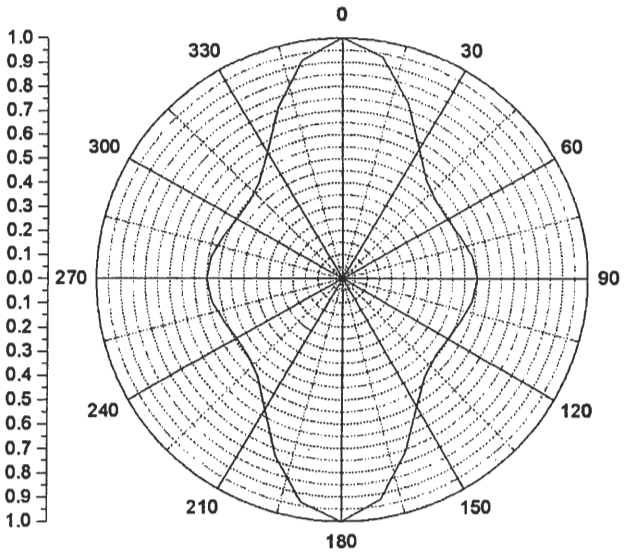

Sample 13-1

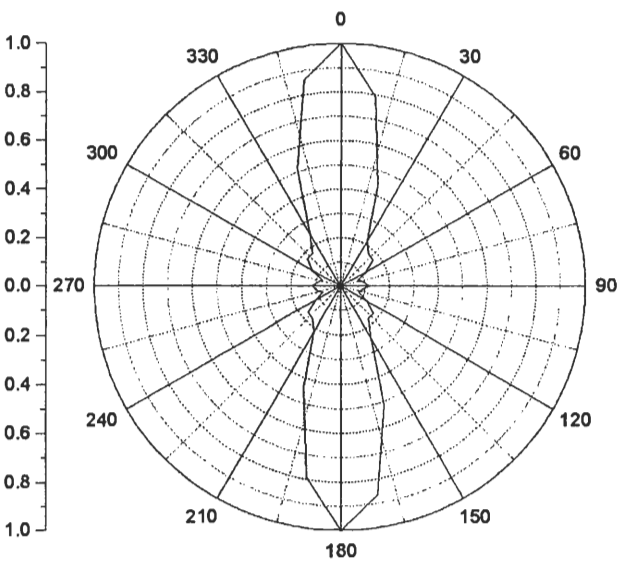

Sample 14-1

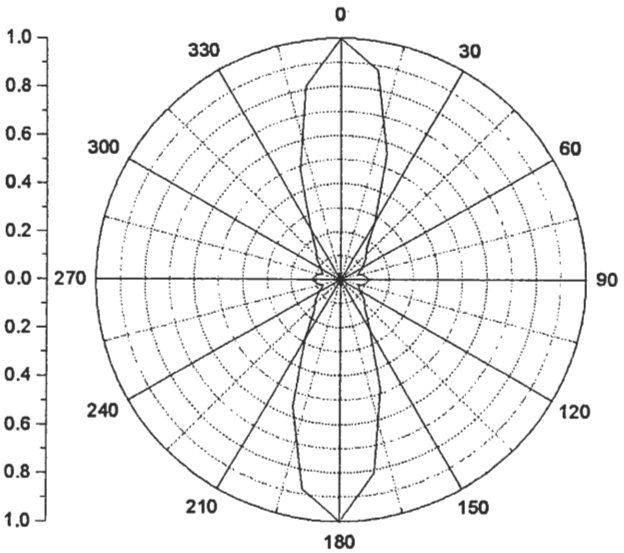

Sample 15-1

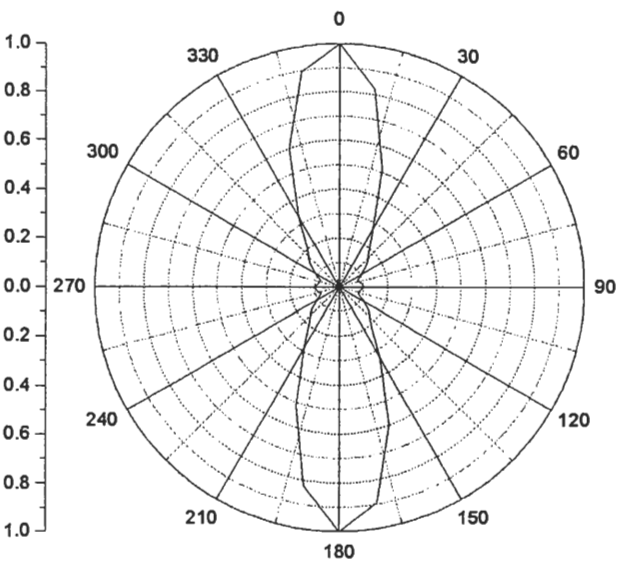

Sample 16-1

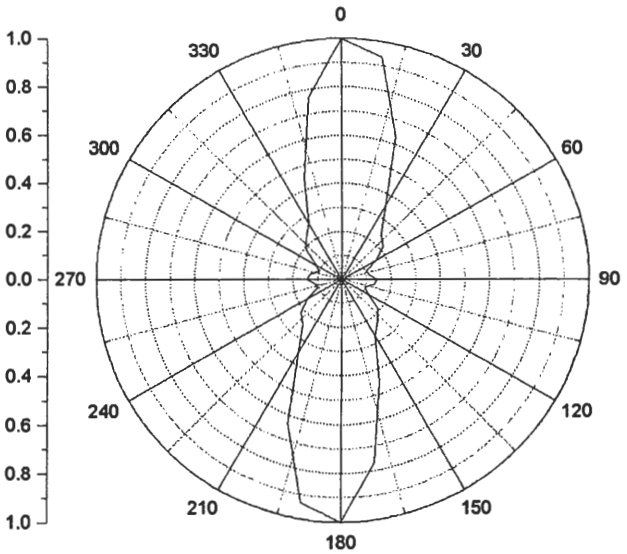

Sample 17-1

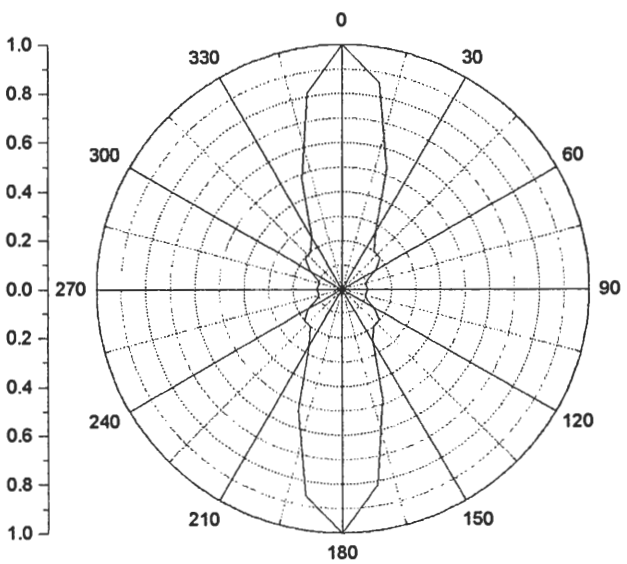

Sample 18-1

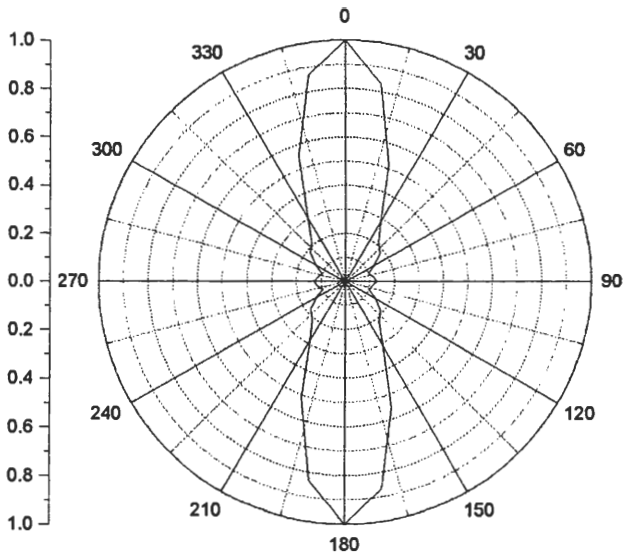

Sample 19-1

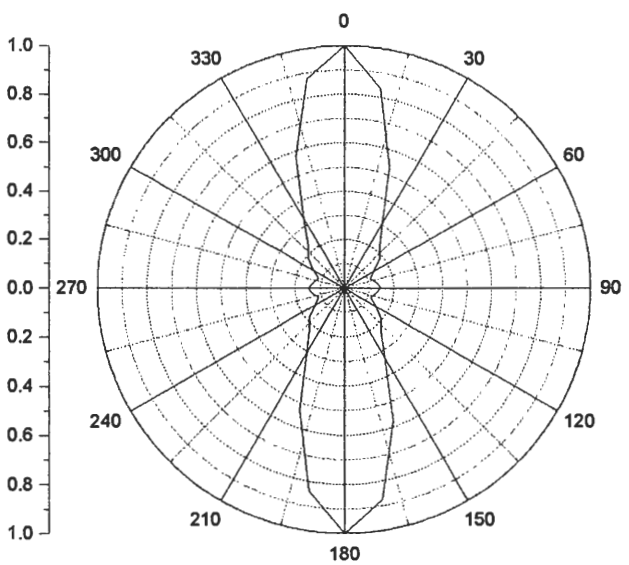

Sample 20-1

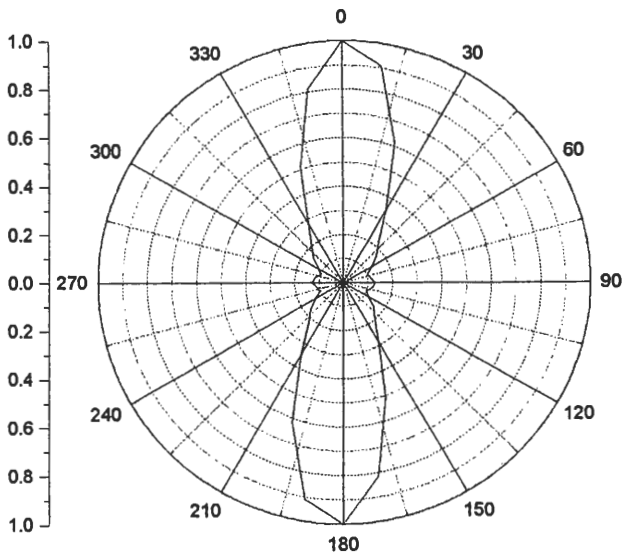

Sample 21-1

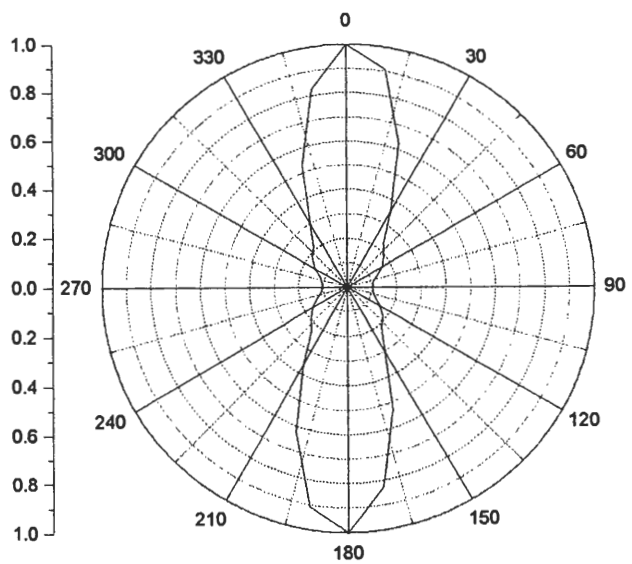

Sample 22-1

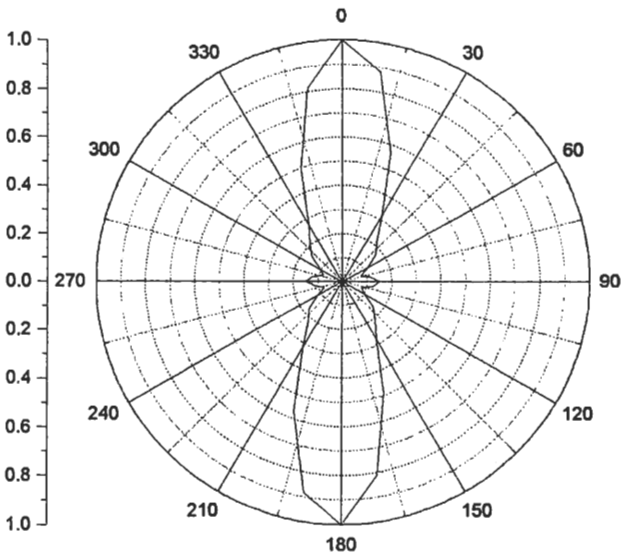

Sample 23-1

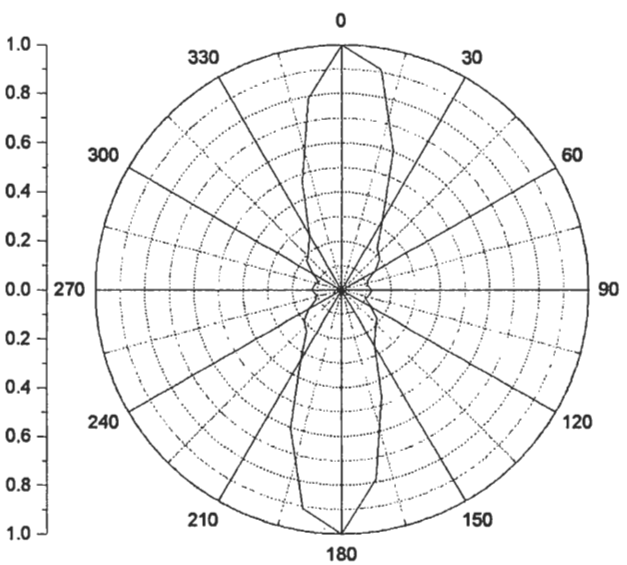

Sample 24-1

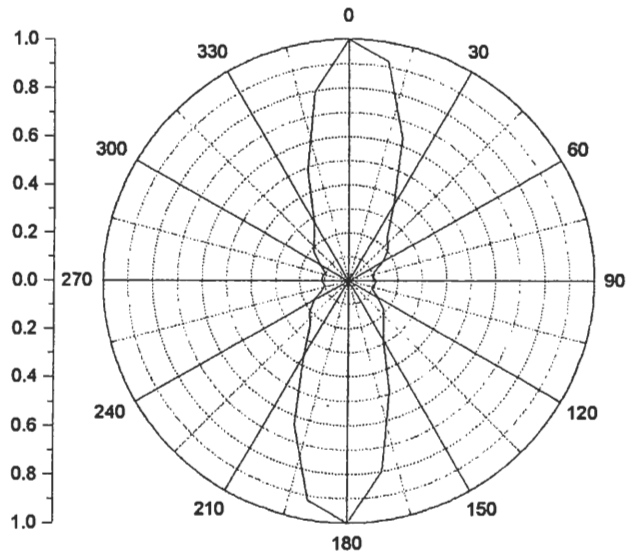

Sample 25-1

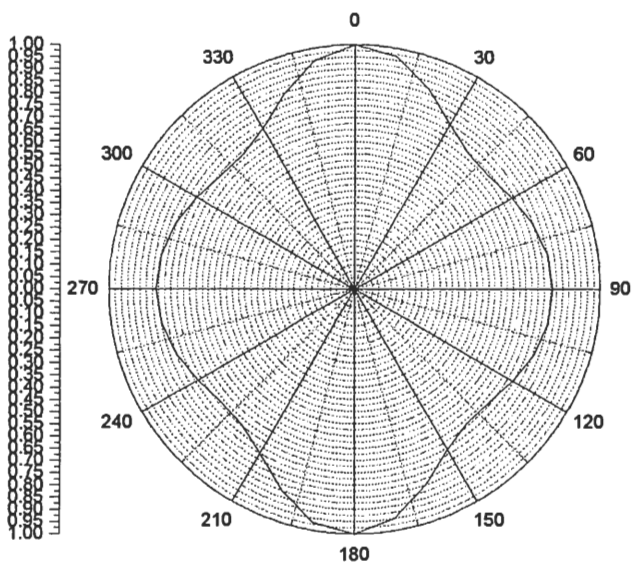

Sample 26-2

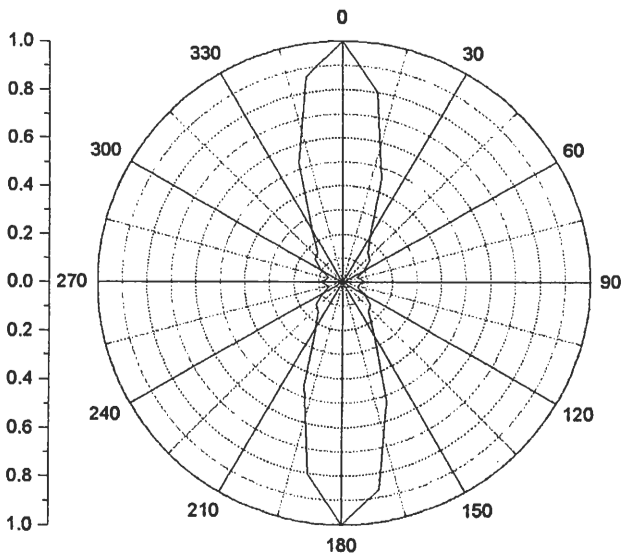

Sample 27-1

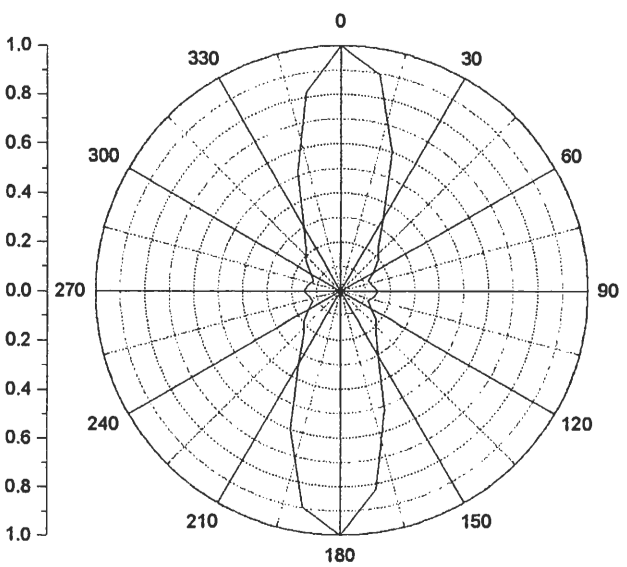

Sample 28-1

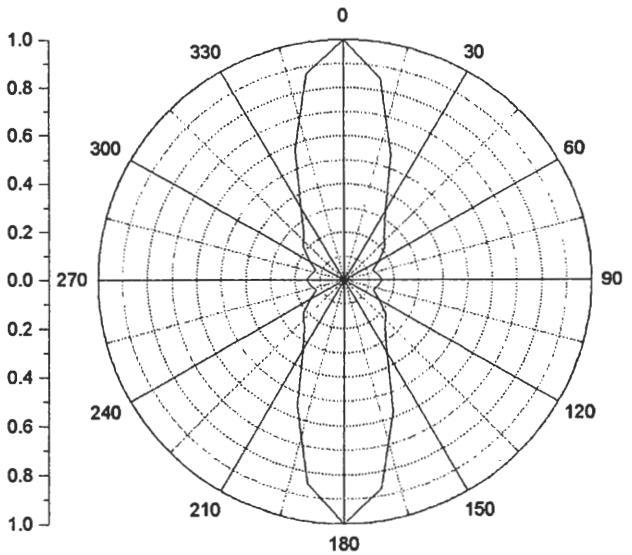

Sample 29-1

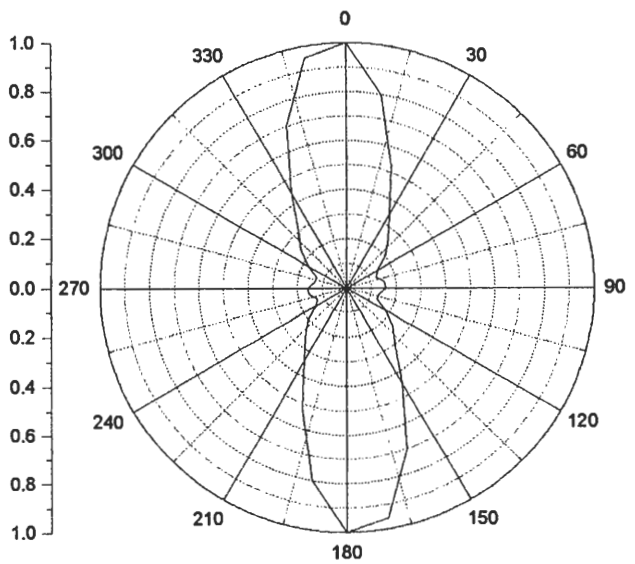

Sample 30-1

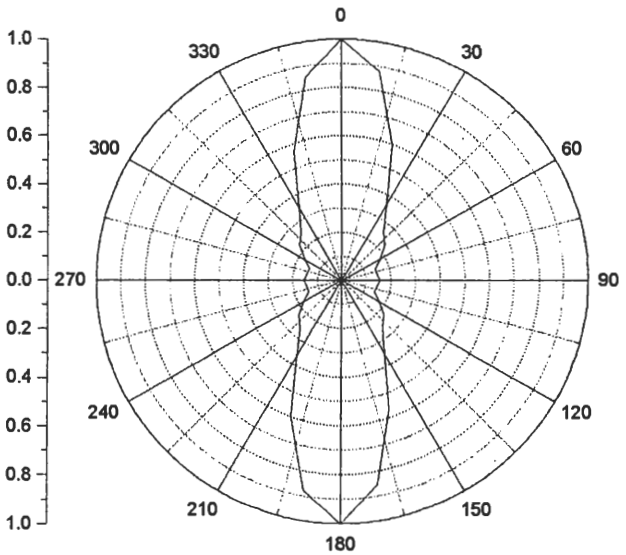

Sample 31-1

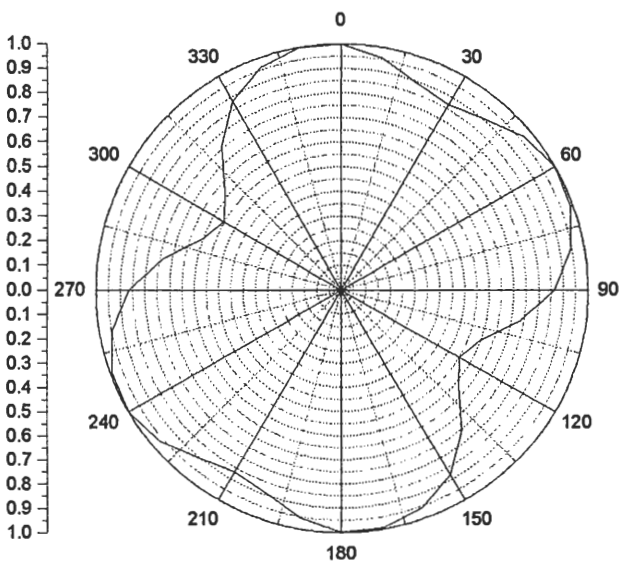

Sample 32-1

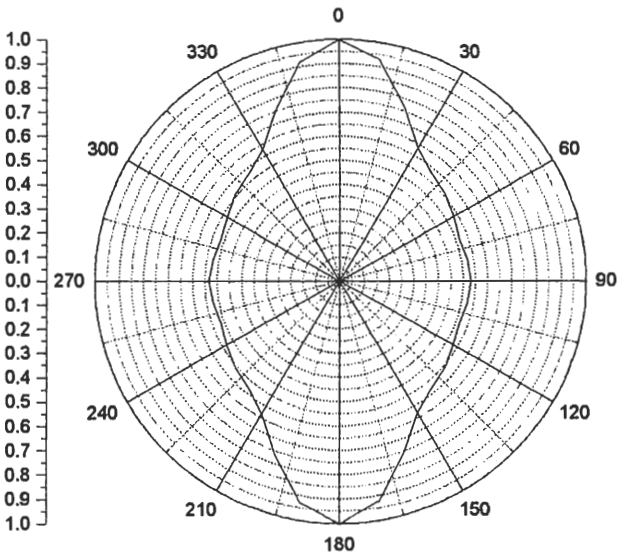

Sample 33-1

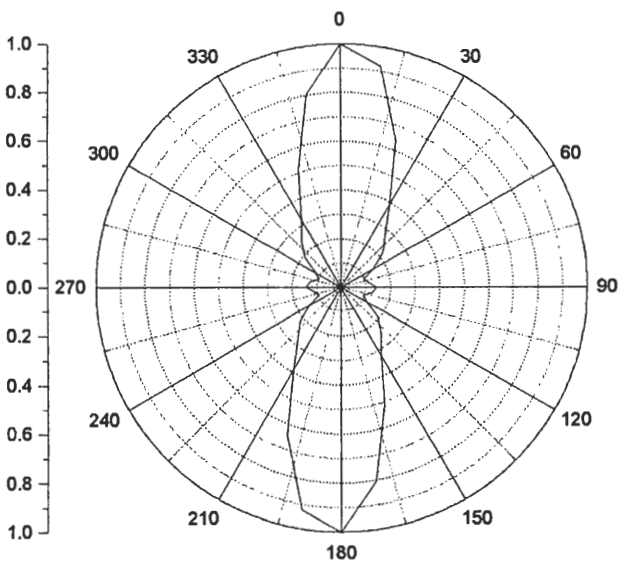

Sample 34-1

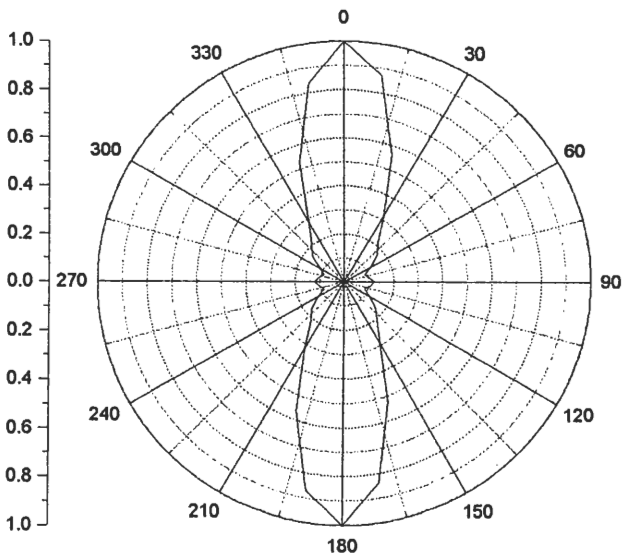

Sample 35-1

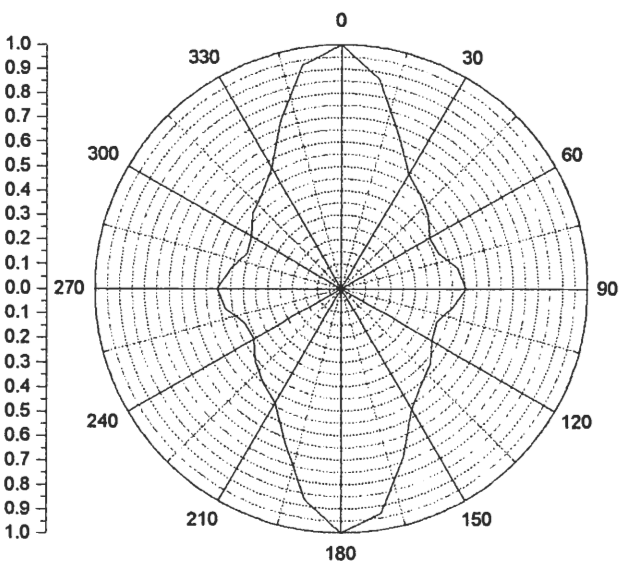

Sample 36-1

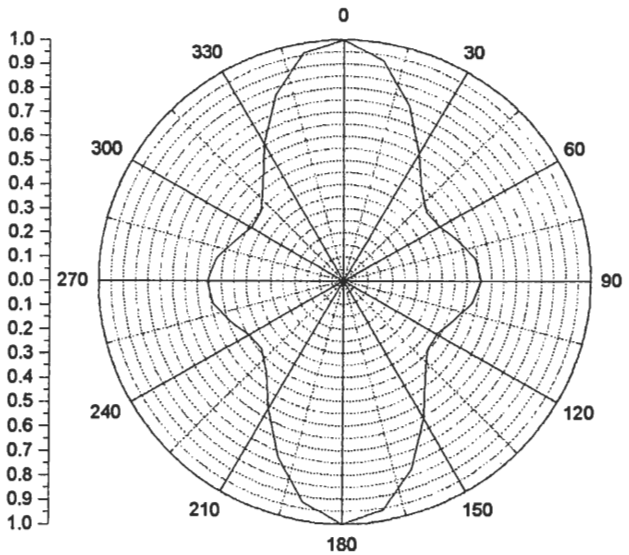

Sample 37-1

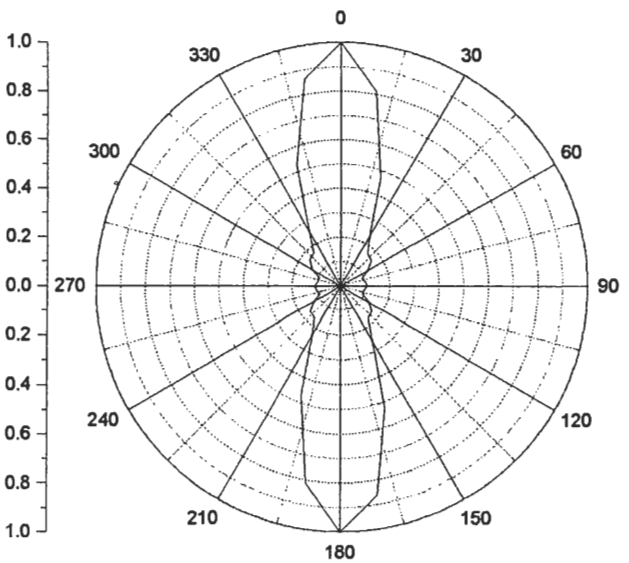

Sample 38-1

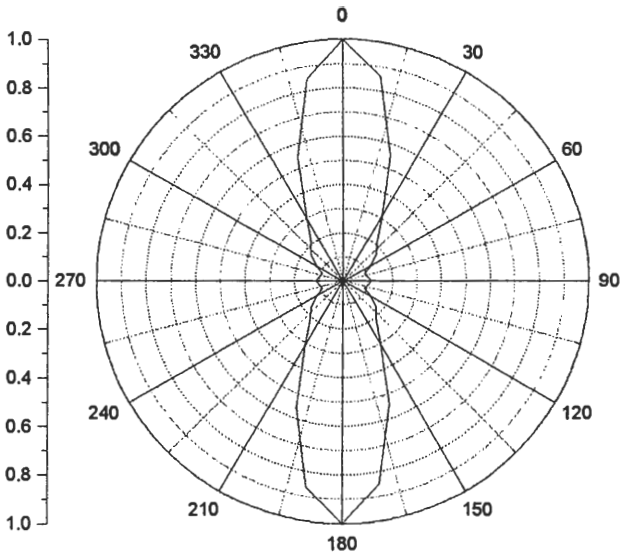

Sample 39-1

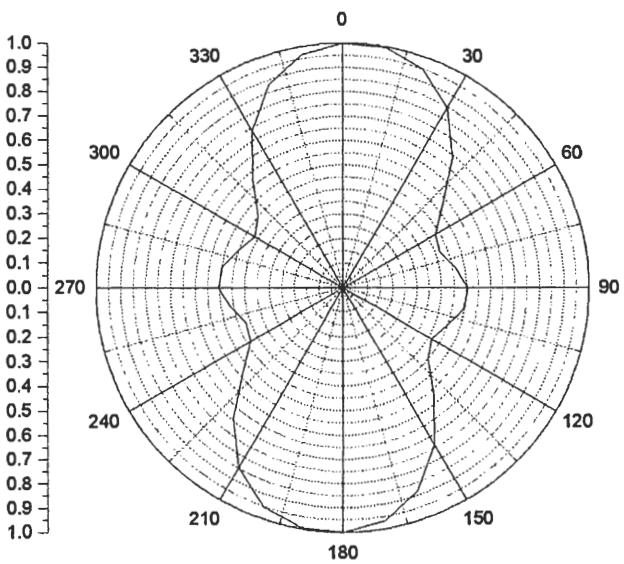

Sample 40-2

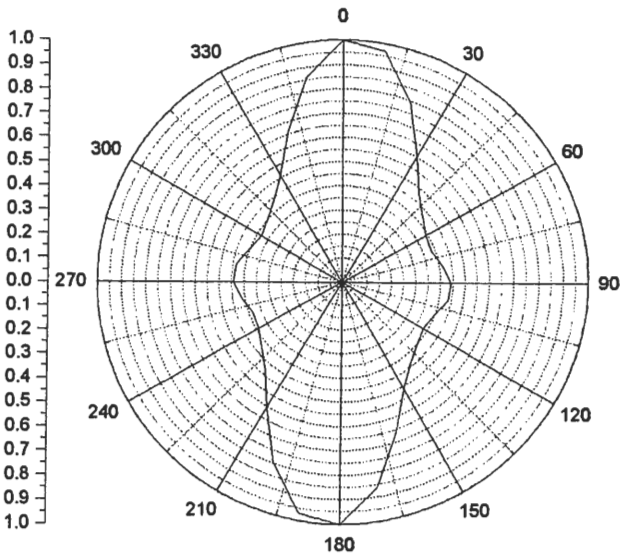

Sample 41-1

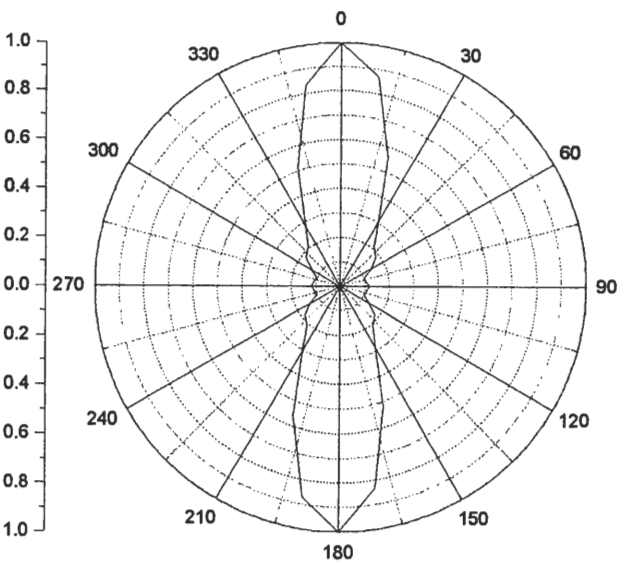

Sample 42-1

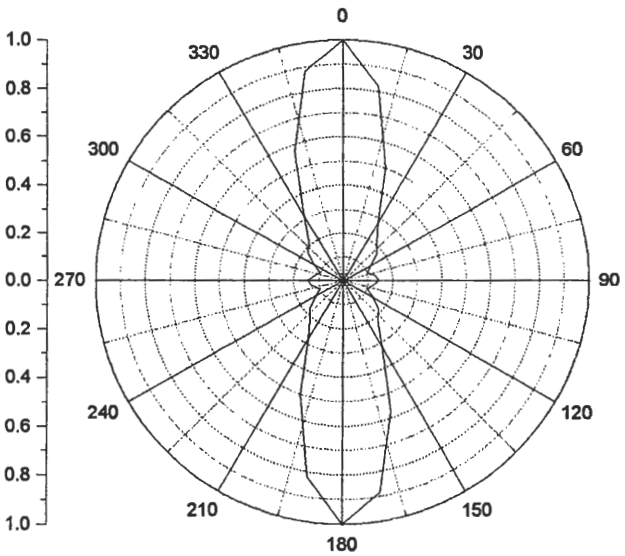

Sample 43-1

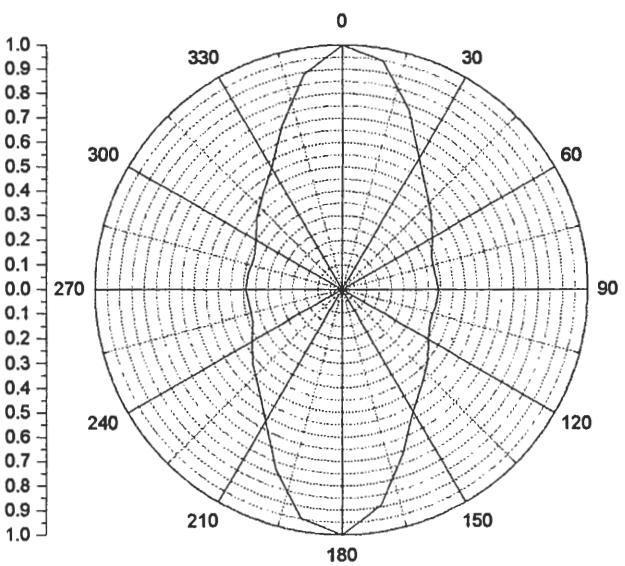

Sample 44-1

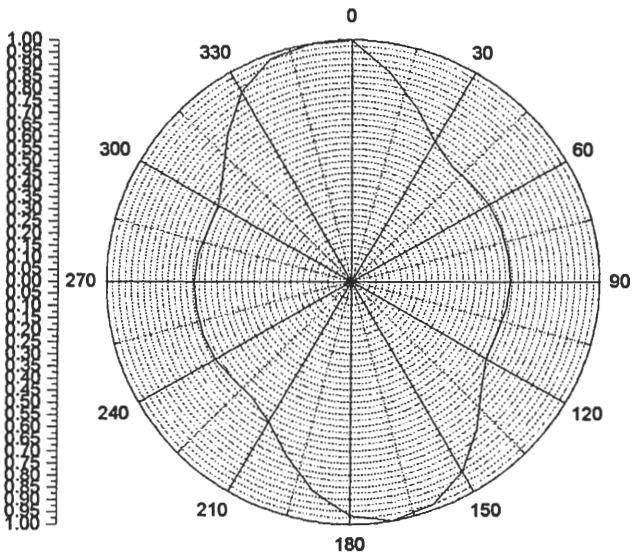

Sample 45-1

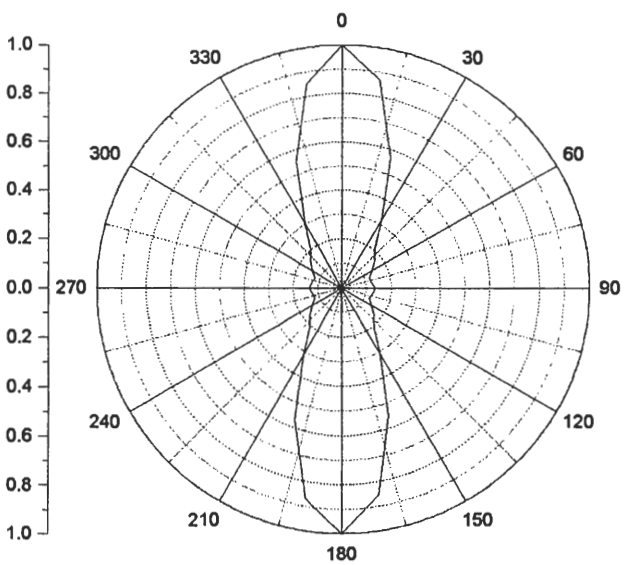

Sample 46-1

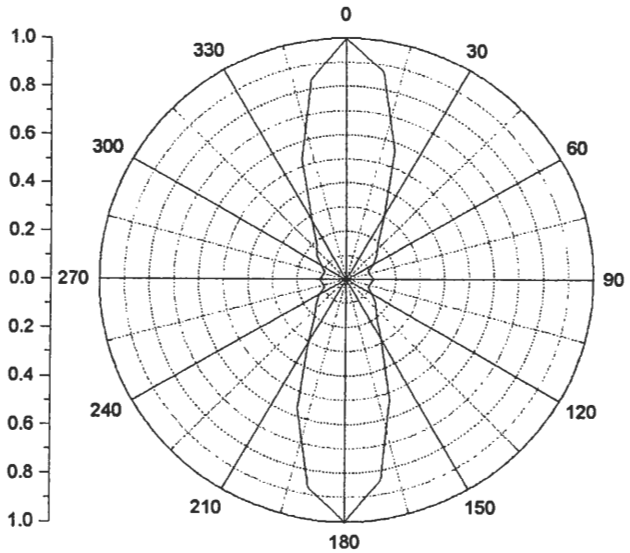

Sample 47-1

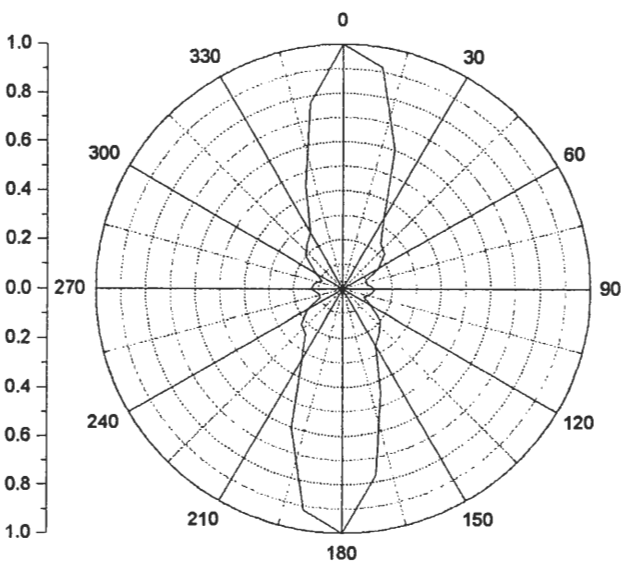

Sample 48-1

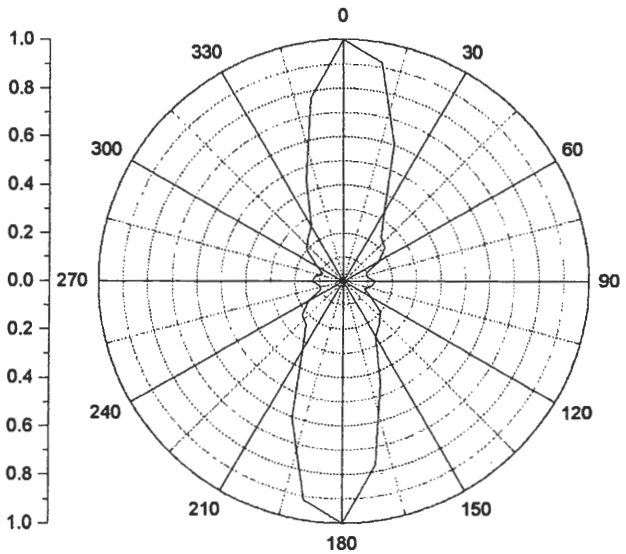

Sample 49-1

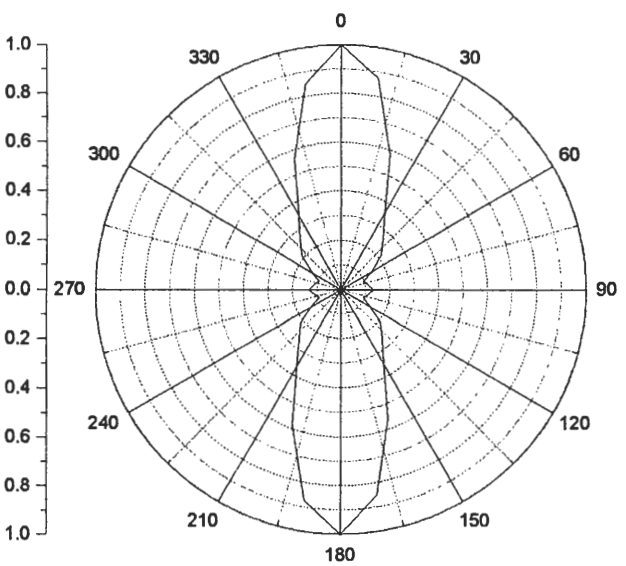

Sample 50-1

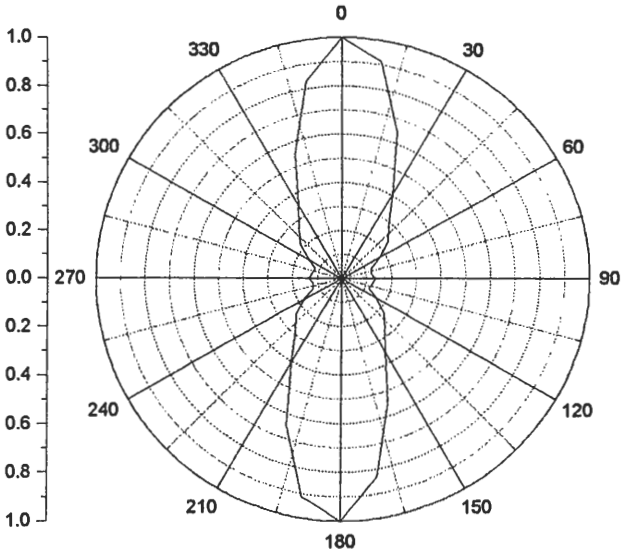

Sample 51-1

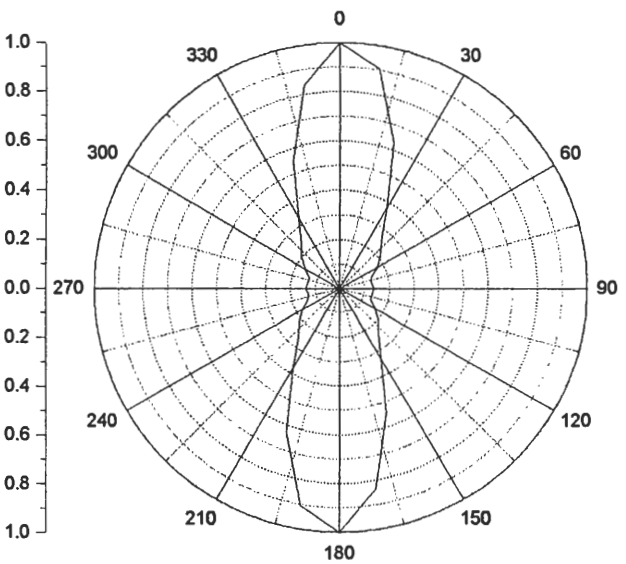

Sample 52-1

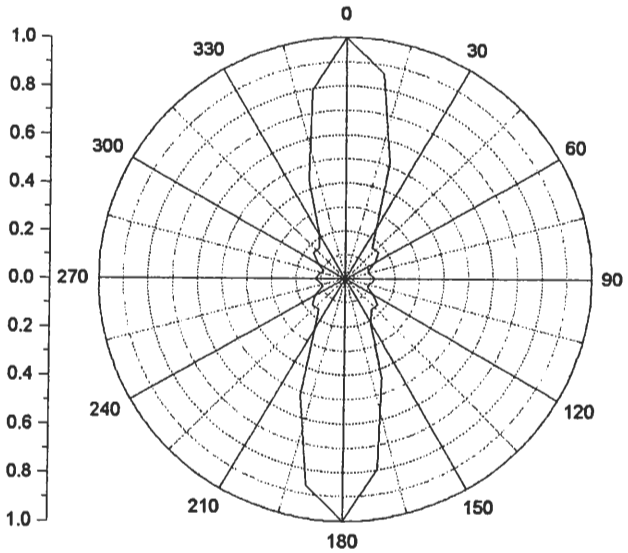

Sample 53-1

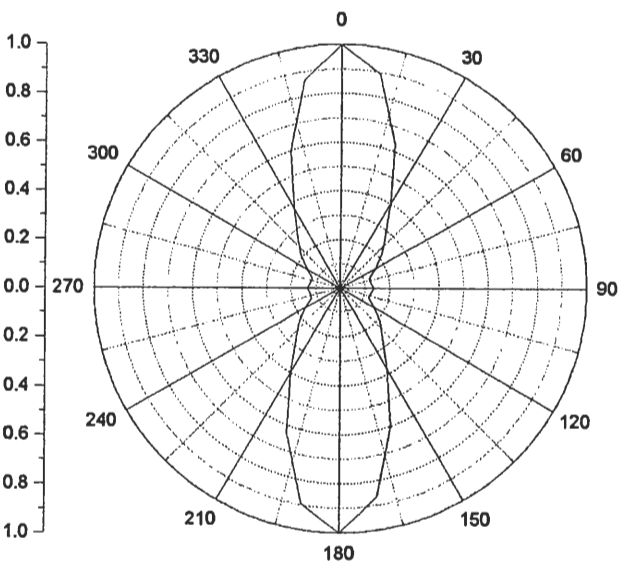

Sample 54-1

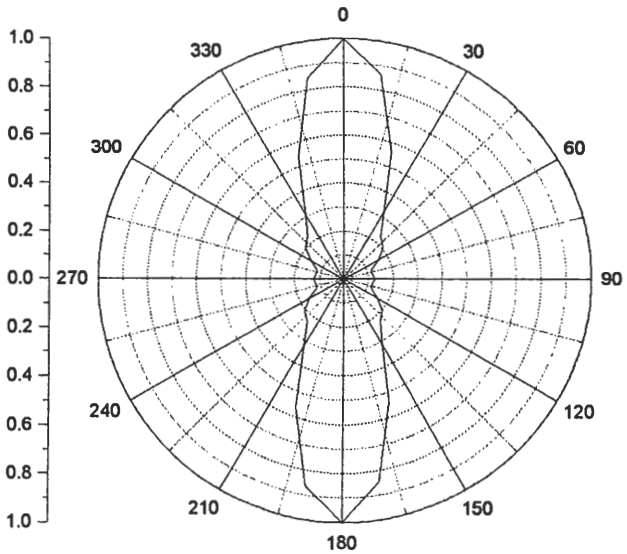

Sample 55-1

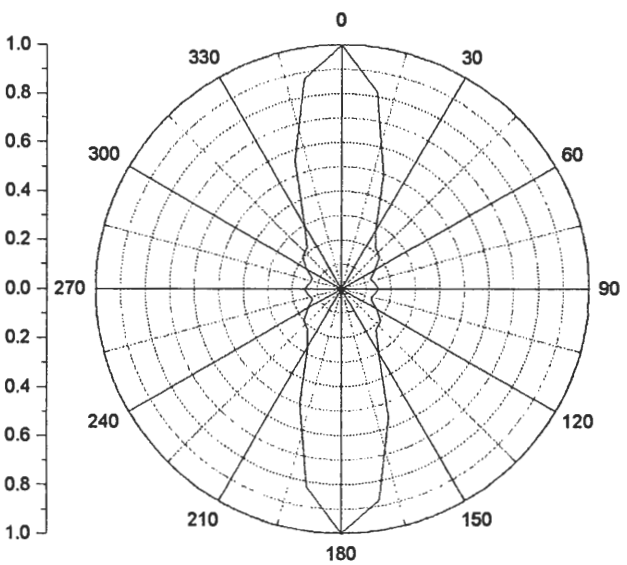

Sample 56-1

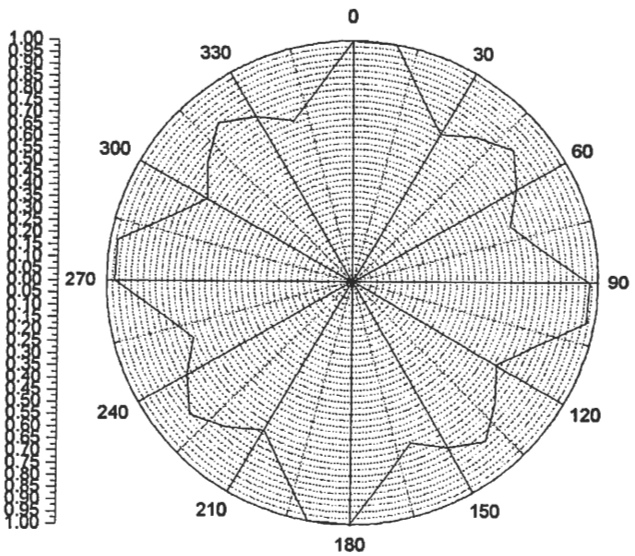

Sample 57-1

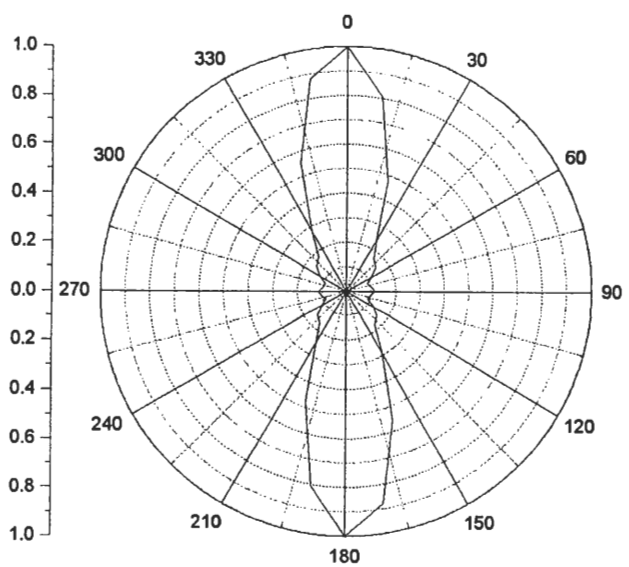

Sample 58-1

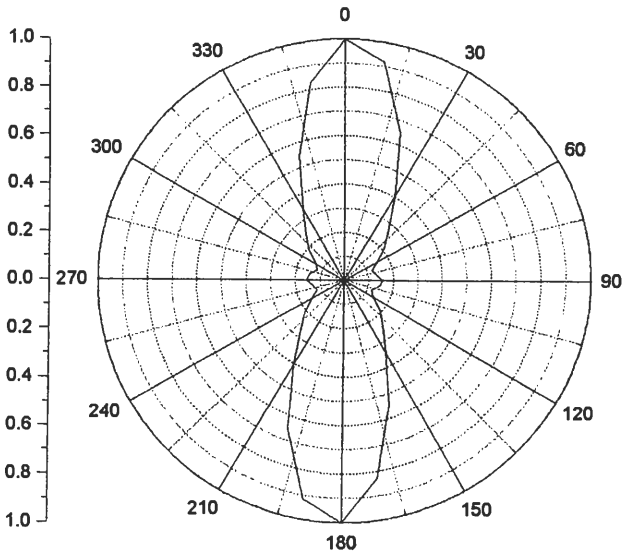

Sample 59-1

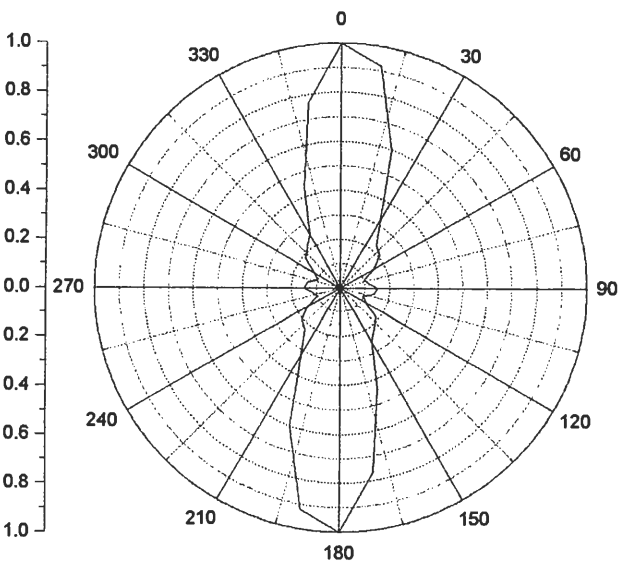

Sample 60-1

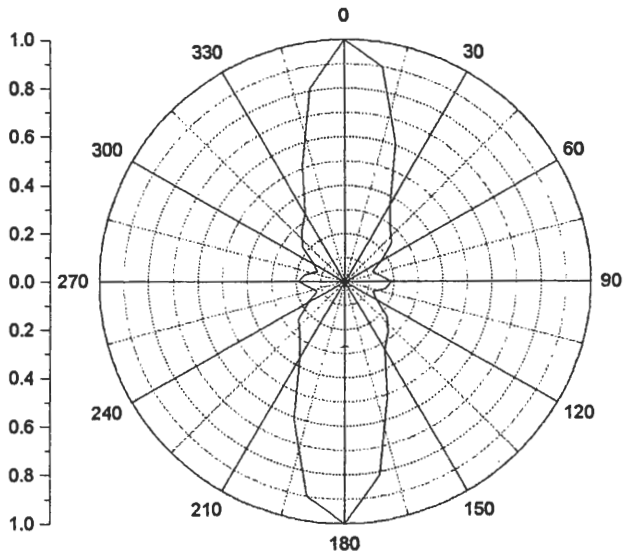

Sample 61-1

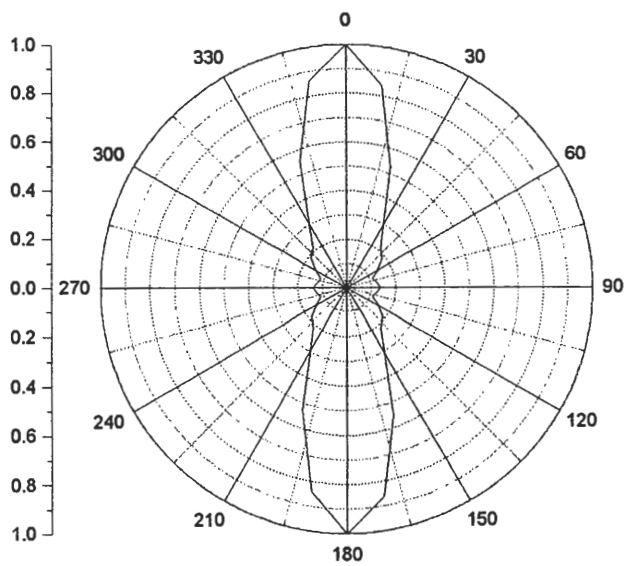

Sample 62-1

APPENDIX V -- DRYING CURVES (FORCE AND DISPLACEMENT)

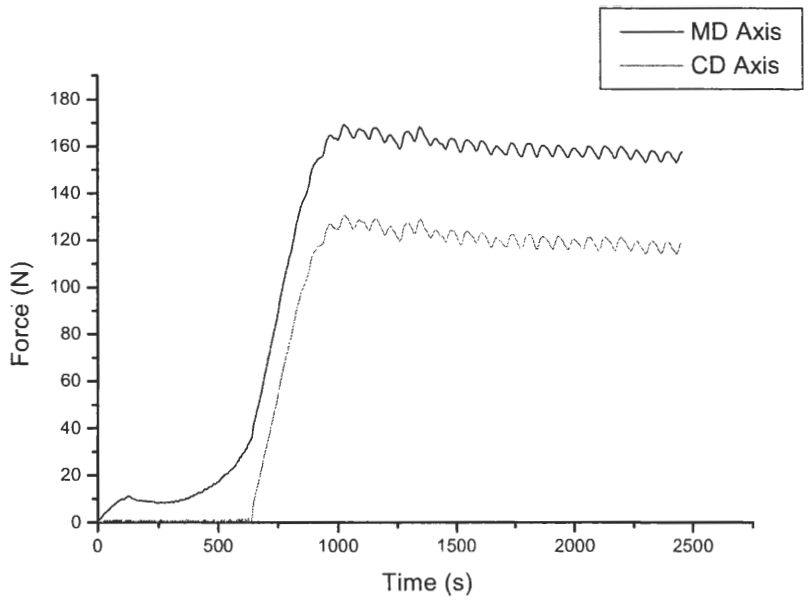

Sample 1-1. Top curve is MD, bottom is CD

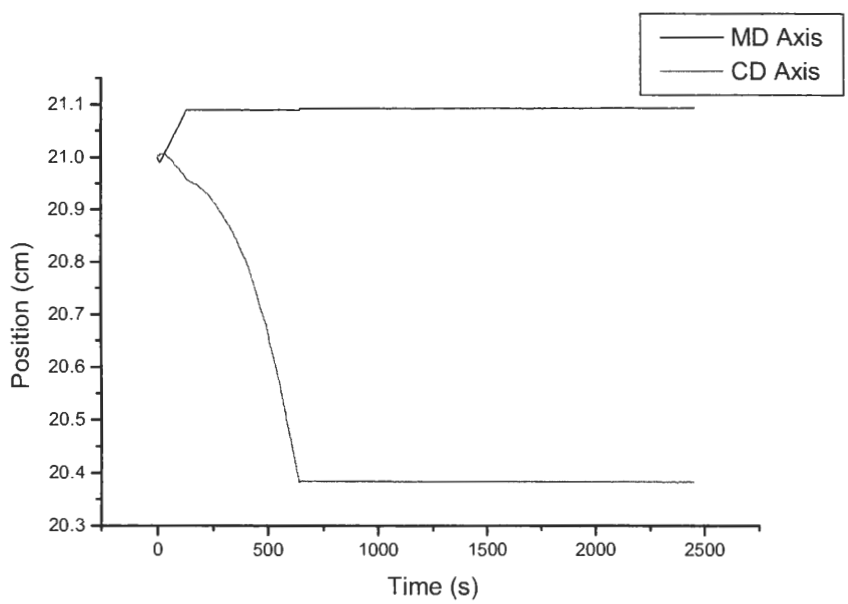

Sample 1-1. Top curve is MD, bottom is CD

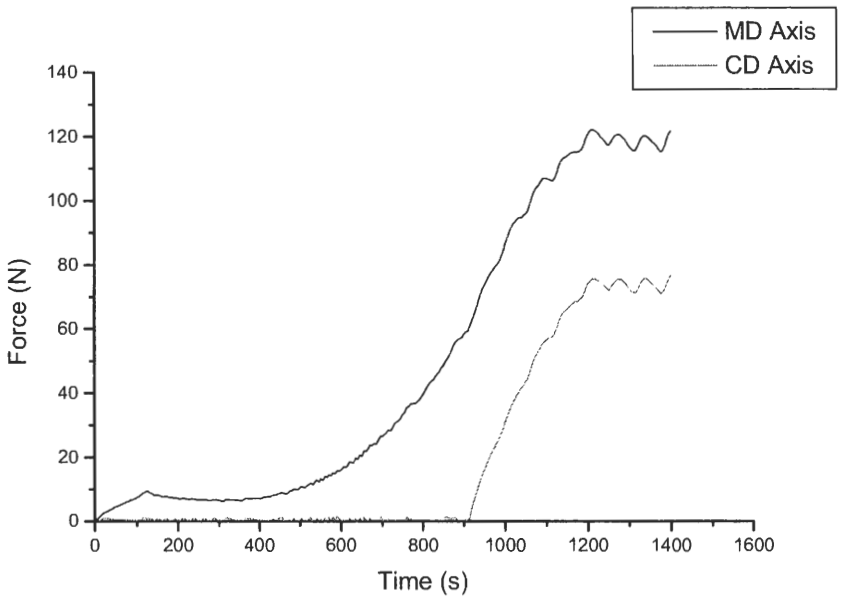

Sample 2-1. Top curve is MD, bottom is CD

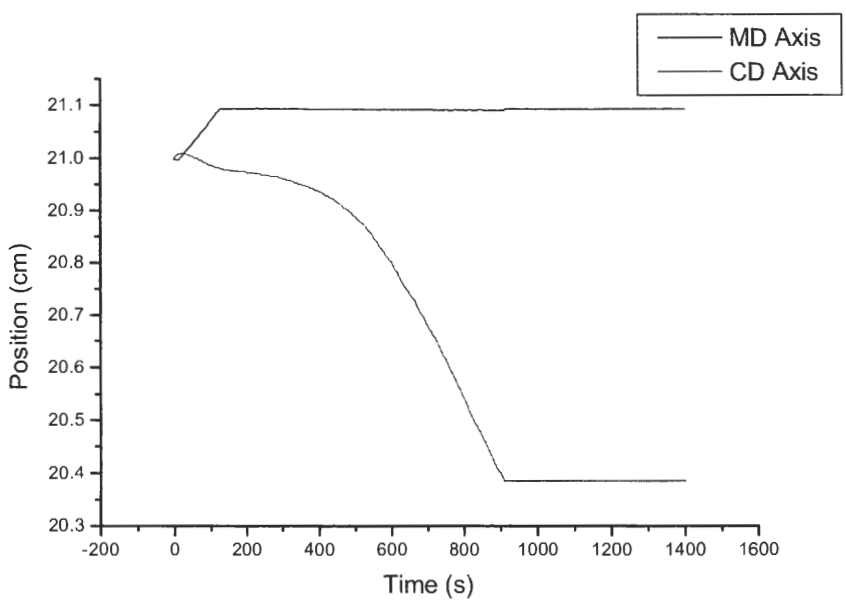

Sample 2-1. Top curve is MD, bottom is CD

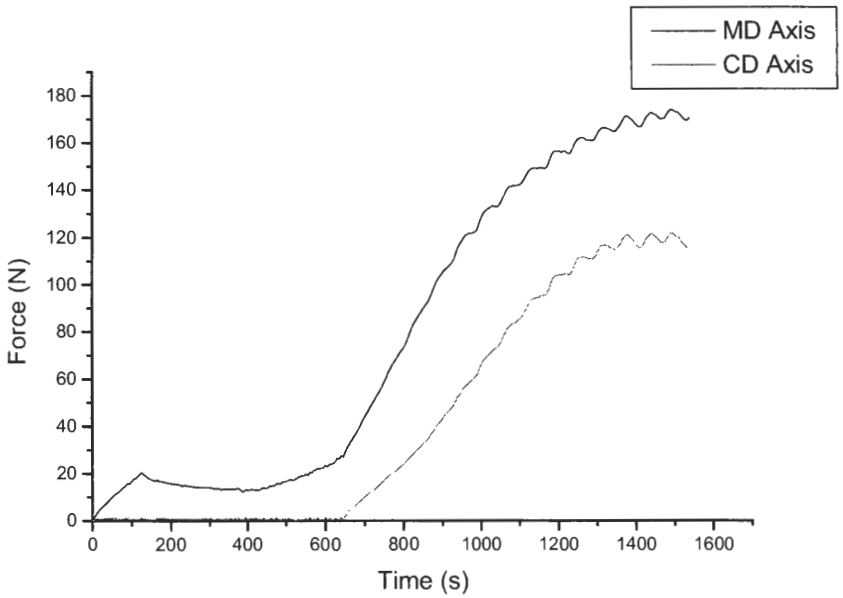

Sample 3-1. Top curve is MD, bottom is CD

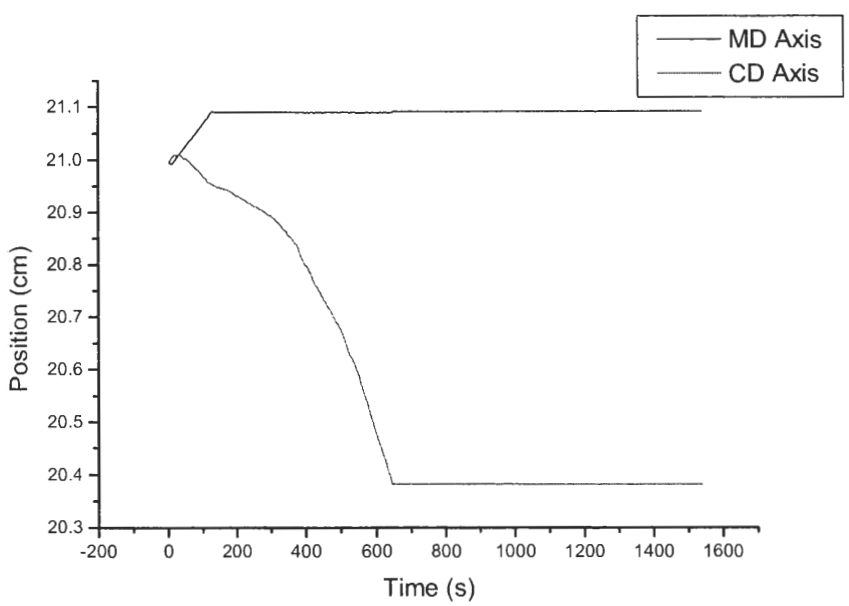

Sample 3-1. Top curve is MD, bottom is CD

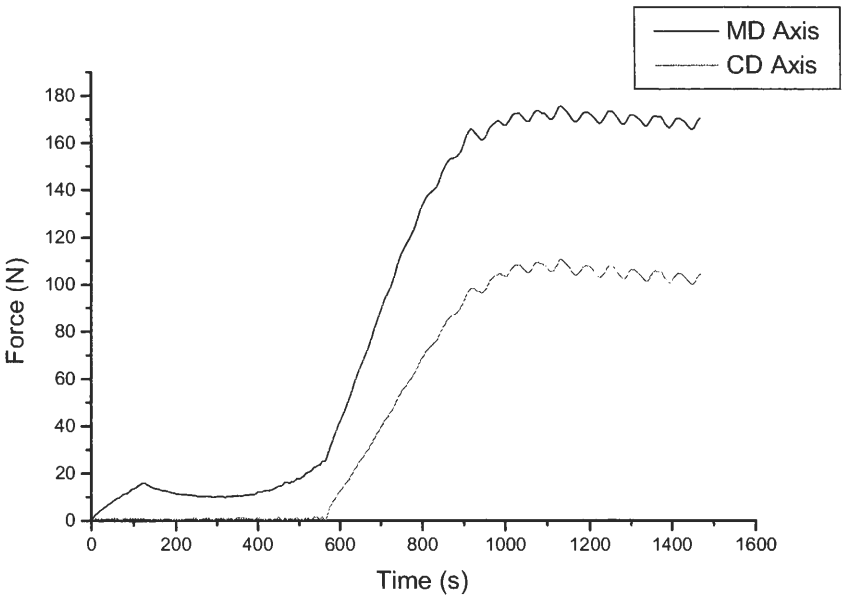

Sample 4-2. Top curve is MD, bottom is CD

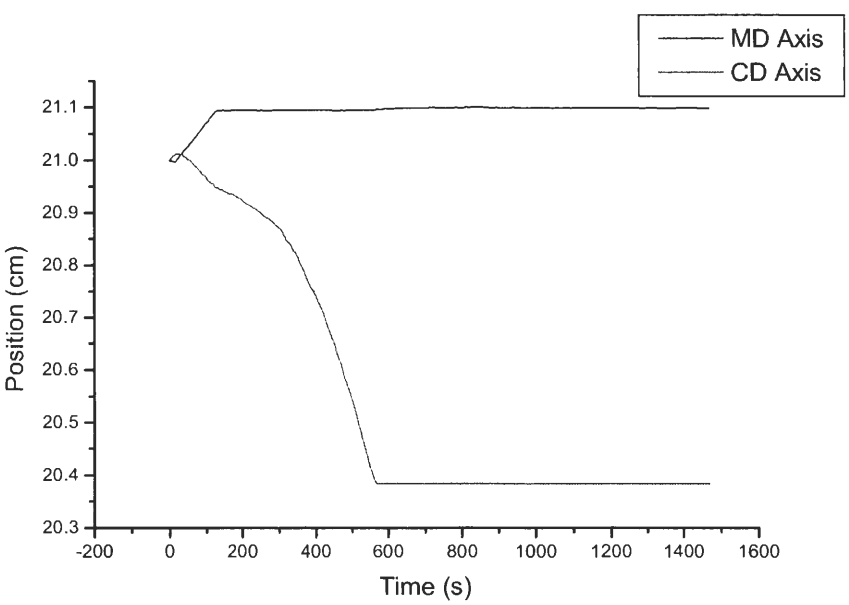

Sample 4-1. Top curve is MD, bottom is CD

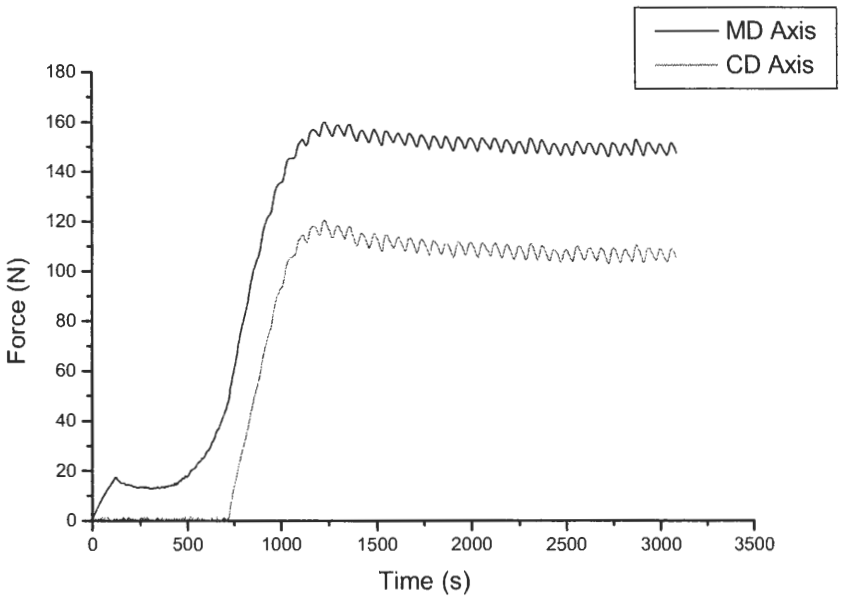

Sample 5-1. Top curve is MD, bottom is CD

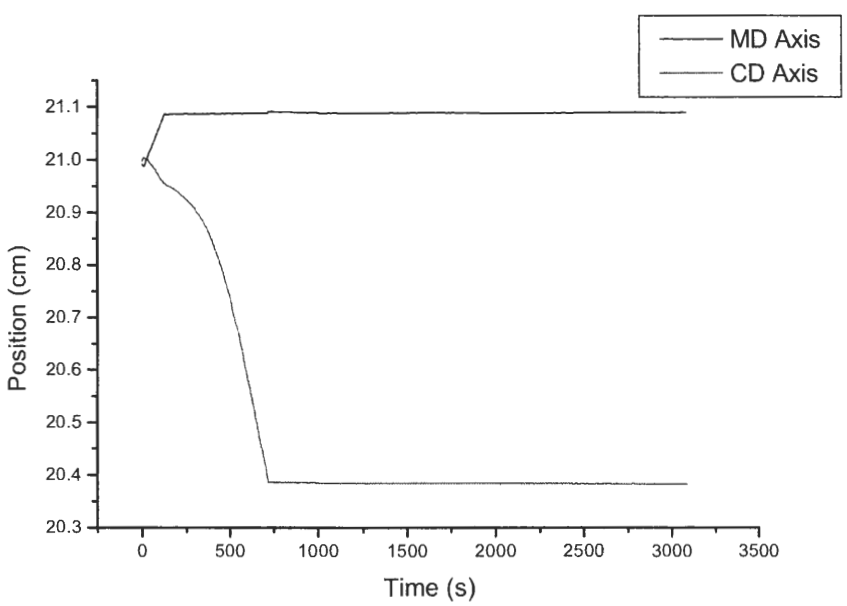

Sample 5-1. Top curve is MD, bottom is CD

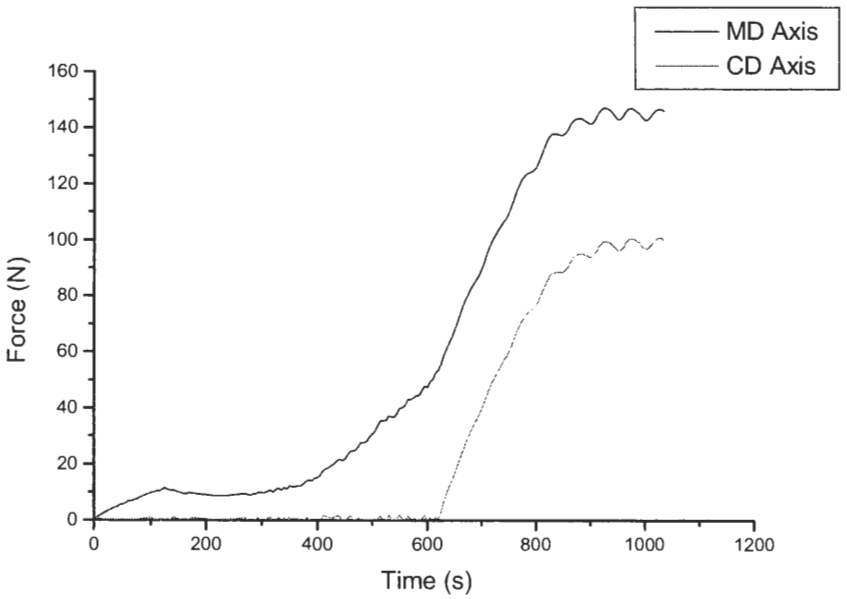

Sample 6-1. Top curve is MD, bottom is CD

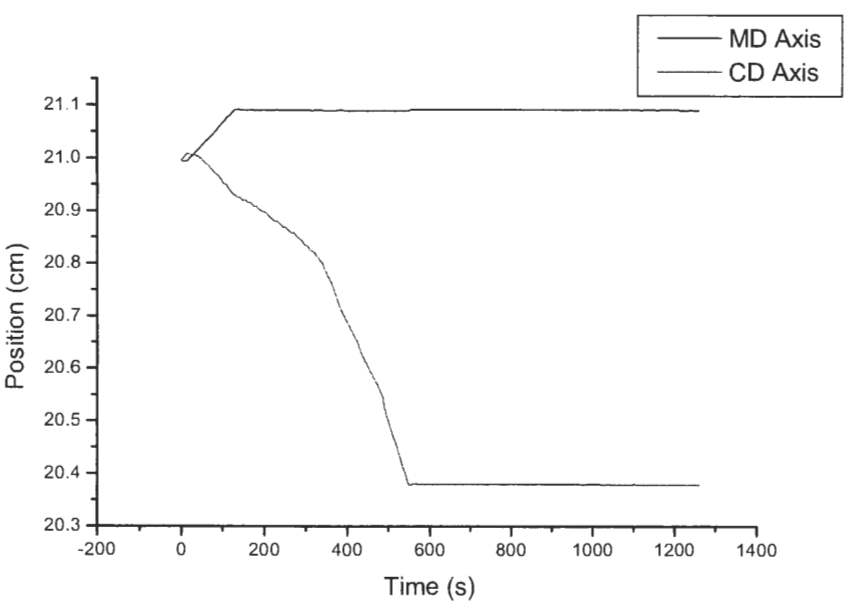

Sample 6-1. Top curve is MD, bottom is CD

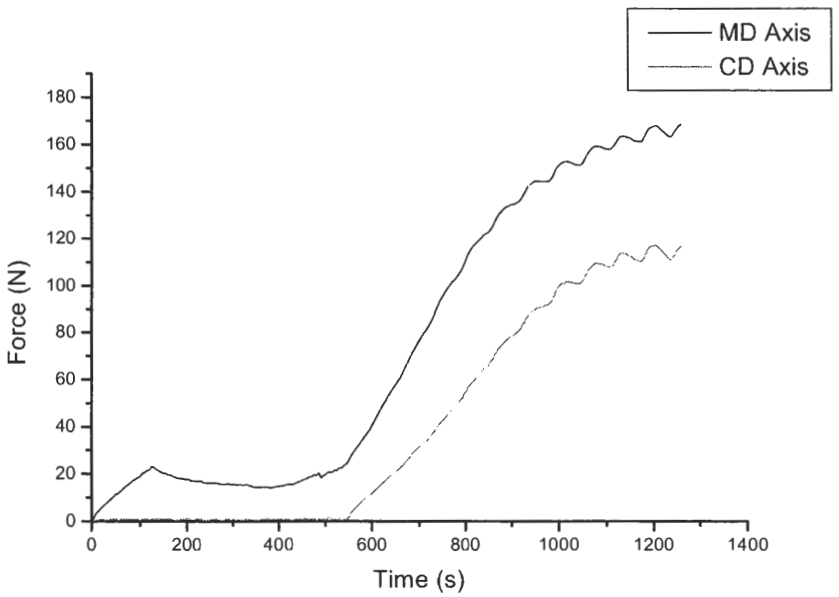

Sample 7-1. Top curve is MD, bottom is CD

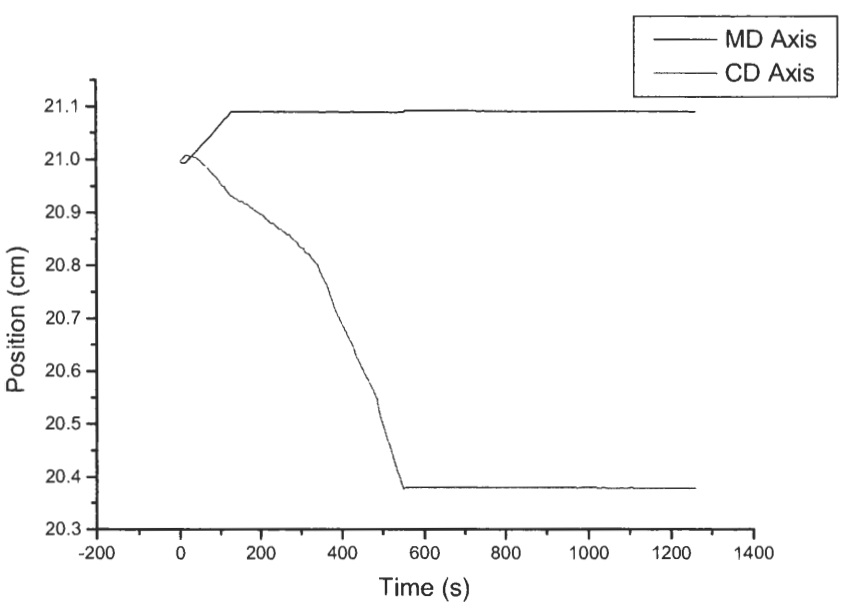

Sample 7-1. Top curve is MD, bottom is CD

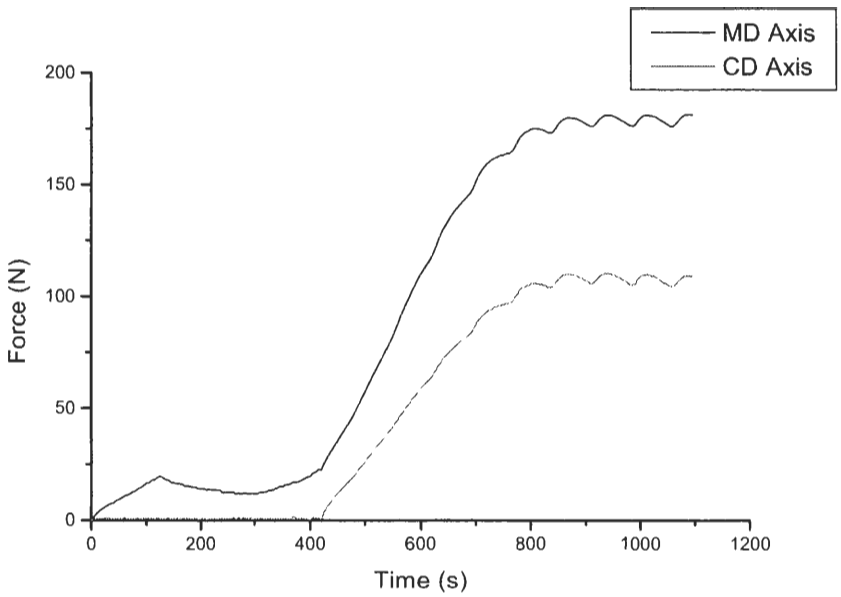

Sample 8-1. Top curve is MD, bottom is CD

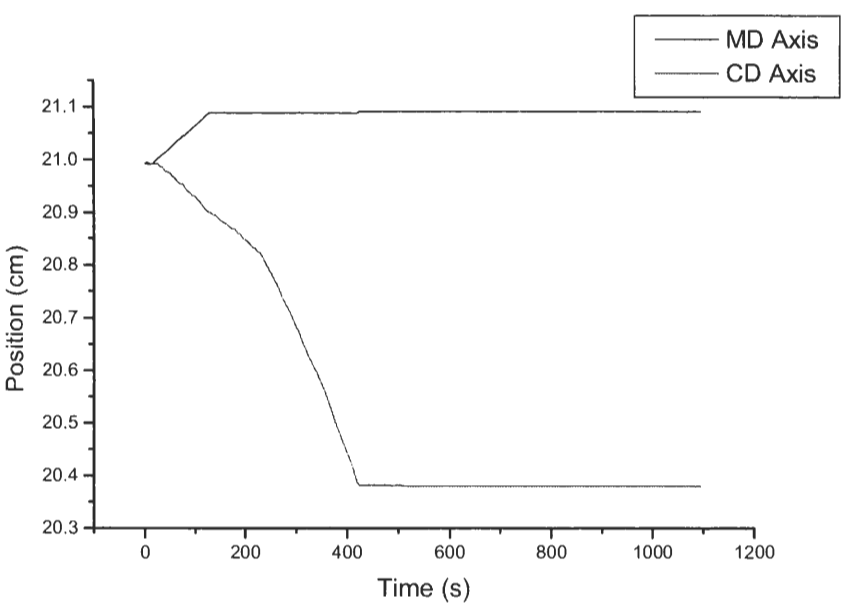

Sample 8-1. Top curve is MD, bottom is CD

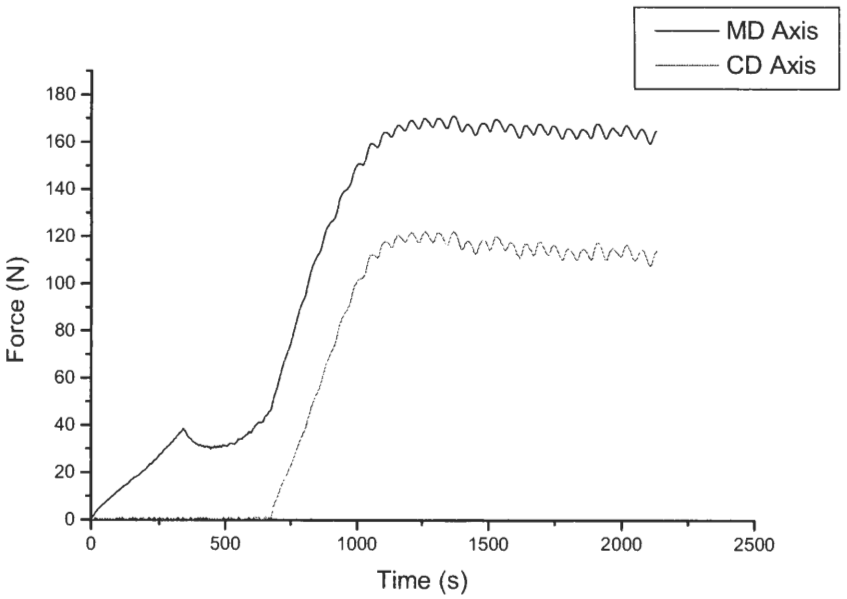

Sample 9-1. Top curve is MD, bottom is CD

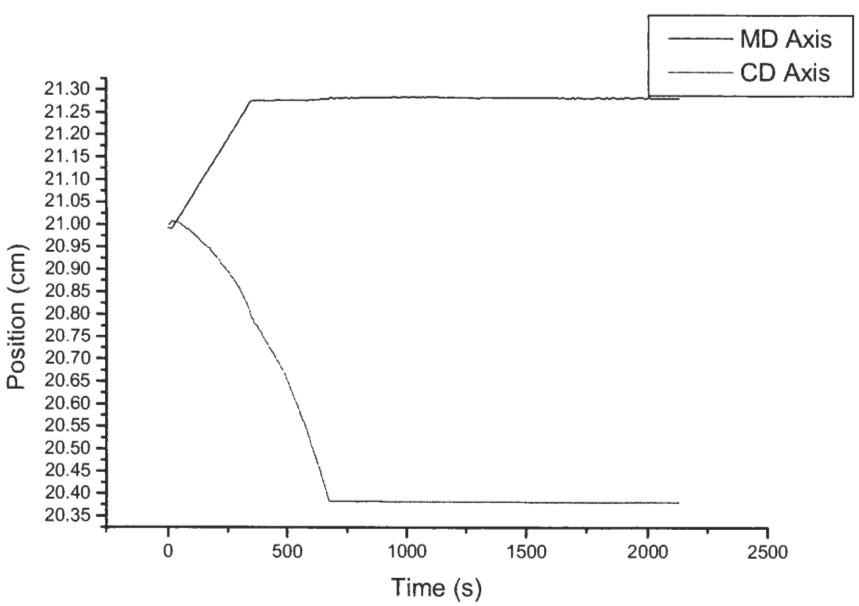

Sample 9-1. Top curve is MD, bottom is CD

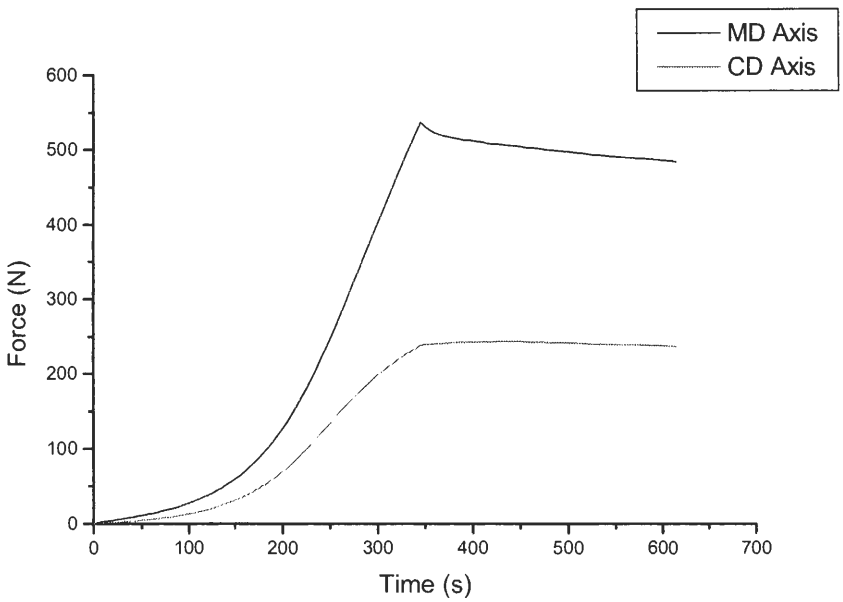

Sample 10-1. Top curve is MD, bottom is CD

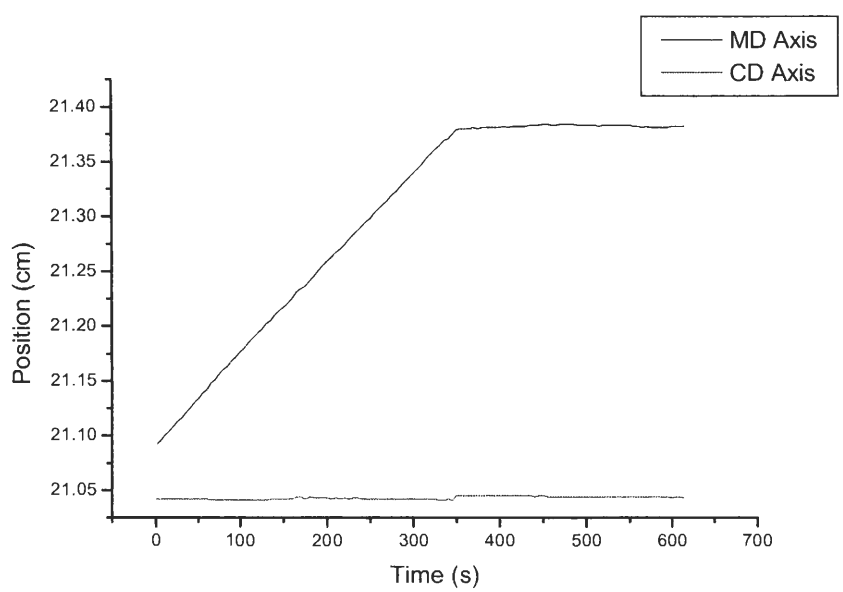

Sample 10-1. Top curve is MD, bottom is CD

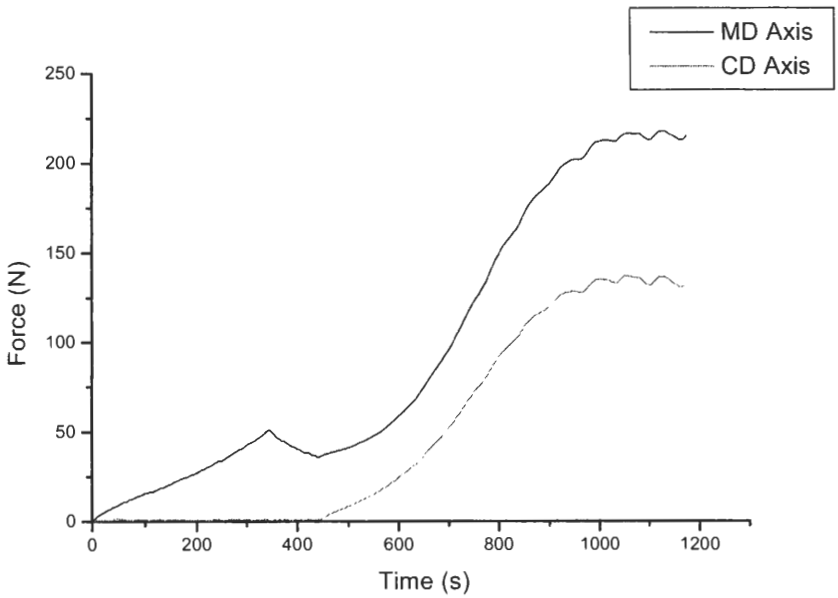

Sample 11-1. Top curve is MD, bottom is CD

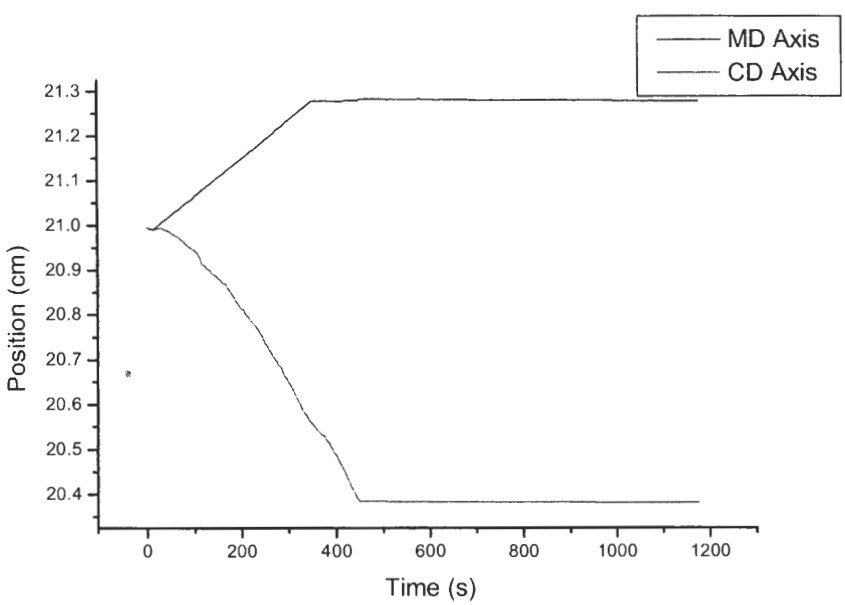

Sample 11-1. Top curve is MD, bottom is CD

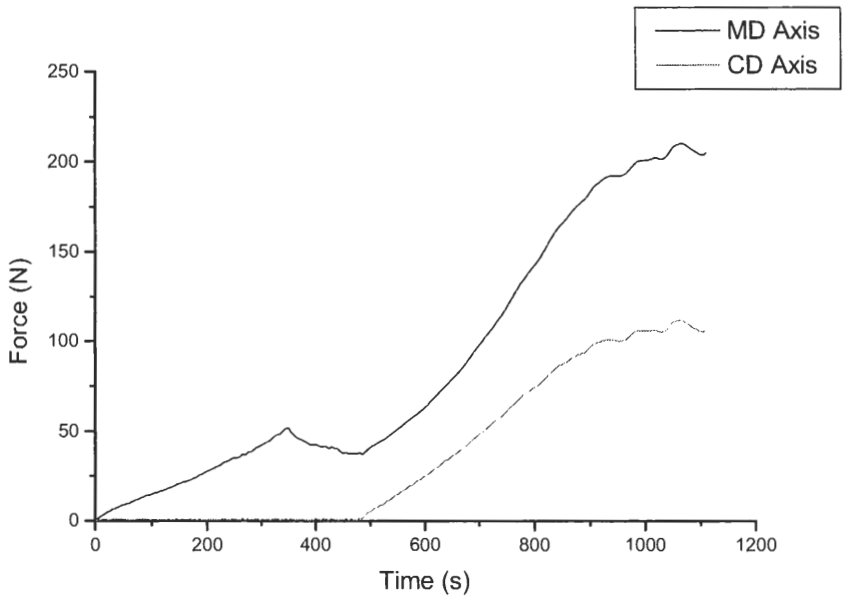

Sample 12-1. Top curve is MD, bottom is CD

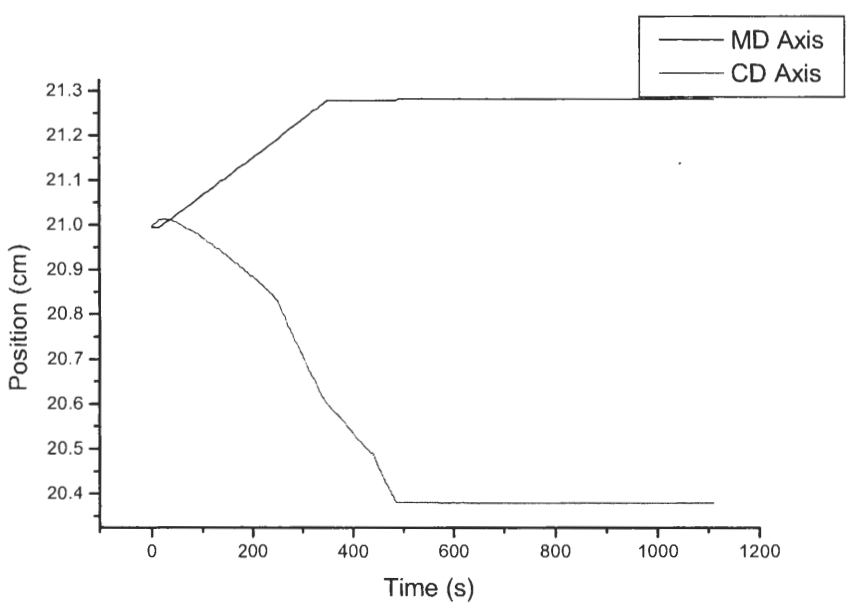

Sample 12-1. Top curve is MD, bottom is CD

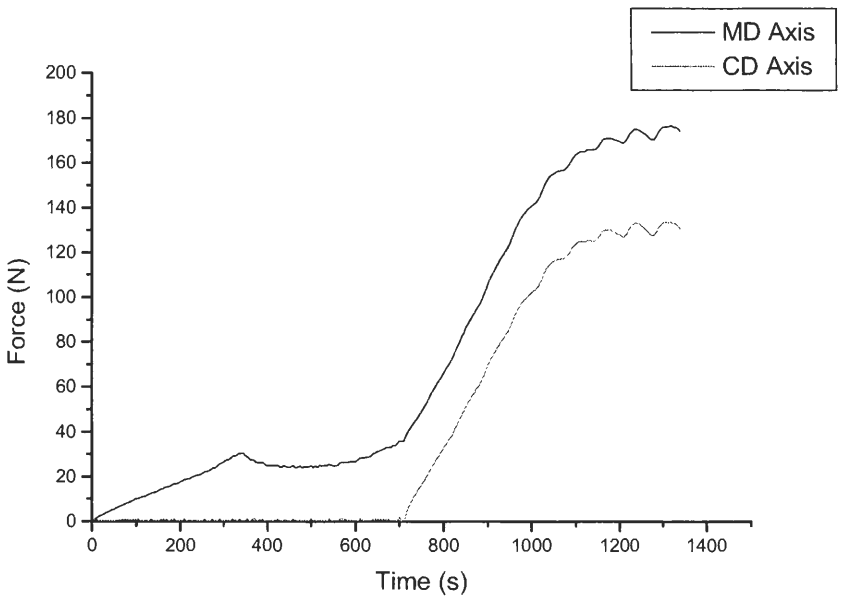

Figure 13-1. Top curve is MD, bottom is CD

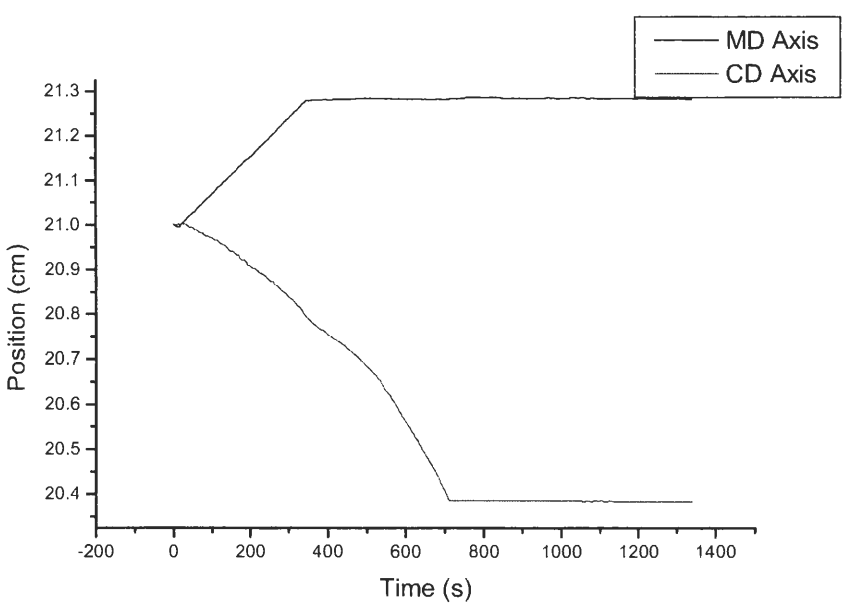

Sample 13-1. Top curve is MD, bottom is CD

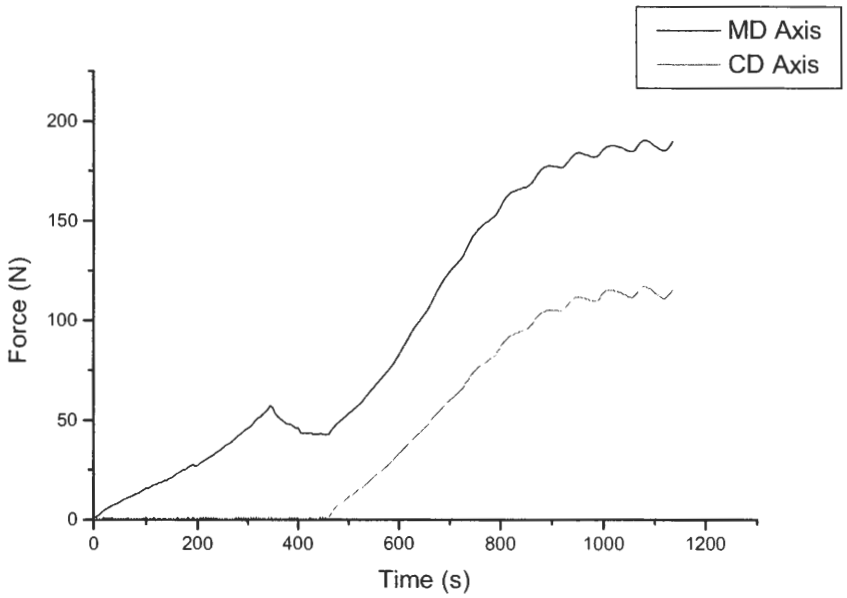

Sample 14-1. Top curve is MD, bottom is CD

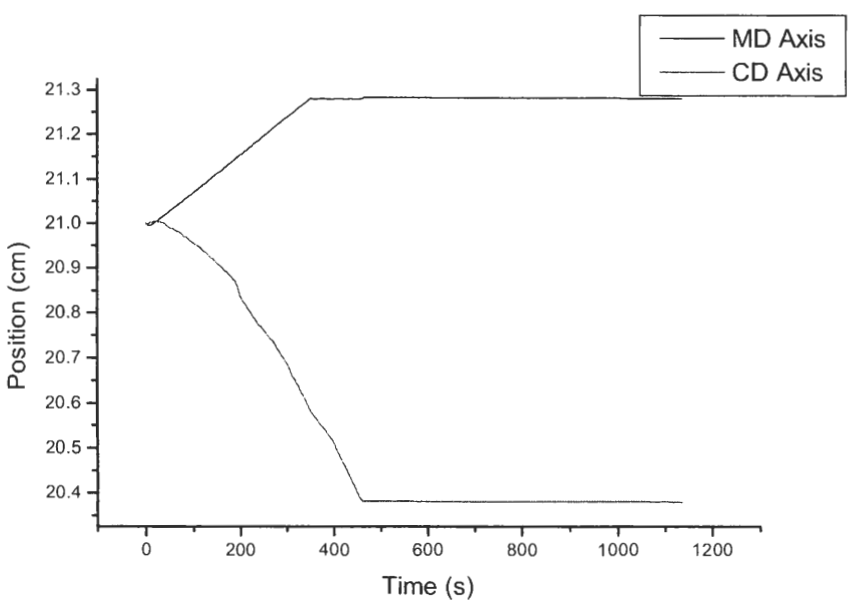

Sample 14-1. Top curve is MD, bottom is CD

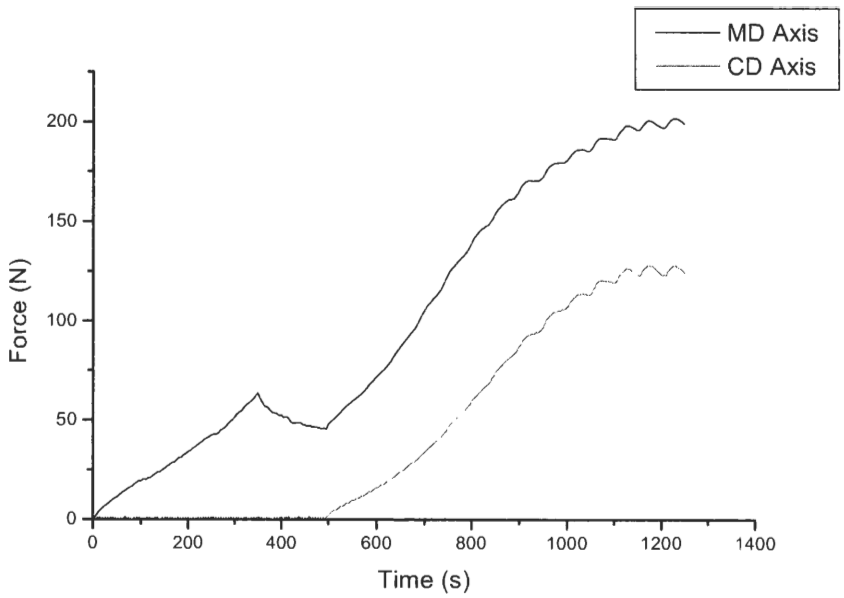

Sample 15-1. Top curve is MD, bottom is CD

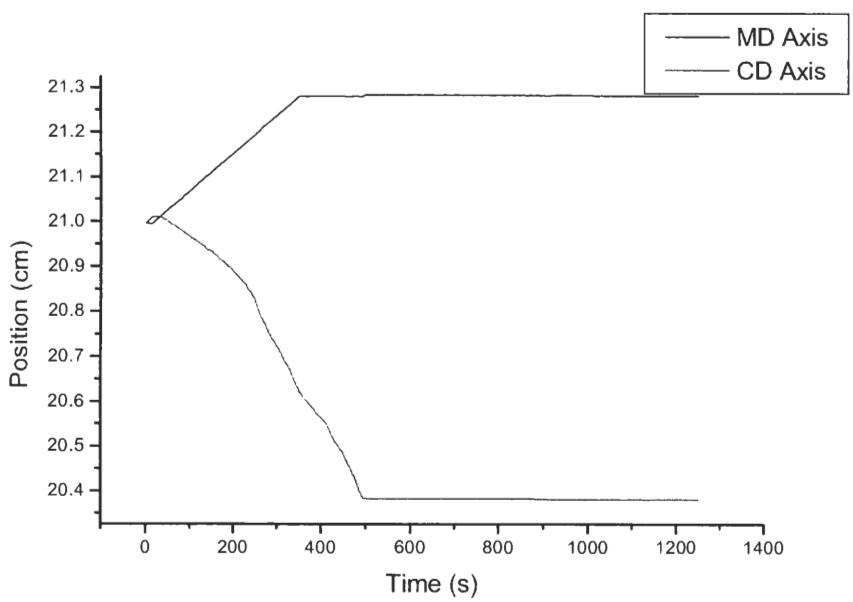

Sample 15-1. Top curve is MD, bottom is CD

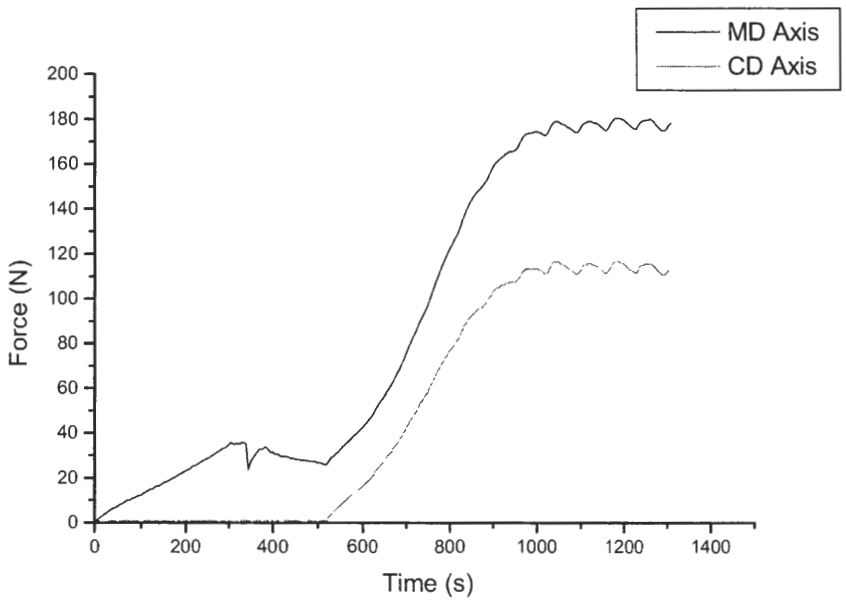

Sample 16-1. Top curve is MD, bottom is CD

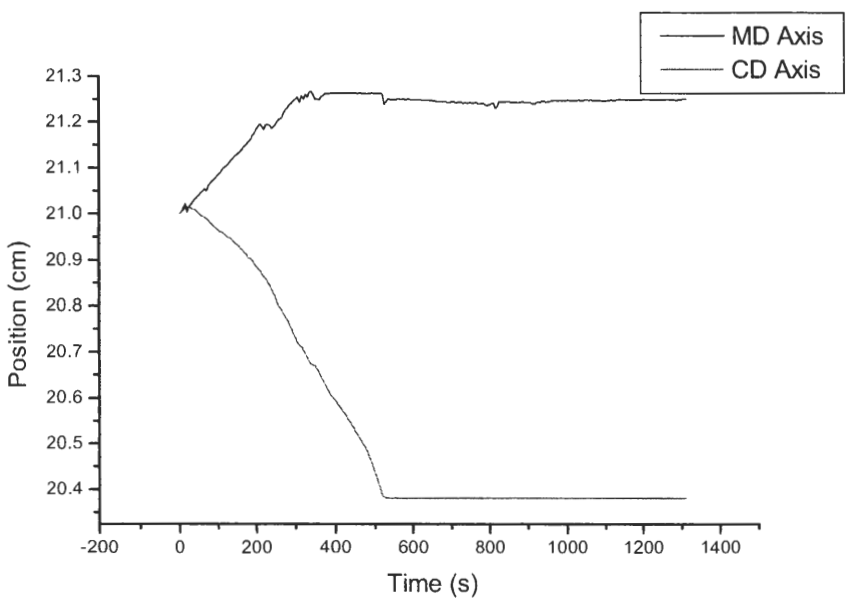

Sample 16-1. Top curve is MD, bottom is CD

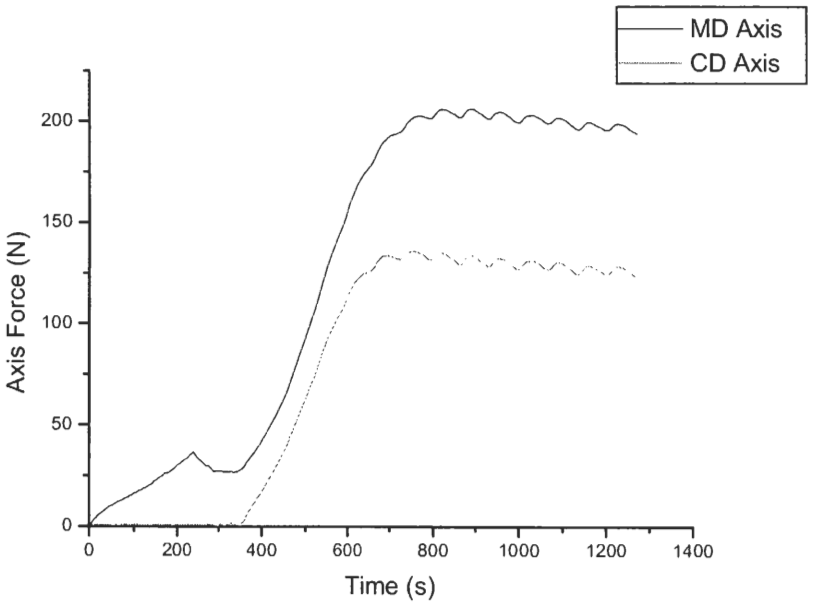

Sample 17-1. Top curve is MD, bottom is CD

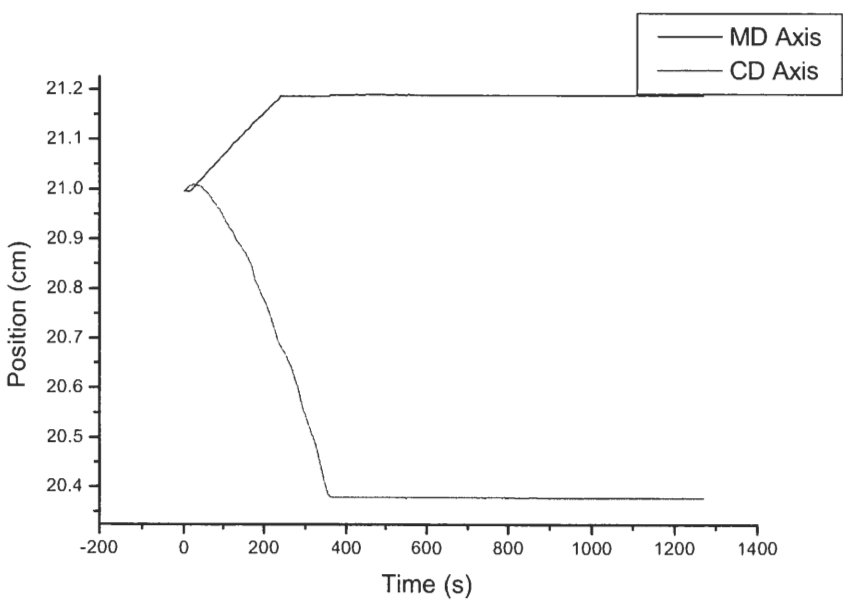

Sample 17-1. Top curve is MD, bottom is CD

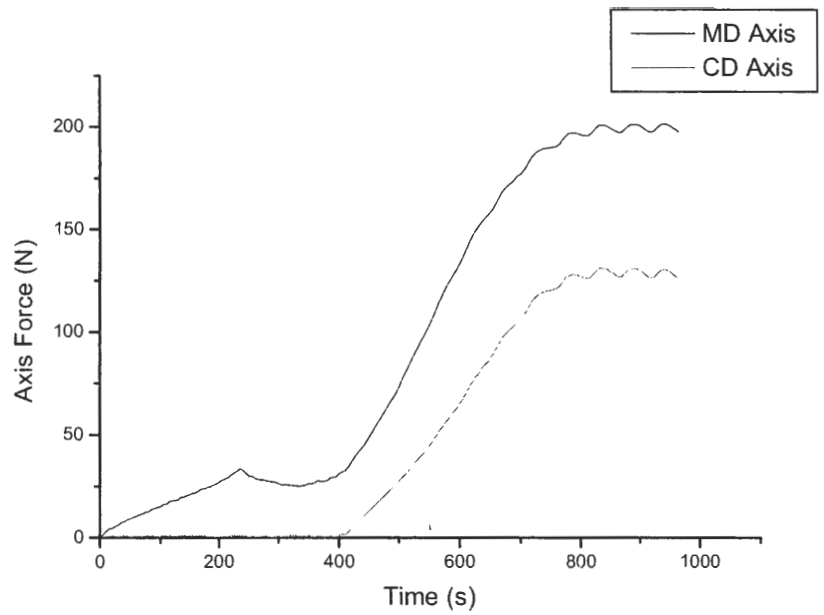

Sample 18-1. Top curve is MD, bottom is CD

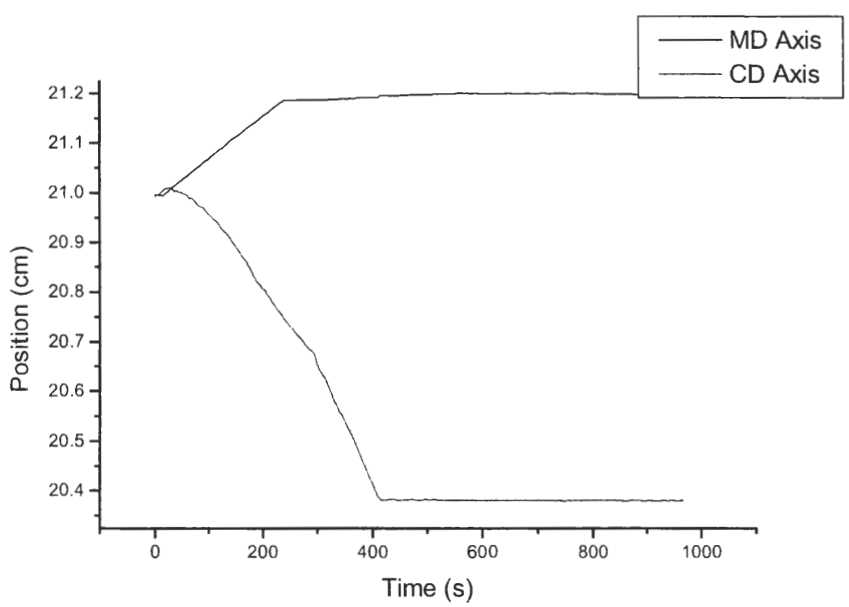

Sample 18-1. Top curve is MD, bottom is CD

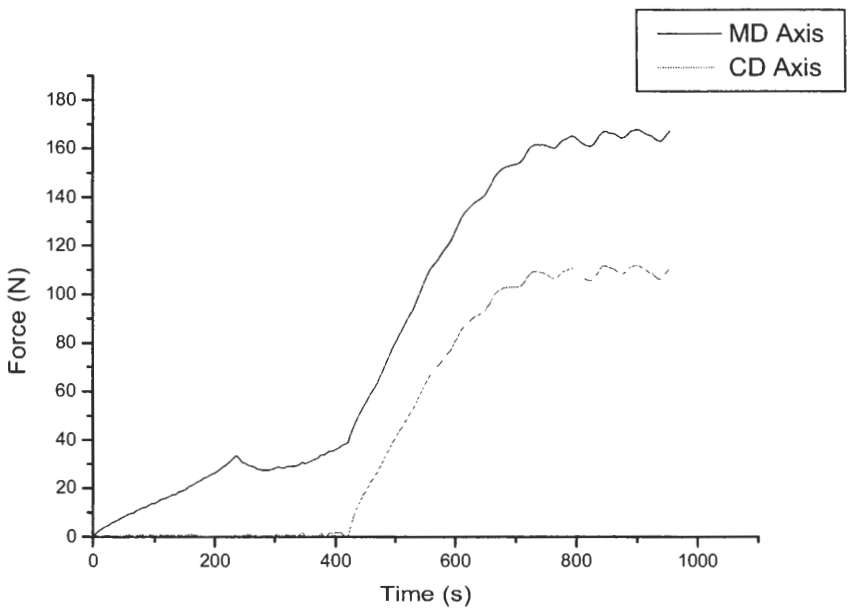

Sample 19-1. Top curve is MD, bottom is CD

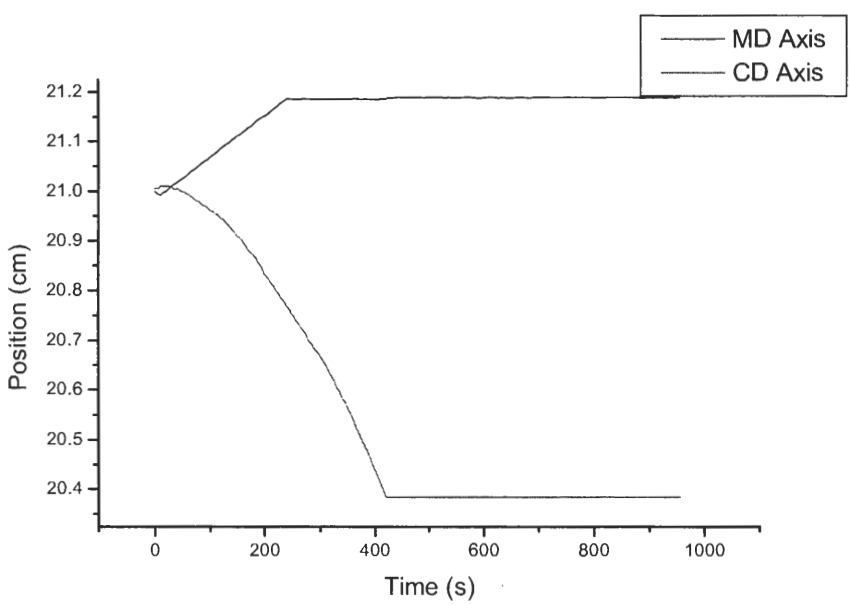

Sample 19-1. Top curve is MD, bottom is CD

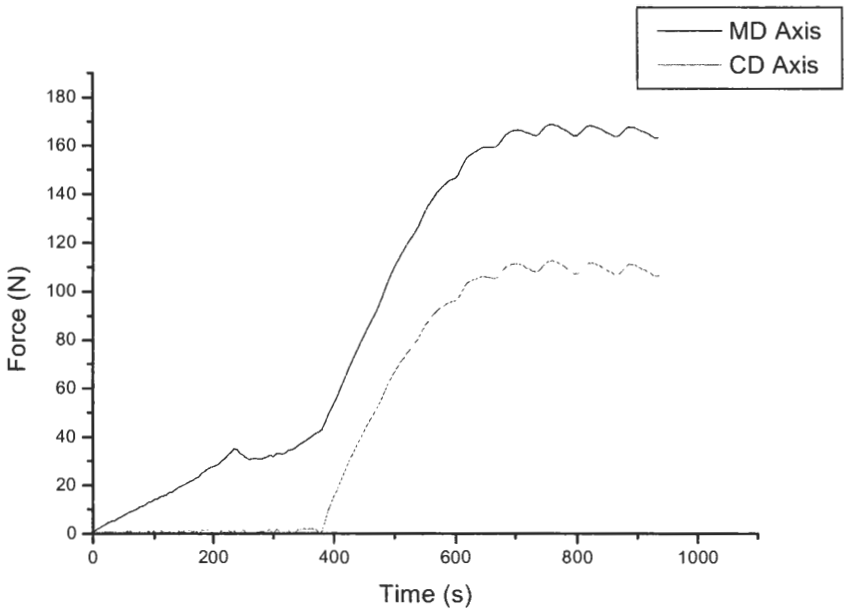

Sample 20-1. Top curve is MD, bottom is CD

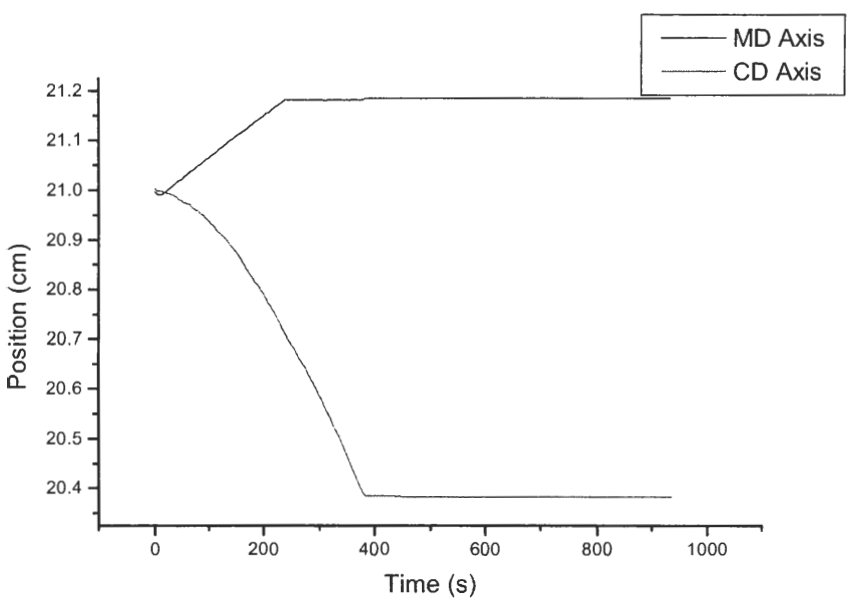

Sample 20-1. Top curve is MD, bottom is CD

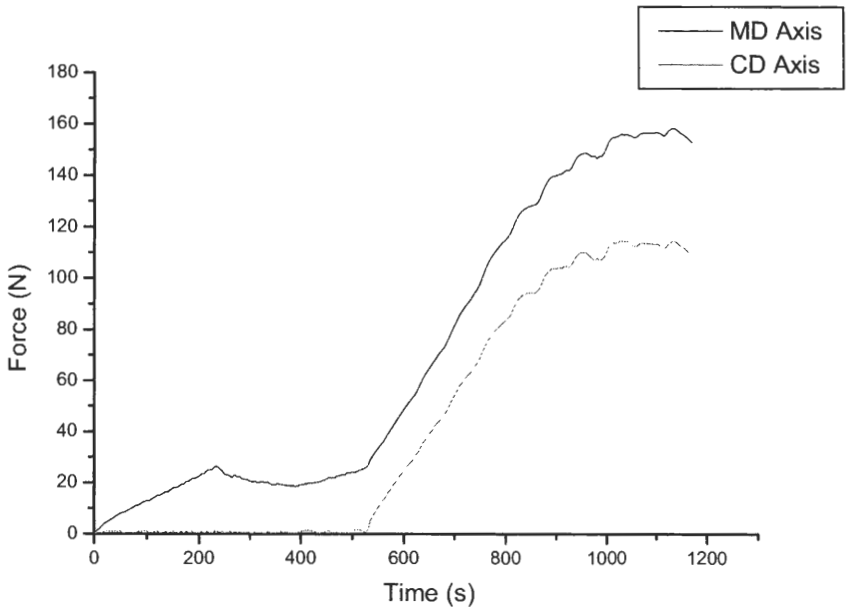

Sample 21-1. Top curve is MD, bottom is CD

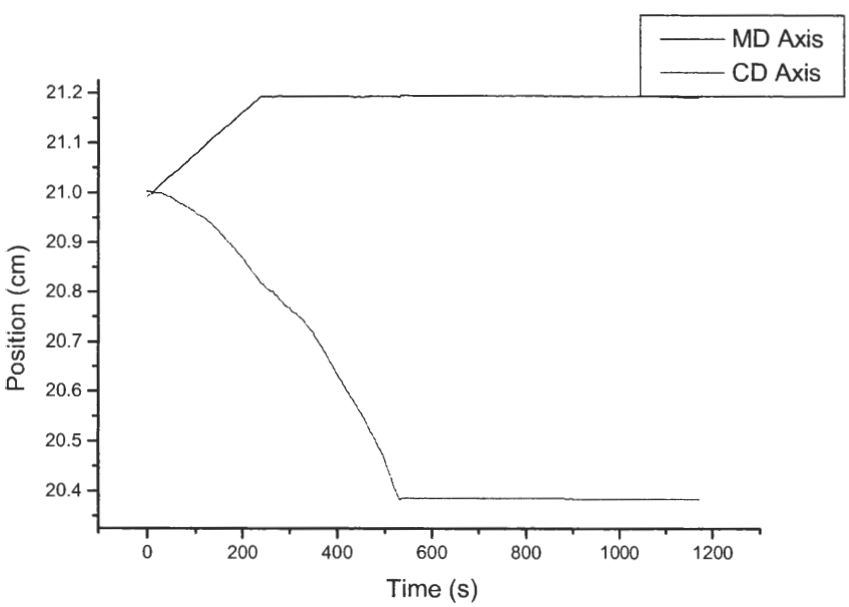

Sample 21-1. Top curve is MD, bottom is CD

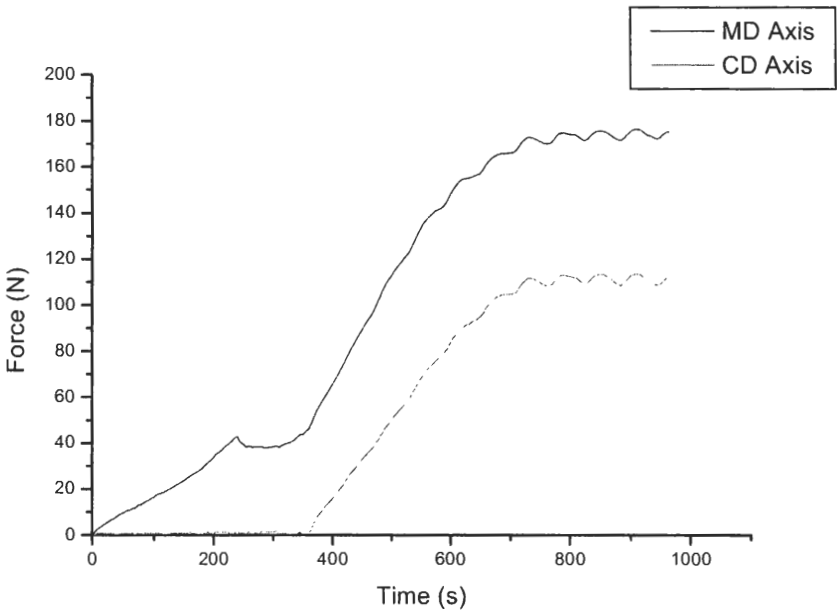

Sample 22-1. Top curve is MD, bottom is CD

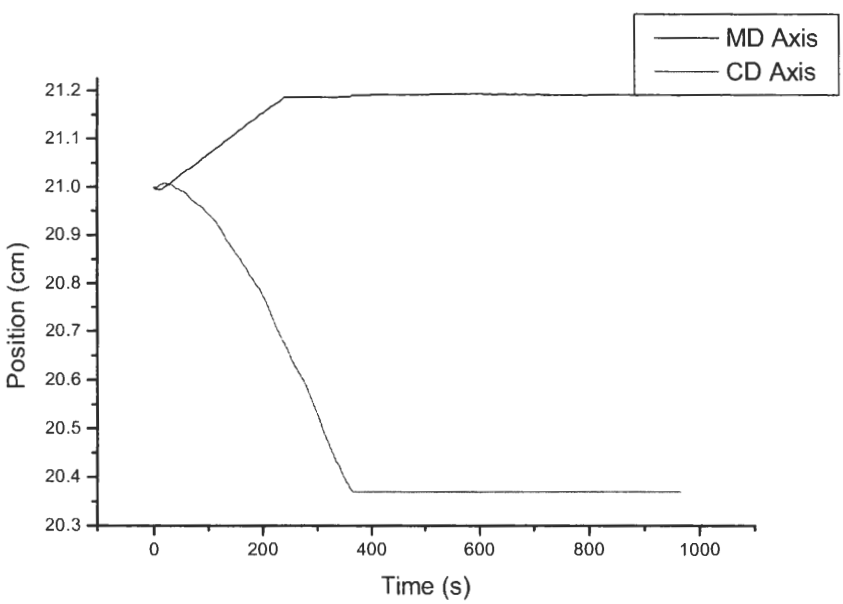

Sample 22-1. Top curve is MD, bottom is CD

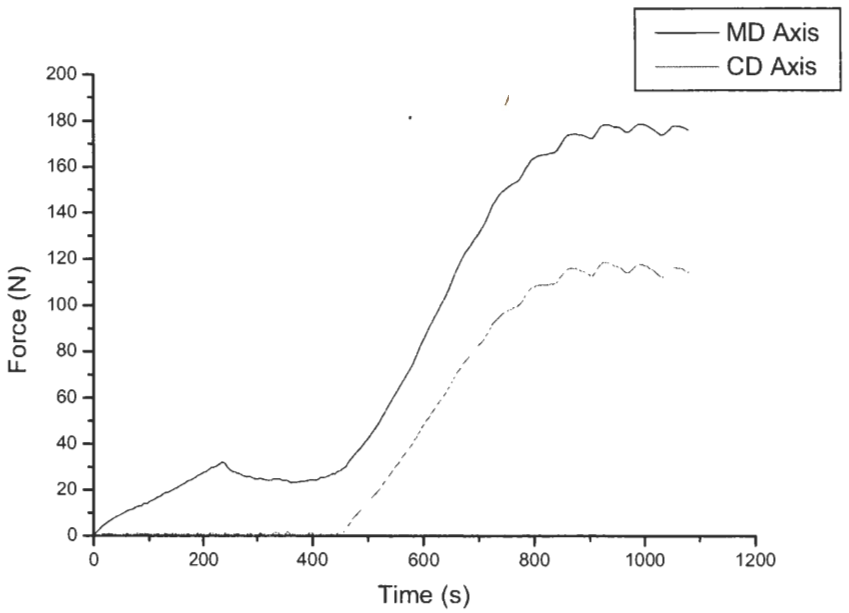

Sample 23-1. Top curve is MD, bottom is CD

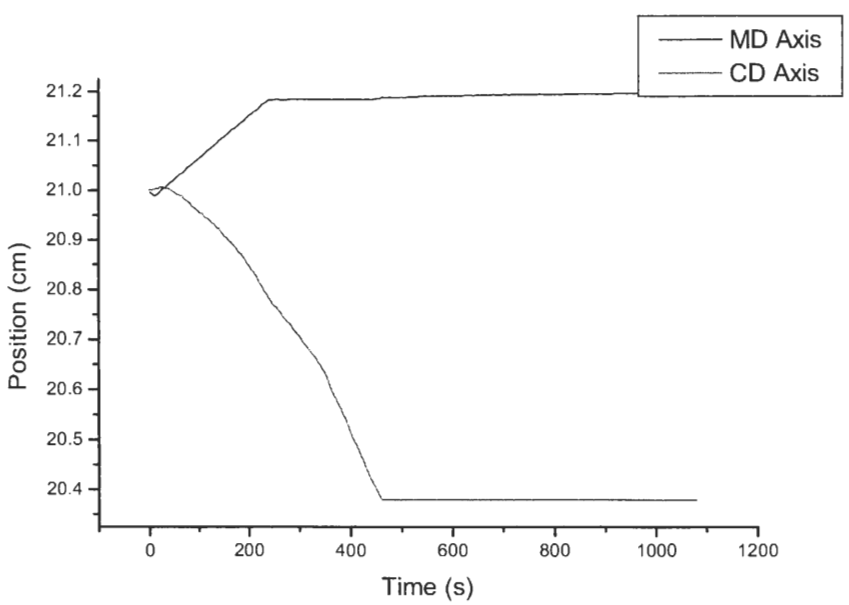

Sample 23-1. Top curve is MD, bottom is CD

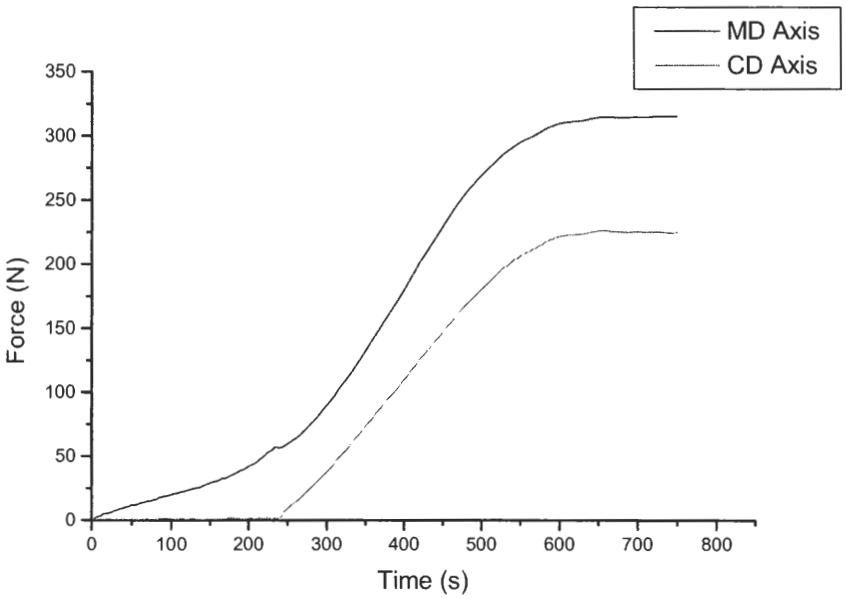

Sample 24-1. Top curve is MD, bottom is CD

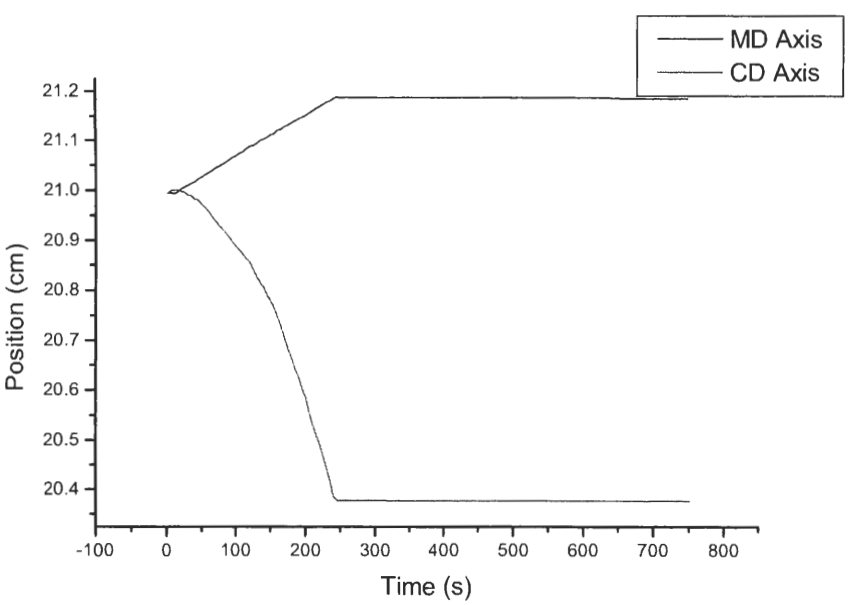

Sample 24-1. Top curve is MD, bottom is CD

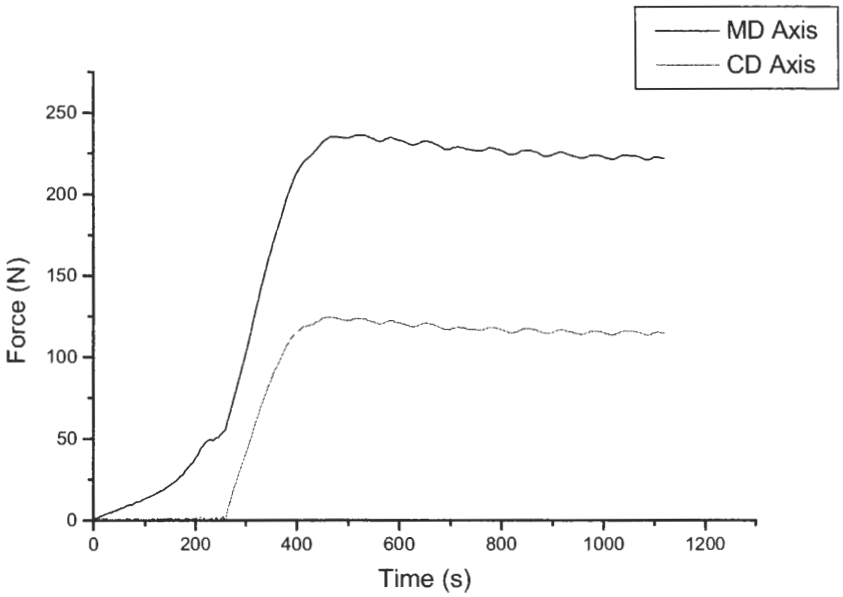

Sample 25-2. Top curve is MD, bottom is CD

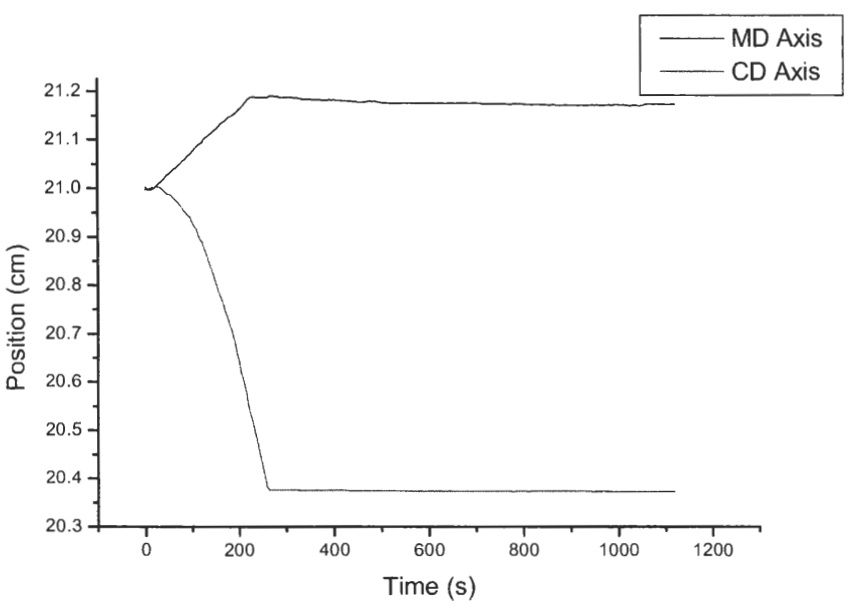

Sample 25-2. Top curve is MD, bottom is CD

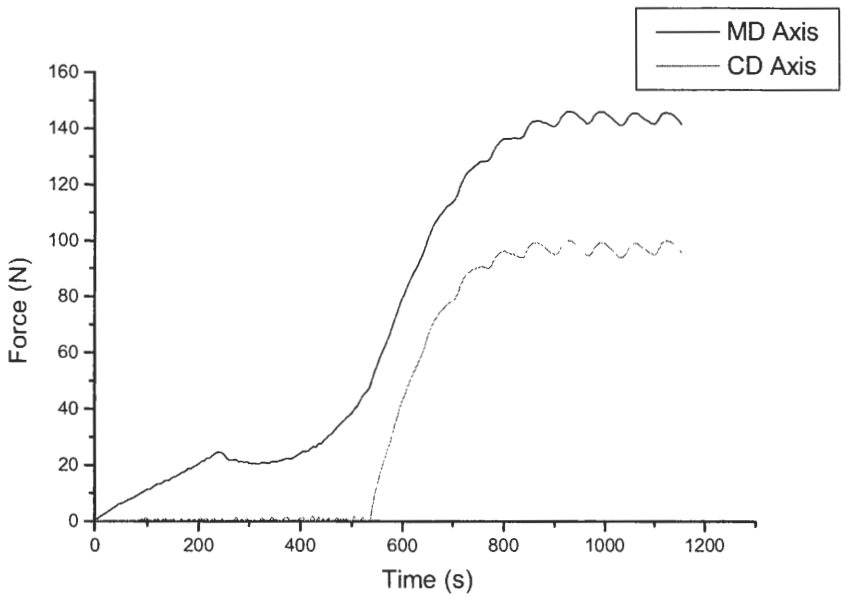

Sample 26-1. Top curve is MD, bottom is CD

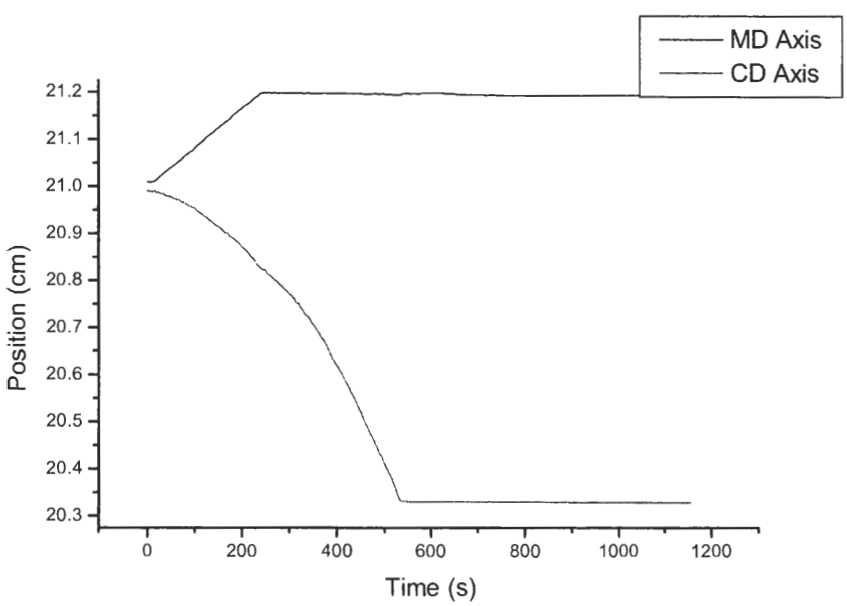

Sample 26-1. Top curve is MD, bottom is CD

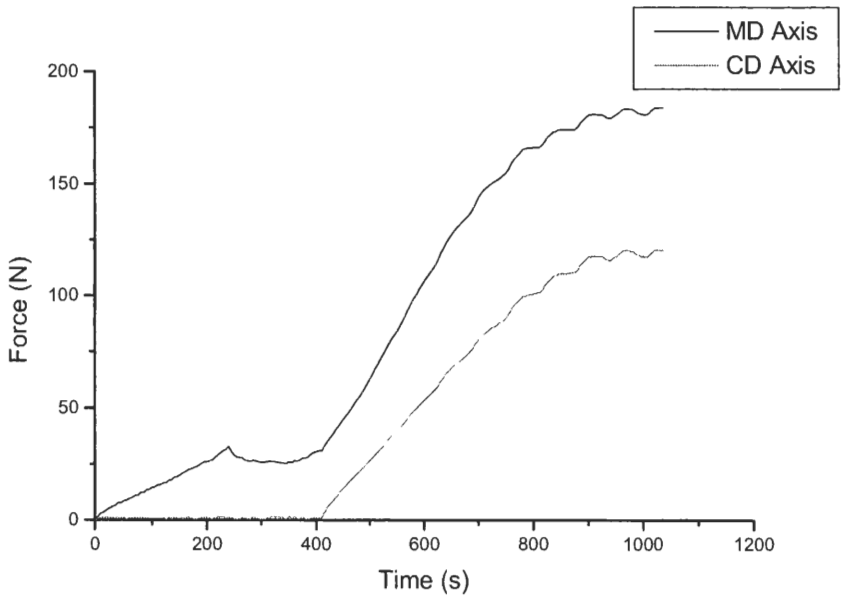

Sample 27-1. Top curve is MD, bottom is CD

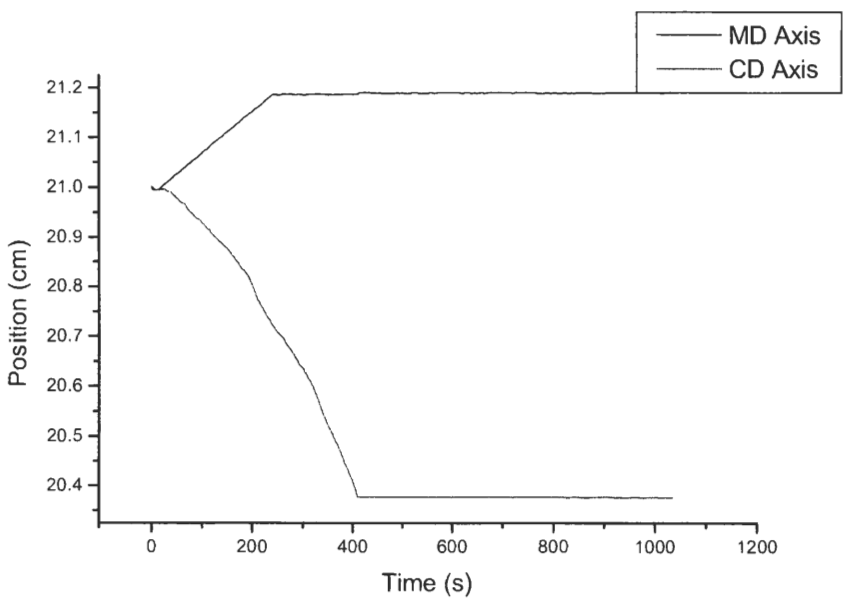

Sample 27-1. Top curve is MD, bottom is CD

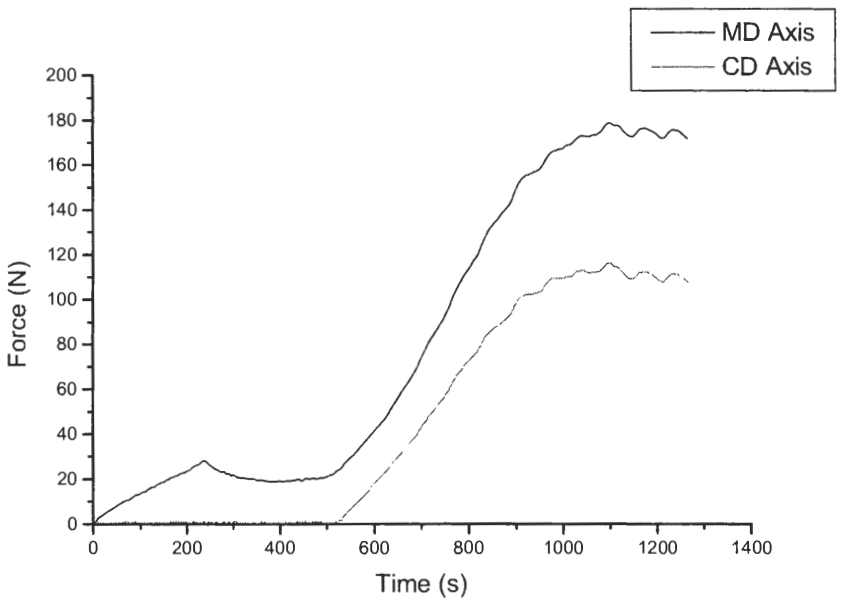

Sample 28-1. Top curve is MD, bottom is CD

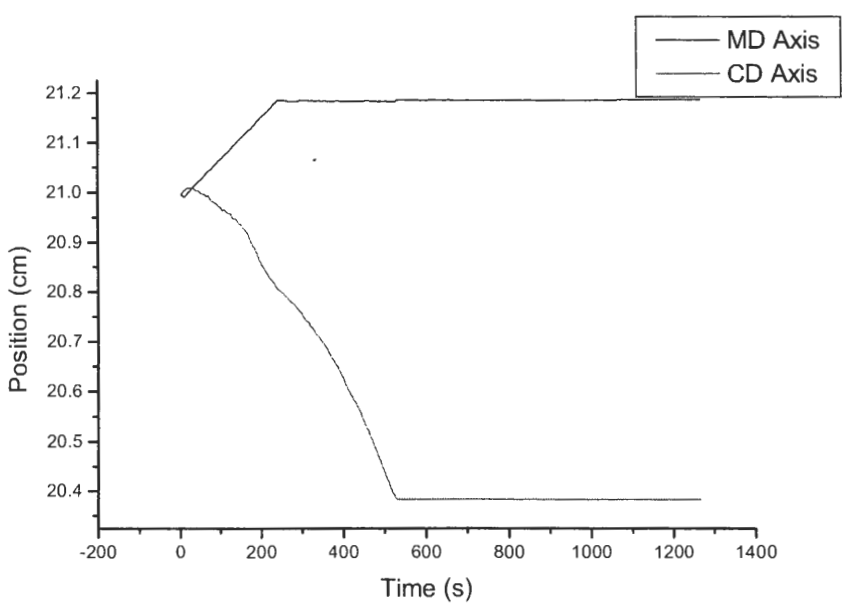

Sample 28-1. Top curve is MD, bottom is CD

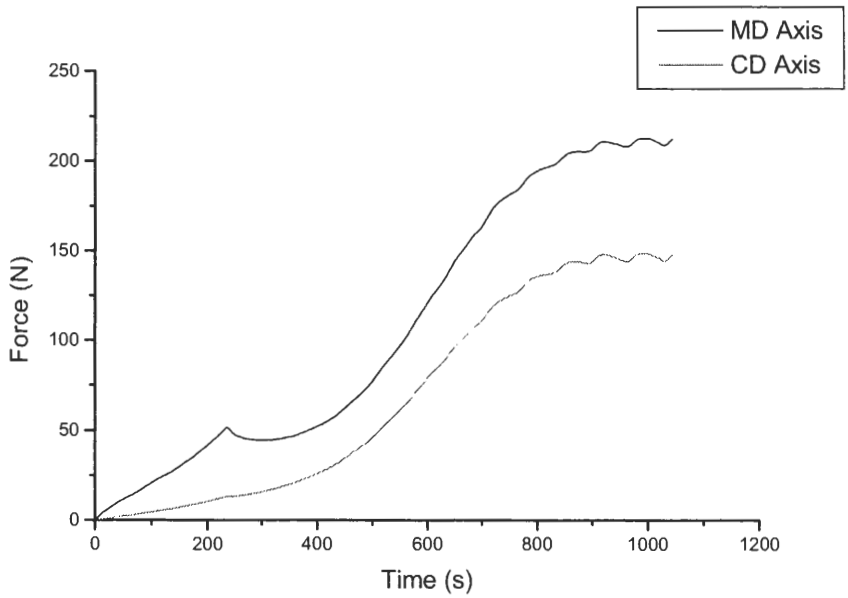

Sample 29-1. Top curve is MD, bottom is CD

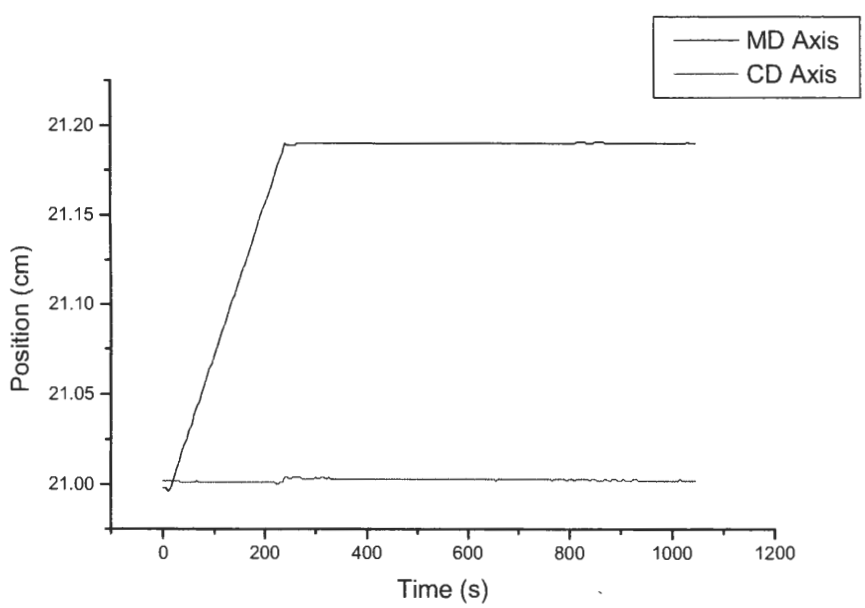

Sample 29-1. Top curve is MD, bottom is CD

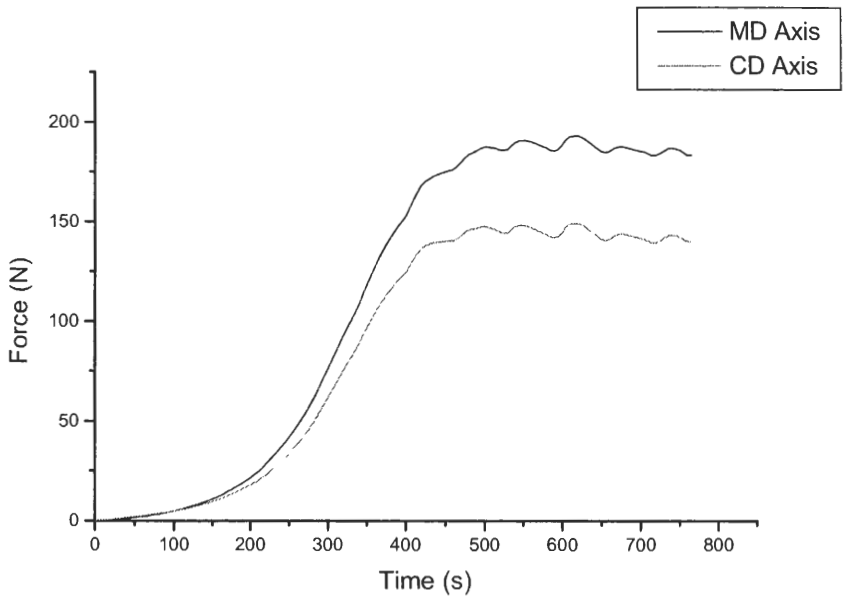

Sample 30-1. Top curve is MD, bottom is CD

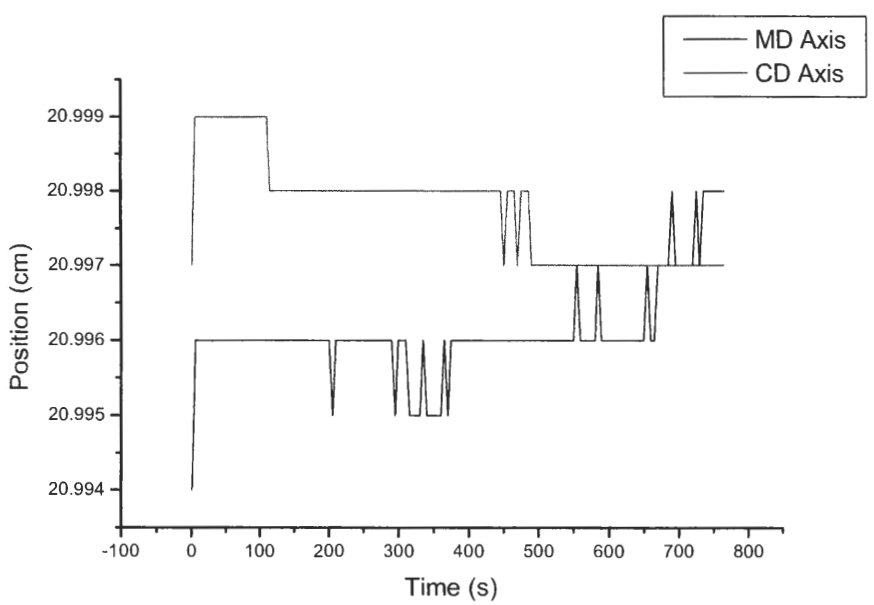

Sample 30-1. Top curve is CD, bottom is MD

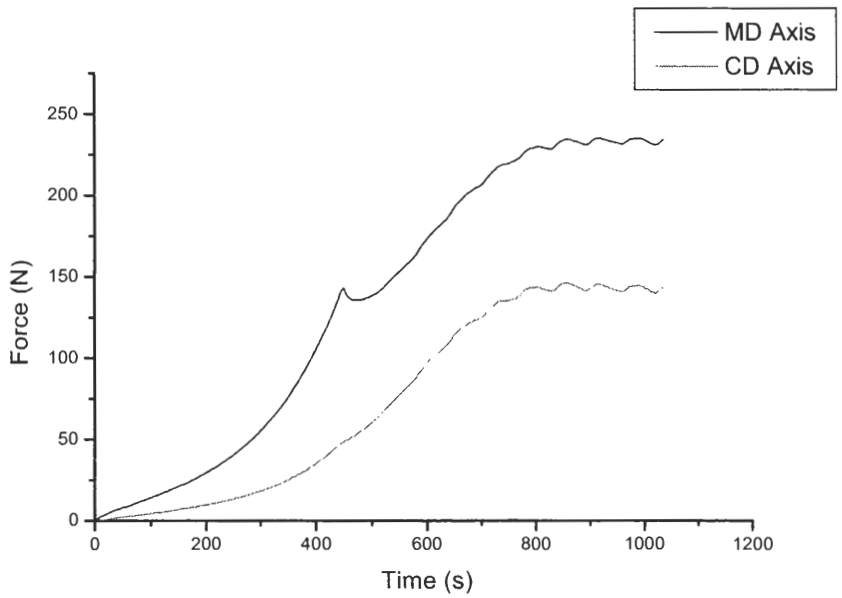

Sample 31-1. Top curve is MD, bottom is CD

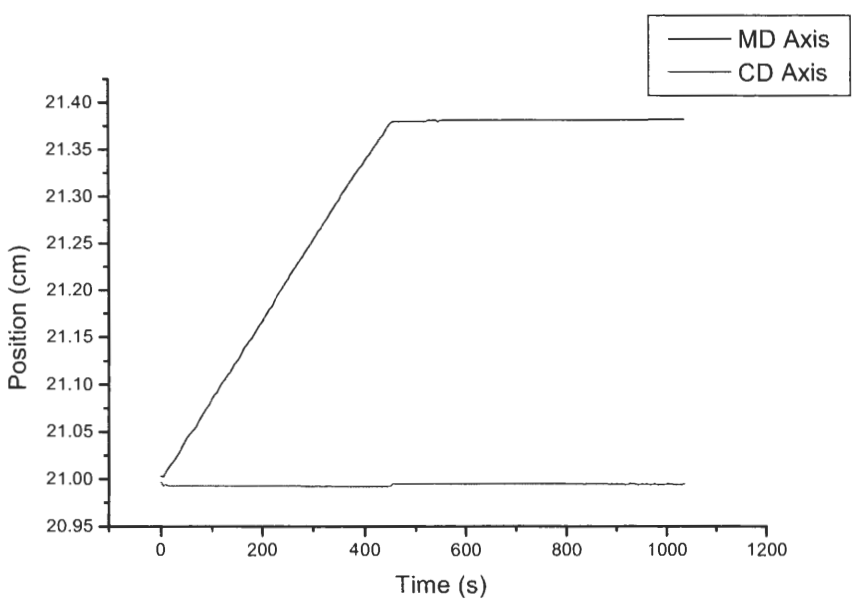

Sample 31-1. Top curve is MD, bottom is CD

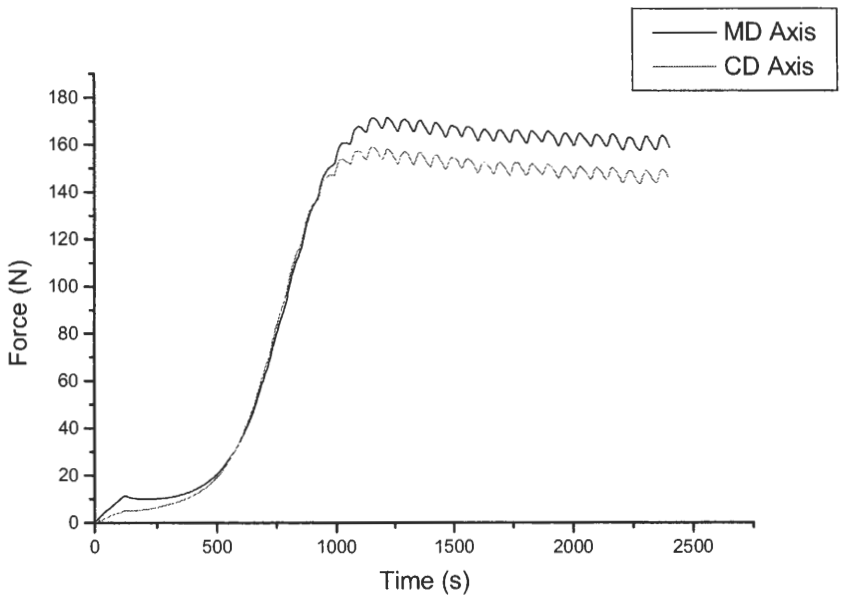

Sample 32-1. Top curve is MD, bottom is CD

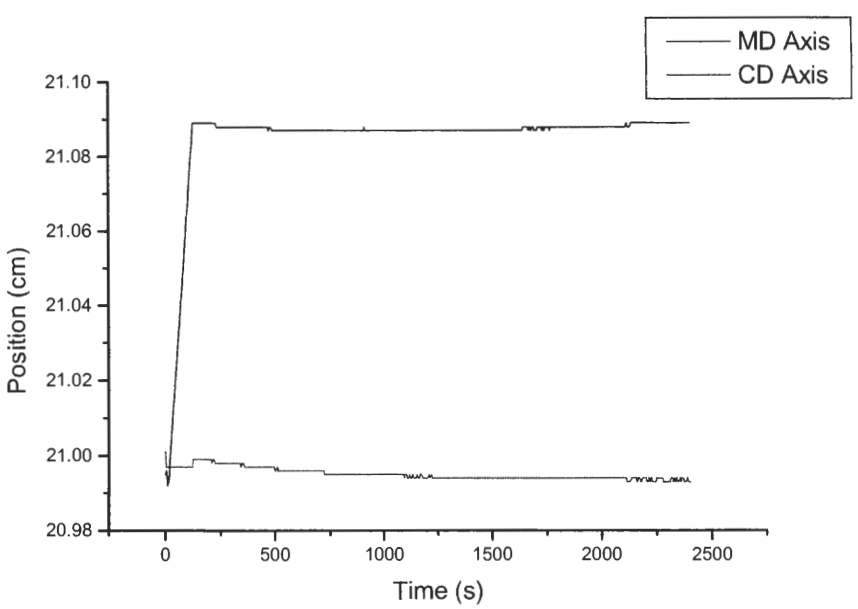

Sample 32-1. Top curve is MD, bottom is CD

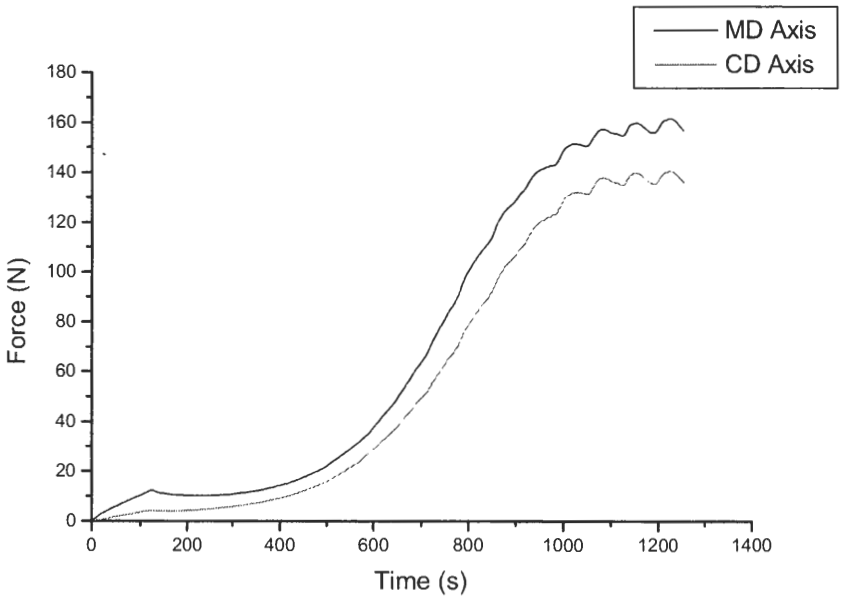

Sample 33-1. Top curve is MD, bottom is CD

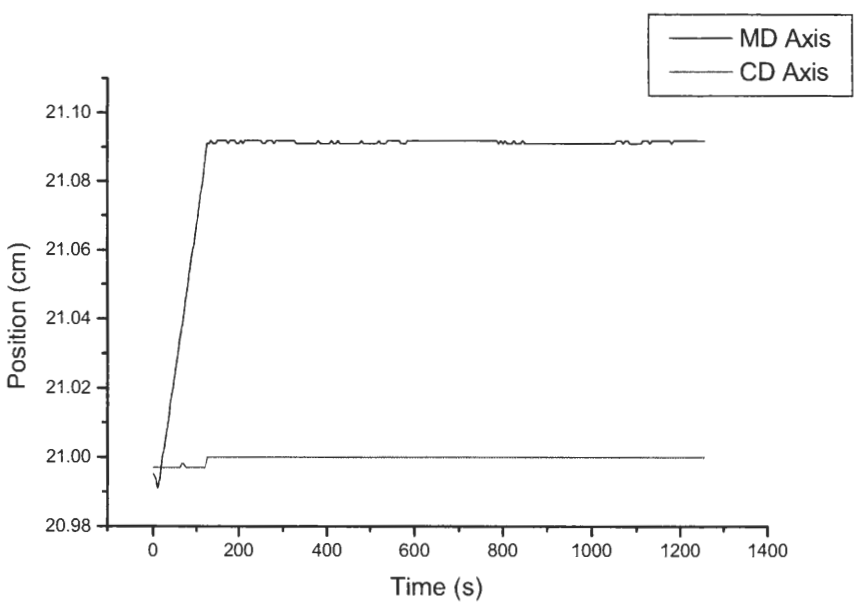

Sample 33-1. Top curve is MD, bottom is CD

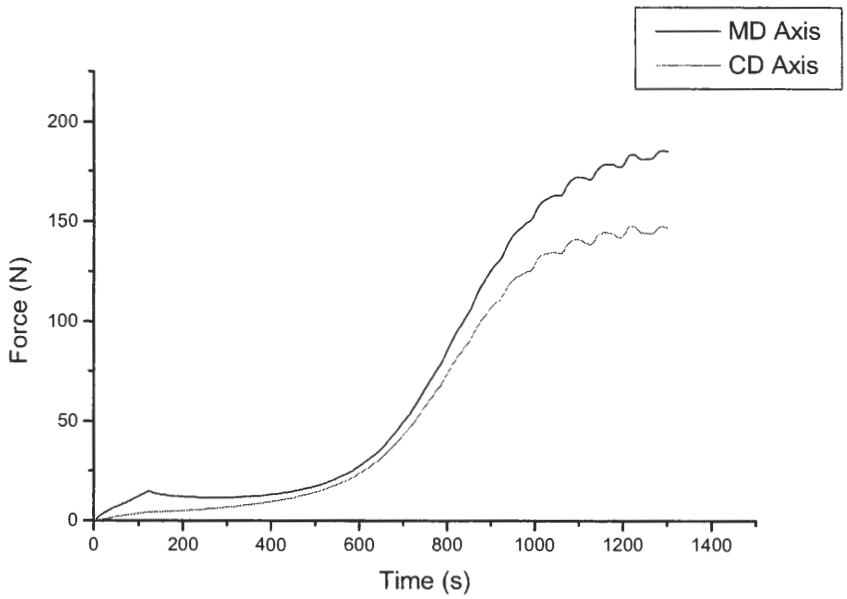

Sample 34-1. Top curve is MD, bottom is CD

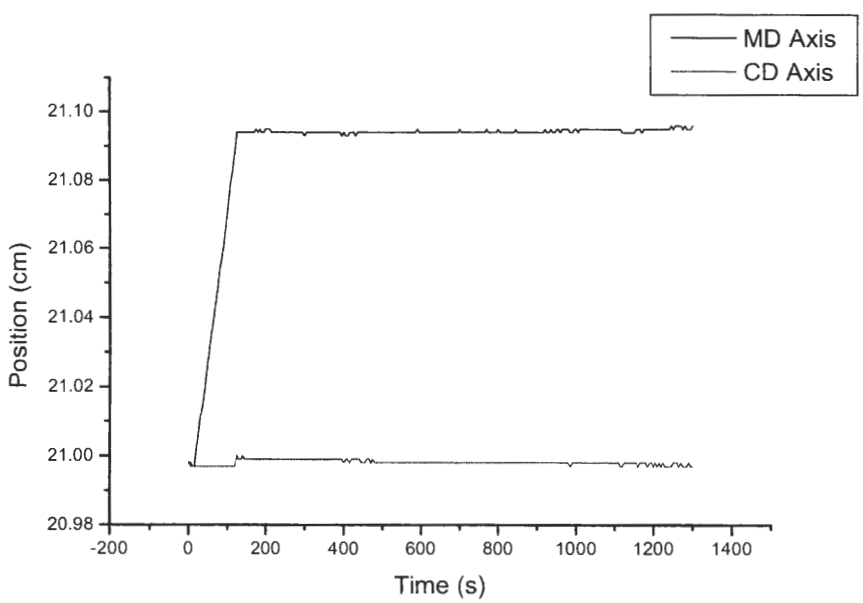

Sample 34-1. Top curve is MD, bottom is CD

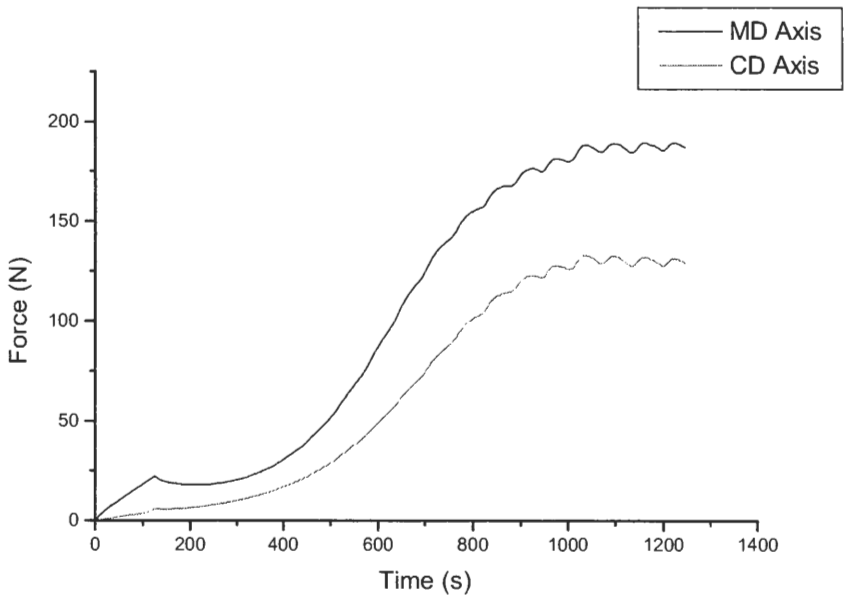

Sample 35-1. Top curve is MD, bottom is CD

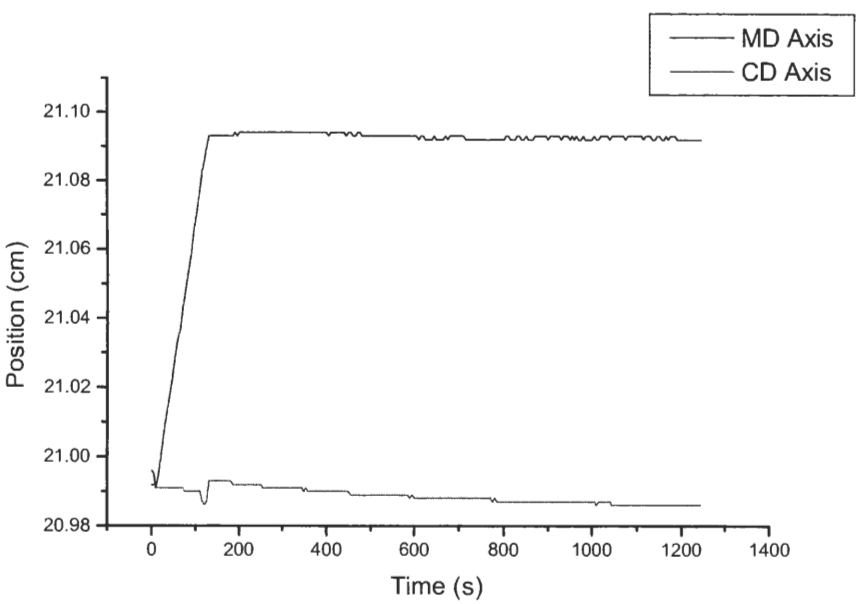

Sample 35-1. Top curve is MD, bottom is CD

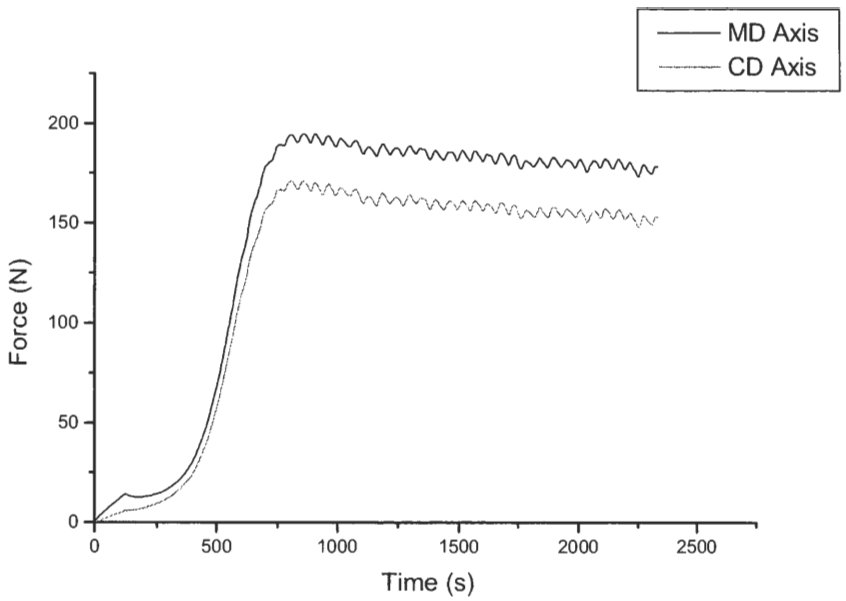

Sample 36-1. Top curve is MD, bottom is CD

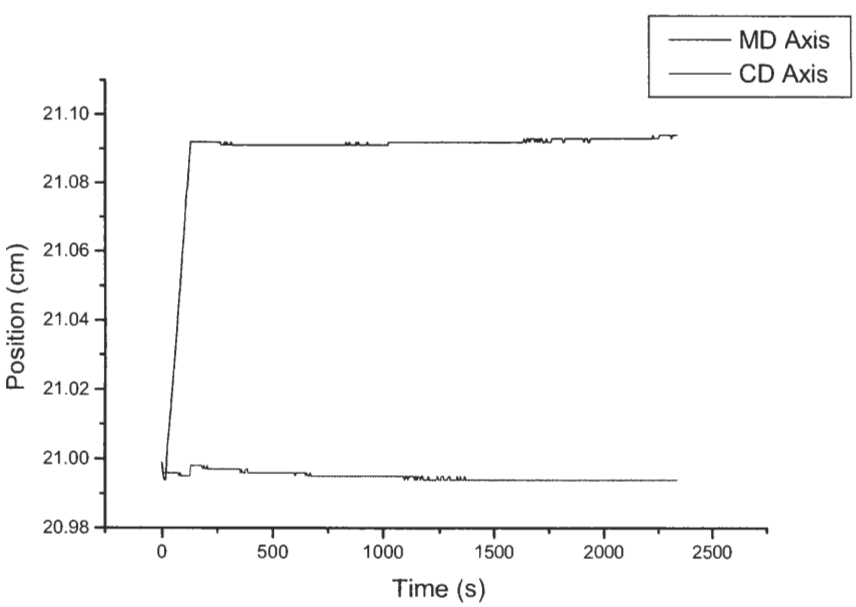

Sample 36-1. Top curve is MD, bottom is CD

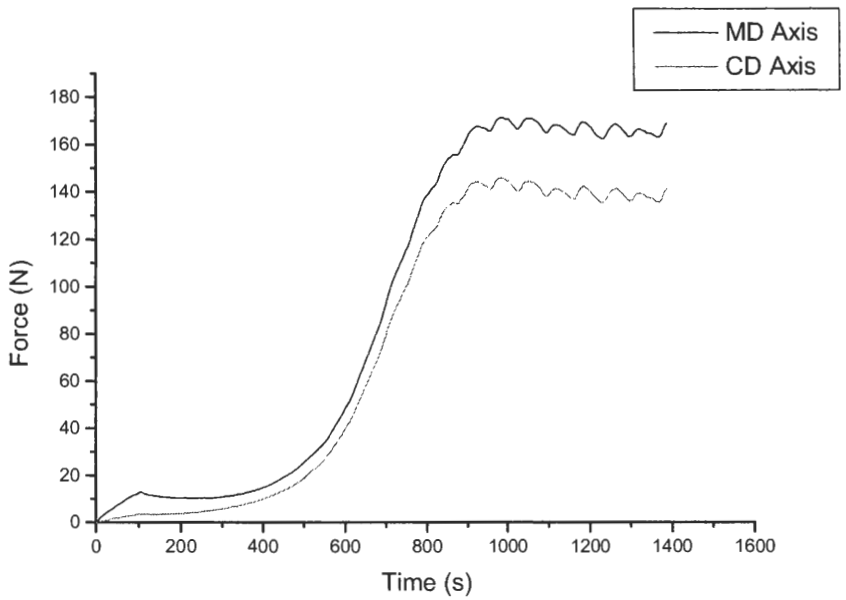

Sample 37-1. Top curve is MD, bottom is CD

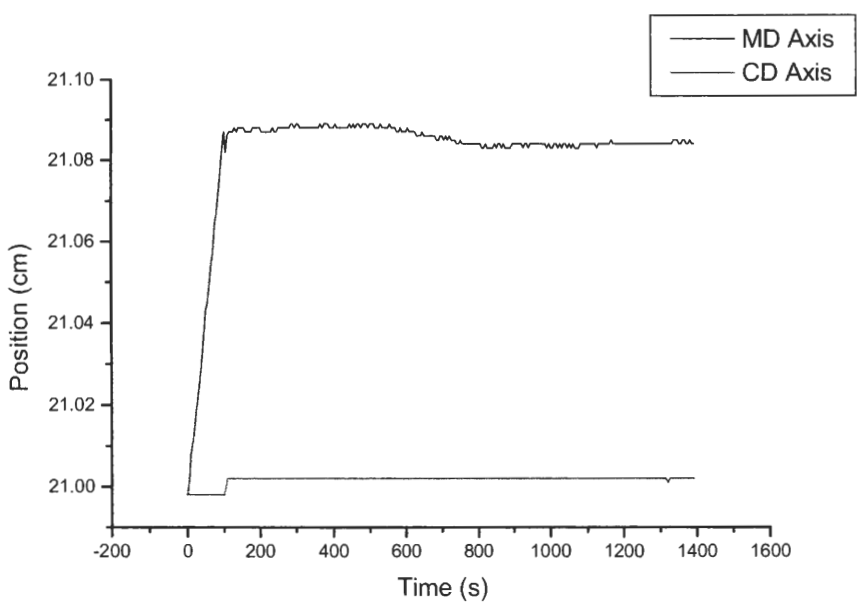

Sample 37-1. Top curve is MD, bottom is CD

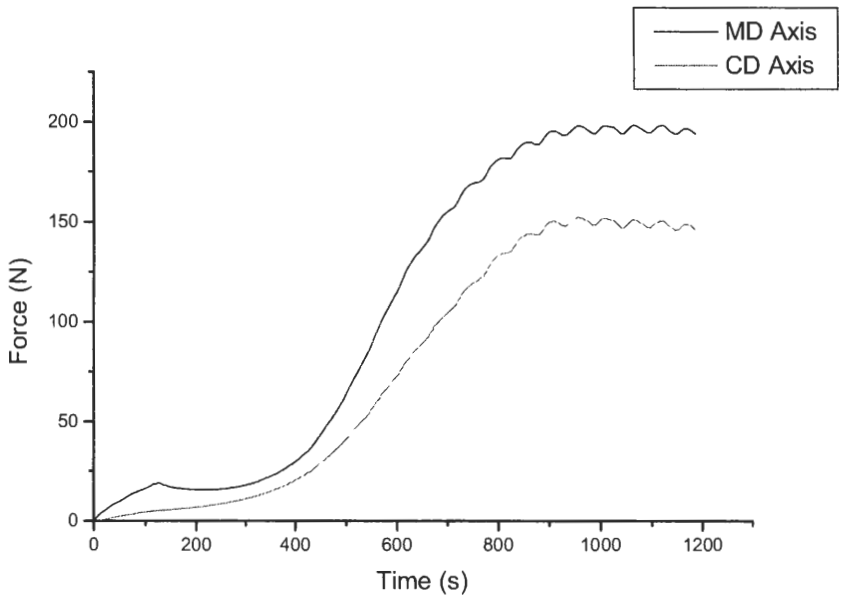

Sample 38-1. Top curve is MD, bottom is CD

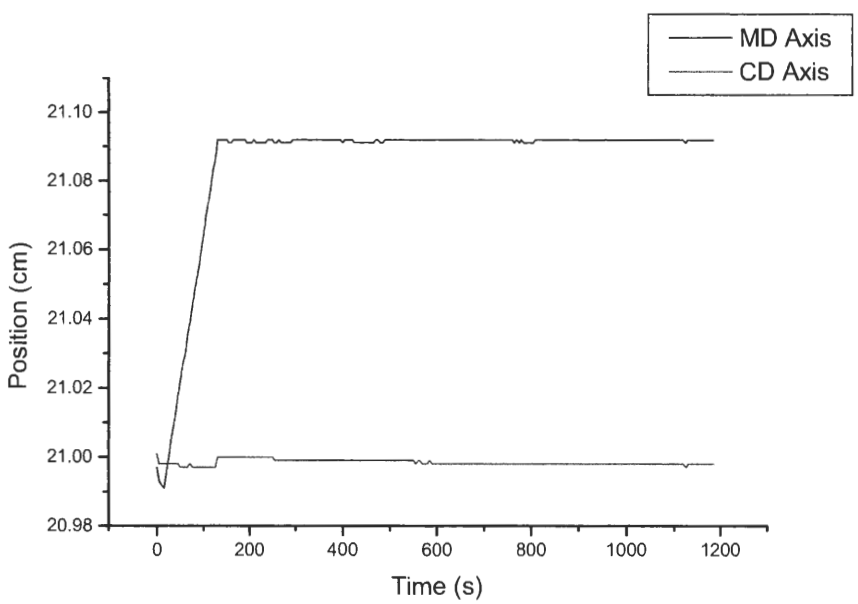

Sample 38-1. Top curve is MD, bottom is CD

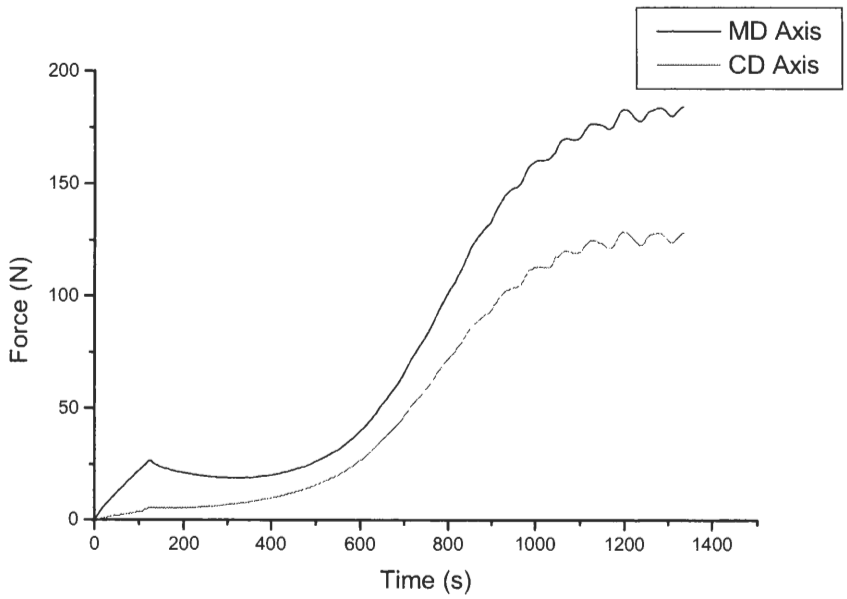

Sample 39-1. Top curve is MD, bottom is CD

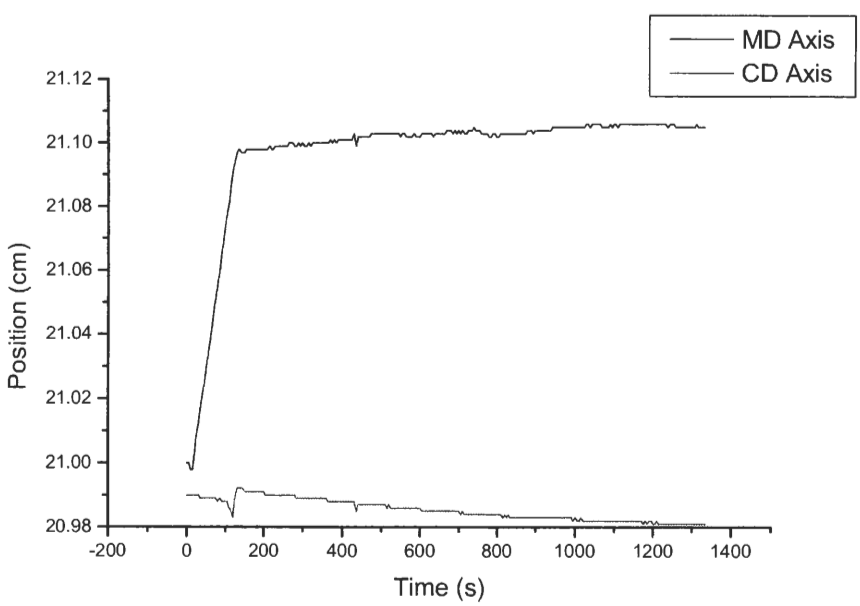

Sample 39-1. Top curve is MD, bottom is CD

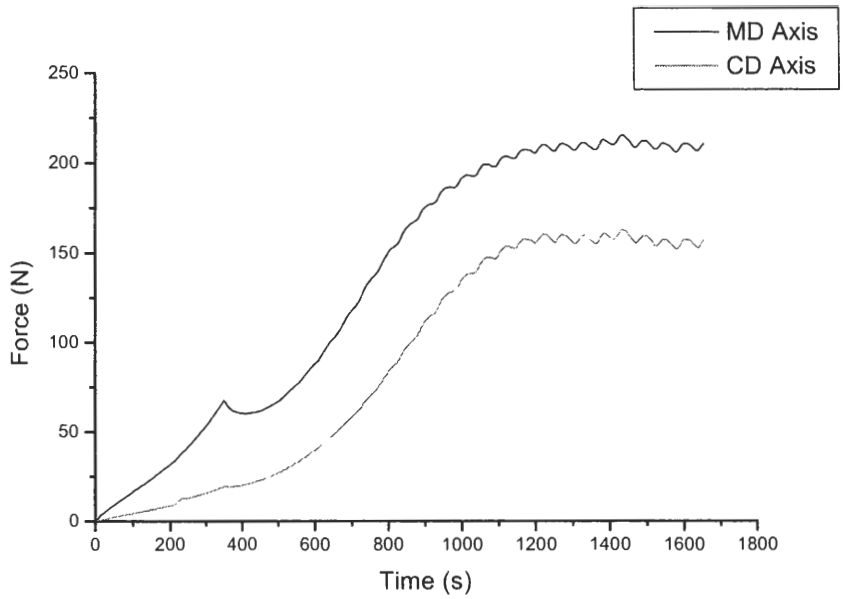

Sample 40-1. Top curve is MD, bottom is CD

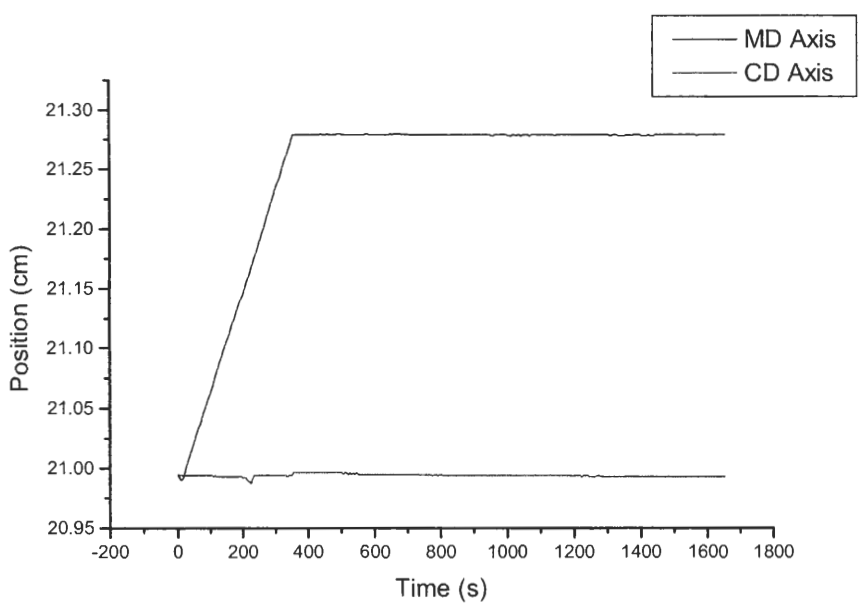

Sample 40-1. Top curve is MD, bottom is CD

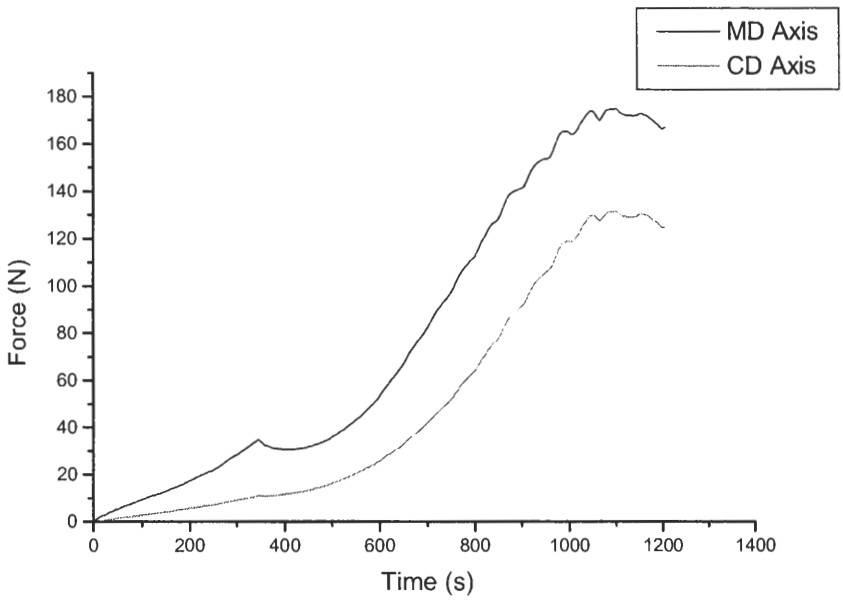

Sample 41-1. Top curve is MD, bottom is CD

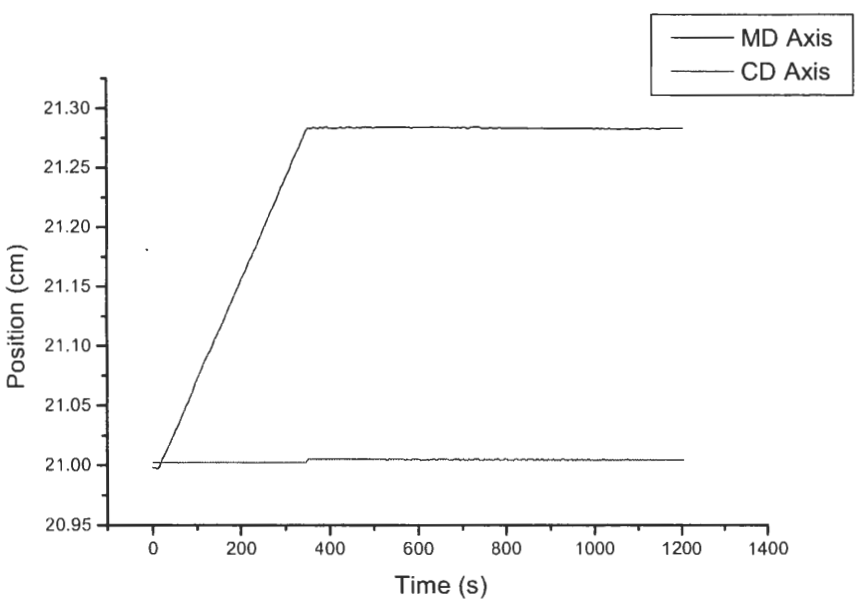

Sample 41-1. Top curve is MD, bottom is CD

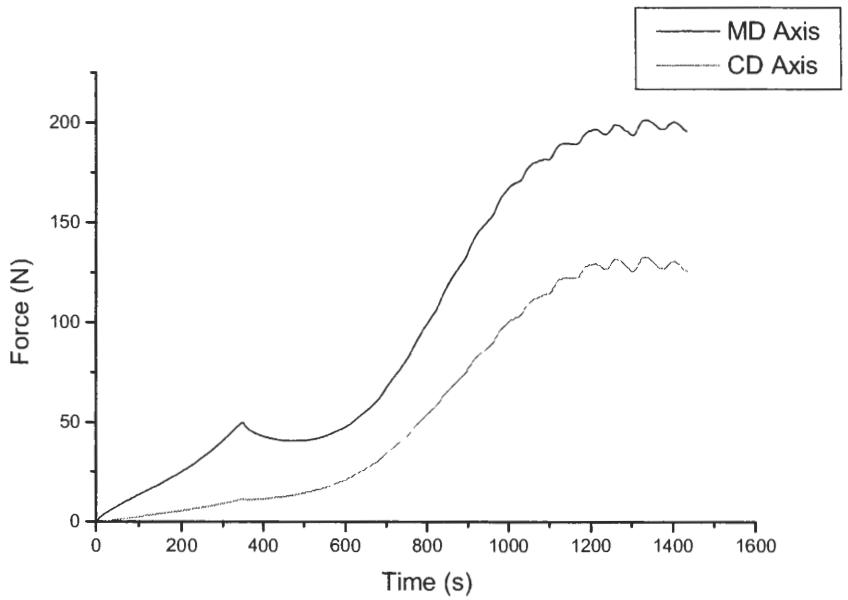

Figure 42-1. Top curve is MD, bottom is CD

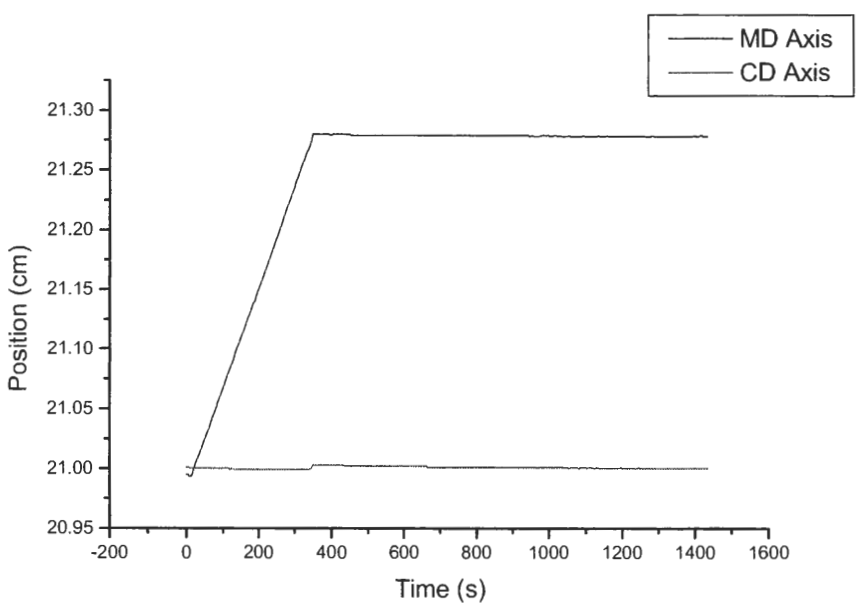

Sample 42-1. Top curve is MD, bottom is CD

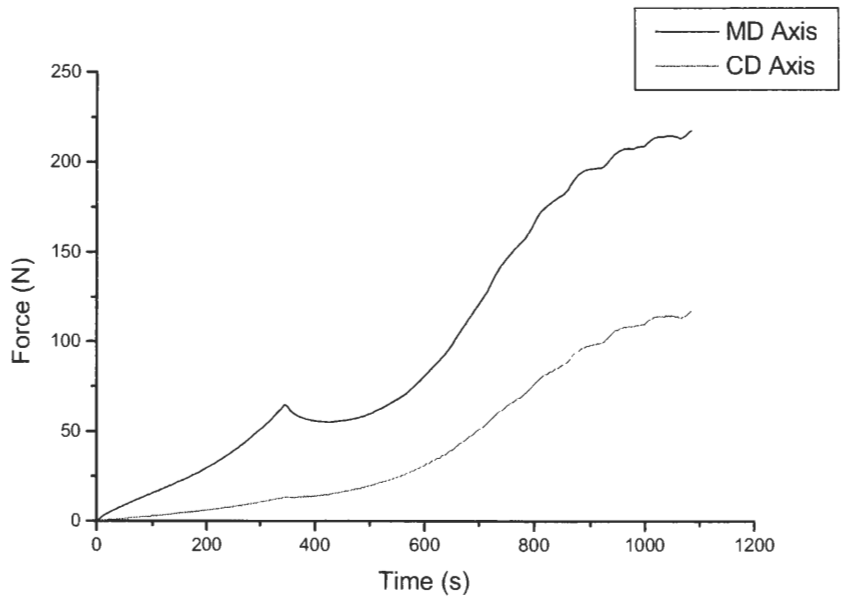

Sample 43-1. Top curve is MD, bottom is CD

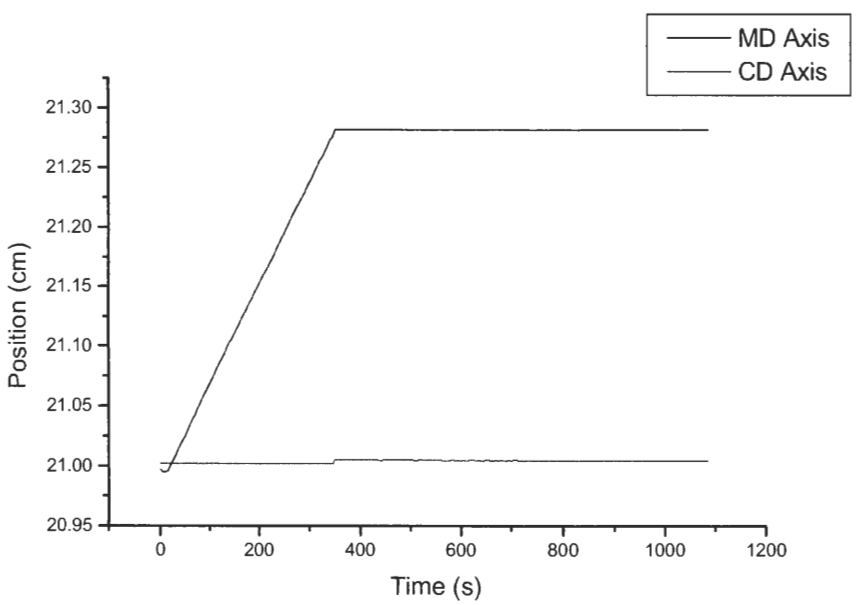

Sample 43-1. Top curve is MD, bottom is CD

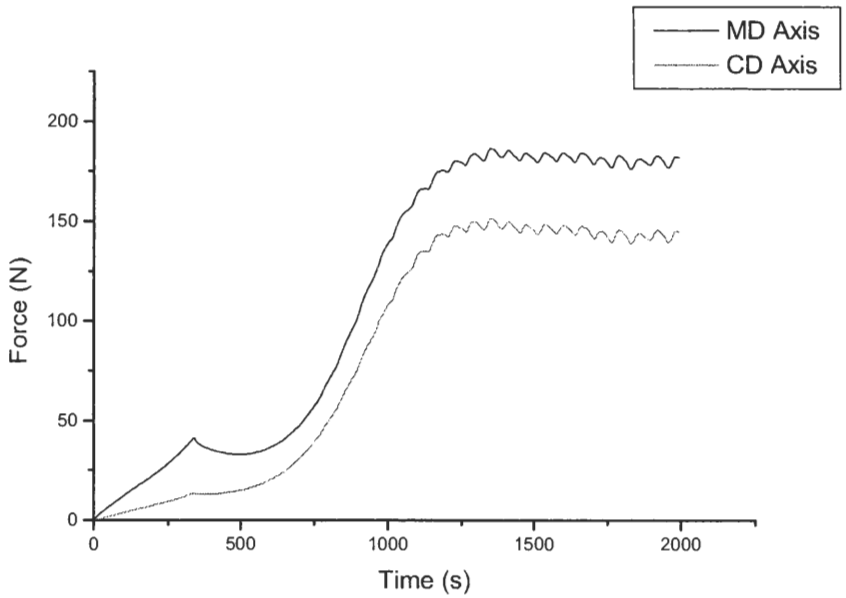

Sample 44-1. Top curve is MD, bottom is CD

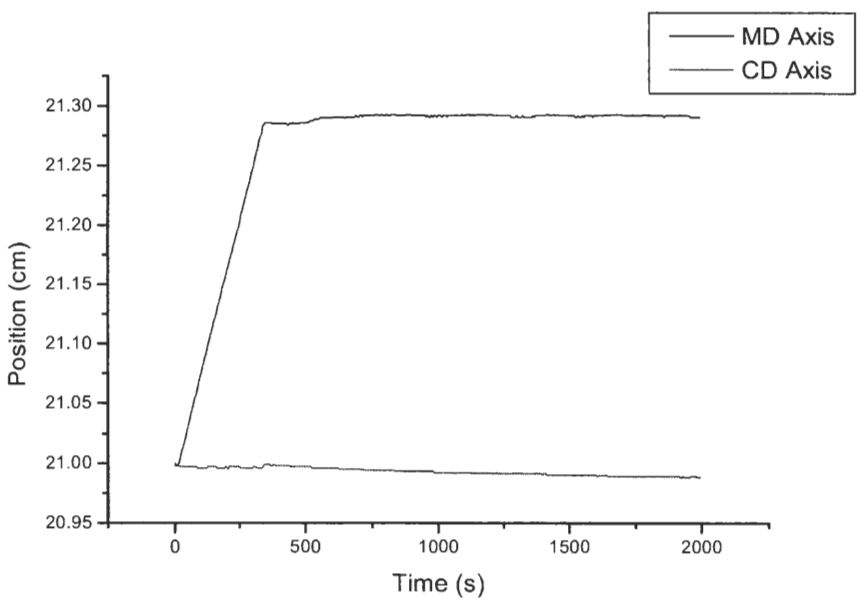

Sample 44-1. Top curve is MD, bottom is CD

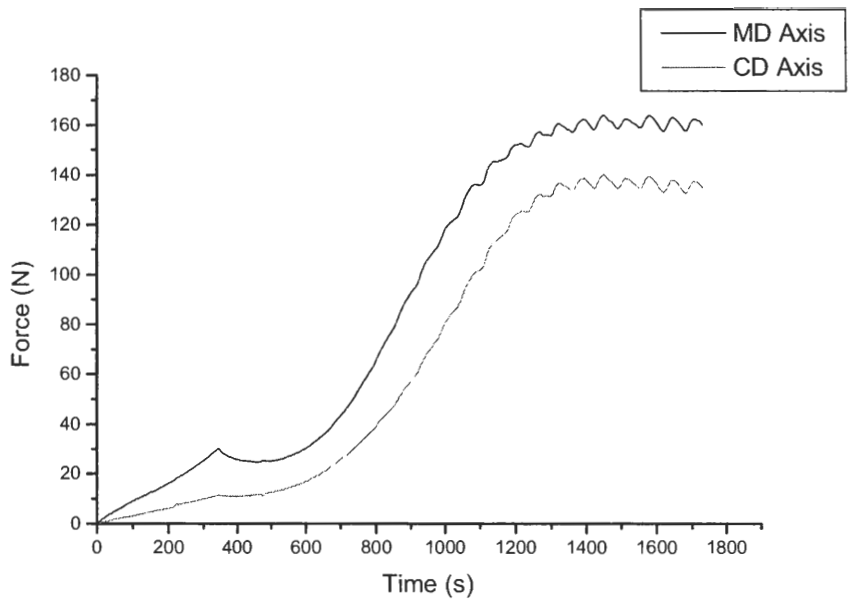

Sample 45-1. Top curve is MD, bottom is CD

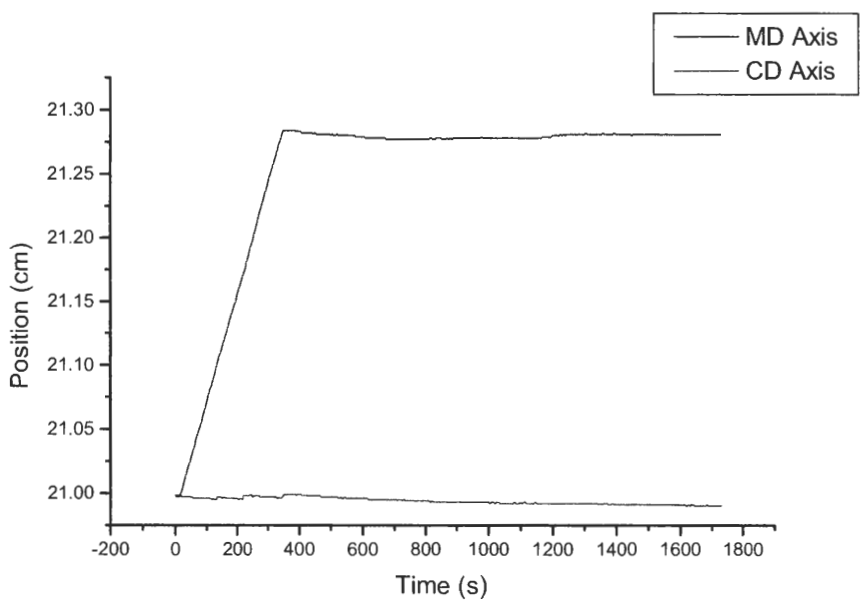

Sample 45-1. Top curve is MD, bottom is CD

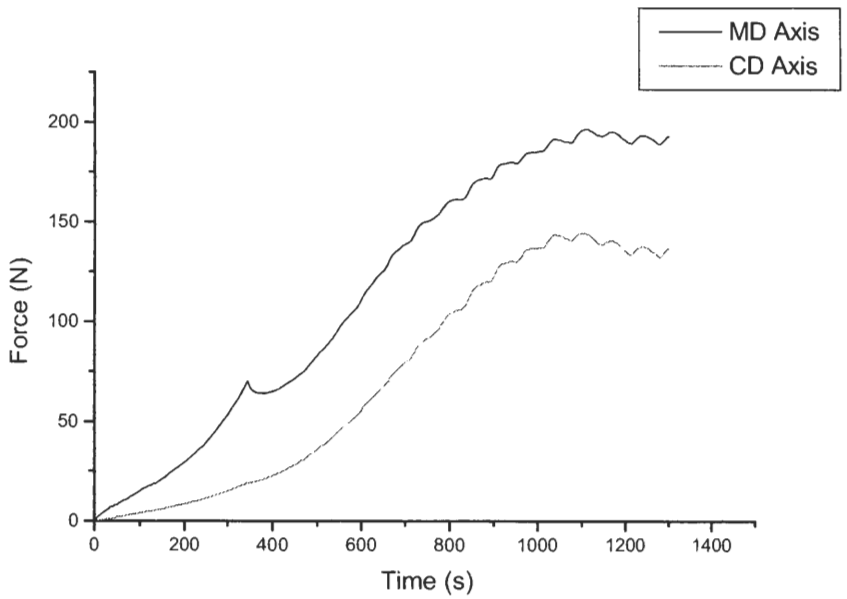

Sample 46-1. Top curve is MD, bottom is CD

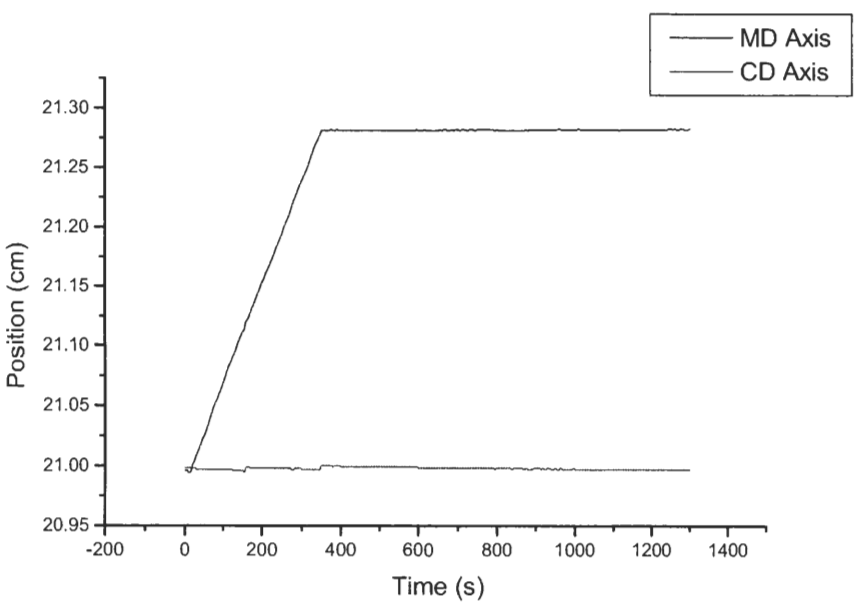

Sample 46-1. Top curve is MD, bottom is CD

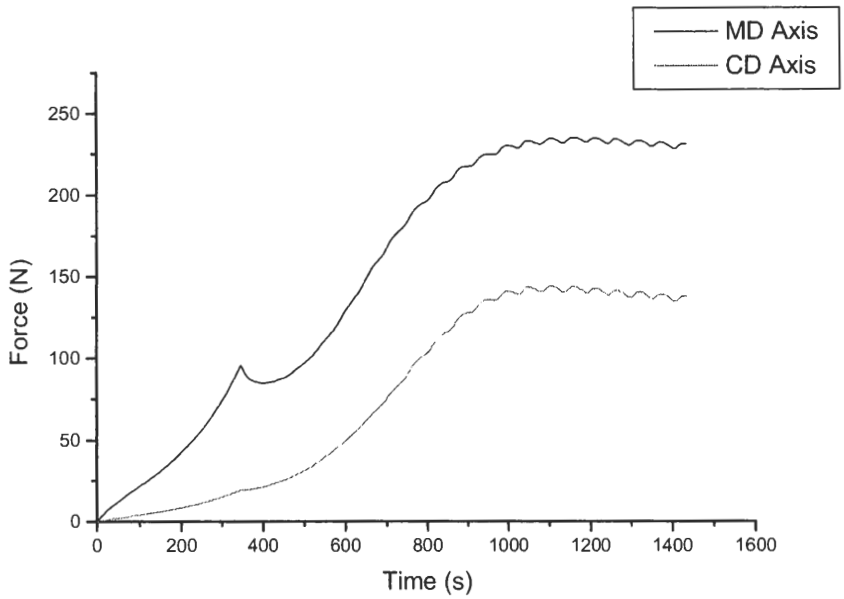

Sample 47-1. Top curve is MD, bottom is CD

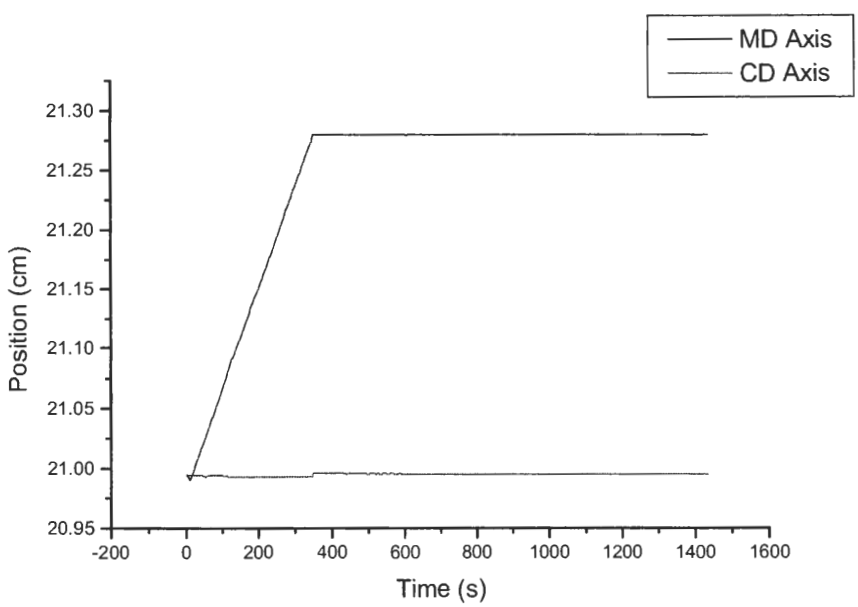

Sample 47-1. Top curve is MD, bottom is CD

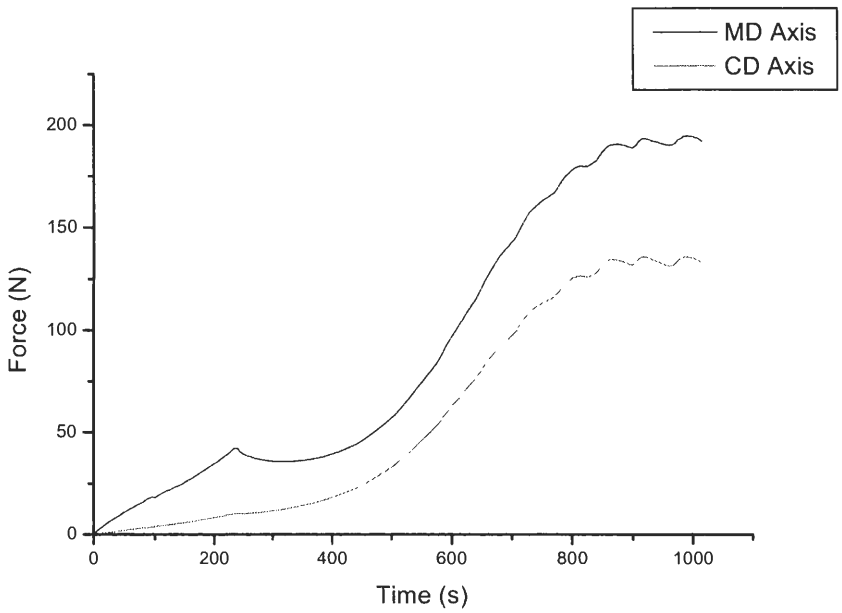

Sample 48-1. Top curve is MD, bottom is CD

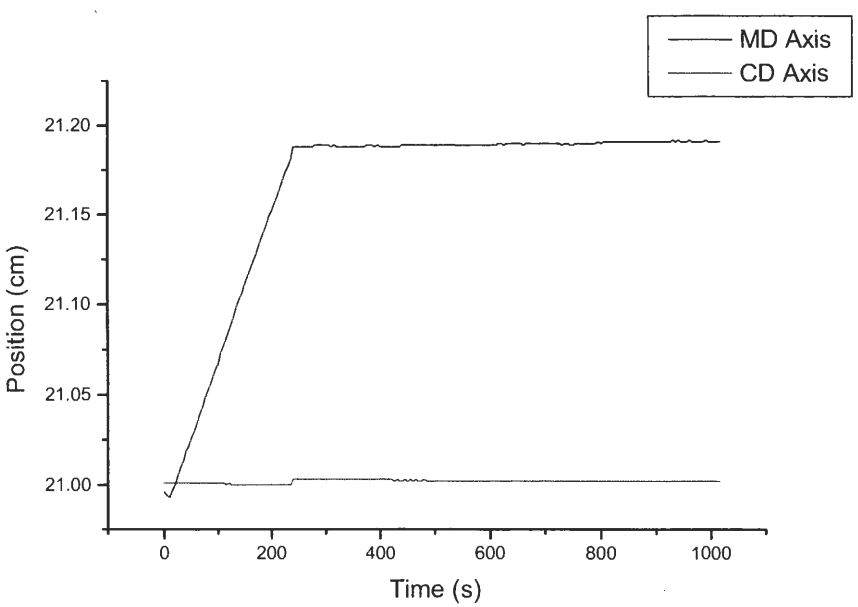

Sample 48-1. Top curve is MD, bottom is CD

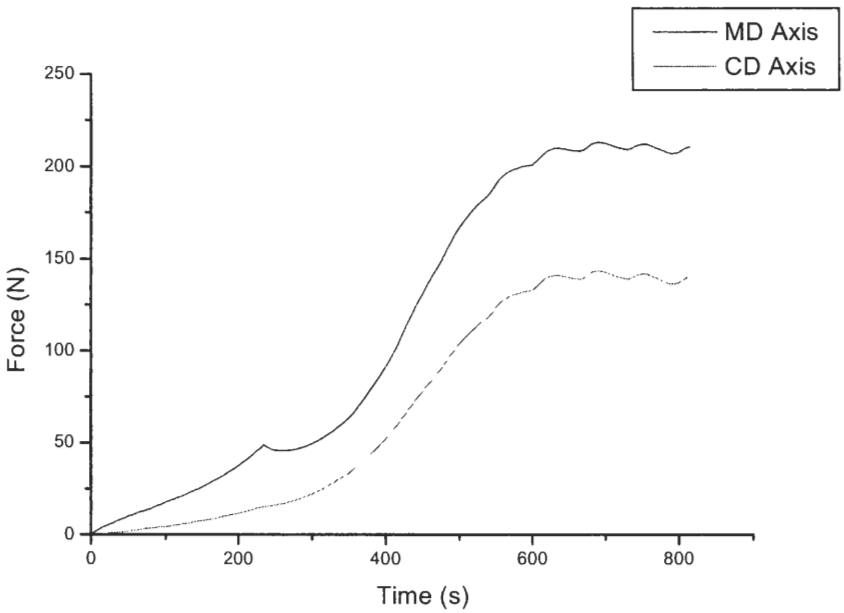

Sample 49-1. Top curve is MD, bottom is CD

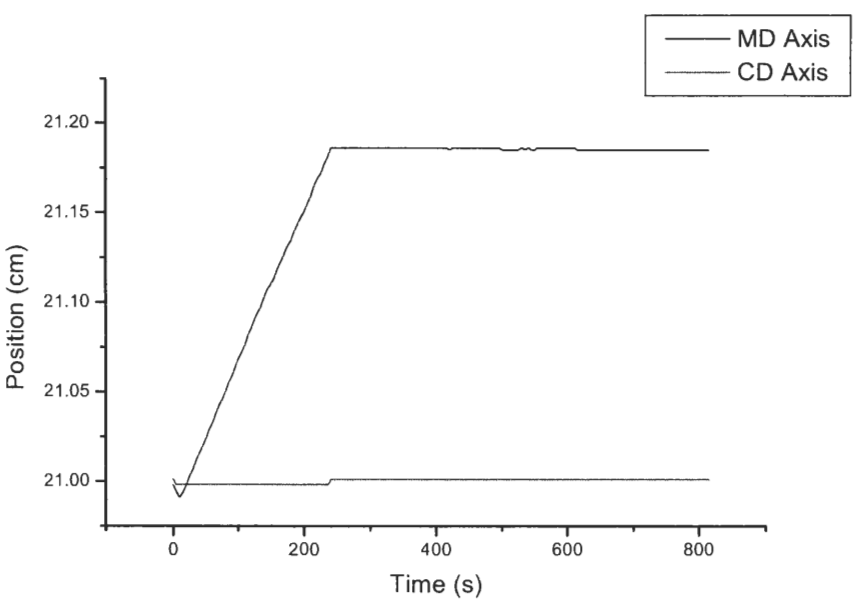

Sample 49-1. Top curve is MD, bottom is CD

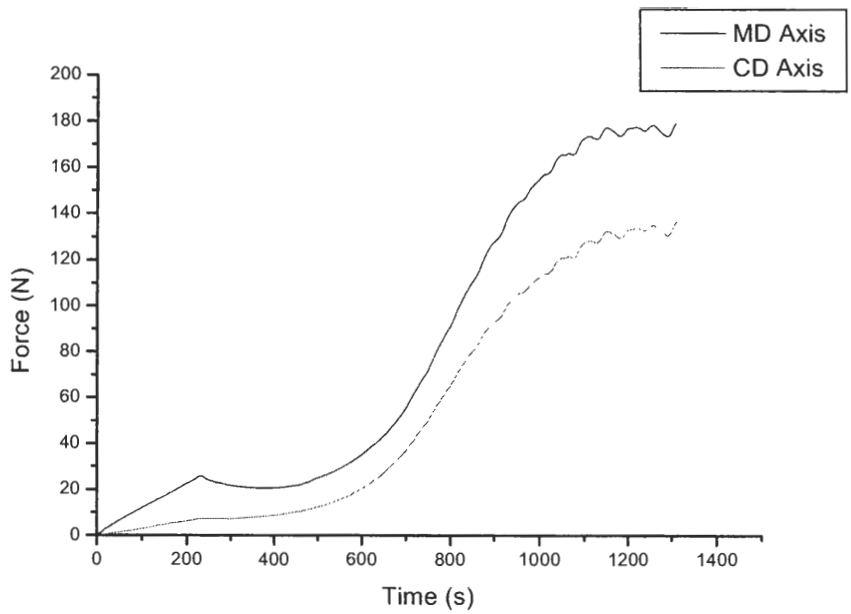

Sample 50-1. Top curve is MD, bottom is CD

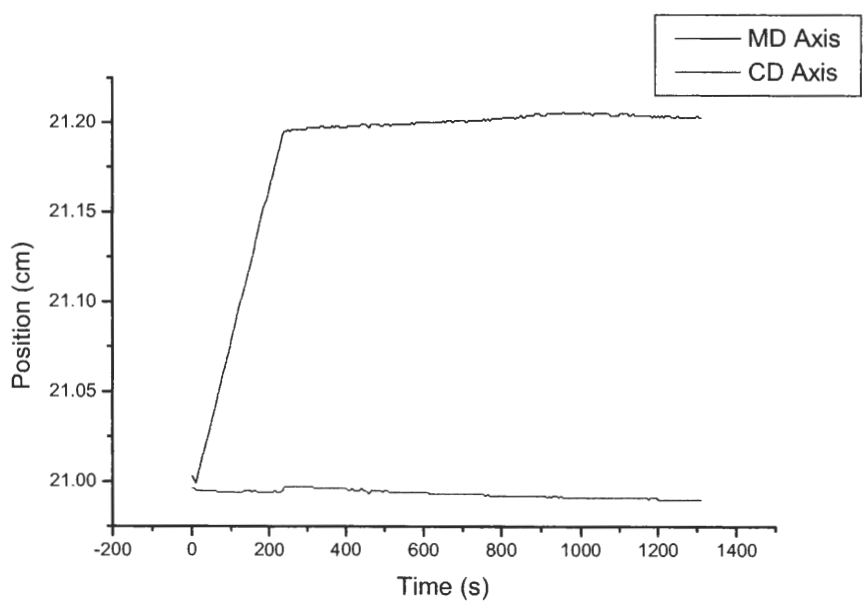

Sample 50-1. Top curve is MD, bottom is CD

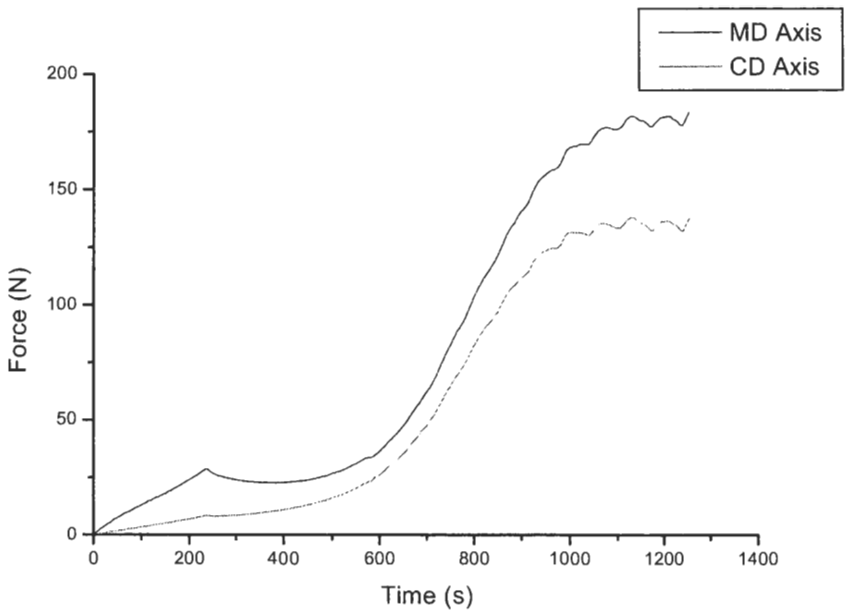

Sample 51-1. Top curve is MD, bottom is CD

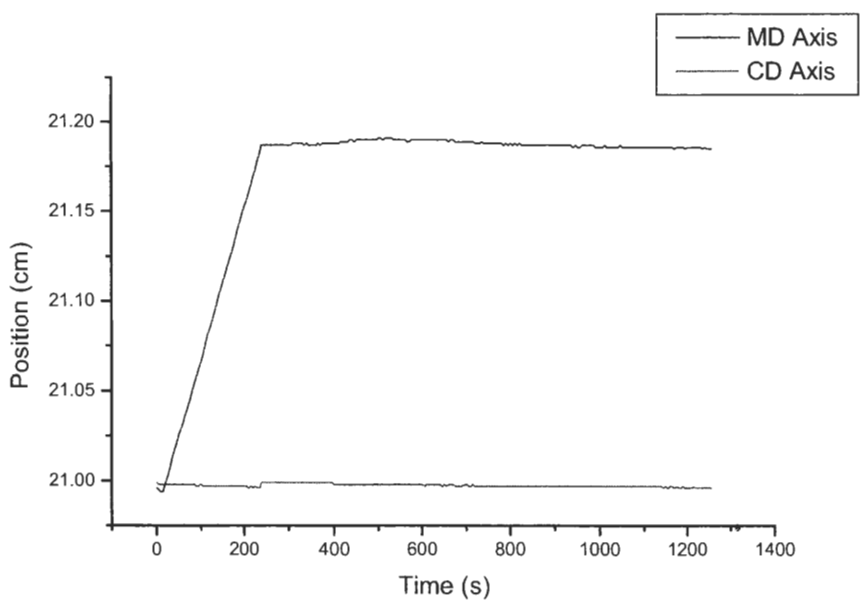

Sample 51-1. Top curve is MD, bottom is CD

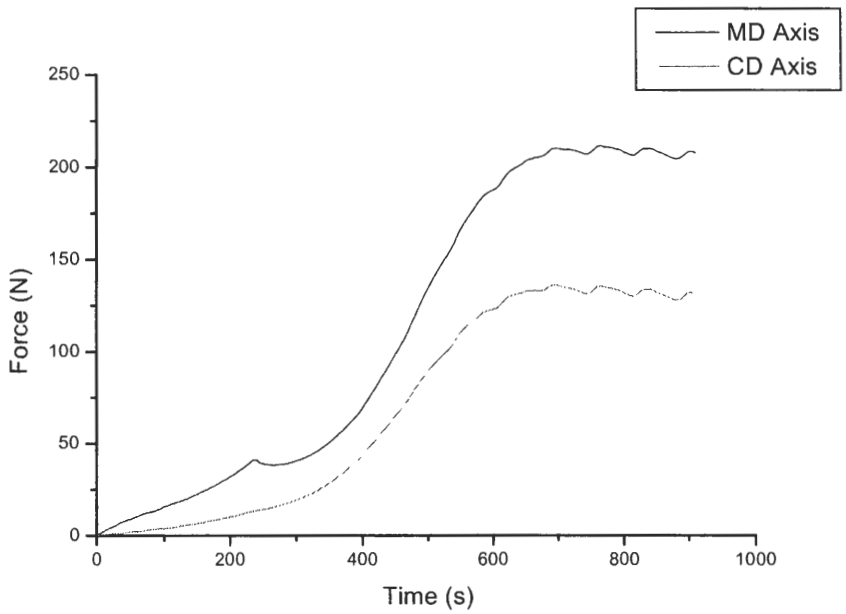

Sample 52-1. Top curve is MD, bottom is CD

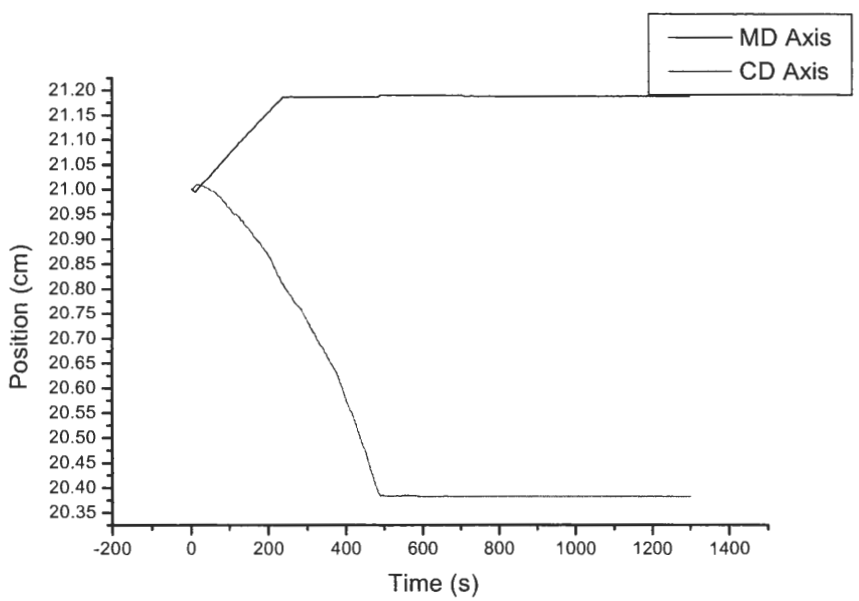

Sample 52-1. Top curve is MD, bottom is CD

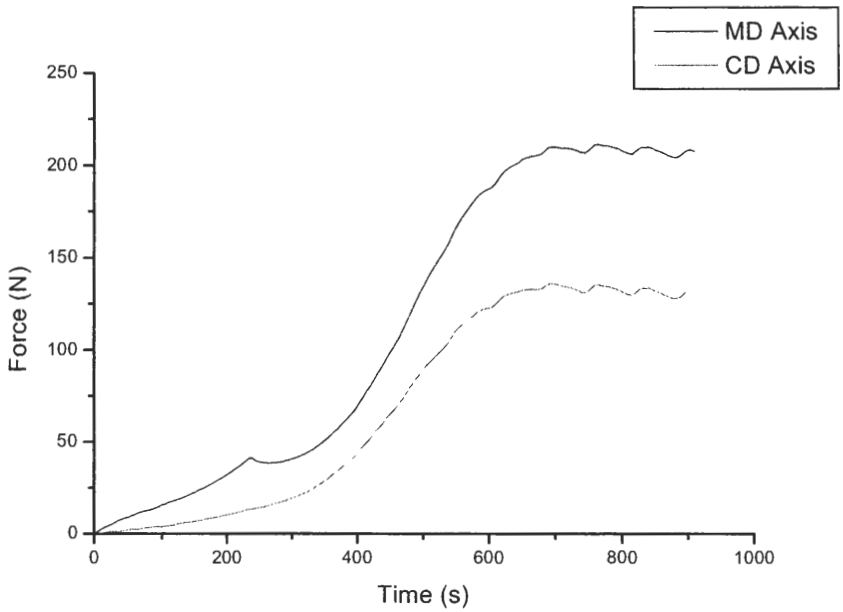

Sample 53-1. Top curve is MD, bottom is CD

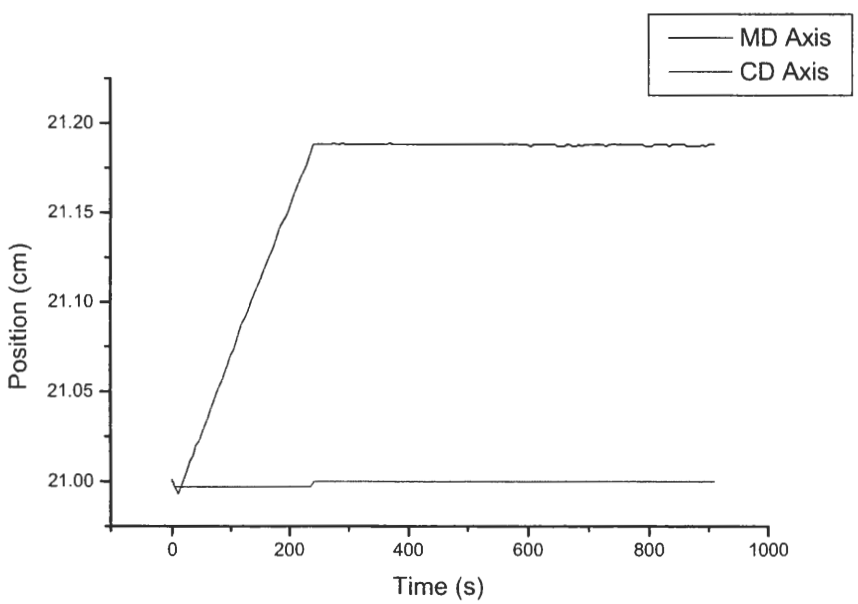

Sample 53-1. Top curve is MD, bottom is CD

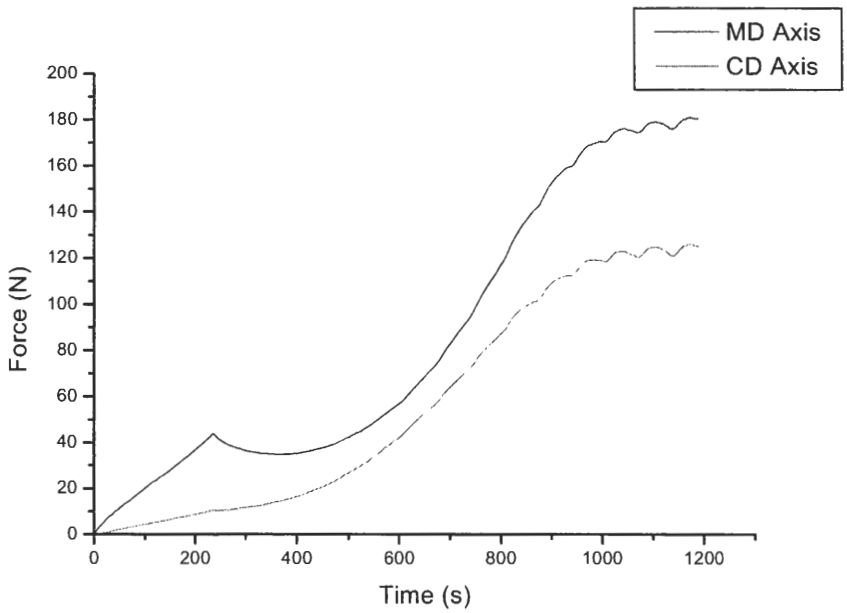

Sample 54-1. Top curve is MD, bottom is CD

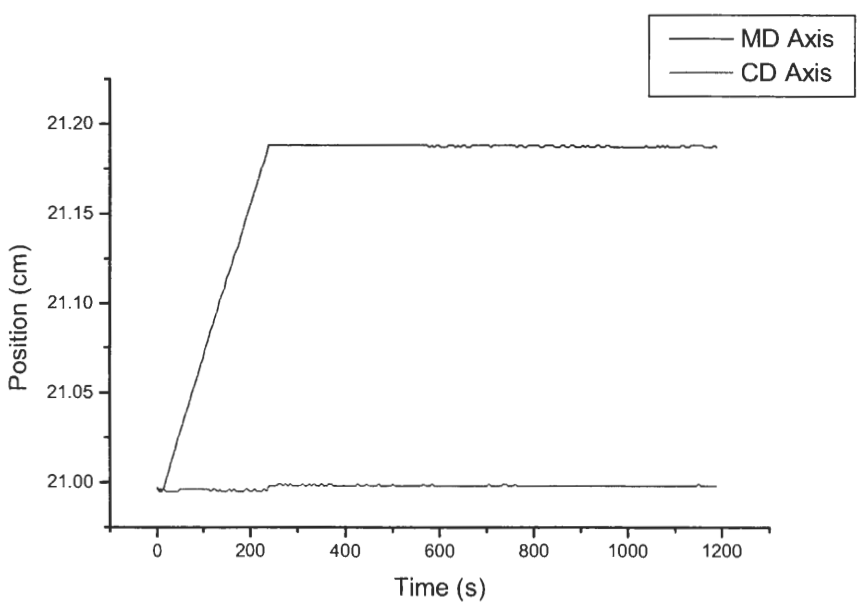

Sample 54-1. Top curve is MD, bottom is CD

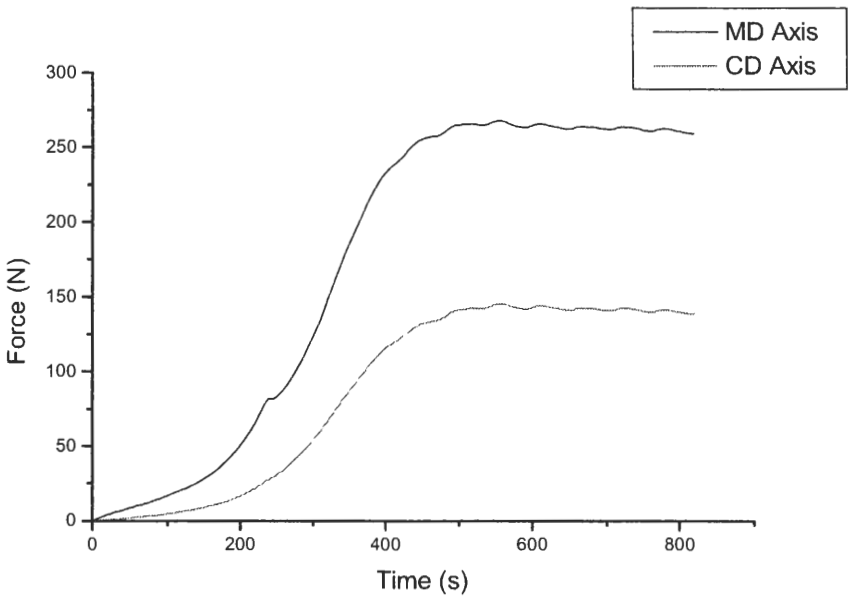

Sample 55-1. Top curve is MD, bottom is CD

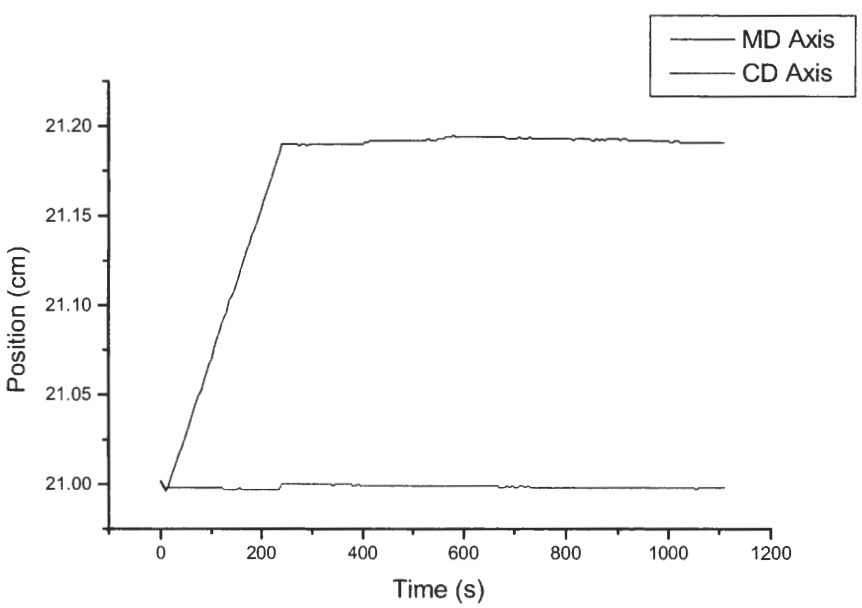

Sample 55-1. Top curve is MD, bottom is CD

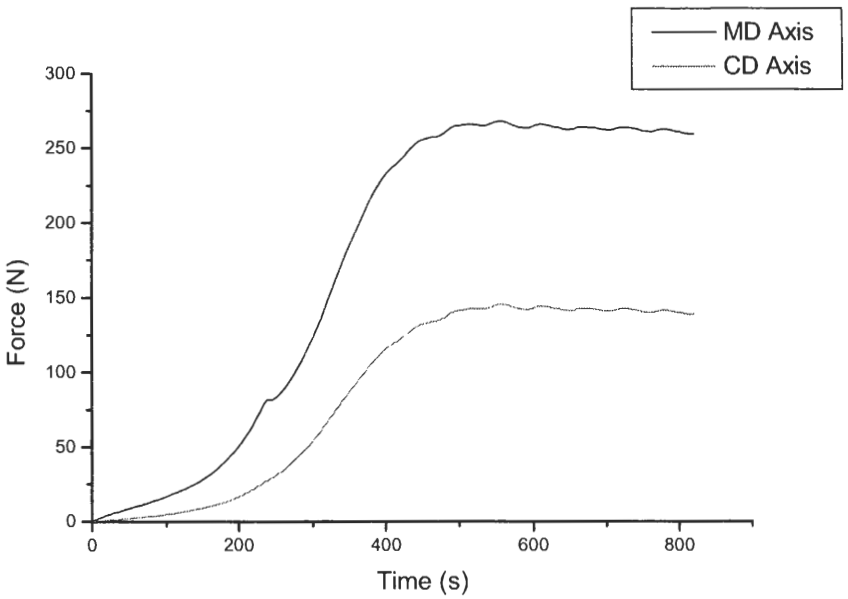

Sample 56-1. Top curve is MD, bottom is CD

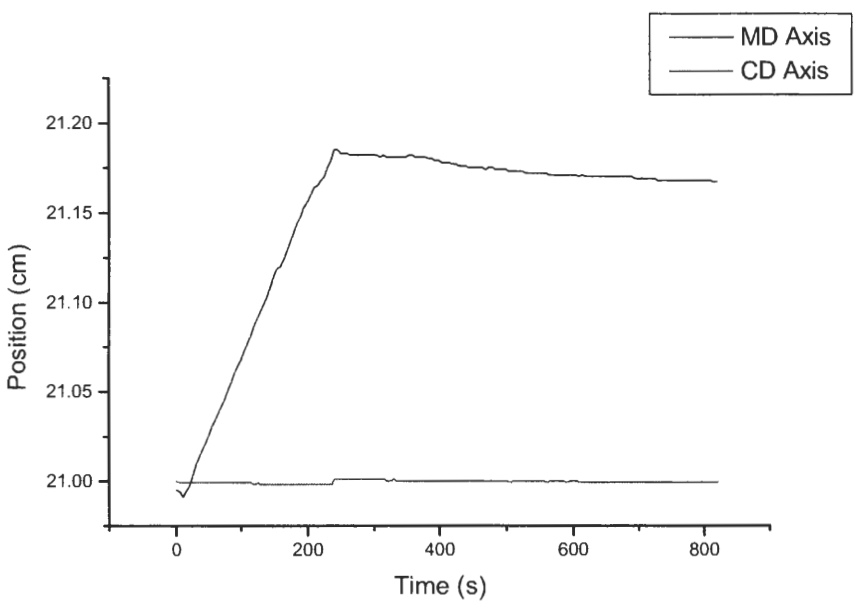

Sample 56-1. Top curve is MD, bottom is CD

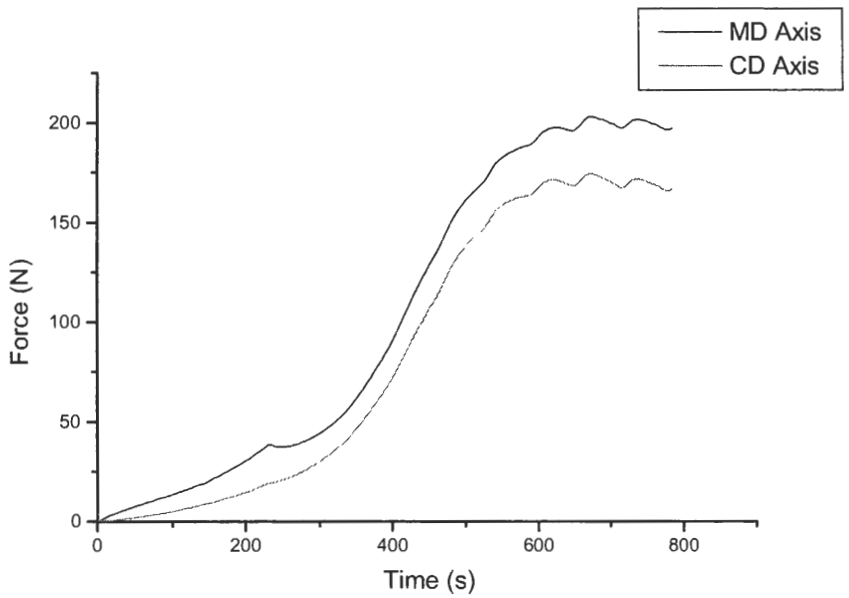

Sample 57-1. Top curve is MD, bottom is CD

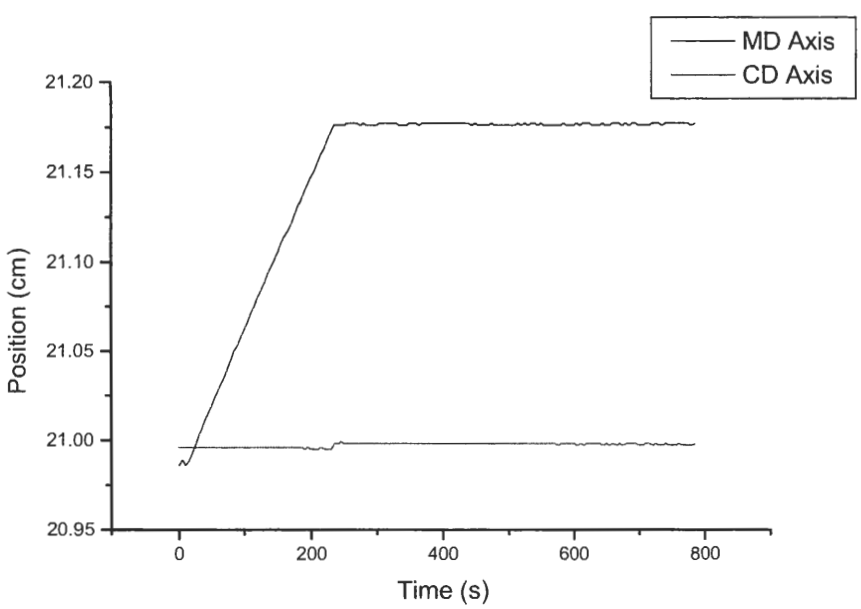

Sample 57-1. Top curve is MD, bottom is CD

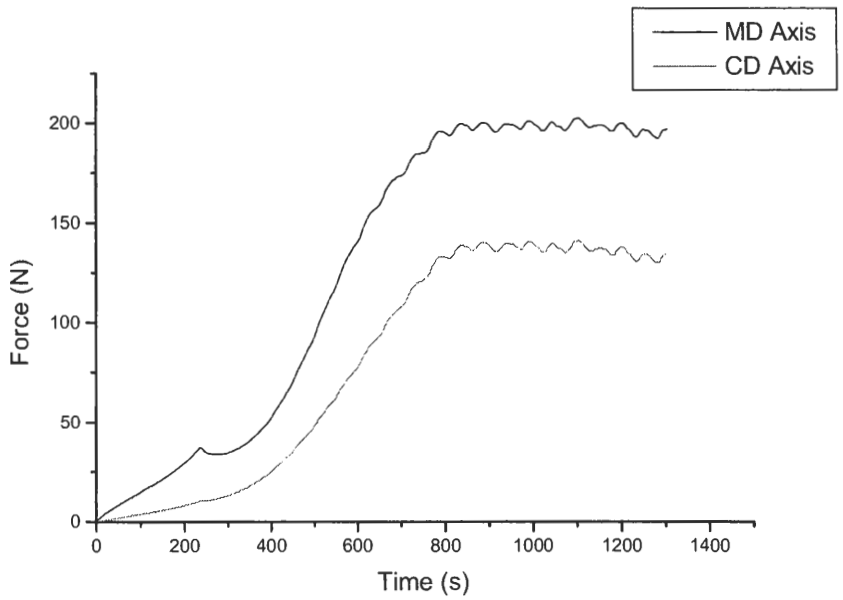

Sample 58-1. Top curve is MD, bottom is CD

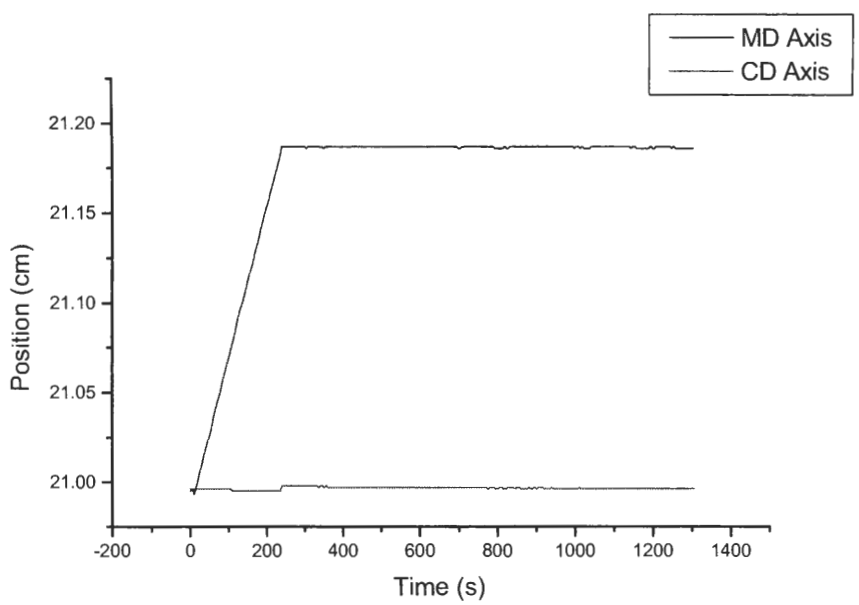

Sample 58-1. Top curve is MD, bottom is CD

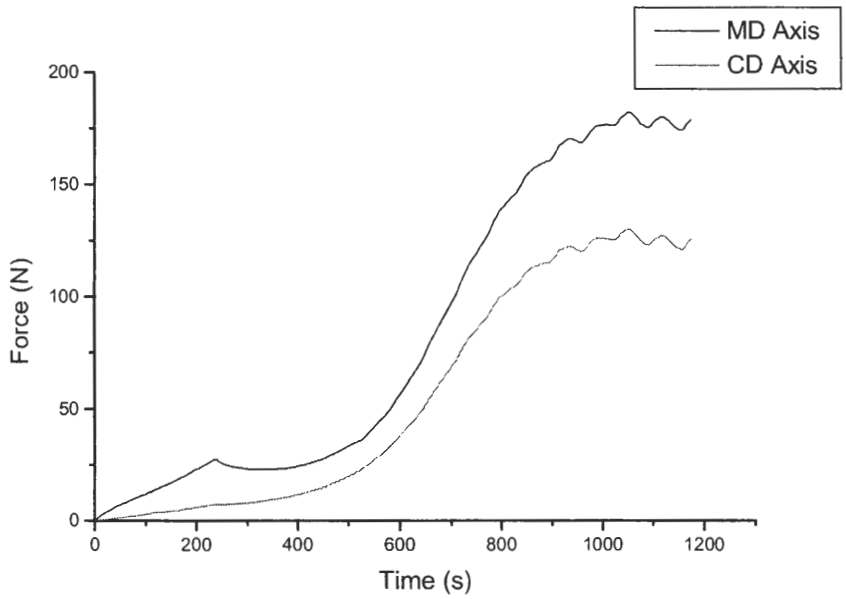

Sample 59-1. Top curve is MD, bottom is CD

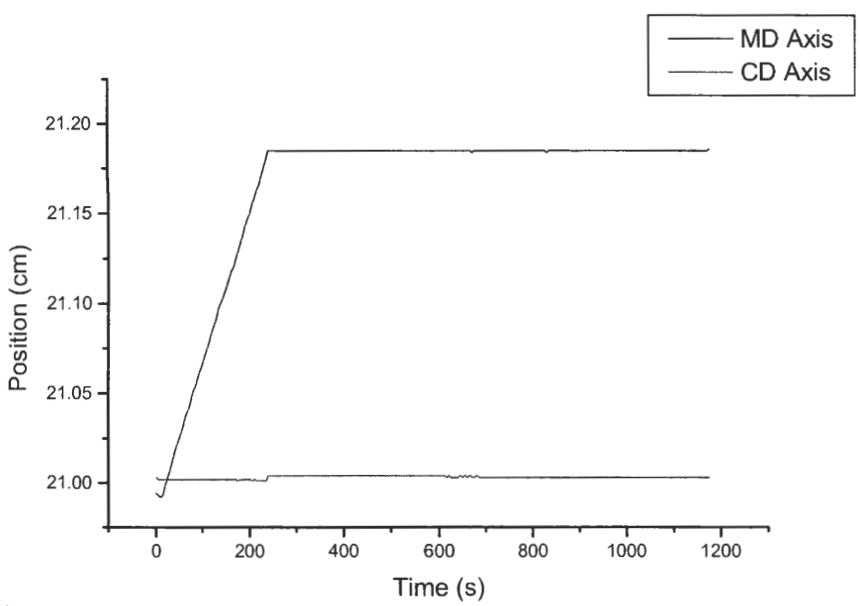

Sample 59-1. Top curve is MD, bottom is CD

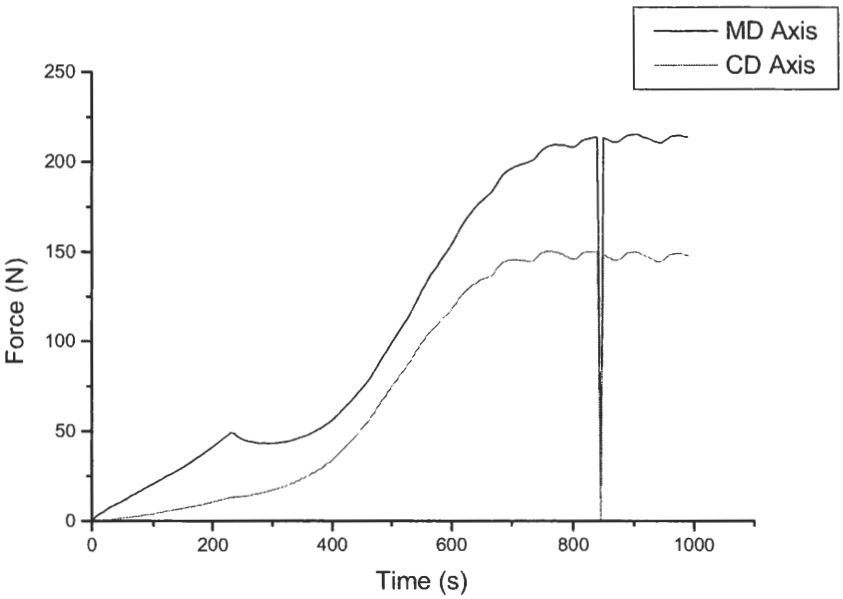

Sample 60-1. Top curve is MD, bottom is CD

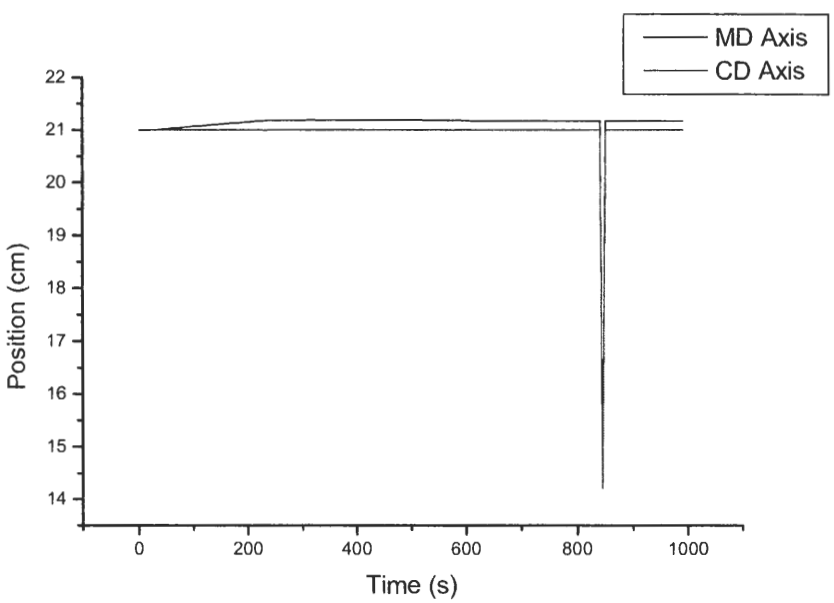

Sample 60-1. Top curve is MD, bottom is CD

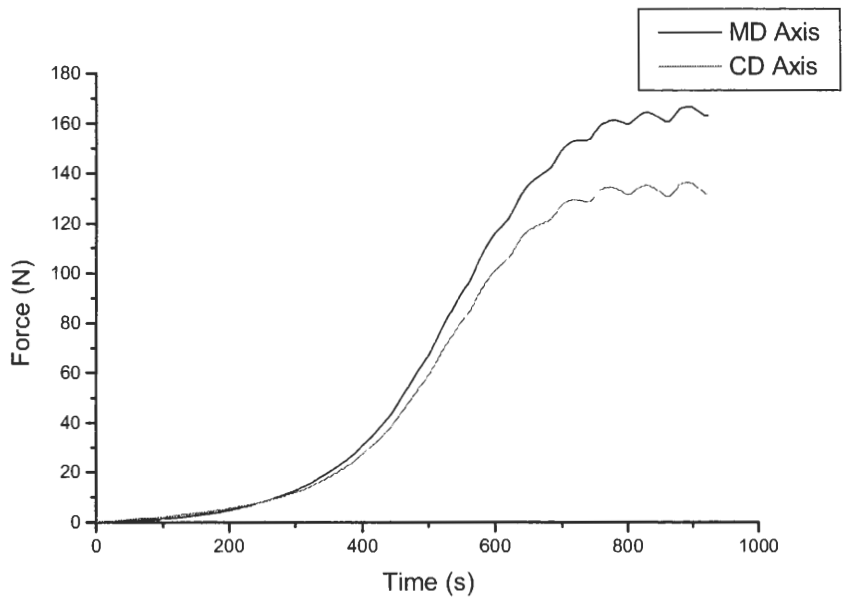

Sample 61-1. Top curve is MD, bottom is CD

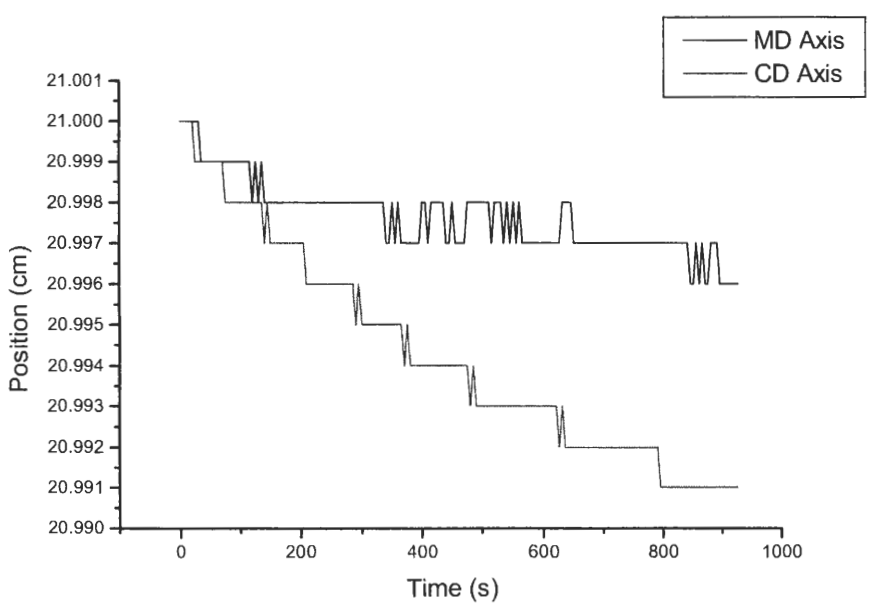

Sample 61-1. Top curve is MD, bottom is CD

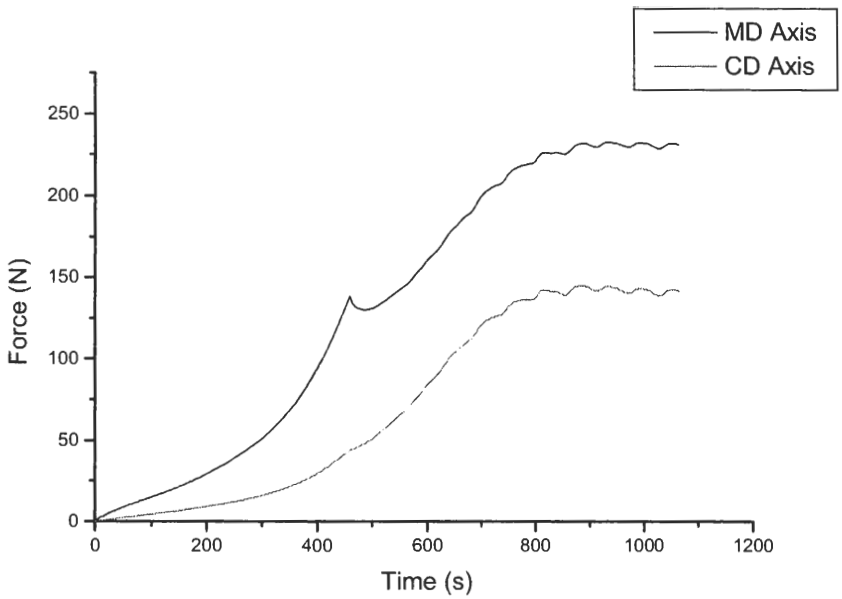

Sample 62-1. Top curve is MD, bottom is CD

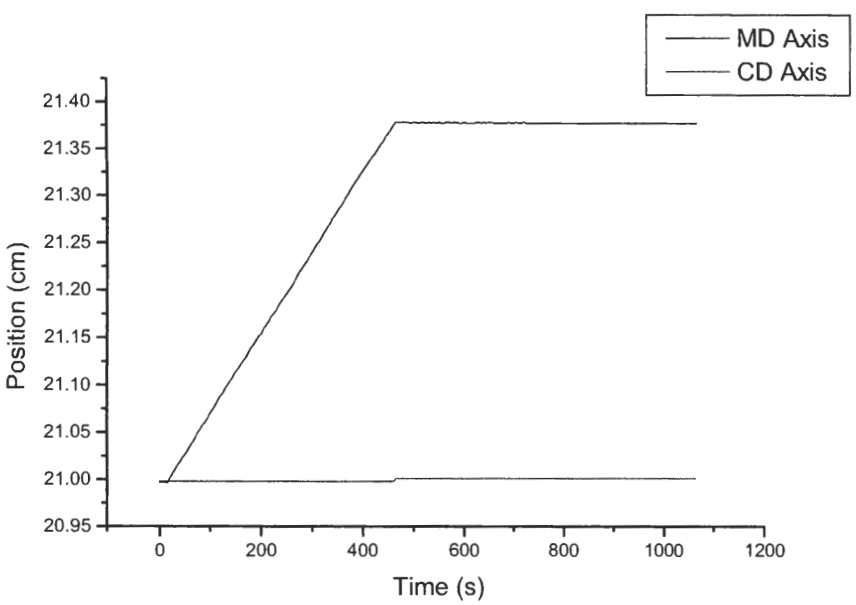

Sample 62-1 Top curve is MD, bottom is CD